



**A genome-wide study to
investigate the organisation of
global genome nucleotide excision
repair in *Saccharomyces cerevisiae***

Matthew Leadbitter

Department of Medical Genetics, Haematology & Pathology
School of Medicine
Cardiff University

A Thesis submitted to Cardiff University for the degree of Doctor of
Philosophy

Ph.D. 2011

UMI Number: U584543

All rights reserved

INFORMATION TO ALL USERS

The quality of this reproduction is dependent upon the quality of the copy submitted.

In the unlikely event that the author did not send a complete manuscript and there are missing pages, these will be noted. Also, if material had to be removed, a note will indicate the deletion.



UMI U584543

Published by ProQuest LLC 2013. Copyright in the Dissertation held by the Author.
Microform Edition © ProQuest LLC.


All rights reserved. This work is protected against
unauthorized copying under Title 17, United States Code.



ProQuest LLC
789 East Eisenhower Parkway
P.O. Box 1346
Ann Arbor, MI 48106-1346


DECLARATION

This work has not previously been accepted in substance for any degree and is not concurrently submitted in candidature for any degree.

Signed  (candidate) Date19.9.11.....

STATEMENT 1


This thesis is being submitted in partial fulfillment of the requirements for the degree of PhD

Signed  (candidate) Date19.9.11.....

STATEMENT 2


This thesis is the result of my own independent work/investigation, except where otherwise stated.

Other sources are acknowledged by explicit references.

Signed  (candidate) Date19.9.11.....

STATEMENT 3

I hereby give consent for my thesis, if accepted, to be available for photocopying and for inter-library loan, and for the title and summary to be made available to outside organisations.

Signed  (candidate) Date19.9.11.....

STATEMENT 4: PREVIOUSLY APPROVED BAR ON ACCESS

I hereby give consent for my thesis, if accepted, to be available for photocopying and for inter-library loans **after expiry of a bar on access previously approved by the Graduate Development Committee.**

Signed (candidate) Date

Acknowledgements

First and foremost, I must express my gratitude to my principal supervisor and friend, Dr. Simon Reed. His scientific passion and understanding have been the driving force behind the completion of my thesis. I thank him for sharing his wisdom and experience with me during both the highs and lows of my academic journey. He has opened my mind and expanded my perspectives. Thank you. I am also very grateful to Professor Raymond Waters for the many scientific discussions and for always being a patient and constructive supervisor when I needed help.

A huge thank you must also be said to all my academic colleagues; Dr. Shirong Yu (who was basically my 'molecular mum') and Dr. Julia Smirnova for teaching me the skills and discipline required of any good scientist. An extra big thank you must also go to Katie Evans (who originally identified and characterised 'angry Mat') and ('Professor' of bioinformatics/'real" ale!) Mark Bennett for all their support/insightful discussion/laughs during my final year especially. But I have met so many wonderful people who have helped along the way, and so in no particular order thanks to; Dr. Yumin Teng, Dr. Yachuan Yu, Dr. Huayun Zhuang-Jackson, Dr. Rhiannon Jones, Mary Alam, Trish, Yanbo Deng, Mark Robinson and the latest batch of Dr's (Zheng, Agi, Neil, Becky, Hannah and Azeem). A special mention must also go to Hefin Gill, who taught me that a western on the floor is still well worth developing.

A thank you must also be made to all my 'non-academic' colleagues in Cardiff that have made living in Wales such a joy. In particular, the lads from 37. Ed, who took me under his wing from day one; I treasure your friendship. And Tom, the wisest 23 year old I have ever met; thank you for the generosity you have shown me over the years. And the rest of them; Hartley, Robbo, Danger and Ed (#2) – there is no-one better to share a cheeky pint (or seven) with. And, Meg Evans – Meg if you ever look this thesis up – you did get a mention!

Finally, I must thank the ones closest to my heart; Suzie, without whom I probably would have finished my thesis in half the time; your love and support have given me the strength and determination I needed. My sister Alice, who equally qualifies for all the same statements made of Suzie; thank you for always being there for me. My dad for just being my dad. And lastly, my mum, whose limitless love and support has always given me the strength to endure. If I were to dedicate this work to anyone (which is a bit much for me), it would be to you.

Summary

In *Saccharomyces cerevisiae* efficient global genome nucleotide excision repair (GGR) requires a heterotrimeric protein complex of Abf1, Rad7 and Rad16 termed the GGR complex. Abf1 is a site specific DNA binding protein with known roles in DNA replication, transcription and repair. Rad16 has a DNA translocase activity and is a functional component of an E3 ubiquitin ligase. Rad16 has recently been shown to regulate the occupancy of Gcn5 and histone H3 K9K14 acetylation in response to UV damage.

The current study investigates how GGR is organised throughout the genome using chromatin-immunoprecipitation coupled to microarrays. Abf1 is observed to bind the genome at a high frequency and is preferentially localised to promoters. By analysing other genome-wide datasets in relation to Abf1 binding, Rad16 dependent histone H3 K9K14 acetylation and efficient GGR are observed to colocalise with Abf1 binding sites at promoters. Rad16 binding is also mapped and is found to colocalise with Abf1 binding sites at many promoters. Peaks of Rad16 binding are lost in a UV dependent manner and based on previous studies, this is suggested to occur by DNA translocation of Rad16. The differences in Rad16 binding levels are found to correlate with Rad16 dependent acetylation and efficient GGR.

In addition to studying the occupancy of Abf1, novel tools are built for the genome-wide analysis of Abf1 DNA binding kinetics. A recombinant protein termed a competitor is designed for this purpose. The competitor consists of an Abf1 DNA binding domain fused to a hormone dependent regulatory cassette. Following activation, the rate at which the competitor replaces Abf1 at a DNA binding site is monitored by chromatin immunoprecipitation to qualitatively measure Abf1 DNA binding kinetics. Preliminary results are shown that might suggest changes in Abf1 DNA binding kinetics following UV are mechanistically linked to GGR.

Abbreviations

(6-4)PP - Pyrimidine (6–4) pyrimidone photoproduct
aa – Amino acid
AD – Activation domain
AR – Androgen receptor
ARR – Access, repair, restore
ATR - Ataxia-telangiectasia mutated and Rad3-related
BER – Base excision repair
CAK- CDK activating kinase
ChIP – Chromatin immunoprecipitation
CPD – Cyclobutane pyrimidine dimer
DBD – DNA binding domain
DBS - (site specific) DNA binding site
DMSO - Dimethyl sulfoxide
DSB – Double strand break
dsDNA – Doubled stranded DNA
EDTA - Ethylenediamine tetraacetic acid
EMSA - Electrophoretic mobility shift assay
ER α - Oestrogen receptor- α
ER α LBD – Oestrogen receptor- α ligand binding domain
FLIP - Fluorescence loss in photobleaching
FRAP – Fluorescence recovery after photobleaching
GFP – Green fluorescent protein
GGR – Global genome NER
GR – Glucocorticoid receptor
GRF – General regulatory factor
HAT – Histone acetyl transferase
HBD – Hormone binding domain
HLB – High level binding
HR – Homologous recombination
IP – Immunoprecipitation/Immunoprecipitate
LBD – Ligand binding domain
LLB – Low level binding
MMR – Mismatch repair
NDR – Nucleosome depleted region
NER – Nucleotide excision repair
NHEJ – Non-homologous end joining
NTS – Non-transcribed strand
OB – Oligonucleotide binding
ORF – Open reading frame
PAR – Poly ADP-ribose
PCNA – Proliferating nuclear antigen
PCR – Polymerase chain reaction
PIC- Preincision complex
qPCR – quantitative PCR
RFC – Replication factor C
RNAPI - RNA polymerase I
RNAPII - RNA polymerase II

Abbreviations continued

ROS – Reactive oxygen species
RPA – Replication protein A
SCP – Scaled chromosomal position
SDS – Sodium dodecyl sulphate
ssDNA – Single stranded DNA
TCR – Transcription coupled NER
TF – Transcription factor
TLS – Translesion synthesis
TR – Thyroid receptor
TS – Transcribed strand
TSS – Transcription start site
UBA – Ubiquitin associated
UbL – Ubiquitin like
UPP – Ubiquitin proteasome pathway
UAS – Upstream activating sequences
WCE – Whole cell extract

Contents

Chapter

Page

1. Introduction

1.1 DNA damage.....	1
- 1.1.1 UV irradiation induced DNA damage and mutagenesis.....	2
- 1.1.2 Cyclobutane pyrimidine dimer (CPD).....	4
- 1.1.3 Pyrimidine-pyrimidone (6-4) photoproducts ((6-4)PP).....	6
1.2 Eukaryotic DNA repair pathways.....	8
- 1.2.1 Double strand break repair.....	8
- 1.2.2 Mismatch repair.....	10
- 1.2.3 Base excision repair.....	12
1.3 Nucleotide excision repair.....	16
- 1.3.1 Transcription coupled repair.....	18
- 1.3.2 Formation of the preincision complex.....	23
- 1.3.3 TFIIH.....	24
- 1.3.4 RPA and XPA.....	27
- 1.3.5 Dual Incision.....	29
- 1.3.6 DNA resynthesis.....	31
1.4 Proteins necessary for GGR.....	33
- 1.4.1 XPC-HR23B-centrin2.....	33
- 1.4.2 Rad4-Rad23-Rad33.....	35
- 1.4.3 UV-DDB complex.....	38
- 1.4.4 The GGR complex.....	40
1.5 Autonomously replicating sequence binding factor I.....	42
- 1.5.1 A role for Abf1 in DNA replication.....	42
- 1.5.2 Abf1 as a transcriptional regulator.....	43
- 1.5.3 Abf1 is important for DNA silencing.....	45
- 1.5.4 The multifunctional roles of Abf1; extensive repertoire of biochemical activities or a universal context dependent role?.....	46
- 1.5.5 The role of Abf1 in GGR.....	49

1.6 DNA binding kinetics.....	50
- 1.6.1 The nomenclature used with respect to transcription factors....	50
- 1.6.2 The in vivo lifetime of TF:DBS complexes.....	51
- 1.6.3 The regulation of DNA binding kinetics.....	53
- 1.6.4 Regulation of DNA binding kinetics by the 19S sub-particle of the proteasome.....	55
- 1.6.5 Is there a physiological rationale in regulating DNA binding kinetics?.....	57
1.7 Aim of the current study.....	60

2. Material and Methods

2.1 Strains, growth and storage.....	61
2.2 UV damage.....	61
2.3 DNA manipulations.....	62
- 2.3.1 DNA gel electrophoresis.....	62
- 2.3.2 Polymerase Chain Reaction (PCR).....	63
- 2.3.3 Cloning.....	64
- 2.3.4 DNA sequencing.....	65
2.4 Yeast transformation.....	66
2.5 Colony PCR.....	67
2.6 Protein work.....	68
- 2.6.1 Yeast whole protein lysates.....	68
- 2.6.2 Bradford Assay.....	69
- 2.6.3 Western blotting.....	70
2.7 Chromatin immunoprecipitation (ChIP).....	72
- 2.7.1 Immunoprecipitation (IP).....	74
- 2.7.2 Preparation of DNA from immunoprecipitated and input samples.....	76
- 2.7.3 Quantification of DNA by qPCR.....	76
- 2.7.4 Quantifying the relative occupancy of protein-chromatin binding.....	78
2.8 ChIP-on-chip.....	79

3. Mapping the genome-wide localisation of Abf1 in the absence and presence of UV damage

3.1 Introduction.....	84
3.2 Materials and Methods.....	89
3.3 Results.....	93
- 3.3.1 Genome-wide analysis of Abf1 binding.....	93
- 3.3.2 Normalisation of data.....	95
- 3.3.3 Investigating the effect of dye bias.....	97
- 3.3.4 Mapping Abf1 binding peaks.....	98
- 3.3.5 Abf1 preferentially binds promoter regions of the genome.....	100
- 3.3.6 UV dependent changes in Abf1 occupancy.....	102
- 3.3.7 Investigating histone H3 K9K14 hyperacetylation at Abf1 binding peaks.....	105
- 3.3.8 Investing GGR at Abf1 binding peaks.....	110
3.4 Discussion.....	113

4. Mapping the genome-wide localisation of Rad16 in the absence and presence of UV damage

4.1 Introduction.....	120
4.2 Materials and Methods.....	124
4.3 Results.....	127
- 4.3.1 Genome-wide analysis of Rad16 binding.....	127
- 4.3.2 The distribution of Rad16 before and after UV irradiation.....	129
- 4.3.3 Rad16 binding colocalises with Abf1 binding in vivo.....	130
- 4.3.4 The UV responsive changes in GGR complex chromatin binding.....	132
- 4.3.5 Investigating CPD repair at regions of the genome where Abf1 and Rad16 binding peaks colocalise.....	134
- 4.3.6 Investigating the relationship between Rad16 binding, Rad16 dependent acetylation and CPD repair.....	136
4.4 Discussion.....	140

5. Developing tools for the in vivo analysis of Abf1 DNA binding kinetics

5.1 Introduction.....	145
- 5.1.1 Molecular biological techniques for the study of DNA binding kinetics in vivo.....	147
- 5.1.2 Competitive ChIP; a novel technique for the analysis of DNA binding kinetics in vivo.....	150
5.2 Materials and Methods.....	154
5.3 Results	161
- 5.3.1 Designing an Abf1 competitor.....	161
- 5.3.2 Construction and expression of an Abf1 competitor.....	162
- 5.3.3 Abf1competitive ChIP.....	164
- 5.3.4 Testing the ability of the competitor to bind chromatin in the absence of Abf1 binding.....	166
- 5.3.5 Redesigning the Abf1 competitor.....	167
- 5.3.6 The in vivo molecular characteristics of the revised Abf1 competitor.....	172
- 5.3.7 Improving the hormonal regulation of the Abf1 competitor.....	173
5.4 Discussion.....	175

6. Investigating Abf1 DNA binding kinetics using Abf1 competitive ChIP

6.1 Introduction.....	180
6.2 Materials and methods.....	182
6.3 Results.....	185
- 6.3.1 Optimising the hormone concentration for competitive ChIP...	185
- 6.3.2 Examining the efficiency of the competition reaction.....	186
- 6.3.3 Potential caveats when investigating DNA binding kinetics at sites of incomplete competitor exchange with Abf1.....	188
- 6.3.4 Comparing the protein level of the competitor to Abf1 in vivo	190
- 6.3.5 Attempts to further improve the efficiency of Abf1 competitive ChIP.....	191
- 6.3.6 Genome-wide analysis of Abf1 competitive ChIP both in the presence and absence of UV damage.....	193
6.4 Discussion.....	197

7. General conclusions and future experiments

7.1 Chapter 3. Mapping the genome-wide localisation of Abf1 in the absence and presence of UV damage..... 202

7.2 Chapter 4. Mapping the genome-wide localisation of Rad16 in the absence and presence of UV damage..... 205

7.3 Chapter 5. Developing tools for the in vivo analysis of Abf1 DNA binding kinetics..... 210

7.4 Chapter 6. Investigating Abf1 DNA binding kinetics using Abf1 competitive ChIP..... 211

Appendix I..... 215

Appendix II..... 216

Appendix III..... 220

Appendix IV..... 223

Appendix V..... 231

References..... 237

1. Introduction

1.1 DNA damage

Deoxyribonucleic acid (DNA) encodes the genetic blueprint of cellular life. Using the four nucleotides of guanine, cytosine, adenine and thymine, DNA functions to store the information necessary for the development of all cellular components including all protein and RNA. Accurate preservation of this molecule and inheritance to the daughter cell is critical to life, and mechanisms that perturb these processes are considered to play fundamental roles within ageing, cancer and cell death. Therefore, maintenance of cellular DNA is imperative for the stable development and replication of all living organisms.

Within the cell, DNA is not inherently stable and is constantly exposed to agents that alter its primary structure, as well as spontaneous alterations. Deamination of four of the five bases present in DNA (cytosine, adenine, guanine and 5-methylcytosine) can result in the conversion to alternative nitrogen bases (uracil, hypoxanthine, xanthine, thymine). In addition, uracil may be introduced into DNA during semi-conservative replication, which may also incorrectly incorporate non-complementary bases resulting in DNA mismatches. Similarly, non-replicative DNA synthesis may also introduce DNA mismatches. Cleavage of the N-glycosyl bond between a base and sugar phosphate within DNA produces an abasic site. Reactive oxygen species (ROS) derived from aerobic respiration and other sources can produce intracellular $\cdot\text{OH}$ radicals which result in electrophilic additions to nucleobases or hydrogen abstraction of deoxyribose sugar, which can induce single strand breaks. A wide variety of DNA damage is also introduced as a result of exogenous environmental factors. Ionizing radiation (from cosmic radiation and radionuclides) can induce regions of localised ROS which can induce a variety of DNA lesions including oxidative damage to bases, as well as single and double strand DNA breaks. UV irradiation (from sunlight) induces the saturation of the 5,6 double bond of pyrimidines to produce a wide variety of lesions including cyclobutane pyrimidine dimers, pyrimidine-pyrimidone (6-4) photoproducts, pyrimidine hydrates and thymine glycol. Alkylating agents (such as methyl chloride or S-adenosylmethionine) transfer alkyl groups to nucleophilic centres within DNA bases and the backbone. Alkylation also weakens the N-glycosyl bond and thus promotes formation of abasic nucleotides.

Further to these examples, a plethora of extra DNA damages and sources of damage have been characterised (Friedberg, 2006).

In order to maintain the structure of DNA and promote cell survival, the cell has evolved a large repertoire of biochemical pathways to both reverse DNA damage and tolerate damage during DNA replication. A wide variety of sources of DNA damage to the cell have existed throughout evolution and these have functioned to impose a high selective pressure for the maintenance of these pathways. Consequently, most DNA repair pathways are highly homologous throughout the eukaryotic kingdom, and as such, model organisms including the yeast *Saccharomyces cerevisiae* have been, and continue to be, implemental in the quest for deciphering the molecular mechanism of eukaryotic DNA repair. The research presented here concerns the repair of UV induced DNA damage by the repair pathway nucleotide excision repair, using *S. cerevisiae* as a model organism.

1.1.1 UV irradiation induced DNA damage and mutagenesis

Ultra-violet radiation (UV) is subdivided into three ranges termed UVA (320-400nm), UVB (290-320nm) and UVC (200-290nm). Exposure of humans to UV from solar radiation principally consists of wavelengths from UVA (95%) and longer wavelengths in UVB (5%), whilst the earth's ozone layer absorbs the majority of shorter wavelengths from UVB and UVC. UV radiation is both cytotoxic and mutagenic and a plethora of evidence demonstrates UV exposure is a primary factor in the development of skin cancers (Pfeifer et al., 2005). This is principally due to UV induced DNA damage. UV is readily absorbed by DNA and exposure induces a wide variety of DNA lesions; principally dipyrimidine photoproducts (discussed below) but also less commonly other damages including interstrand crosslinks, ssDNA breaks and oxidative lesions (Bourre et al., 1987; Douki et al., 2003; Ravanat et al., 2001). Pyrimidine photoproducts are refractory to DNA replication and if they are not tolerated by the cell, can result in necrosis (Prakash et al., 2005). Nucleotide excision repair (NER) is the principle pathway for the repair of UV damaged DNA (discussed below). Mutations which inactivate this pathway are the molecular cause of the homozygous recessive genetic disease Xeroderma pigmentosum (XP). This disease exemplifies the role of DNA damage in UV induced cytotoxicity and mutagenesis; XP patients show severe sensitivity to sunlight and a ~2000-fold increase in the incidence of skin cancer (Friedberg, 2006).

In the absence of repair, DNA damage may be tolerated during DNA replication by a host of specialised polymerases termed translesion synthesis (TLS) polymerases, which mediate DNA replication past a lesion (Prakash et al., 2005). Although this process can occur via one polymerase, often damage is bypassed by the combinatorial activities of two polymerases; the first adds nucleotides opposite a lesion and the second extends synthesis beyond the lesion. Whilst these activities promote the tolerance of DNA damage, and cell survival, because the enzymes typically have a low fidelity this occurs at the cost of accurate DNA replication (Prakash et al., 2005). This inaccurate replication drives mutagenesis, and the vast majority of UV induced DNA mutagenesis in eukaryotes is dependent upon the activity of TLS polymerases (Abdulovic and Jinks-Robertson, 2006; Yoon et al., 2009, 2010).

Most DNA mutations induced by UVB or UVC light are base substitutions at dipyrimidines, most commonly C->T transition events (Armstrong and Kunz, 1992; Brash et al., 1987; Drobetsky et al., 1987; Dumstorf et al., 2006; Gueranger et al., 2008). UVA induced DNA mutagenesis is currently a hot topic of debate, and in some experimental setups, it appears UVA induces a differential pattern of mutagenesis to that of UVB or UVC (Runger and Kappes, 2008). This correlates with a differential pattern of UVA induced DNA damage (Douki et al., 2003). However, as with UVB and UVC, pyrimidine photoproducts still remain the primary DNA damage and these lesions have been correlated with UVA mutagenesis including the prototypical C->T transition (Mouret et al., 2006; Rochette et al., 2003; Runger and Kappes, 2008). In addition, UVA is considered only to contribute 0.01-10% of DNA damage from solar radiation (Runger and Kappes, 2008). Within the laboratory, UV damage is commonly induced by a germicidal lamp emitting principally wavelengths close to 254nm, in the UVC range. This wavelength is not readily absorbed by proteins, but is near to the absorption maxima of DNA, permitting experimental selectivity for UV induced DNA lesions (Friedberg, 2006). It may thus be observed that whilst this does not recapitulate UV exposure from natural sunlight, the experimental procedure remains highly biologically relevant by inducing the same DNA damage and mutations as natural sunlight.

1.1.2 Cyclobutane pyrimidine dimer (CPD)

The most common DNA lesion induced by UV irradiation occurs between adjacent pyrimidines which covalently link between the C5 and C6 double bonds of the respective bases to form a 4 carbon ring (Fig. 1.1). Such lesions are termed cyclobutane pyrimidine dimers or CPDs, and are classically represented between bases with "<>" such that a CPD between two thymines is denoted as T<>T. Theoretically four stereoisomers of the CPD exist, although in B-form DNA the lesion predominately occurs as the cis-syn isomer (Friedberg, 2006).

CPDs may form between any dipyrimidines, however lesion incidence is influenced by multiple factors. In this respect, base composition of the dipyrimidine appears to be important. Treatment of naked DNA with UVC induces CPDs between the adjacent pyrimidines T<>T, C<>T, T<>C, C<>C, at a ratio of 68:13:16:3, whilst UVB treatment achieves a similar ratio of 52:19:21:7 (Mitchell et al., 1992). The formation of CPDs plateaus at high levels of UV irradiation (Douki and Cadet, 2001; Douki et al., 2000). It should be noted that numerous studies have analysed the incidence of the CPD lesion for these four dipyrimidines using various techniques with both in vitro and in vivo DNA substrates. Whilst the ratios reported do differ from those stated above, two universal observations generally hold; that UVB and UVC induce CPD lesions at similar ratios for the dipyrimidines (and a given experimental condition) and that the T<>T CPD is the most frequent lesion observed (Bourre et al., 1987; Brash and Haseltine, 1982; Douki and Cadet, 2001; Rochette et al., 2003). Furthermore, the intracellular environment does not have a large influence upon the relative distribution of CPD incidence at dipyrimidines (Douki and Cadet, 2001; Lippke et al., 1981; Teng et al., 2010). Interestingly, application of UVA to DNA does not induce the same pattern of DNA damage as that of UVB or UVC; neither C<>C CPDs nor (6-4)PPs (see below) are detectably induced and the ratio of T<>T CPD to other CPD lesions is far greater (Besaratina et al., 2005; Courdavault et al., 2004; Douki et al., 2003; Rochette et al., 2003). Whilst this was predicted to suggest that UVA may induce CPD formation via an indirect method (thus contrasting with UVB and UVC), two recent reports strongly suggest damage induction occurs via direct absorption of the wavelength (Douki et al., 2003; Jiang et al., 2009; Mouret et al., 2010). As with UVB and UVC irradiation, the predominant lesion in UVA damaged DNA is the CPD (Courdavault et al., 2004; Douki et al., 2003; Mouret et al., 2006).

The CPD has long been suspected to be the principle mutagenic lesion induced by UV irradiation due to its abundant presence and slow repair in vivo (Courdavault et al., 2005). In support of this, selectively repairing CPDs after UV damage by photoreversal, drastically reduces UV induced mutagenesis in both yeast and mammalian cells (Armstrong and Kunz, 1992; Brash et al., 1987; Jans et al., 2005; Yoon et al., 2010; You et al., 2001). The most common base substitution at a CPD is a C->T transition (Yoon et al., 2009; You et al., 2001). Interestingly however, TLS past the cis-syn T<>T CPD is not a highly mutagenic process in vivo (Gibbs et al., 1993; Yoon et al., 2009). Indeed, it has been demonstrated that a T<>T CPD may be efficiently bypassed in an error-free manner by the TLS polymerase Pol η (Johnson et al., 1999b; Masutani et al., 1999a; Washington et al., 2000; Yoon et al., 2009). Furthermore, genetic abnormalities within this polymerase are the molecular basis of a variant form of XP (termed XPV) in which UV induced mutagenesis is highly prevalent (Johnson et al., 1999a; Masutani et al., 1999b). This suggests Pol η is the principle polymerase involved in CPD TLS; the same conclusion is also made in yeast (Gibbs et al., 2005).

In a recent study it was shown that mammalian polymerases Pol κ and Pol ζ function in independent mutagenic TLS pathways for the CPD (Yoon et al., 2009). Pol κ cannot bypass this lesion, whilst Pol ζ bypass occurs infrequently (Johnson et al., 2000a; Johnson et al., 2000b; Nelson et al., 1996). However, both can extend from a nucleotide opposite the 3' thymine of a T<>T CPD, and both do this preferentially from an incorrectly incorporated guanine base (Johnson et al., 2000b; Washington et al., 2002). Therefore, it is predicted that an as yet to be identified TLS polymerase functions upstream of both Pol κ and Pol ζ dependent TLS to insert a nucleotide(s) opposite the CPD lesion (Yoon et al., 2009). Interestingly, two further human studies have produced contrasting results with that of Yoon et al. (2009) for CPD mutagenesis. Ziv et al. (2009) found that whilst Pol ζ was necessary for CPD mutagenesis, their study suggested the polymerase functioned in two TLS pathways; one of which was dependent upon Pol ι and the other Pol κ (Ziv et al., 2009). In further contrast to these reports, a third study has suggested Pol ζ does not have a role in CPD mutagenesis (Shachar et al., 2009). At least some of these differences probably reflect the disparity in the experimental conditions; whilst all studies used plasmid based assays to assess mutagenesis, the latter two studies introduced the lesion upon a region of single stranded DNA and thus probably reflect TLS at post replication gaps

rather than replication forks (Shachar et al., 2009). Finally, whilst human Pol η has been demonstrated to efficiently bypass a CPD under certain in vitro conditions, this polymerase does not seem to significantly influence CPD mutagenicity in vivo (Gueranger et al., 2008; Vaisman et al., 2003; Yoon et al., 2009).

The molecular mechanism of the common UV/CPD induced C->T transition remains to be determined (Pfeifer et al., 2005). However, it has been speculated that this may be due to spontaneous deamination of cytosine within a CPD, producing uracil which, if correctly bypassed by TLS would incorporate a guanine and thus result in the C->T transition observed at this lesion (Vaisman et al., 2006).

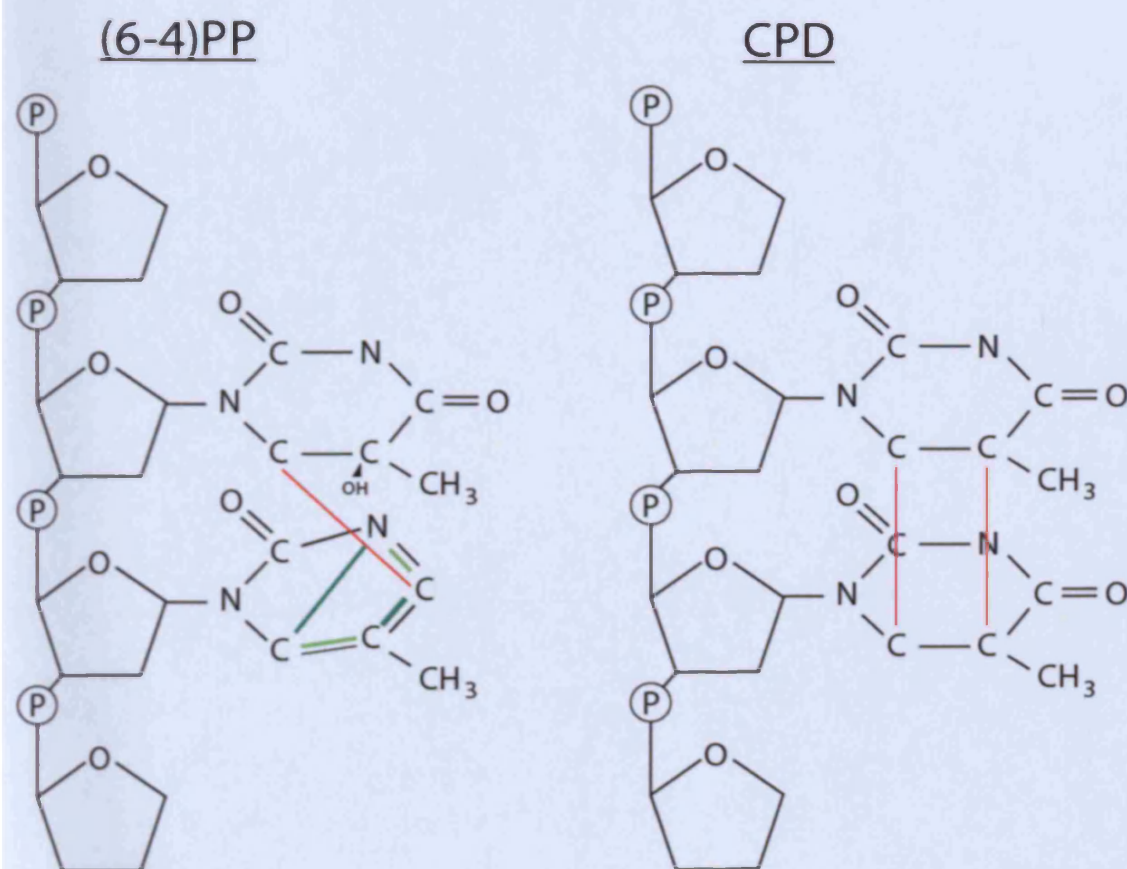


Figure 1.1. The chemical structure of the (6-4)PP and CPD. Both UV lesions are shown between two thymine bases. The aberrant covalent bonds in each lesion are shown in red. The two covalent bonds in light green represent bonds found in a standard (6-4)PP valence isomer, whilst these are replaced with the two covalent bonds represented in dark green for a Dewar valence (6-4)PP.

1.1.3 Pyrimidine-pyrimidone (6-4) photoproducts ((6-4)PP)

A second prevalent damage within DNA following UV irradiation covalently links the C6 position of a 5' pyrimidine to the C4 position of a 3' pyrimidine (Fig.

1.1) (Lippke et al., 1981). The damage is termed a pyrimidine-pyrimidone (6-4) photoproduct or (6-4)PP. The incidence of CPD relative to the (6-4) PP DNA damage depends both upon flanking DNA sequence and the wavelength of UV radiation; estimates typically calculate between three to ten fold higher levels of CPD incidence (Bourre et al., 1987; Brash and Haseltine, 1982; Douki et al., 2003; Perdiz et al., 2000). In addition, the (6-4)PP also exists as a Dewar valence isomer (see Fig 1.1). As with the CPD, the incidence of (6-4)PP DNA damage is influenced by its nucleotide sequence. For both UVB and UVC irradiation, the (6-4)PP is most prevalent at TC dimers, while TT or CC (6-4)PPs occur around 5-10 times less often and CT (6-4)PPs are very uncommon; this pattern is true of both purified and intracellular DNA (Brash and Haseltine, 1982; Douki and Cadet, 2001; Lippke et al., 1981). Under conditions where the relationship between lesion formation and UVB/UVC irradiation is linear, the only Dewar valence isomer detected is the CC (6-4)PP isomer (Douki and Cadet, 2001). However, as UV irradiation exposure increases the relative distribution of damage alters such that (6-4)PP formation plateaus, whilst Dewar (6-4)PP continues to increase (Douki and Cadet, 2001; Douki et al., 2000). Whilst UVA irradiation cannot induce the formation of (6-4)PPs in DNA, it has been demonstrated to photoisomerize the damage into its Dewar valence isomer (Besaratina et al., 2005; Douki et al., 2003; Rochette et al., 2003). As a consequence, simulated sunlight (95% UVA, 5% UVB) DNA damage results in high levels of Dewar valence isomers at a cost of (6-4)PPs when compared with UVB DNA damage alone (Douki et al., 2003; Perdiz et al., 2000). The nucleotide composition of the dipyrimidine also influences this process and TT (6-4)PPs are photoisomerized more efficiently than TC (6-4)PPs by UVA (Courdavault et al., 2005).

The most common base substitution induced by the (6-4)PP is a T->C transition for both yeast and mammalian cells (Bresson and Fuchs, 2002; Gibbs et al., 1995; Yoon et al., 2010). Interestingly, despite its error-free role in CPD TLS, Pol η is responsible for the majority of (6-4)PP induced mutagenesis in yeast (Bresson and Fuchs, 2002; Zhang and Siede, 2002). In vitro the polymerase preferentially inserts guanine opposite the 3' thymine of a TT (6-4)PP (Johnson et al., 2001). This activity would result in the T->C transition mutations most frequently observed at the (6-4)PP in vivo. Pol ι may also insert nucleotides opposite a TT (6-4)PP and does this with a low fidelity (Haracska et al., 2001; Johnson et al., 2000b; Tissier et al., 2000; Vaisman et al., 2003). Irrespective of which polymerase inserts a nucleotide(s)

opposite the (6-4)PP, neither can bypass the damage in vitro (Johnson et al., 2001; Seki and Wood, 2008; Vaisman et al., 2003). In both circumstances addition of Polζ continues DNA polymerisation, which occurs consistently with the stated mutagenesis of a (6-4)PP above, by preferentially extending from an incorrectly inserted guanine nucleotide opposite a lesion thymine (Johnson et al., 2001; Johnson et al., 2000b). In vivo, Polζ is considered to be the principle polymerase for TLS of the (6-4)PP in yeast (Gibbs et al., 2005).

In contrast with yeast, in humans these three polymerases appear to function independently in (6-4)PP TLS pathways; Polη and Polι function in error-prone pathways whilst Polζ is necessary for error free bypass of the lesion (Yoon et al., 2010). Given the above biochemical properties of these polymerases, this suggests that at least two more TLS polymerases must exist; one to extend from Polη and Polι nucleotide insertion opposite the lesion, and another to act upstream of Polζ extension. Polθ may be one likely candidate given that it can efficiently extend TLS across a (6-4)PP with Polι in vitro (Seki and Wood, 2008). A second recent human study has also explored (6-4)PP mutagenesis pathways but produced contrasting results with Yoon et al. (2010), suggesting Polζ is the predominant driver of (6-4)PP mutagenesis (Shachar et al., 2009). As discussed above, the differences may result from the experimental setup reflecting different types of TLS at ssDNA and dsDNA lesion substrates.

1.2 Eukaryotic DNA repair pathways

By way of introduction to eukaryotic DNA repair the following account briefly summarises the repair pathways common to all eukaryotes; double strand break repair, mismatch repair and base excision repair, followed by a detailed account of nucleotide excision repair.

1.2.1 Double strand break repair

DNA double strand breaks (DSBs) are a highly cytotoxic DNA lesion and are the product of multiple sources including ionizing radiation, oxidative stress and replication of damaged DNA. DSB repair can occur via two repair mechanisms; non-homologous end joining (NHEJ) or homologous recombination (HR) (Heyer et al., 2010; San Filippo et al., 2008). Since HR requires a second region of dsDNA homologous to the region in which a DSB has occurred, NHEJ is the only DSB repair option in any circumstance where this template is unavailable. NHEJ occurs using

various functional components including a DSB multifunctional recruitment factor, a polymerase, nuclease, kinase/phosphatase and ligase, members of which are given for both yeast and humans in Fig. 1.2. For vertebrate NHEJ, when a DSB breaks forms, the DNA ends are bound by Ku and this complex functions to recruit the nuclease, polymerase and ligase activities (Lieber, 2010). Artemis:DNA-PKcs has a 5' exonuclease activity as well as 5' and 3' endonucleolytic activities and is able to process a wide variety of damaged DNA overhangs. Pol λ and Pol μ bind Ku, and the latter is able to perform template independent DNA synthesis. A complex of XLF:XRCC4:DNA ligase IV functions as a flexible ligase able to ligate incompatible DNA ends and across gaps. Ku does not sequentially recruit these processive factors and thus DNA duplex ends may be processed by any one of these catalytic activities at any one time. Processing may transiently terminate when two strands anneal, or permanently terminate when one or both of the duplex strands ligate (Lieber, 2010).

When a DSB is repaired by HR, DNA ends are processed by nucleolytic resection in the 5'→3' direction to leave 3' ssDNA ends (San Filippo et al., 2008). In *S. cerevisiae* this processing involves four nucleases Mre11-Rad50-Xrs2, Exo1, Dna2 and Sae2 as well as the helicase Sgs1 (Heyer et al., 2010). ssDNA ends are coated with RPA to prevent secondary structures forming, but subsequent recombination requires the formation of a nucleoprotein filament of Rad51 and the ssDNA termed the presynaptic filament. Formation of the filament is mediated through three classes of factors; Rad51 paralogues, Rad52 and BRCA2 (the latter is only present in higher eukaryotes). The presynaptic filament then searches for homologous dsDNA and subsequent Rad54 mediated strand invasion results in formation of the D loop (see Fig. 1.2). Formation of the D-loop represents a branching point whereby three pathways may occur (Heyer et al., 2010). DNA polymerase extension of the 3' invaded strand may extend the filament beyond the point at which the DSB occurred. In the absence of a complementary presynaptic filament the D-loop may become a replication fork in a process termed break induced replication. Alternatively, the extended filament may re-anneal with the reciprocal resected 3' DNA filament restoring the dsDNA; this mechanism is termed synthesis dependent strand annealing. The second presynaptic filament may also anneal to the D-loop to produce two holiday junctions which may both be extended by DNA polymerisation. These junctions may be resolved in a variety of ways to produce both recombinant and non-recombinant dsDNA. Finally, if following nucleolytic resection the two ssDNA

filaments are complementary distal to the DSB, these may anneal followed by removal of the 3' ssDNA ends in a mechanism call single strand annealing (Heyer et al., 2010; San Filippo et al., 2008).

A. Table of functional homologues in NHEJ

Functional component	<i>S.cerevisiae</i>	Multicellular eukaryote
Recruitment factor	Ku 70/80	Ku 70/80
Polymerase	Pol4	Pol μ and pol λ
Nuclease	Rad50:Mre11:Xrs2	Artemis:DNA-PKcs
Kinase/Phosphatase	Tpp1 and others	PNK and others
Ligase	Nej1:Lif1:Dnl4	XLJ:XRCC4: DNA ligase IV

B.

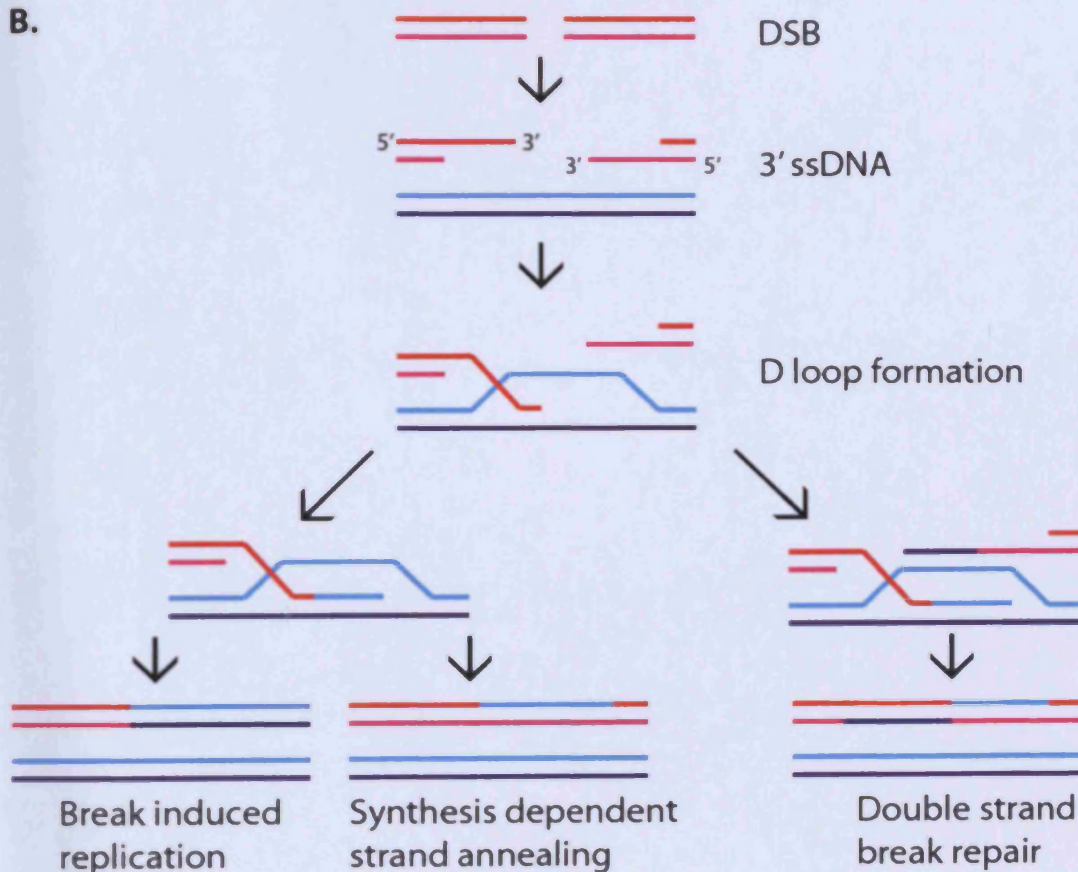


Figure 1.2. A. Table of NHEJ homologues adapted from (Lieber, 2010) B. DSB repair DNA intermediates and products. Redrawn from (Heyer et al., 2010)

1.2.2 Mismatch repair

Mismatch repair (MMR) is essential for the repair of base-base mismatches as well as insertion/deletions loops, both of which are primarily products of inaccurate DNA replication (Jiricny, 2006b; Pluciennik et al., 2010). In the absence of MMR,

accumulation of these mutations promotes carcinogenesis. MMR principally occurs via a mechanism that involves ssDNA resection over the mismatched DNA, followed by DNA polymerase dependent resynthesis. Crucially, this pathway requires a mechanism to discriminate newly synthesised DNA with a mismatch from the template DNA to prevent 'repair' of the template and thus mutagenesis.

In eukaryotes, DNA mismatches are recognised by the MutS homologues MSH2, MSH3 and MSH6 (Kunkel and Erie, 2005). These proteins function as heterodimers of MSH2-MSH6 (MutS α) or MSH2-MSH3 (MutS β), which encircle the DNA at a mismatch in an asymmetric binding manner. Msh2-Msh6 (the yeast homologue of human MSH2-MSH6) can slide along DNA in an ATP independent manner in the absence of rapid deassociation/reassociation events (Gorman et al., 2007). Upon encountering DNA mismatches the complex is kinetically stabilised, which is predicted to signal MMR events (Zhai and Hingorani, 2010). MSH3 and MSH6 physically interact with proliferating cell nuclear antigen (PCNA), and this interaction has been predicted to couple MMR with DNA replication (Kunkel and Erie, 2005). A second heterodimeric complex important for MMR includes the MutL homologues which exist as MutL α (MLH1-PMS2 in humans, Mlh1-Pms1 in yeast), MutL β (MLH1-PMS1, Mlh1-Mlh2 in yeast) and MutL γ (MLH1-MLH3). MutL α has been demonstrated to function as a nicking endonuclease able to produce single stranded nicks in dsDNA (Kadyrov et al., 2006). MutL α is recruited by MutS α , and both PCNA, MutL α and MutS α can form complexes on DNA. The interaction with PCNA is necessary to activate the endonucleolytic activity of MutL α , and it appears that the orientation upon which PCNA is loaded onto DNA dictates which strand is incised (Pluciennik et al., 2010).

Bidirectional eukaryotic MMR has been reconstituted in vitro with the human proteins MutS α , MutL α , Exo1, replication protein A (RPA), replication factor C (RFC), PCNA, DNA polymerase δ (Pol δ) and DNA ligase I (Constantin et al., 2005; Jiricny, 2006b). Reconstitution of efficient MMR requires both a mismatch and a single strand nick, which may be situated either 5' or 3' to the mismatch. DNA is resected in an Exo1 dependent manner between the nick and the mismatch, and subsequent DNA polymerisation by Pol δ restores the DNA. However, a second pathway that depends upon nucleotide displacement by Pol δ instead of Exo1 resection has also been implicated (Kadyrov et al., 2009). One paradox of these observations was that Exo1 is a 5'->3' exonuclease and yet DNA was resected irrespective of the

orientation of the nick to the mismatch. In the absence of RFC and PCNA, DNA is only resected in the 5'→3' direction by Exo1, even if the mismatch is found in the opposite direction. However, in their presence RFC can suppress futile 5'→3' exonuclease activity from a nick that lies 3' to the mismatch (Dzantiev et al., 2004). In addition RFC loads PCNA and this induces the MutLα endonucleolytic activity which may then introduce new nicks into the dsDNA 5' to the mismatch. From these novel nucleation sites DNA may then be resected by Exo1 (Jiricny, 2006a).

In addition to in vitro studies, a nick or DNA end may also provide a strand discrimination signal in vivo, and these signals are predicted to arise from the ends of actively replicating DNA (Crouse, 2010). In support of this model, a recent publication using DNA polymerase mutants demonstrated MMR of base substitutions by Polα are corrected several fold more efficiently than those of Polδ (Nick McElhinny et al., 2010). Given that DNA polymerised by Polα (on the lagging strand) will always be more proximal to the end of the replicating strand (and thus a discrimination signal) than DNA polymerised by Polδ, it was suggested MMR is more likely to occur within the former.

1.2.3 Base excision repair

The base excision repair (BER) pathway is important for the repair of a wide variety of chemical lesions at the base of a single deoxyribonucleic acid. Toxicological chemical modifications repaired by BER include oxidation, alkylation and base deamination, however subdivisions of the BER pathway are also important for the repair of covalently attached DNA topoisomerase and the repair of DNA single strand breaks (Almeida and Sobol, 2007). Whilst the repair mechanism is well conserved throughout the eukaryotic kingdom, many of the biochemical roles in BER are performed by non-homologous factors when comparing BER of *S. cerevisiae* with that of *H.sapiens* (Kelley et al., 2003). The minimal BER pathway may be reconstituted with only 4 or 5 enzymes, consisting of a DNA glycosylase, AP endonuclease, DNA polymerase and a DNA ligase. BER is initiated through the activity of a DNA glycosylase, which functions to recognise a lesion and cleave the N-glycosidic bond between a damaged base and the deoxyribose sugar, thus removing the lesion from the DNA molecule. Following this, the deoxyribose phosphate backbone adjacent to the apyrimidic/apurinic (AP) site is cleaved, either 5' to the AP site by an AP endonuclease or 3' to the AP site via an AP lyase activity present in

some AP glycosylases. The cleaved DNA backbone may then be further processed by a variety of enzymes to produce a substrate compatible for DNA replication. The missing nucleotide is ultimately replaced by a DNA polymerase (primarily DNA pol β in mammals or pol ϵ in yeast), and the nicked DNA ligated by DNA ligase III (or ligase I, and in yeast Cdc9). The process of DNA replication may function to add a single nucleotide, a mechanism termed short-patch BER, or alternatively replace a further 1-12 downstream nucleotides in a mechanism termed long-patch BER. In long patch BER, DNA, cleaved by the AP endonuclease APE1 (or in yeast Apn1), is displaced by DNA polymerase in a PCNA dependent manner during replication. The displaced ssDNA fragment then is resolved by the endonuclease FEN1 (Rad27 in yeast) allowing DNA ligation to complete the reaction.

The eukaryotic cell contains a diverse range of DNA glycosylases; to date 11 different mammalian glycosylases have been identified, a list of which, along with *S. cerevisiae* homologues, are given in Table 1.1 (Robertson et al., 2009). Most DNA glycosylases are promiscuous, thus many DNA damages are known to be repaired by numerous glycosylases with differing kinetics according to their substrate preference (Hegde et al., 2008). Following the activity of a DNA glycosylase the primary AP endonuclease in mammalian cells termed APE1 (or Apn1 in *S. cerevisiae*), incises the DNA backbone (Boiteux and Guillet, 2004). This incision either occurs 5' to an AP site to leave a 3'-OH and 5' deoxyribophosphate (dRP), or if the DNA backbone was cleaved by a bifunctional DNA glycosylase, a 3' phosphodiesterase activity may eliminate the 3'- α,β unsaturated aldehyde (see Fig. 1.3) (Chen et al., 1991; Robson and Hickson, 1991; Winters et al., 1994). Whilst the latter incision produces a substrate compatible for nucleotide incorporation by Pol β , the former requires that the 5'dRP is eliminated through a catalytic activity present within this polymerase (Matsumoto and Kim, 1995). Interestingly, both APE1 and Apn1 have also been demonstrated to nick DNA 5' to many base lesions independent to prior detection by a DNA glycosylase, initiating a repair pathway termed nucleotide incision repair (Daviet et al., 2007; Ischenko and Saparbaev, 2002).

Whilst APE1 is the archetypal enzyme necessary for the tailoring of DNA suitable for gap filling by DNA polymerase, other proteins have been demonstrated to play such roles in BER. One special case is seen with the bifunctional DNA glycosylases NEIL1 and NEIL2. In addition to their DNA glycosylase activity, these enzymes can perform a β,δ elimination of the DNA ribose backbone yielding a gap

with both 5' and 3' phosphates (Hazra et al., 2002). In this circumstance, PNKP, which possesses a far stronger 3'-phosphatase activity than APE1, functions to eliminate the 3' phosphate (Wiederhold et al., 2004). A second example is the activity of tyrosyl-DNA phosphodiesterase (TDP1). This protein is able to cleave peptides covalently attached to the 3' phosphate of the DNA backbone via a tyrosyl residue (Interthal et al., 2001). The activity is important for the repair of stalled topoisomerase covalently linked to DNA (Pouliot et al., 1999). The resultant nick may then be repaired by downstream BER enzymes. In addition to TDP1, APE1 is also known to be able to cleave 3'-phosphotyrosyl bonds, and recently a human enzyme that cleaves 5'-phosphotyrosyl bonds was also identified (Cortes Ledesma et al., 2009; Wilson, 2003).

DNA glycosylase	<i>S. cerevisiae</i>	<i>H. sapiens</i>
3-Methyl-adenine DNA glycoylase II	MAG1	
8-Oxoguanine DNA glycosylase	OGG1	OGG1
Endonuclease III/ endonuclease III like-1	NTG1/NTG2	NTHL1
Adenine-DNA glycosylase		MUTYH
Methyl-CpG binding domain protein 4		MBD4
Uracil-DNA glycosylase	UNG1	UNG
Single-strand selective monofunctional uracil-DNA glycosylase I		SMUG1
G:U mismatch specific DNA glycosylase/ thymine-DNA glycosylase		TDG
Endonuclease VIII-like 1		NEIL1
Endonuclease VIII-like 2		NEIL2
N-Methylpurine-DNA glycosylase		MPG

Table 1.1. List of known DNA glycosylases from *Homo sapiens* and *Saccharomyces cerevisiae*, derived from (Robertson et al., 2009).

Following incision of the DNA backbone, two further proteins are considered to be important for the mechanism of BER termed XRCC1 and PARP1. XRCC1 has been demonstrated to bind a wide variety of BER enzymes including multiple DNA glycosylases, PARP1, DNA ligase III and DNA pol β , (Caldecott et al., 1996; Campalans et al., 2005; Masson et al., 1998). A catalytic activity is not associated with this protein, and it is thought to function as a scaffold protein by recruiting a protein complex necessary for BER to a lesion. PARP1 has long been identified as a molecular sensor of single stranded DNA nicks, and is considered to initiate repair of such lesions derived from endogenous oxidative metabolism or exogenous

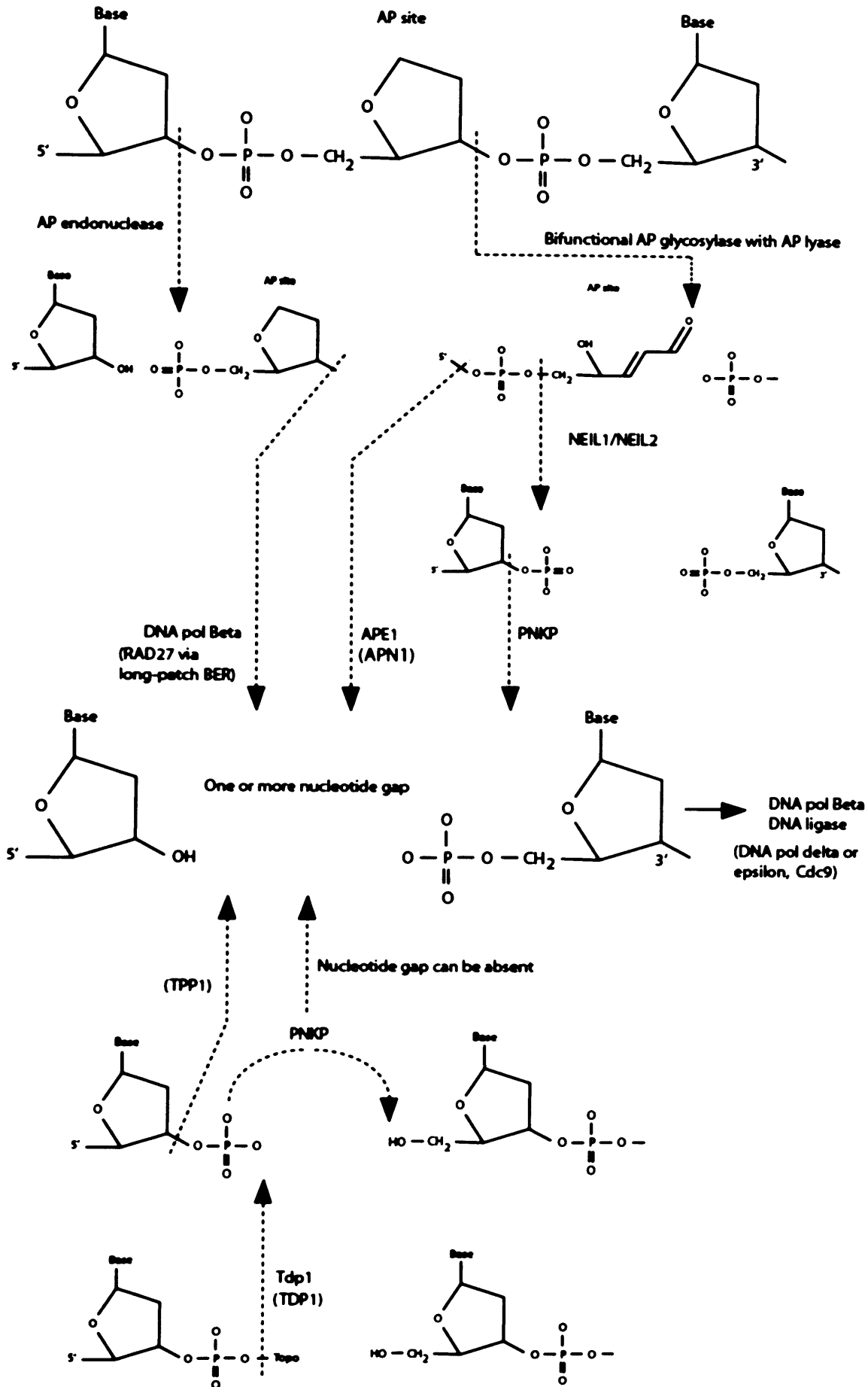


Figure 1.3. Molecular mechanisms of BER. Dashed lines pass through covalent bonds broken by the named enzyme next to the line. *S. cerevisiae* homologues are shown in brackets.

environmental agents (Almeida and Sobol, 2007; de Murcia and Ménissier de Murcia, 1994). The enzyme catalyses the polymerisation of a covalently attached poly(ADP-ribose) (PAR) moiety to various protein targets including itself, in response to DNA damage. PARP1 dependent PAR polymerisation is readily detected at single strand breaks; the role of this activity is not fully understood but there is good evidence that the mechanism includes the ability to recruit XRCC1 to the damage site (El-Khamisy et al., 2003; Okano et al., 2003). Whilst PARP-1 could conceivably play a similar role for the repair of single strand breaks from BER reaction intermediates this has not yet been demonstrated.

1.3 Nucleotide excision repair

Nucleotide excision repair (NER) is a powerful repair mechanism within the cell and the principle repair pathway for the restoration of DNA following UV damage. The pathway is also observed to repair a wide range of helix distorting lesions, including those induced by aromatic hydrocarbons or electrophilic molecules such as cisplatin, as well as intrastrand cross-links (Gillet and Scharer, 2006). The basic mechanism of NER entails five stages; DNA damage detection, separation of the dsDNA surrounding the lesion, incision of ssDNA both 5' and 3' to the lesion, extrusion of the damage containing oligonucleotide and finally DNA resynthesis (Fig. 1.4). The pathway is split into two subpathways which differ only in their mechanism of damage detection. Transcription coupled NER (TCR) is initiated through damage mediated inhibition of RNA polymerase II (RNAPII) transcription (Hanawalt and Spivak, 2008). TCR is confined to only the transcribed strand (TS) of active genes, and is classically observed to promote rapid repair in these regions in comparison to the remaining genome. The second subpathway, termed global genome NER (GGR), restores DNA damage throughout the entire genome and repairs both active and inactive genes as well as intergenic regions. Damage detection in this pathway principally requires the mammalian protein XPC. Interestingly, the *S. cerevisiae* orthologue of XPC, Rad4, is required for damage detection in GGR, but in contrast to XPC, also has an essential role in TCR (Prakash and Prakash, 2000). With minor exceptions, the molecular mechanism of mammalian NER and *S. cerevisiae* NER are highly homologous. As exemplified in table 1.2, nearly all NER factors implicated in the pathway from damage detection through to damage incision have equivalent orthologues between human and *S. cerevisiae*. The following account of this repair

pathway will first consider the entire TCR reaction from all eukaryotic model organisms. This is followed by a detailed discussion of the various factors necessary for GGR in humans and the yeast *S. cerevisiae*.

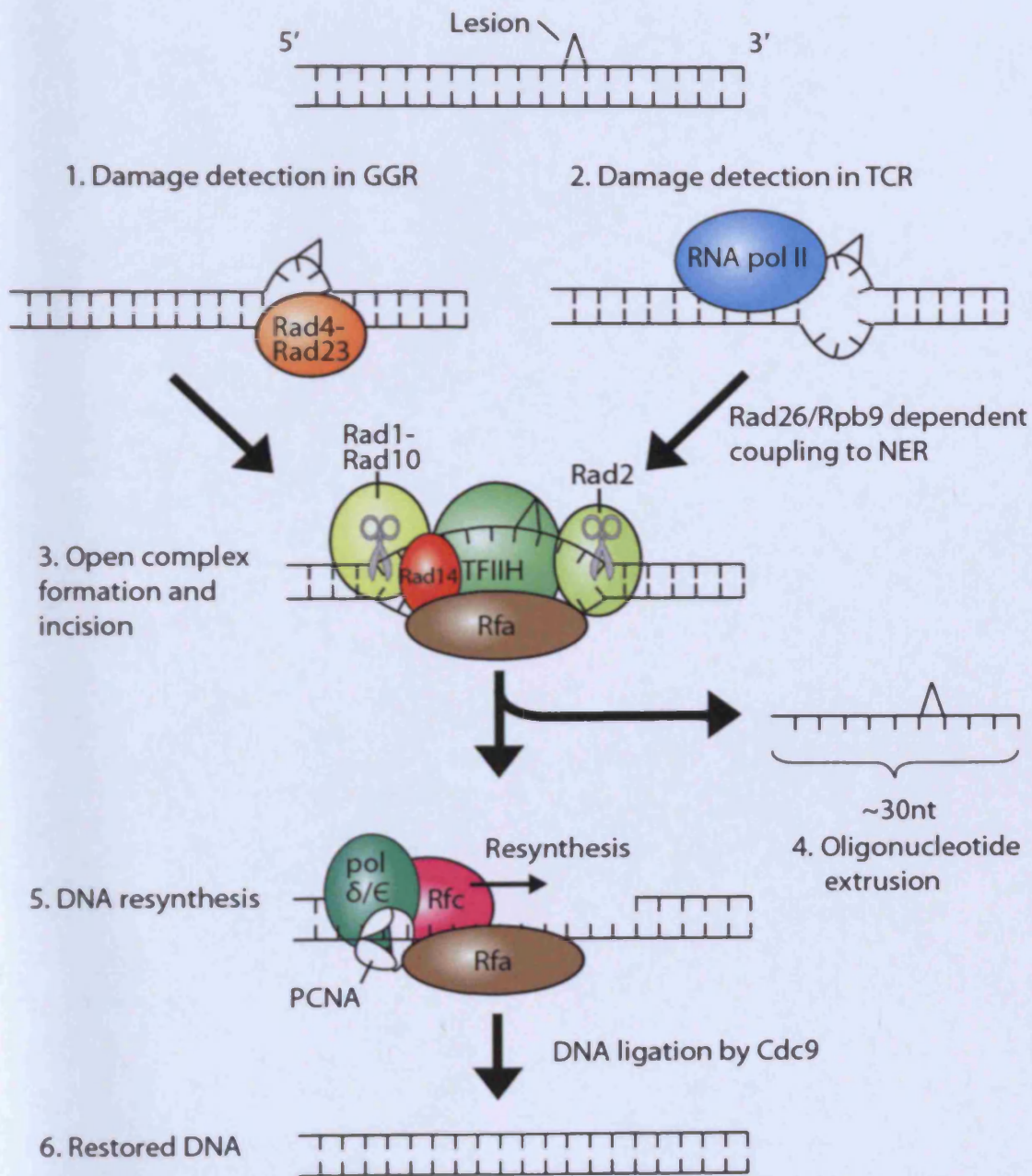


Figure 1.4. Cartoon representing the molecular mechanism of *S. cerevisiae* NER.

<u>Main activity</u>	<u><i>S. cerevisiae</i></u>	<u><i>H. sapiens</i></u>	<u>Description/Activity</u>
Damage detection in GGR	RAD4 RAD23 RAD33	XPC HR23B CEN2	DNA damage recognition Downstream recruitment of NER factors
	? ?	DDB1 DDB2	DNA damage recognition; chromatin remodelling?
Pre-incision complex	RAD3	XPD	5' → 3' DNA helicase
	RAD25	XPB	3' → 5' DNA helicase
	SSL1	GTF2H2	Core TFIIH subunit p44
	TFB1	GTF2H1	Core TFIIH subunit p62
	TFB2	GTF2H4	Core TFIIH subunit p52
	TFB4	GTF2H3	Core TFIIH subunit p34
	TFB5	TTDA	Stabilise TFIIH
	TFB3	MAT1	Member of kinase complex CAK/TFIIK
	KIN28	CDK7	Member of kinase complex CAK/TFIIK
	CCL1	Cyclin H	Member of kinase complex CAK/TFIIK
	RAD14	XPA	Structural role? Damage verification?
	RFA1-3	RPA1-3	ssDNA binding protein
Dual Incision	RAD1 RAD10	XPF ERCC1	Endonuclease for incision of ssDNA 5' to damage
	RAD2	XPG	Endonuclease for incision of ssDNA 3' to damage
GGR specific	ABF1	?	Site specific DNA binding protein
	RAD7	?	SOCS box E3 ligase component
	RAD16	?	SnF2 family ATPase, RING finger
TCR specific	RAD28	CSA	WD40 repeat E3 ligase component
	RAD26	CSB	SnF2 family ATPase

Table 1.2. List of core NER genes for both *S.cerevisiae* and *H.sapiens*. Homologues are presented in the same rows.

1.3.1 Transcription coupled repair

RNAPII is proposed to function as the initiator of the TCR pathway by arresting at a lesion during transcription elongation. This proposition is based upon a plethora of experimental observations. Firstly, lesions within DNA that function to inhibit transcription elongation by RNAPII are repaired by TCR. Such lesions include cisplatin or a CPD (Laine and Egly, 2006; Sarker et al., 2005; Selby et al., 1997a; Tornaletti, 2009; Tornaletti and Hanawalt, 1999; Tremeau-Bravard et al., 2004). Conversely, an *N*-2-aminofluorene adduct, which fails to inhibit RNAPII elongation, is not preferentially repaired within the TS of a gene; the operational definition of functional TCR (Donahue et al., 1996; Tang et al., 1989). Secondly, functional TCR requires ongoing transcription. Inhibiting RNAPII function either through chemical inhibition or through the use of temperature sensitive RNAPII mutants prohibits preferential repair of the TS of a gene (Christians and Hanawalt, 1992; Sweder and

Hanawalt, 1992). Thirdly, using high resolution technologies, it has been observed that preferential repair of the TS begins adjacent to a transcription start site (TSS), and that the kinetics of repair are uniform along the TS (Teng et al., 1997; Tijsterman et al., 1999; Tijsterman et al., 1997). The latter observation is important since chromatin structure is known to strongly influence GGR repair kinetics (Li and Smerdon, 2004; Tijsterman et al., 1999; Waters et al., 2009). Damage recognition is commonly considered the rate limiting step in NER (Chaudhuri et al., 2009; Lommel et al., 2000b). Thus, RNAPII, as a processive tracker along DNA, conceivably cannot preferentially distinguish lesions according to their position in chromatin. This provides a tantalising model to explain the absence of chromatin influence upon repair kinetics in TCR. Lastly, the incision reaction of TCR can be reconstituted *in vitro* at a lesion arrested RNAPII with recombinant NER proteins excluding the addition of XPC (Laine and Egly, 2006). In GGR, XPC is considered a fundamental damage recognition factor and is absolutely required for reconstitution of the reaction *in vitro* (Mu et al., 1996b; Rademakers et al., 2003; Volker et al., 2001).

The current model for TCR states that following arrest of RNAPII at a lesion, downstream NER factors are recruited (Laine and Egly, 2006). The exact order in which this occurs, and the molecular mechanisms necessary for this process are still an area of intense research. Of the factors common to both TCR and GGR, TFIIH and XPA are predicted to preclude the arrival of further downstream repair proteins (Laine and Egly, 2006). In contrast, other studies have indicated XPG is independently able to recognise and bind RNAPII arrested at a lesion; indeed the two proteins interact *in vivo* (Sarker et al., 2005). However, the strongest candidate necessary for the molecular mechanism of TCR following RNAPII is the mammalian protein CSB. An interaction between CSB and RNAPII has been confirmed *in vivo*, and is stimulated upon UV damage (Fousteri et al., 2006a; van Gool et al., 1997). *In vitro*, this factor has been demonstrated to facilitate binding of TFIIH, CSA and XPG to RNAPII (Sarker et al., 2005; Tantin, 1998). More recently, it has been demonstrated *in vivo*, that CSB is essential for the recruitment of a wide array of NER factors to RNAPII in response to UV damage, including TFIIH, XPG, XPA, ERCC1 and CSA (Fousteri et al., 2006a). Lastly, in further support of the role of CSB to recruit TFIIH, in yeast, an absolute requirement for the CSB homologue Rad26 in TCR, is alleviated in regions of a gene promoter where TFIIH remains associated with RNAPII (Tijsterman et al., 1997).

Historically, the potential role of CSB in TCR was originally implicated by its structural similarities to an important TCR repair protein in *Escherichia coli* (*E. coli*) termed Mfd. In *E. coli*, RNA polymerase (RNAP) stalls at a DNA lesion and restricts damage binding by the recognition factors UvrA and UvrB. Upon binding RNAP, Mfd translocates along DNA and is thought to push RNAP toward a lesion, causing it to dissociate from the damaged DNA; Mfd then functions to recruit UvrA through a direct protein interaction (Deaconescu et al., 2007). Mfd is a member of the family 2 ATPases/helicases, containing the seven signature domains necessary for ATPase activity that drives the Mfd translocase. CSB is also a member of this family, and thus has been suggested to similarly function to recruit NER factors by displacing RNAPII (Svejstrup, 2003; Troelstra et al., 1992). Indeed CSB/Rad26 is known to be a DNA dependent ATPase without detectable helicase activity, akin to Mfd (Citterio et al., 1998; Guzder et al., 1996a; Selby and Sancar, 1997). However, in contrast to Mfd, CSB cannot displace RNAPII stalled at a lesion in vitro (Selby and Sancar, 1997). Interestingly, in a second contrast to the TCR pathway in *E. coli*, both DNA incision and oligonucleotide extrusion have been observed in vitro without the dissociation of RNAPII, despite the fact that DNA footprinting suggests RNAPII occupies a 30-40 nucleotide territory around a CPD (Selby et al., 1997b; Tornaletti et al., 1999; Tremeau-Bravard et al., 2004). Therefore, despite sequence similarities, the biochemical activities of CSB and Mfd may well contrast.

How CSB is recruited to RNAPII, and how this functions to recruit downstream NER factors remains elusive. An intimate link between CSB and transcription has been previously reported suggesting that not only may the protein interact with RNAPII in the absence of damage, but that it may also have a role in transcription (Malik et al., 2010; van den Boom et al., 2004). Upon UV damage this interaction with RNAPII is stabilised and a net recruitment of CSB to chromatin is observed (Fousteri et al., 2006a; van den Boom et al., 2004). Chromatin recruitment, but not DNA binding, requires the ATPase activity of CSB, which has been shown to relieve an autorepressive N-terminal domain within the protein (Lake et al., 2010). How might CSB proceed to function in TCR? CSB has been demonstrated to induce negative supercoiling in dsDNA, have an ATPase dependent chromatin remodelling activity and the ability to catalyse both ssDNA annealing and strand exchange in vitro (Beerens et al., 2005; Citterio et al., 2000; Muftuoglu et al., 2006; Newman et al., 2006). Furthermore, CSB has also been indicated to physically interact with TFIIH,

XPA and CSA (Groisman et al., 2006; Henning et al., 1995; Selby and Sancar, 1997). How each of these properties play a role in recruiting downstream NER factors and/or contribute to as yet undefined molecular mechanisms remains to be seen.

Studies in *S. cerevisiae* that have explored the roles of Rad26 in TCR have revealed some contrasting features with CSB. In yeast there are two apparent subpathways of TCR; the first is dependent upon Rad26, whilst the second is dependent upon a non-essential subunit of RNAPII, Rpb9. Thus Rad26 is not essential for TCR in yeast (Li and Smerdon, 2002; Li and Smerdon, 2004). Rpb9 TCR strictly depends upon active transcription of a gene, whilst Rad26-mediated TCR is unaffected by temperature sensitive inhibition of transcription (Li et al., 2006a; Li et al., 2006c). In addition to this, *RAD26* dependent NER has also been observed within the non-transcribed strand (NTS) of a repressed gene (Li et al., 2006a; Li et al., 2007). These observations clearly make it difficult to implicate Rad26 in a role that functions to couple the transcription machinery with core NER factors. Indeed, the requirement for Rad26 and Rpb9 in TCR is abolished in a *spt4Δ* mutant (Jansen et al., 2000; Li et al., 2006c). How Spt4 functions to prohibit TCR is unknown, but the observation has important implications. It demonstrates coupling of the transcription machinery to the NER machinery can occur independently of both Rad26 and Rpb9, which may imply that RNAPII is in fact intrinsically competent to do this itself. In support of this model, in vitro a mammalian lesion stalled RNAPII can recruit most core NER factors in the absence of CSB (Laine et al., 2006; Tremeau-Bravard et al., 2004). Therefore, CSB may function to alleviate conditions refractory to the recruitment of NER factors (such as chromatin environment or RNAPII binding proteins), rather than coupling RNAPII with them as seen for Mfd. Finally, another study in *S. cerevisiae* has also implicated *RAD51* dependent homologous recombination to functionally couple transcription to NER in vivo (Aboussekhra and Al-Sharif, 2005).

Like CSB, CSA is also known to be exclusively required for TCR. In humans CSA is essential for TCR, whilst surprisingly, mutation of the yeast homologue *RAD28* does not seem to affect repair kinetics (Bhatia et al., 1996; Venema et al., 1990). As observed with CSB, CSA shows a UV dependent accumulation at lesion arrested RNAPII (Fousteri et al., 2006a; Groisman et al., 2003). CSA is a member of an E3 ubiquitin ligase complex, that includes Cul4A, Roc1 and all eight subunits of the COP9 signalosome (Groisman et al., 2003). E3 ubiquitin ligases target the covalent addition of an ubiquitin molecule to protein lysines, which often initiates

proteasomal degradation of the protein (Finley, 2009). Remarkably, the GGR specific factor DDB2 also resides in an identical complex in place of CSA. COP9 functions to negatively regulate the CSA E3 ubiquitin ligase. To date, the only known substrate of this ligase is CSB (Groisman et al., 2006). Studies by Groisman et al., have shown that following UV damage, CSA mediated ubiquitin ligation targets CSB for proteasomal degradation, depleting cellular CSB hours after UV irradiation. Remarkably, they show that this activity is necessary for the recovery of RNA synthesis following UV damage. Unlike CSA, deletion of Rad28 does not affect post-UV recovery of RNA synthesis (Reagan and Friedberg, 1997). CSA is not considered to reside in a stable complex with CSB, and the two are thus considered to only transiently interact in vivo (van Gool et al., 1997). Furthermore, CSA is only required for the recruitment of TFIIS, HMGN1 and XAB2 to RNPAII for TCR, and thus plays a functionally distinguishable role in TCR from CSB (Fousteri et al., 2006a).

One of the latest concepts to emerge in DNA repair is the importance of post-translational modifications to both core and accessory repair factors for the molecular mechanism of DNA repair. In particular, the covalent attachment of ubiquitin, through E3 ubiquitin ligases such as the CSA complex, and the structurally related SUMO polypeptides to repair proteins is highly prevalent (Bergink and Jentsch, 2009). In addition to CSB, the large subunit of RNAPII (PolII LS) is also known to be ubiquitylated in response to UV damage, resulting in proteasomal degradation of the protein (Ratner et al., 1998; Woudstra et al., 2002). Interestingly, this phenotype strictly depends upon the presence of both CSA and CSB, which founded the hypothesis that the modification was necessary for the mechanism of TCR. In support of this, DNA damage that is not repaired by TCR cannot induce this phenotype (Bregman et al., 1996). Arrest of an elongating RNAPII (by DNA damage or through chemical inhibition) appears to be the primary stimulus for PolII LS ubiquitylation, thus DNA damage per se is not a pre-requisite (Lee et al., 2002a; Somesh et al., 2005). In *S. cerevisiae* it was later shown that inhibition of PolII LS ubiquitylation did not affect TCR in vivo, and that the E3 ligase that targeted PolII LS was not Rad28 (Lommel et al., 2000a; Somesh et al., 2005). Whilst ubiquitylation and degradation of PolII LS are important for UV survival, mutations of this pathway are not epistatic with mutations in Rad26 (Somesh et al., 2007; Woudstra et al., 2002). These observations have led to the proposal that in the absence of successful TCR, an arrested RNAPII may be removed through degradation of PolII LS by the proteasome

as ‘a last resort’ mechanism (Somesh et al., 2005; Svejstrup, 2007). If the two pathways are independent, then how are CSA and CSB required for PolII LS ubiquitylation? In fact the E3 ubiquitin ligase that targets PolII LS is conserved from *S. cerevisiae* to humans and the repair proteins are not required for this activity. This was recently established in an elegant study that demonstrated mutations in CSA/CSB that function to delay recovery of RNAPII transcription after UV treatment, actually cause a reduction of the substrate of PolII LS ubiquitylation, a lesion arrested RNAPII (Anindya et al., 2007). Despite this evidence, and that RNAPII does not sterically inhibit TCR in vitro, the degradation of PolII LS and subsequent elimination of RNAPII for TCR is still a working model (Fousteri et al., 2006a; Malik et al., 2010; Tremereau-Bravard et al., 2004). Finally, in *S. cerevisiae*, transcription arrested RNAPII also induces SUMOylation of PolII LS, however the covalent modification does not seem to influence TCR or degradation but instead looks to mediate activation of downstream DNA damage response pathways (Chen et al., 2009).

Very recently, CSB was identified to possess an ubiquitin binding domain (UBD) at its C-terminus (Anindya et al., 2010). In the absence of this domain, CSB is unable to dynamically associate with TCR complexes resulting in sequestration of the protein at a lesion. Remarkably, the truncated protein can still function to recruit all the proteins necessary for DNA incision and oligonucleotide extrusion at a lesion, however neither activity can be detected (Laine and Egly, 2006). Thus an ubiquitylation event seems absolutely required for onset of TCR via a CSB directed regulation mechanism. Interestingly, the yeast homologue of CSA, Rad28, is not essential for Rad26 dependent TCR (Bhatia et al., 1996). Given that Rad26 does not contain the UBD identified in CSB, this ubiquitin mediated regulation mechanism appears exclusive to higher eukaryotic TCR and most probably occurs through the E3 ubiquitin ligase activity of CSA, which may explain the difference in necessity for CSA to Rad28 in TCR.

1.3.2 Formation of the preincision complex

Following DNA damage recognition a collection of factors associate with the lesion forming a multi-protein complex termed the preincision complex (PIC) (Mu et al., 1997; Wakasugi and Sancar, 1998). Sequential construction of the PIC leads to separation of the dsDNA around a lesion, followed by dual incision of ssDNA and subsequent extrusion of the damaged oligonucleotide. Oligonucleotide extrusion has

been recapitulated in vitro with purified proteins for both GGR and TCR (Lainé and Egly, 2006; Riedl et al., 2003). Whilst GGR requires the addition of XPC-HR23B for damage recognition and TCR requires RNAPII and CSB, all other additional factors required are identical and thus, following damage recognition, the two pathways converge.

1.3.3 TFIIH

The exact order of recruitment, if indeed an order exists, for the factors necessary to form the PIC has been a topic of debate for well over ten years (Gillet and Scharer, 2006; Reardon and Sancar, 2004). Following damage recognition, in vitro binding of the three factors TFIIH, XPA and RPA to a lesion are partially interdependent both for GGR and TCR (Lainé and Egly, 2006; Mu et al., 1997; Wakasugi and Sancar, 1998). However, more sensitive in vitro studies and in vivo evidence strongly suggest TFIIH is the first protein complex to join a damage site following detection (Riedl et al., 2003; Tapias et al., 2004; Volker et al., 2001; Zotter et al., 2006). TFIIH is a multi-subunit complex necessary for the transcription of RNA polymerase I and II genes (Thomas and Chiang, 2006). It consists of a core complex of XPD, XPB, p62, p44, p34, p52, and TTDA, and an associated three subunit complex termed the CDK activating kinase (CAK). Of special interest, are the XPD and XPB subunits (yeast homologues Rad3 and Rad25), which possess 5' → 3' and 3' → 5' helicase activity respectively (Drapkin et al., 1994; Guzder et al., 1994; Schaeffer et al., 1994; Schaeffer et al., 1993; Sung et al., 1993; Sung et al., 1987). For GGR, TFIIH is recruited through a direct protein-protein interaction with XPC (Araujo et al., 2001; Uchida et al., 2002; Yokoi et al., 2000). In vitro this recruitment seems to be ATP independent, whilst recent in vivo data suggests the ATPase activity of XPB is absolutely required for recruitment to damage sites in chromatin (Oksenych et al., 2009; Riedl et al., 2003).

Following recruitment, TFIIH has been previously suggested to verify the presence of a lesion. This bipartite damage recognition mechanism was originally proposed based upon the observation that lesions which fail to significantly alter DNA structure, are only efficiently repaired by NER if combined with a mismatch loop (Hess et al., 1997; Sugasawa et al., 2001). Given that a mismatch loop without a lesion is not a target for NER, these results indicate repair requires both DNA distortion and a lesion to initiate. Recently, an elegant study has extrapolated upon

these observations (Sugasawa et al., 2009). Here the authors demonstrated that a mismatch loop up to 160 nucleotides away from a CPD lesion remarkably enhanced the efficiency of its NER. Interestingly, the enhanced repair was only apparent when a loop was situated 5' to a lesion (see Fig. 1.5). Given that XPC preferentially binds a mismatched loop over a CPD, in an orientation specific manner, the results suggest that an NER complex would have to translocate in a 5' → 3' direction to locate the damage (Sugasawa et al., 2002). This activity is likely driven by the 5' → 3' helicase of XPD, and in support of this, addition of TFIIH and XPA to an electrophoretic mobility shift assay (EMSA) containing XPC, relocalises the XPC bound complex from the mismatch loop to the damage site. Interestingly, both the ATPase and helicase activity of Rad3, is attenuated by UV induced DNA lesions (Naegeli et al., 1992). However, attenuation strictly depends upon the presence of damage within the strand upon which Rad3 translocates. This strand is predicted to pass through a small pore of XPD, which conceivably could provide a mechanistic explanation for damage perception (Wolski et al., 2010). Complementary to the studies in yeast, archaeal XPD helicase activity has also recently been demonstrated to be attenuated by a CPD, resulting in a stable interaction between XPD and the damage site (Mathieu et al., 2010). Interestingly however, the CPD does not function to attenuate the ATPase activity of XPD. Collectively, these data strongly suggest that damage dependent inhibition of TFIIH translocation functions to verify the presence of a lesion and situate PIC formation (Fig 1.5).

Once localised to a damage site, TFIIH subsequently functions to separate the dsDNA surrounding a lesion (Evans et al., 1997a; Evans et al., 1997b). Strand separation by TFIIH requires ATP hydrolysis and is thus predicted to be a function of the two helicases XPB and XPD (Tapias et al., 2004). More recent in vivo evidence has suggested that whilst the helicase activity of XPD is essential for NER, an ATPase activity devoid of helicase function within XPB is sufficient to support the reaction (Coin et al., 2007). In light of the recent data indicating TFIIH translocation in NER, Sugawasa et al. have suggested the above result indicates that XPB may separate DNA using an ATPase activity alone, whilst XPD functions to translocate TFIIH along DNA and separate the strands (Sugasawa et al., 2009). Given this translocation is in a 5' → 3' direction, it may be predicted that inhibition of motility by a lesion would result in a bubble of separated DNA primarily situated 5' to the damage. Indeed, experiments that analyse either strand separation or cleavage of DNA relative

to a lesion, suggest the bubble of separated DNA is positioned toward the 5' of the damage (Evans et al., 1997b; Huang et al., 1992; Matsunaga et al., 1995; Moggs et al., 1996; Tapias et al., 2004).

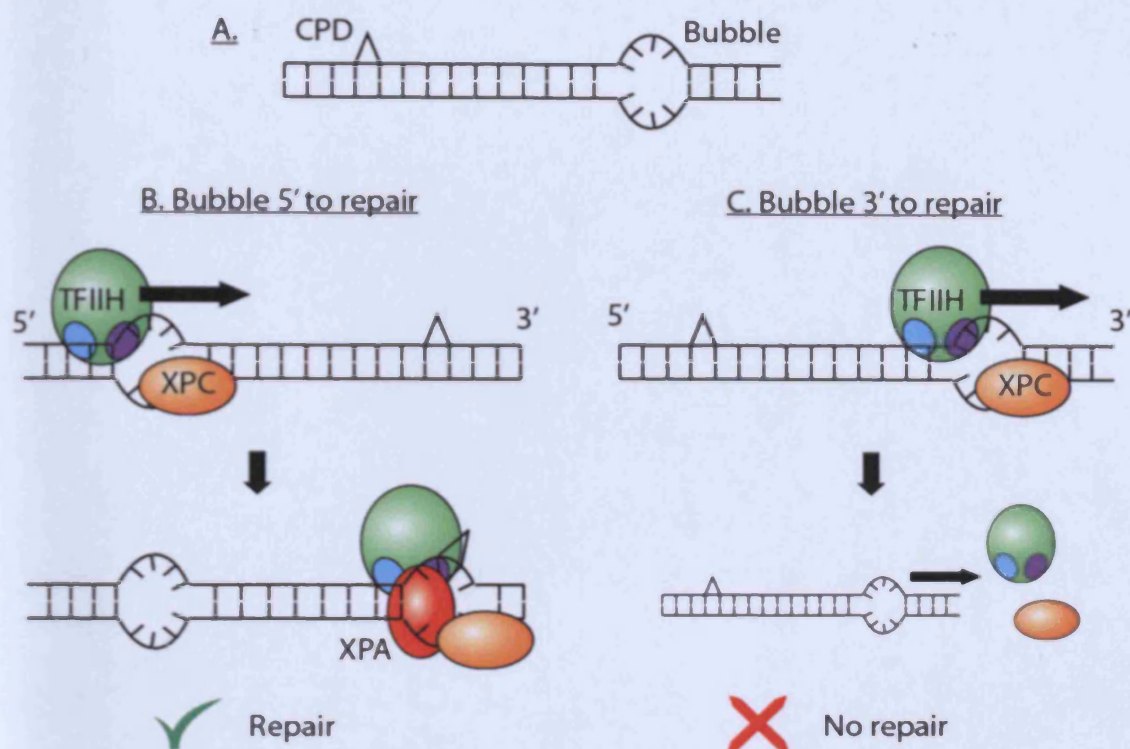


Figure 1.5. Bipartite damage recognition by XPC and TFIIH. A. Schematic of the substrate used in (Sugasawa et al., 2009). B. In scenario B XPC binds the mismatch bubble in preference to the CPD and recruits TFIIH 5' to the lesion. TFIIH translocation is attenuated by the CPD and repair is initiated. C. In scenario C the bubble lies 3' to the CPD and TFIIH recruitment and subsequent translocation is orientated away from the damage prohibiting functional repair.

More recent research has also focused upon how other constituents of TFIIH may function in NER. One example of this is the tenth member of the TFIIH complex to be discovered, TTDA. Mutations within this small protein are the molecular cause of the UV sensitive condition trichothiodystrophy (Giglia-Mari et al., 2004). Absence of TTDA from TFIIH prohibits functional NER and causes a reduction in cellular TFIIH levels (Giglia-Mari et al., 2004; Giglia-Mari et al., 2006). TTDA does not seem to have a role in XPC dependent damage recruitment for TFIIH, however, in its absence, strand separation and subsequent recruitment of NER factors is inhibited (Coin et al., 2006). A second example, from the same laboratory, has recently contradicted one of the paradigms of mammalian NER. The study demonstrated that the engagement of TFIIH in NER coincides with subsequent loss of the CAK complex, resulting in a form that cannot instigate transcriptional activation (Coin et

al., 2008). This suggests TFIIH is a dynamic complex in NER, in complete contrast with previous mammalian studies which suggested that CAK was statically engaged with TFIIH both during repair and transcription (Araujo et al., 2001; Mu et al., 1996a; Riedl et al., 2003). However, in support of these observations, *S. cerevisiae* NER has also been demonstrated to utilise TFIIH independent of the CAK complex (termed TFIIK in yeast) (Svejstrup et al., 1995).

1.3.4 RPA and XPA

Once the DNA strands are separated by TFIIH, recruitment of XPA, RPA and XPG functions to further separate the DNA around a lesion and this completes formation of the PIC (Tapias et al., 2004). The first stable NER multi-factor complex detectable upon a lesion in vitro consists of XPC-HR23B, TFIIH, RPA and XPA, with damage binding affinity increased upon introduction of XPG (Riedl et al., 2003; Wakasugi and Sancar, 1998). Binding of XPG is thought to be concurrent with the loss of XPC-HR23B from the PIC, whilst other studies have implicated XPA-RPA to stimulate the loss of XPC-HR23B (Mu et al., 1996a; Riedl et al., 2003; Wakasugi and Sancar, 1998; You et al., 2003). In vivo, there is no apparent interdependence between these three factors for damage binding, and thus a strict order of recruitment cannot be ascertained (Rademakers et al., 2003; Volker et al., 2001).

RPA is a heterotrimeric complex composed of subunits 70, 32 and 14kDa, commonly referred to as RPA1, RPA2 and RPA3 respectively (or Rfa1, Rfa2 and Rfa3, in yeast) (Friedberg, 2006). Recently, a homologue of RPA2, termed RPA4, has also been identified and heterotrimeric complexes with either RPA2 paralogue can support NER (Kemp et al., 2010). RPA has a high affinity for ssDNA and stable interaction of the complex with ssDNA occludes a region of ~30 nucleotides, however RPA may also bind shorter DNA fragments with a lower affinity (Kim et al., 1994; Kim et al., 1992; Matsunaga et al., 1996). Interestingly, the 30 nucleotide DNA binding mode of RPA corresponds well with the predicted size of DNA strand separation during NER (Evans et al., 1997a; Mu et al., 1997; Riedl et al., 2003). RPA is also known to have a high preference for binding pyrimidines and UV induced DNA lesions such as (6-4)PPs (Kim et al., 1992; Wakasugi and Sancar, 1999). DNA binding is conferred by oligonucleotide binding (OB) domains; RPA1 contains 4 OB domains, whilst RPA2 and RPA3 each have one, and all three subunits contribute to DNA binding (Bastin-Shanower and Brill, 2001; Bochkarev et al., 1997; Bochkareva

et al., 2002; Salas et al., 2009). DNA binding by RPA occurs with a strict polarity. When bound to ssDNA, RPA aligns such that RPA1 is located toward the 5' of the strand with RPA2 and RPA3 following distally toward the 3' of the strand (Bochkareva et al., 2002; Khlimankov et al., 2001; Kolpashchikov et al., 2001; Salas et al., 2009). High affinity DNA binding occurs at the 5' of ssDNA via the RPA1 OB domain DBDA, and this is required for all DNA binding, whilst the weaker DNA interactions that occur toward the 3' (by subsequent OB domains in RPA1 and 2) are required specifically for binding with longer nucleotide sequences (>12nt) (Bastin-Shanower and Brill, 2001; de Laat et al., 1998b).

During NER, binding of RPA to the separated DNA strands is thought to both stabilise the ssDNA intermediates whilst co-ordinating PIC formation through specific protein-protein interactions (de Laat et al., 1998b). Both RPA1 and RPA2 physically interact with XPA (He et al., 1995; Kemp et al., 2010; Li et al., 1995a; Stigger et al., 1998). In vitro, addition of RPA has been demonstrated to co-operatively enhance damage binding by XPA (He et al., 1995; Kemp et al., 2010; Wakasugi and Sancar, 1998; Wakasugi and Sancar, 1999). Thus, a stable interaction between XPA and RPA occurs at a damage site, and RPA protein domains necessary for both ssDNA binding and binding of XPA are essential for efficient NER (Stigger et al., 1998). Given the polarity of RPA ssDNA binding, and the strong interaction between RPA2 and XPA, it has been suggested that RPA may function to position XPA toward the 5' of a DNA lesion (Mer et al., 2000). RPA also has roles in positioning and regulating the activities of XPG and XPF-ERCC1. RPA physically interacts with and stimulates the DNA incision activity of both endonucleases (He et al., 1995; Matsunaga et al., 1996). Importantly, RPA only functions to recruit both endonucleases to their specific DNA junctions in one DNA binding orientation (de Laat et al., 1998b). Binding of RPA in the opposing direction prohibits binding of the endonucleases. These data strongly suggest RPA must bind the PIC with specific polarity to functionally recruit XPG and XPF-ERCC1. These conclusions also indicate that RPA must therefore bind the non-damaged ssDNA of the NER PIC.

XPA, and the yeast orthologue Rad14, both contain a zinc finger motif and preferentially bind UV damaged DNA (Guzder et al., 1993; Tanaka et al., 1990; Wakasugi and Sancar, 1998). XPA is known to bind UV lesions in a co-operative manner with RPA, and is predicted to function as a dimer (Wakasugi and Sancar, 1998; Wakasugi and Sancar, 1999; Yang et al., 2002b). Whilst this has implicated the

protein in damage detection, XPA is no longer considered to play this primordial role due to the absolute requirement of XPC for damage localisation of XPA *in vivo* (Volker et al., 2001). In addition, direct lesion recognition by XPA is not a prerequisite for repair excision (Missura et al., 2001). Indeed rather than detecting lesions *per se*, XPA has been demonstrated to have a high affinity for kinked DNA structures (Camenisch et al., 2006). This activity, in combination with the single stranded DNA binding affinity of RPA, has been suggested to provide XPA-RPA with a highly sensitive method for molecular verification of the early NER PIC (Missura et al., 2001). However, the exact molecular function of XPA for the core NER reaction is unknown. It is noteworthy that the protein interacts with a remarkable number of the core NER factors and is thus likely to play a scaffold-like function within the PIC (reviewed in Gillet and Scharer, 2006). It is also known to be necessary for the recruitment of XPF-ERCC1 (Orelli et al., 2009).

More recent research has further identified XPA as a potential pivotal intermediate between the core NER reaction and DNA damage responsive checkpoint proteins. Numerous studies have demonstrated NER functions both upstream of, and downstream to cellular responses to DNA damage mediated by checkpoint proteins (Auclair et al., 2008; Giannattasio et al., 2004; Yu et al., 2001). Rad14 physically interacts with Ddc1 and Mec3, two checkpoint proteins, and thus may play a role in damage recruitment of these factors necessary for activation of DNA damage responses (Giannattasio et al., 2004). Conversely, in mammals XPA is known to physically interact with the checkpoint protein ataxia-telangiectasia mutated and Rad3-related (ATR), and this interaction is required for UV dependent nuclear localisation of XPA (Shell et al., 2009; Wu et al., 2007). In addition, in response to UV, ATR functions to phosphorylate XPA and this modification improves CPD repair kinetics and post-UV cellular survival (Wu et al., 2006). Furthermore, XPA is acetylated and SIRT1 (Sir2 in yeast) mediated deacetylation, induced by UV damage, is necessary for proficient CPD repair (Fan and Luo, 2010). Together, these data suggest that post-translational modifications of XPA may function to modulate NER activity.

1.3.5 Dual Incision

Binding of XPG completes formation of the PIC and subsequent recruitment of XPF-ERCC1 results in dual incision and oligonucleotide extrusion (Constantinou

et al., 1999; Evans et al., 1997a; Evans et al., 1997b; Mu et al., 1997; Riedl et al., 2003). In vitro, addition of XPG is absolutely required for the recruitment of XPF-ERCC1 suggesting this factor is the last to join prior to DNA incision (Riedl et al., 2003). XPG and XPF-ERCC1 are structure specific endonucleases which function to incise the lesion containing oligonucleotide 3' and 5' to the damage respectively (O'Donovan et al., 1994; Sijbers et al., 1996a). The 5' incision is made 15-24 nucleotides from the lesion whilst the 3' incision occurs 2-8 nucleotides away, releasing an oligonucleotide of ~27 nucleotides (Huang et al., 1992; Matsunaga et al., 1995; Moggs et al., 1996). Interestingly in vitro studies of yeast GGR demonstrate extrusion of the oligonucleotide is an active process requiring superhelical torsion produced by a heterotrimeric complex termed the GGR complex (discussed below) (Yu et al., 2004). This observation is reminiscent of the role of UvrD for oligonucleotide extrusion in prokaryotes, although in contrast to UvrD, the GGR complex is not a DNA helicase (Orren et al., 1992; Yu et al., 2009). Whether mammalian NER requires active extrusion of the oligonucleotide remains to be determined.

XPG is a structure specific endonuclease and incises ds/ssDNA junctions, splayed arms and bubble structures within the 5' extending ssDNA (Evans et al., 1997a; Hohl et al., 2003; Matsunaga et al., 1995; O'Donovan et al., 1994). This incision occurs within one nucleotide of the ds/ss junction depending upon the structure of the substrate (Hohl et al., 2003). The yeast homologue of XPG, Rad2, has also been demonstrated to possess an identical structural specificity, and activity in NER (Habraken et al., 1995). XPG/Rad2 interacts with TFIIH and this interaction is important for the stable recruitment of XPG to damage in vivo, and functional repair (Araujo et al., 2001; Dunand-Sauthier et al., 2005; Habraken et al., 1996; Ito et al., 2007; Thorel et al., 2004). XPF-ERCC1 is an obligate heterodimer, which functions to incise DNA structures with an exact opposite polarity to that by XPG (Sijbers et al., 1996a). Incision occurs within 2-8 nucleotides of the ds/ss junction (de Laat et al., 1998a). The dimer interacts at the C-terminal of both proteins, and the interaction is essential for functional NER (de Laat et al., 1998c; Sijbers et al., 1996b). The yeast orthologue, Rad1-Rad10, functions in NER in an identical manner although the protein interaction domains between the two complexes are non-homologous (Bailly et al., 1992; Bardwell et al., 1993; Bardwell et al., 1994; de Laat et al., 1998c). XPF-ERCC1 and Rad1-Rad10 are recruited to the NER PIC by TFIIH and this interaction

is essential for functional NER (Guzder et al., 2006; Guzder et al., 1996b; Li et al., 1995b; Orelli et al., 2009; Tsodikov et al., 2007).

Whilst the order of recruitment for the two endonucleases is well defined in vitro, an outstanding controversy has remained over the order in which the two incise DNA during NER. In contrast to reconstituted NER in *S. cerevisiae*, under certain conditions both uncoupled 5' and 3' incisions have been observed in mammalian NER (Evans et al., 1997a; Guzder et al., 1995; Matsunaga et al., 1995). Whilst XPG can perform an incision in the absence of XPF-ERCC1, XPF-ERCC1 requires the presence but not the catalytic activity of XPG for incision (Constantinou et al., 1999; Mu et al., 1996a; Wakasugi et al., 1997). However, efficient XPG incision requires both the presence and catalytic activity of XPF-ERCC1 (Tapias et al., 2004). A recent report demonstrated in vivo that the incision by XPF-ERCC1 was sufficient to initiate downstream DNA synthesis, in the absence of the XPG incision (Staresincic et al., 2009). Given this observation, the authors concluded that the 5' incision of NER may occur prior to and be necessary for the 3' incision in vivo. This observation is difficult to reconcile with previous reports of uncoupled 3' incisions, however, to date such studies have only been performed upon naked DNA templates. Whether 3' uncoupled incisions may occur in vivo is as yet to be ascertained, and will be fundamentally important for understanding the regulation of dual incision.

1.3.6 DNA resynthesis

Following extrusion of the damaged oligonucleotide, resynthesis of the DNA molecule restores its native structure. In vitro, reconstitution of NER DNA resynthesis can be achieved through the addition of RPA, PCNA, RFC, DNA polymerase δ or ϵ (pol δ/ϵ) and DNA ligase I (Aboussekhra et al., 1995; Araujo et al., 2000; Mocquet et al., 2008; Shivji et al., 1995). This pathway with respect to NER is poorly characterised and thus the molecular mechanism is extrapolated from supposed parallels in DNA replication (Gillet and Scharer, 2006). RFC is a pentameric complex which functions to load the trimeric ring structure of PCNA proximal to 3' primer DNA. PCNA then interacts with a DNA polymerase and the complex functions to resynthesise DNA, thus replacing the lost oligonucleotide. DNA ligase subsequently restores the missing phosphodiester bond between the final nucleotide incorporated and the dsDNA molecule.

Evidence for an *in vivo* role for these DNA replication factors in NER is also apparent. Cell free extracts depleted of PCNA cannot perform DNA resynthesis of NER substrates (Shivji et al., 1992). Furthermore, PCNA co-localises to UV damage *in vivo* and complexes with RPA in a UV dependent manner (Essers et al., 2005; Green and Almouzni, 2003; Mocquet et al., 2008; Moser et al., 2007). In yeast, temperature sensitive mutants of pol δ / ϵ fail to progress beyond the incision step of NER (Budd and Campbell, 1995). As shown for PCNA, mammalian pol δ also colocalises with UV damage and complexes with RPA (Mocquet et al., 2008; Moser et al., 2007). *In vitro*, RFC is absolutely required for efficient catalytic activity of pol δ / ϵ implying an *in vivo* role for NER (Podust et al., 1992). Finally, temperature sensitive mutants of *S. cerevisiae* DNA ligase I (Cdc9) fail to ligate the DNA backbone following repair of NER substrates (Wu et al., 1999). Mammalian DNA ligase I also localises to UV damage in a cell-cycle regulated manner (Moser et al., 2007).

More recent research in mammalian NER has also implicated another DNA polymerase, pol κ , and ligase, XRCC1-DNA ligase III α (DNA ligase III), to be important for resynthesis (Moser et al., 2007; Ogi and Lehmann, 2006). Pol δ and pol κ apparently function within the same pathway, and depleting all three polymerases is sufficient to inhibit DNA resynthesis *in vivo* (Ogi et al., 2010). Recruitment of pol δ to the NER reaction is mediated by RFC, whilst pol ϵ requires the alternative clamp loader CTF18-RFC and pol κ requires XRCC1 and ubiquitylated PCNA. DNA ligase III localises to UV damage *in vivo*, and in contrast to DNA ligase I, at all stages of the cell cycle and is apparently the predominant ligase in mammalian NER. Interestingly, pol ϵ has an identical cell cycle dependence for UV damage localisation to DNA ligase I, whilst pol δ is independent of the cell cycle, suggesting the two polymerases may utilise the different ligases (Moser et al., 2007).

Another aspect of NER that is poorly understood is the transition between incision (extrusion) and DNA resynthesis. A recent *in vitro* study demonstrated that proficient DNA resynthesis of an oligonucleotide extruded substrate required both RPA and XPG (Mocquet et al., 2008). RPA is known to remain associated with DNA following oligonucleotide extrusion, perhaps without surprise given its fundamental role in the resynthesis stage (Riedl et al., 2003; Shivji et al., 1995). XPG is also known to physically interact with PCNA and thus may play a role in recruiting this factor, although the requirement of this interaction for NER is yet to be proven (Gary

et al., 1997). XPF is refractory to RFC and PCNA recruitment and thus is predicted to leave prior to their recruitment; this may support a model whereby XPF incision and DNA resynthesis occur prior to XPG incision (Mocquet et al., 2008; Staresincic et al., 2009). Mechanisms that co-ordinate this transition are particularly topical given the recent observation that attenuation of DNA resynthesis in NER promotes activation of DNA damage responsive checkpoint proteins (Giannattasio et al., 2010). Checkpoint activation depends upon the nuclease Exo1, which was demonstrated to promote long strands of ssDNA in an UV damage and Rad14 dependent manner. Thus it was proposed that in the absence of DNA resynthesis, Exo1 resects the ssDNA gap to produce longer gaps that promote checkpoint activation (Giannattasio et al., 2010).

1.4 Proteins necessary for GGR

1.4.1 XPC-HR23B-centrin2

In mammals mutations within XPC specifically inhibit GRR but do not affect TCR (Venema et al., 1991). In vivo, XPC is a constituent of a heterotrimeric complex of XPC-HR23B-centrin2, which is known to have a fundamental role in DNA damage detection (Nishi et al., 2005; Volker et al., 2001).

In vitro, XPC-HR23B binds dsDNA but has a greater affinity for UV or cisplatin damaged dsDNA or dsDNA containing a (6-4)PP, platinum crosslink or cholesterol moiety (Batty and Wood, 2000; Kusumoto et al., 2001; Sugasawa et al., 1998; Wakasugi and Sancar, 1999; You et al., 2003). DNA binding is mediated by the XPC protein (Yokoi et al., 2000). The ability of XPC to bind a broad variety of structurally unrelated DNA lesions suggests the protein must utilise a non-specific binding mode, which is thought to function by detecting perturbations in the canonical DNA structure caused by lesions (Sugasawa, 2009). In support of this, a non-lesion containing 5bp mismatch in dsDNA is readily bound by XPC-HR23B, however it is not excised by the NER machinery (Sugasawa et al., 2001). Furthermore, the CPD lesion, which is known to cause minimal alterations to the DNA helical structure is poorly bound by XPC-HR23B and poorly repaired when compared with (6-4)PPs (Batty et al., 2000; Kusumoto et al., 2001; Sugasawa et al., 2009). However, if the CPD is incorporated into a mismatch, the binding affinity of XPC-HR23B is higher and the efficiency of repair is dramatically increased (Mu and Sancar, 1997; Sugasawa et al., 2001). XPC binds ss/dsDNA junctions with high affinity and thus separation of the dsDNA by a lesion is considered the primary determinant for

damage binding (Buterin et al., 2005; Sugasawa et al., 2002). Indeed, a recent study of DNA adduct structure demonstrated a good correlation between lesion derived dsDNA separation, XPC binding affinity and NER efficiency (Mocquet et al., 2007). Further studies have shown XPC also has a very high affinity for ssDNA, which is attenuated by UV damage, implying the protein may in fact primarily bind the non-damaged strand at a lesion (Maillard et al., 2007). This conclusion is heavily supported by two other recent studies demonstrating that eliminating perturbations in the non-damaged DNA strand suppressed NER damage excision (Buterin et al., 2005; Sugasawa et al., 2009). Remarkably, a very recent study has functionally uncoupled the ability of XPC to bind dsDNA mismatch loops and ssDNA (Camenisch et al., 2009). The two activities lie within different regions of the XPC DNA binding domain (DBD), and suggest XPC binds lesions with a bipartite recognition mechanism. XPC binds dsDNA mismatches asymmetrically aligning toward the 5' of such structures (Sugasawa et al., 2002). Damage binding is concurrent with further separation of the dsDNA at a lesion (Evans et al., 1997b; Tapias et al., 2004).

XPC is known to be post-translationally modified by both ubiquitin and SUMO1 in a UV dependent manner (Sugasawa et al., 2005; Wang et al., 2005). Both modifications require DDB2 (discussed below). SUMOylation appears to be important for the stabilisation of XPC following UV (Wang et al., 2005). The stability of XPC is reduced after UV, and whilst this requires the activity of the proteasome, surprisingly it does not require ubiquitylation of the protein (Wang et al., 2007). Indeed, XPC ubiquitylation is readily reversible within the cell (Sugasawa et al., 2005). Mutation of lysine 655 inhibits post-translational modifications of XPC, recruitment of XPG to UV damage (although XPA and XPB are unaffected) and abolishes GGR (Wang et al., 2007).

The role/s for HR23B in GGR are less clear. In mammalian cells, HR23B is known to express a paralogue called HR23A. Whilst the two proteins seem to play a functionally redundant role in NER, the majority of XPC complexes with HR23B (Araki et al., 2001; Ng et al., 2003). In vitro, addition of HR23B stimulates NER activity, and both the HR23B N-terminal ubiquitin like domain and XPC interaction domain are required for this activity (Masutani et al., 1997; Sugasawa et al., 1996). Currently, the only role attributed to HR23B in NER is its ability to stabilise XPC levels, and over-expression of XPC functions to partially relieve the UV sensitivity of

mHR23A^{-/-}, mHR23B^{-/-} cell lines (Ng et al., 2003). The protein has also been suggested to contribute to turnover of XPC-HR23B at the PIC (You et al., 2003).

More recently XPC-HR23B was found to be in complex with centrin2; centrin2 binds XPC (Araki et al., 2001). Centrin2 is a calcium binding protein, whose affinity for an XPC peptide is strongly promoted by calcium presence (Popescu et al., 2003). Binding of XPC by centrin2 is necessary for efficient repair in vivo and is demonstrated to increase damage binding by XPC in vitro (Nishi et al., 2005).

1.4.2 Rad4-Rad23-Rad33

S. cerevisiae contains homologues of XPC, termed Rad4, and HR23B, termed Rad23 which form a stable heterodimeric complex (Guzder et al., 1998a; Wang et al., 1997). In addition, a likely homologue of centrin2 also exists, termed Rad33, which physically interacts with Rad4 (den Dulk et al., 2008). In contrast to mammalian NER, Rad4 is absolutely required for both GGR and TCR, however the role of Rad4 in TCR is unknown (Teng et al., 2010). Similarly, mutations in *RAD23* and *RAD33* also prohibit efficient GGR and TCR (den Dulk et al., 2006; He et al., 1996; Mueller and Smerdon, 1996).

Rad4-Rad23 shows high affinity binding for lesions including (6-4)PPs and N-acetyl-2-aminofluorene adducts, but poorly recognises CPDs (Guzder et al., 1998a; Jansen et al., 1998; Xie et al., 2004). The structure of Rad4-Rad23 binding a CPD within a 3bp mismatch was recently solved (Min and Pavletich, 2007). In agreement with damage binding models of XPC, Rad4 primarily binds DNA at a lesion through interactions with the non-damaged strand. Rad4 binding is concurrent with dinucleotide flipping at both the lesion and at the opposing complementary nucleotides, and a β -hairpin of Rad4 inserts between the double stranded DNA at this position. This structure predicts that lesions which function to locally destabilise the structure of dsDNA will facilitate both nucleotide flipping and β -hairpin insertion, and thus be readily bound by Rad4; again in agreement with observations described for XPC above.

In contrast to mammalian cells, the role yeast Rad23 plays within the cell has been extensively characterised. Like its mammalian homologue, Rad23 consists of an N-terminal ubiquitin-like domain (UbL domain), a Rad4 binding domain and two ubiquitin associated domains (UBA domains), which lie either side of the Rad4 binding domain (Dantuma et al., 2009). Rad23 is known to interact with the

proteasome and is thought to function to target this to the various cellular pathways to which it contributes.

The ubiquitin-proteasome pathway (UPP) is responsible for the targeted degradation of proteins. The proteasome is a large multisubunit complex consisting of two principle particles termed the 19S regulatory particle and the 20S core particle (Finley, 2009). The 20S forms a large barrel-like structure; at either end there is an opening to which a 19S complex may interact. The 19S is further divided into two structures termed the base, which interacts with the 20S, and a peripheral lid. Proteins are targeted for degradation through covalent attachment of at least four ubiquitin molecules (Thrower et al., 2000). The 19S functions to recruit, unfold and translocate such targeted proteins into the 20S core where they are subsequently cleaved into small peptides.

The UbL domain of Rad23 is known to bind the Rpn1 subunit of the 19S base subcomplex (Elsasser et al., 2002; Saeki et al., 2002). This functions to recruit Rad23 to the proteasome but does not result in its rapid degradation (Schauber et al., 1998; Watkins et al., 1993). Indeed the UBA2 domain of Rad23 has been demonstrated to protect the protein from proteolytic degradation (Heessen et al., 2005). Both UBA domains have been demonstrated to bind mono-, di- and tetraubiquitin species (Bertolaet et al., 2001; Chen et al., 2001; Raasi et al., 2005; Rao and Sastry, 2002; Verma et al., 2004). However, the predominant physiological target of the UBA domains appears to be ubiquitylated proteins rather than free ubiquitin chains (Chen and Madura, 2002). The simultaneous binding of UBA domains to ubiquitylated substrates and the UbL domain to the proteasome has founded the hypothesis that Rad23 is important for the recruitment of ubiquitylated proteins to the proteasome (Elsasser et al., 2004; Verma et al., 2004). In support of this model, various proteolytic substrates have been demonstrated to be stabilised in *rad23Δ* mutants, concurrent with increased cellular levels of polyubiquitylated proteins (Lambertson et al., 1999; Rao and Sastry, 2002; Verma et al., 2004). Furthermore, Rad23 also binds the E4 ubiquitin chain elongation factor Ufd2 via its UbL domain suggesting it may couple ubiquitylation to subsequent degradation (Kim et al., 2004). However, the Rad23 UBA domains have also been shown to suppress polyubiquitin chain polymerisation in vitro (Chen et al., 2001; Ortolan et al., 2000). Similarly, the UBA domains of the *Schizosaccharomyces pombe* orthologue of Rad23, Rhp3, have also been shown to suppress de-ubiquitylation of polyubiquitylated substrates (Hartmann-

Petersen et al., 2003). These observations suggest Rad23 could also stabilise protein substrates by regulating polyubiquitylation, and overexpressing Rad23 has been shown to increase the half life of some UPP targets (Chen and Madura, 2002; Ortolan et al., 2000). Interestingly, the effect Rad23 has on protein stabilisation in vitro is dose dependent; Rad23 promotes protein degradation unless a large molar excess is added whereby it inhibits the same activity (Verma et al., 2004). Thus although Rad23 can inhibit substrate polyubiquitylation, at physiological concentrations the protein is currently regarded to primarily promote UPP dependent degradation.

S. cerevisiae rad23Δ mutants are known to have an intermediate repair capacity and UV survival compared to mutants of essential NER genes such as Rad4 or Rad14, suggesting it may have a regulatory role in the reaction (He et al., 1996; Mueller and Smerdon, 1996; Prakash and Prakash, 2000). As with mammals, Rad23 has been suggested to be important for the stability of Rad4 in vivo, although this has been disputed (Gillette et al., 2006; Lommel et al., 2002; Ortolan et al., 2004). Expression of the Rad4 binding domain of Rad23 alone, which functions to stabilise Rad4, or overexpressing Rad4 in the absence of Rad23, is not sufficient to restore wild type UV survival demonstrating Rad23 plays a role beyond stabilising Rad4 in NER (Ortolan et al., 2004; Xie et al., 2004). Deletion of the UbL domain of Rad23 renders cells with an intermediate UV sensitivity between wild type and *rad23Δ* mutants; interestingly replacing the UbL domain with ubiquitin suppresses the UV sensitivity (Watkins 1993). Given an alternative proteasome interaction module can suppress the UV sensitivity of *Ubl1 Rad23* it is likely the primary role of this domain is to accommodate an interaction with the proteasome (Dantuma et al., 2009). Whilst Rad4, Rad23 and the proteasome have been co-purified suggesting a role for the UPP pathway in NER, only mutations in the 19S specifically affect NER, suggesting a role independent of proteolysis is important in the molecular mechanism (Russell et al., 1999; Schaubert et al., 1998). The 19S has been demonstrated to negatively regulate the rate of lesion removal in vivo; however this activity is modulated through an interaction with the UbL domain of Rad23 which functions to suppress this (Gillette et al., 2001). Currently, the molecular mechanism behind these observations is unknown, however it has been shown that the pathway functions independent of de novo protein synthesis (Gillette et al., 2006).

Finally, whilst some previous reports have not seen UV sensitivity in *RAD23* with UBA domain mutations, it has been reported that UV sensitivity is observed

when doses of UV are repeatedly applied (Bertolaet et al., 2001; Heessen et al., 2005; Ortolan et al., 2004). The authors suggested that the already low levels of Rad23 with a mutation in the UBA2 domain are depleted following a single UV dose rendering the cells sensitive to a subsequent UV dose.

1.4.3 UV-DDB complex

A second complex implicated in damage recognition in mammalian cells is termed the UV damaged DNA binding complex (UV-DDB) (Sugasawa, 2009). The complex consisting of the two subunits termed DDB1 (p127) and DDB2 (p48) is able to bind a variety of DNA lesions including (6-4)PPs, CPD and AP sites (Wittschieben et al., 2005). Mutations of DDB2 are the molecular defect in XPE patients, cell lines of which are known to have defects exclusively in GGR (Hwang et al., 1999; Tang and Chu, 2002). XPE lines are known to have highly deficient CPD repair but only mild defects in (6-4)PP repair. In vivo, the UV-DDB complex has been demonstrated to bind both (6-4)PPs and CPDs, and damage recognition occurs independent of XPC-HR23B-Centrin2 (Luijsterburg et al., 2007; Moser et al., 2005). Interestingly, despite the molecular defect of XPE, cell-free extracts do not require the UV-DDB complex for efficient NER, however addition of the complex has been shown to have a stimulatory role for the repair of CPD (Wakasugi et al., 2002). Such assays employ naked DNA for repair, implying that UV-DDB may have a predominant role in the repair of chromatin (Rapic-Otrin et al., 2002).

The above data strongly indicate a role for UV-DDB in damage recognition and specifically a role in promoting CPD repair in vivo. Recently, the X-ray crystal structure of UV-DDB was resolved bound to DNA containing a (6-4)PP or abasic analog lesion, tetrahydrofuran (Scrima et al., 2008). The study demonstrated DNA damage recognition occurs exclusively through DDB2. Binding of DDB2 results in flipping of a dinucleotide at the lesion and insertion of a three residue hairpin into this region, thus separating the DNA strands. The protein-DNA complex also results in extensive kinking of the DNA at the lesion. Both UV-DDB and XPC-HR23B bind DNA damage, but only XPC is essential for GGR (Hwang et al., 1999). Therefore, UV-DDB is proposed to function to bind DNA damage and promote XPC recruitment thereby enhancing GGR, especially so at lesions that are poorly recognised by XPC such as the CPD (Scrima et al., 2008). Indeed, there are many examples demonstrating enhanced damage binding of XPC as a consequence of UV-DDB

(Fitch et al., 2003; Moser et al., 2005; Yasuda et al., 2007). Furthermore, XPC and UV-DDB have been shown to physically interact (Sugasawa et al., 2005). Comparison of the structure of UV-DDB and the XPC homolog Rad4 suggests that the two damage binding complexes could not bind a lesion simultaneously, however given that XPC DNA binding is bipartite utilising two domains (that bind both DNA strands around a lesion) a ternary complex of DDB2-DNA-XPC may transition the exchange (Scrima et al., 2008).

In vivo the UV-DDB complex is part of an E3 ubiquitin ligase, including Cul4A (or Cul4B), Roc1, and all members of the COP9 signalosome (Groisman et al., 2003; Guerrero-Santoro et al., 2008). The COP9 signalosome functions to negatively regulate the E3 ubiquitin ligase and dissociates from this in response to UV damage. Both UV-DDB and associated E3 ubiquitin ligase subunits are recruited to damage sites as a complex (Luijsterburg et al., 2007). Following UV, the UV-DDB complex has been demonstrated to ubiquitylate a variety of targets including DDB2, XPC and histones H2A, H3 and H4 (El-Mahdy et al., 2006; Kapetanaki et al., 2006; Sugasawa et al., 2005; Wang et al., 2006). DDB2 is degraded in an UV-dose dependent manner, and it was suggested that ubiquitylated DDB2 is degraded to allow access of XPC to a lesion (Kapetanaki et al., 2006; Sugasawa et al., 2005). However, recent evidence has demonstrated that the damage binding of UV-DDB is far more rapid than the half life of DDB2 in response to UV, and that UV dependent degradation occurs independent of XPC (Alekseev et al., 2008; Luijsterburg et al., 2007). Instead, UV-DDB ubiquitylation has been hypothesised to recruit XPC through an ubiquitin dependent interaction with HR23B, or degrade DDB2 to release DDB1 for subsequent damage responsive ubiquitylation activities (Alekseev et al., 2008; Kapetanaki et al., 2006). In contrast to DDB2, low-level degradation of XPC occurs in an UV-dose independent manner and a large fraction of the protein is known to be reversibly polyubiquitylated in response to damage (El-Mahdy et al., 2006; Sugasawa et al., 2005). The mechanistic significance of XPC ubiquitylation is unknown, however the post-translationally modified protein is observed to have a higher DNA binding affinity. The functional significance of histone ubiquitylation is also unknown; it has been suggested to help recruit XPC through HR23B or by changing nucleosome structure and therefore increasing DNA accessibility (Kapetanaki et al., 2006; Wang et al., 2006).

1.4.4 The GGR complex

In *S. cerevisiae* no direct homologues of UV-DDB are known, however it is emerging that functional homologues may instead exist. The genetics and biochemical properties of UV-DDB share considerable similarities with a heterotrimeric complex of Rad7, Rad16 and Abf1 (discussed below), termed the GGR complex (Reed and Gillette, 2007; Yu et al., 2004). In contrast to UV-DDB, the genes *RAD7* and *RAD16* are essential for the majority of GGR for both (6-4)PPs and CPDs (Teng et al., 1997; Terleth et al., 1990; Tijsterman et al., 1999; Verhage et al., 1994; Wang et al., 1997). Interestingly, two recent reports have indicated the potential of Rad16 independent GGR specifically within the NTS of repressed genes (Li et al., 2006a; Li et al., 2007). This repair activity is strictly dependent upon Rad26 and is attenuated by transcriptional activation of the gene.

In vitro, the dimeric complex of Rad7 and Rad16 has been demonstrated to possess high affinity binding for UV-damaged DNA (Guzder et al., 1997). Damage binding requires ATP and is independent of Rad7 alone, thus it is likely to depend upon the two zinc dependent DBDs of Rad16 (Bang et al., 1992; Guzder et al., 1998b, 1999). Rad16 is a member of the Snf2 family of ATPases, many members of which are known to remodel chromatin (Durr et al., 2006; Flaus et al., 2006). This suggests that Rad16 is also important for chromatin remodelling (further discussed in Chapter 4.1). Through the activity of Rad16, the GGR complex functions as a DNA translocase (Yu et al., 2009). In vitro, Rad16 ATP hydrolysis is stimulated in the presence of DNA, however, addition of UV-damaged DNA attenuates this activity (Guzder et al., 1998b). This observation has led to the hypothesis that the GGR complex functions to translocate along DNA until encountering a lesion, to which the complex binds, attenuating DNA translocation and ATP hydrolysis.

The GGR complex has been implicated to be important for UV responsive NER dependent and NER independent events (Guzder et al., 1997; Reed et al., 1998; Yu et al., 2005). In vitro, addition of both Rad7-Rad16 and Rad4-Rad23 to UV-damaged DNA results in synergistic binding of both complexes to a lesion (Guzder et al., 1999). Rad7 and Rad4 are known to interact, and deletions in Rad7 that disrupt this interaction render the cell with a UV sensitivity equivalent to *rad7Δ* (Wang et al., 1997). This result implies all activities that the GGR complex contributes to the survival of the cell following UV damage require an interaction with Rad4. Interestingly, like UV-DDB, the GGR complex has been implicated in damage

responsive activities independent of Rad4 (see below). In contrast to UV-DDB however, a potential role for the GGR complex in promoting the recruitment of Rad4-Rad23 (or the reverse) to a lesion is yet to be explored *in vivo*. Recently, it has been demonstrated that Rad16 is important for global histone H3 K9K14 hyperacetylation in response to UV damage (Teng et al., 2008). Damage responsive increases in H3 acetylation, which are a requisite for efficient GGR, occur independently of both Rad4 and Rad14, but not Rad16 (Yu et al., 2005). Given that Rad16 is not a histone acetyl transferase (HAT) it has been predicted that the GGR complex may function to remodel chromatin and thus facilitate the recruitment of HATs (Teng et al., 2008). A recent report provided strong evidence that Rad16 regulates UV dependent histone H3 K9K14 hyperacetylation by regulating the occupancy of HATs such as Gcn5 (see Chapter 4.1, Yu et al., 2011). Following dual incision around a lesion, the extrusion of a damage containing oligonucleotide has been demonstrated to require a domain of superhelicity *in vitro* (Yu et al., 2004). The GGR complex is able to produce negative superhelical torsion through a catalytic activity in Rad16, and this has been shown to be necessary for damage excision *in vitro*. As observed with other members of the Snf2 protein family, this superhelical torsion is predicted to result from the activity of translocation (Lia et al., 2006; Yu et al., 2009).

The GGR complex is also part of an E3 ubiquitin ligase with the factors Cul3 and Elc1 (Gillette et al., 2006; Ramsey et al., 2004). This complex has been demonstrated to ubiquitylate Rad4 in response to UV, which results in UPP dependent degradation of the protein (Gillette et al., 2006). Interestingly, both Rad23 and the E3 ligase of the GGR complex play functionally redundant roles for cellular UV survival. It was shown that the ubiquitylation event, rather than subsequent degradation of Rad4, was important for UV survival. The functional contribution of Rad4 ubiquitylation to UV survival depended upon *de novo* protein synthesis, strongly suggesting the post-translational modification regulates a transcriptional response to UV. To date the only known target of the GGR complex E3 ubiquitin ligase is Rad4, however, whilst mutations that eliminate the ability of the complex to ubiquitylate Rad4 do not predispose cells sensitive to UV, mutations designed to eliminate the RING domain of Rad16, and thus all E3 ligase activity, do (Deshaies and Joazeiro, 2009; Gillette et al., 2006; Ramsey et al., 2004; Yu et al., 2011). This result implies that the E3 ligase may have more as yet unidentified targets, which could include those already discussed for UV-DDB.

1.5 Autonomously replicating sequence binding factor I

Autonomously replicating sequence binding factor I (Abf1) was originally identified for its ability to bind DNA at a variety of origins of DNA replication, as well as the silencing loci *HML* and *HMR* (Diffley, 1992). A plethora of literature subsequently identified Abf1 to bind within the upstream activating sequences (UASs) of a large array of gene promoters. It is now well established that Abf1 is an abundant, essential, global site-specific DNA binding protein (Yarragudi and Morse, 2006). The protein has been physically mapped to 1964 unique binding sites throughout the genome (Schlecht et al., 2008). The protein binds the DNA consensus sequence 5'-CGTnnnnnnTGAT-3', which is predicted to be found at thousands of sites throughout the genome (Mukherjee et al., 2004; Yu et al., 2009). In addition Abf1 has been demonstrated to bind at sites that do not match this consensus sequence (Della Seta et al., 1990; Schroeder and Weil, 1998). Abf1 is known to play roles in many areas of chromatin metabolism including transcription, silencing, DNA replication and repair (Loo et al., 1995; Reed et al., 1999; Rhode et al., 1992). Its multifunctional character has resulted in the classification of the protein as a General Regulatory Factor (GRF), of which members also include Rap1 and Reb1 (Fourel et al., 2002). Like many transcription factors (TF), Abf1 is bipartite consisting of N-terminal DBDs and a C-terminal activation domain (AD) (Yarragudi and Morse, 2006). The AD is further subdivided into two domains termed CS1 and CS2 (Miyake et al., 2002). Abf1 DNA binding alone is not sufficient for its many activities and the C-terminal AD is known to be necessary for its roles in replication, transcription and silencing (Li et al., 1998; Miyake et al., 2002). The following account reviews the characteristics of the protein in its many roles and discusses the molecular mechanisms proposed to account for these activities.

1.5.1 A role for Abf1 in DNA replication

Abf1 is known to bind only a subset of replication origins within the genome at an auxiliary element such as the B3 element of *ARS1* (Marahrens and Stillman, 1992). A role for Abf1 in DNA replication was first demonstrated when plasmids based upon the *ARS1* or *ARS121* origin of replication were shown to have a reduced stability when their Abf1 binding site/s were mutated (Walker et al., 1990; Walker et al., 1989). Cells expressing a temperature sensitive DNA binding mutant of Abf1, termed abf1-1, also show a reduced stability of such plasmids (Rhode et al., 1992).

These results demonstrated that Abf1 is not essential for DNA replication but instead stimulates the efficiency of replication at *ARSs* to which it binds. The stimulatory role for Abf1 binding seems to be independent of both orientation and distance; functioning to stimulate DNA replication when placed up to 1.2Kb away from the essential *ARS* core element (Walker et al., 1990). Furthermore, the Abf1 binding site of *ARS1* can be functionally replaced by either a Rap1 or Gal4 binding site, or by tethering various TF acidic ADs proximal to the *ARS* core element (Hu et al., 1999; Li et al., 1998; Marahrens and Stillman, 1992; Salghetti et al., 2001).

The functional redundancy of many DNA binding proteins at the B3 element of *ARS1* has been proposed to implicate that these must function in a similar manner; suggested to include chromatin remodelling (Venditti et al., 1994). However, the functional redundancy shown between various TFs is not always observed and in the case of *ARS121* only Abf1 functions to stimulate efficient DNA replication (Wiltshire et al., 1997). Furthermore, a second study which used an *ARS1* derived plasmid devoid of a centromere and selectable marker found no stimulatory role for Abf1 binding (Kohzaki et al., 1999). The latter result demonstrates the role which Abf1 plays in replication is context dependent. In support of this concept, addition of an Abf1 binding site to certain *ARS* devoid of this element can inhibit replication efficiency (Kohzaki et al., 1999).

1.5.2 Abf1 as a transcriptional regulator

Following identification of a consensus DNA binding site (DBS) for Abf1, the protein was quickly recognised to bind a large number of gene UASs. Such Abf1 binding domains are able to activate transcription when placed upstream of a reporter construct devoid of a promoter (Della Seta et al., 1990). Furthermore, Abf1 binding sites isolated from either an origin of replication or silencer are also competent in transcriptional activation (Buchman and Kornberg, 1990). However, Abf1 alone is a weak transactivator compared with other prototypical TFs such as Gal4. A strong transactivation potential is only achieved when the binding site is combined with a second UAS element (Buchman and Kornberg, 1990; de Winde and Grivell, 1992). Abf1 functions to synergistically activate transcription with a variety of other cis-acting regulatory elements (Martens and Brandl, 1994; Trawick et al., 1992; Yarragudi et al., 2004). The synergistic activation of genes is also known to occur with other GRFs such as Rap1 and Reb1 (Buchman and Kornberg, 1990; Chasman et

al., 1990). However, Abf1 binding upstream of a gene does not always function as a transactivator. For example, mutation of the Abf1 binding site at *FOX3* functions to alleviate transcriptional repression of the gene under non-inducing conditions (Einerhand et al., 1995). More recent microarray analysis, using the DNA binding temperature sensitive *abf1-1* allele identified 50 Abf1 activated genes and 36 Abf1 repressed genes (Miyake et al., 2004). This is remarkably lower than the number of genes predicted to be bound by Abf1 (Lee et al., 2002b; Schlecht et al., 2008). Indeed, two latter studies have predicted Abf1 to regulate up to 235 or even 3214 genes (Schlecht et al., 2008; Yarragudi et al., 2007).

Akin to its role in DNA replication, Abf1 seems to function as a transactivator in an orientation independent manner (Yoo et al., 1995). Often Abf1 binding sites known to be important for activation are found hundreds of bases away of a TSS (Trawick et al., 1992; Yoo et al., 1995). Furthermore, the role Abf1 binding plays in transcription seems to be functionally redundant with numerous other DNA binding factors. A Rap1 or Reb1 DBS can functionally substitute for an Abf1 DBS within a promoter without loss of transcriptional activity (Kraakman et al., 1991; Martens and Brandl, 1994). Conversely, an Abf1 or Rap1 DBS may functionally replace a Reb1 DBS at a promoter (Martens and Brandl, 1994; Remacle and Holmberg, 1992).

The precise activities through which Abf1 functions to regulate transcription are unknown. Abf1 binds to the promoters of multiple proteins that contribute to the same protein complex, indicating the protein is likely involved in co-regulating gene clusters (Tan et al., 2007). Indeed, Abf1 and Rap1 are known to bind to nearly all ribosomal protein genes. Interestingly, Esa1, the catalytic subunit of the histone acetyltransferase complex NuA4 also co-localises to these gene promoters suggesting Abf1 and Rap1 may recruit histone modifiers (Reid et al., 2000). Indeed, mutation of a Rap1 binding site was found to eliminate recruitment of Esa1, although the same experiment was not performed for Abf1. Deletion of the transcriptional co-activators *EAF5*, *EAF7*, *GCN5*, *HOS2*, *ISW2*, *SET1*, *SPT3*, *TAF1* and *TBP* all affect the expression of genes that overlap significantly with those bound by Abf1 (Steinfeld et al., 2007). Therefore, the protein could potentially stimulate transcription by recruiting some of these factors also, although it is not known to physically interact with any of them.

1.5.3 Abf1 is important for DNA silencing

The two mating type cassettes *HML α* and *HMR α* are maintained transcriptionally inactive in co-ordination with cis-acting DNA regulatory sequences termed silencers, and the Silence Information Regulator genes (*SIR* genes) (Loo and Rine, 1994). Each cassette is flanked by one E silencer, and at the other end, one I silencer. Each silencer contains an ARS domain and may also contain an Abf1 and/or Rap1 DBS. Abf1 is known to bind sites at *HMR-E*, *HMR-I* and *HML-I* (Buchman et al., 1988). A genetic screen for temperature sensitive mutants of silencing, identified that Abf1 is important for efficient silencing at both *HML* and *HMR* (Loo et al., 1995). *HMR-E* consists of three cis regulatory elements termed A, E and B bound by the origin recognition complex (ORC), Rap1 and Abf1 respectively (Brand et al., 1987; Kelly et al., 1994). These three factors show a functional redundancy since only two of the three elements are required for maintenance of silencing. This is also observed at *HML-I* (Boscheron et al., 1996). This is thought to relate to a shared ability of all factors to ultimately recruit the SIR complex (Allis et al., 2006). Individually these DNA elements do not function as a bona fide silencer, however artificially combining all three can produce a functional silencer (McNally and Rine, 1991; Rivier et al., 1999). Given that these DNA elements are often found in pairs where they do not function as silencers clearly demonstrates their effects are context dependent. The combinatorial necessity for the three binding sites has resulted in each individually being dubbed a 'protosilencer'. Each protosilencer is able to co-operate with a silencer up to 4kb away, in an orientation independent manner, to establish a repressed domain, but cannot alone function to silence chromatin (Boscheron et al., 1996).

A second example where Abf1 is known to function as a protosilencer is within the subtelomeric regions. All telomeres contain a region termed the core X element, a 473bp region with a strong ability to silence genes (Pryde and Louis, 1999). All core X elements contain an ARS consensus sequence (ACS) and 31 of 32 also contain a consensus Abf1 DBS. Mutation of either of these elements strongly relieves the repressive activity. Interestingly, the core X element alone does not function as a silencer but instead is able to potentiate the activity of a proximal silencer, at either the telomere or the mating type cassettes (Lebrun et al., 2001).

1.5.4 The multifunctional roles of Abf1; extensive repertoire of biochemical activities or a universal context dependent role?

Having observed the large spectrum of roles Abf1 plays in chromatin metabolism, the obvious question arises as to how Abf1 achieves so many, and in some circumstances contrasting, activities. Abf1 itself is thought to possess little intrinsic regulatory activity, but is known to have a large array of interacting partners involved in histone methylation and acetylation, nucleosome assembly, cell cycle checkpoints, DNA repair and replication, and posttranslational protein modification (28 partners in total from last count at *Saccharomyces* Genome Database; www.yeastgenome.org). In many circumstances, Abf1 has been observed to amplify the activity of its interaction partners, and has hence been dubbed an 'obligate synergiser' (Fourel et al., 2002).

Models attempting to explain the role of Abf1 in transcriptional regulation, silencing and replication share many commonalities, all implicating the protein to be fundamentally important for chromatin organisation. Mutations in Abf1 DBSs are often associated with a loss in chromatin organisation. Specifically, it has been observed that areas proximal to Abf1 DBSs often pertain defined nucleosome positions, which in response to loss of the binding site result in either changes in this positioning or a loss of definition. This has been observed at multiple ARS, silencers and UASs (de Winde and Grivell, 1992; Ganapathi et al., 2010; Hu et al., 1999; Lascaris et al., 2000; Lipford and Bell, 2001). At *ARS1*, Abf1 binding has been demonstrated to prevent the encroachment of nucleosomes into the ACS and B elements, occupancy of which is known to inhibit DNA replication; this activity correlates well with its ability to stimulate DNA replication (Bodmer-Glavas et al., 2001; Hu et al., 1999; Simpson, 1990; Venditti et al., 1994). Nucleosome remodelling at *ARS1* specifically requires the CS2 domain of Abf1 (Miyake et al., 2002). The same activity has also been demonstrated for various DNA binding proteins that can substitute for Abf1 at *ARS1* (Bodmer-Glavas et al., 2001; Hu et al., 1999). Similarly, abolition of Abf1 occupancy at *RPS28A* causes a loss in the strict positioning of nucleosomes; the authors here suggested a model in which Abf1 defines nucleosome positioning by forming a physical boundary for nucleosomes (Lascaris et al., 2000). Abf1 is also proposed to position a defined nucleosome proximal to its DBS at the silencers HML-I and HMR-E. In this circumstance it has been predicted that the

positioned nucleosome facilitates the SIR complex to propagate silenced chromatin, thereby defining the directionality of silencing (Zou et al., 2006).

A second commonly observed property of Abf1 is the ability to define a nucleosome depleted region (NDR) (Badis et al., 2008; Ganapathi et al., 2010). Abf1 binding is commonly associated with an area of MNase/DNase hypersensitivity (Ganapathi et al., 2010; Hartley and Madhani, 2009; Hesselberth et al., 2009). In a genome wide study, binding sequences for Reb1 and Abf1 were two of the five most commonly associated sequences with a NDR (Lee et al., 2007b). Furthermore, introduction of an Abf1 binding site into a nucleosomal domain often repositions the nucleosome, excluding it from the Abf1 DBS (Hartley and Madhani, 2009; Lipford and Bell, 2001; Yarragudi et al., 2004). Interestingly, the ability to compete with nucleosome occupancy and chromatin remodelling have been suggested to be mutually exclusive activities since only the former activity appears to be independent of CS1 and CS2 (Yarragudi et al., 2004). Loss of the AD of Abf1 is known to only affect expression of some genes under Abf1 regulation implying the protein may function to activate transcription by more than one mechanism (Yarragudi et al., 2007). It has been predicted that the combined effects of chromatin remodelling and maintaining a NDR are necessary for facilitating the access of secondary TFs to their cis elements (Yarragudi et al., 2004; Yarragudi and Morse, 2006). In support of this model, the requirement of a Rap1 binding site at *HIS4* for Gcn4 dependent transcription is abrogated when Gcn4 is artificially tethered to the promoter (Yu and Morse, 1999). An Abf1 binding site may also functionally substitute for a Rap1 binding site at *HIS4* (Yarragudi et al., 2004).

In addition to these properties Abf1 binding has the ability to confine areas of differing chromatin states, most commonly between regions of silenced and active chromatin (Fourel et al., 2002; Yu et al., 2003). Binding of the protein to chromatin prevents spreading of a silenced domain beyond it; a protein with such property may be referred to as a genome partitioner, barrier element or insulator. By defining a NDR, Abf1 is believed to inhibit the spread of silenced chromatin by inhibiting the propagation of the Sir complex along a nucleosomal array (Bi et al., 2004). In addition, Abf1 and Rap1 are known to be able to bend DNA upon binding (McBroom and Sadowski, 1994b). Other GRFs that may functionally substitute for Abf1 have many of the above characteristics described. For example, both Rap1 and Reb1 have been demonstrated to remodel chromatin, define NDRs and function as barrier

elements (Bernstein et al., 2004; Hartley and Madhani, 2009; Lee et al., 2007b; Yu and Morse, 1999; Yu et al., 2003). Cells expressing a fusion protein which replaces the essential AD of Abf1 for a partially homologous domain in Rap1 are viable (Goncalves et al., 1996). The functional redundancy between GRFs suggests their molecular functions must be similar.

The C-terminal domain CS2 is necessary for the role of Abf1 in silencing, transcriptional regulation, barrier activity and DNA replication (Fourel et al., 2002; Miyake et al., 2002). Given the interdependence of these activities it is tempting to speculate that the fundamental molecular mechanism through which Abf1 acts is the same in all these circumstances. However, it should be noted that in some circumstances the relative affects of Abf1 mutants do not equally attenuate its ability to function in its various contexts (Fourel et al., 2002; Reed et al., 1999; Rhode et al., 1992; Yarragudi et al., 2004). This potentially implies that Abf1 may in fact play multiple roles in chromatin metabolism at a single binding site (Yarragudi et al., 2004). It is now also apparent that only subsets of promoters regulated by GRFs share the same cofactors (Deminoff and Santangelo, 2001; Reid et al., 2000). Clearly the physiological consequence of Abf1 binding is not always completely consistent and is dependent upon the context in which the protein binds. The interplay between Abf1 and its various cofactors, and how these contribute to chromatin metabolism remain to be elucidated. Furthermore, other mechanisms disparate to the protein's role as a chromatin organiser have been proposed to account for Abf1's activities; these include recruitment of chromatin to nuclear subcompartments and chromatin looping (Fourel et al., 2002). Further investigation at the level of the gene in combination with both genome-wide and three dimensional studies will be required to elucidate how GRFs regulate such a diverse range of nuclear functions.

Lastly, it is worth noting that investigations into GRFs in yeast are likely to provide insights into the molecular biology of higher eukaryotes. Whilst a homologue of Abf1 has not been identified in metazoans, proteins with highly similar properties to GRFs have been identified. A good example of this is CTCF; an abundant site specific genome-wide DNA binding protein. CTCF has been implicated in context dependent promoter activation/repression, silencing, barrier activity and long-range chromatin interactions (Phillips and Corces, 2009). The protein is highly conserved, ubiquitously expressed and essential. Many other similar examples are also appearing

(Fourel et al., 2002; Phillips and Corces, 2009 and references therein). Therefore, GRFs may emerge as fundamental regulators of all eukaryotic genomes.

1.5.5 The role of Abf1 in GGR

A role for Abf1 in GGR was originally implicated from the observation that the protein co-purifies with Rad7 (Reed et al., 1999). In the absence of UV damage, Abf1 forms a stable heterotrimeric complex with Rad7 and Rad16, termed the GGR complex. However, approximately only one third of cellular Abf1 is predicted to be in complex with Rad7 and Rad16. A temperature sensitive DNA binding mutant of Abf1, termed *abf1-1*, was demonstrated to possess a highly deficient repair activity of UV damage at the restrictive temperature. Subsequent to this observation, it was demonstrated that mutating an Abf1 DBS inhibited efficient GGR both in vitro and in vivo (Yu et al., 2009). These results demonstrate that Abf1 promotes efficient GGR through its site specific DNA binding activity. In vitro, mutation of an Abf1 DBS at the *HML α -I* silencer inhibited efficient binding of Abf1, Rad7 and Rad16. When this mutation was incorporated in vivo, a ~400bp domain of deficient repair was situated upstream of the mutated Abf1 DBS. These observations were interpreted to suggest that Abf1 promotes efficient binding of the GGR complex to a consensus DBS, which facilitates the formation of GGR domains in response to DNA damage (Yu et al., 2009). The unidirectional defect in repair at *HML α -I* with the DBS mutation suggests that Abf1 may direct the biochemical activities of the GGR complex in an orientation specific manner. Indeed, Abf1 DNA binding has been suggested to be strictly orientated such that it predominantly contacts one face of the DNA helix at the adjacent major grooves 3'-GCA-5' and 3'-YYRCTR-5' of the DNA binding consensus sequence (McBroom and Sadowski, 1994a). This could subsequently direct the activity of the Rad16 DNA translocase, which promotes GGR (Ramsey et al., 2004; Yu et al., 2004; Yu et al., 2009). Indeed, in response to UV damage, Abf1 occupancy was shown to fall at *HML-I*, potentially reflecting a relocalisation of the GGR complex following UV. The above observations have been consolidated as a model presented in Fig. 1.6 (Yu et al., 2009).

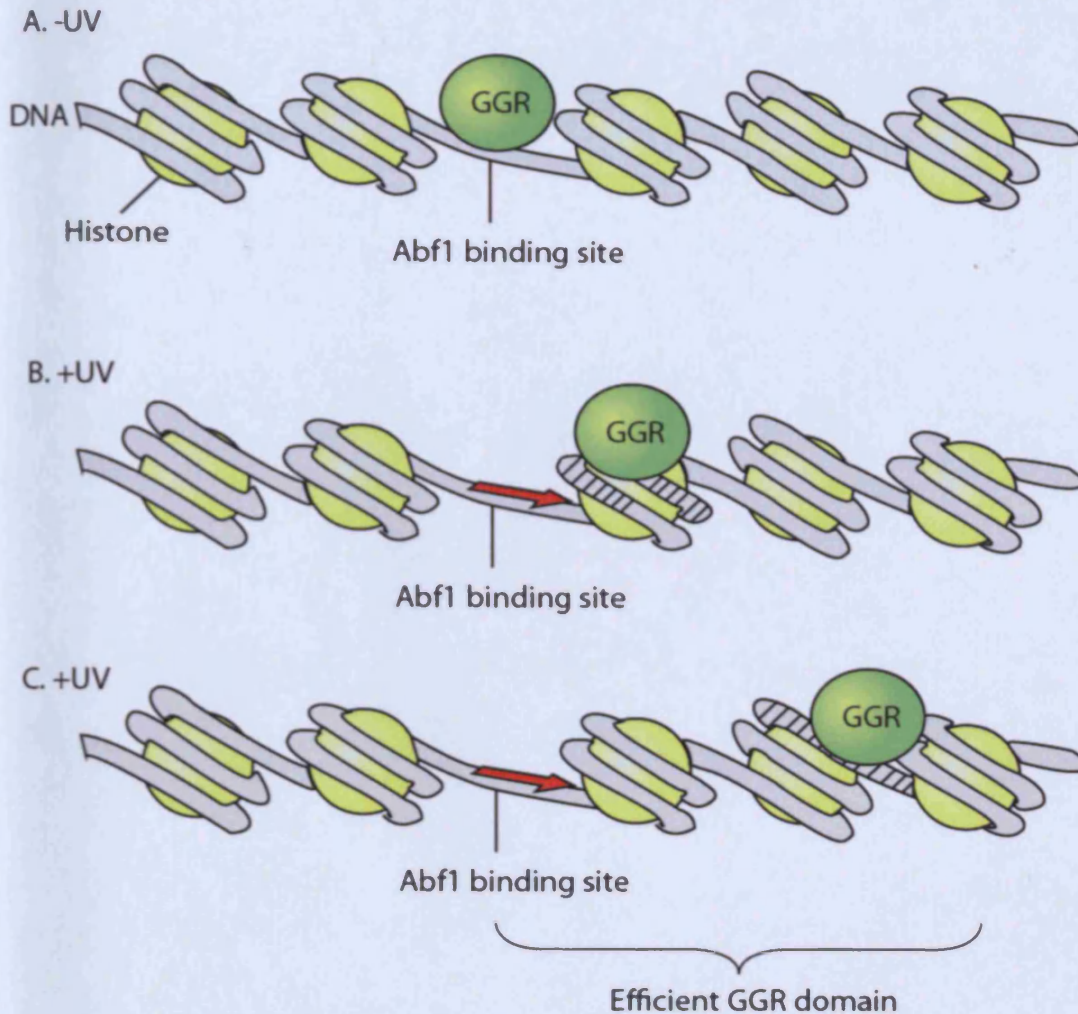


Figure 1.6. A. In the absence of DNA damage the GGR complex (represented as a green complex) is predicted to reside at various Abf1 DBSs throughout the genome. B. In response to damage, the GGR complex induces superhelical torsion in DNA following unidirectional translocation initiated from the Abf1 binding site. This creates domains of superhelical torsion (represented by striped DNA), the activity of which promotes efficient GGR. The GGR complex may translocate either short (B) or long distances (C) to promote GGR within a domain from the Abf1 DBS.

1.6 DNA binding kinetics

1.6.1 The nomenclature used with respect to transcription factors

The principles from which many of the proceeding studies and discussions are derived concern site specific DNA binding regulators of transcription. Unfortunately, this field uses a range of loosely defined terms to describe the various proteins that bind chromatin necessary for transcription. Here, the term transcription factor (TF) is used to describe a site specific DNA binding protein which binds DNA at a region either proximal or distal to a core promoter and either positively or negatively regulates transcription of the promoter. This does not include any of the basal (or

general) TFs, including site specific DNA binding proteins such as TBP. Nor does it include proteins that influence transcriptional regulation via recruitment by TFs (termed co-activators/co-repressors) such as histone modifiers or chromatin remodellers. A TF, in this sense, is equivalent to any protein categorised in transcriptional 'orchestration' from the given reference (Venters et al., 2011).

1.6.2 The in vivo lifetime of TF:DBS complexes

It is now well established that the regulation of transcription is at least partially controlled through TFs; proteins that function to recognise and bind a site specific DNA binding site (DBS) proximal to a gene's core promoter and initiate a progressive recruitment of protein factors necessary for RNA polymerase mediated transcription (Weake and Workman, 2010). Prior to the advent of in vivo technologies such as chromatin immunoprecipitation (ChIP) or live-cell imagery, the delineation of this complex mechanism was established using in vitro assays. Using such assays, it was commonly observed that site specific DNA binding by a TF resulted in a highly stable complex with DNA. For example, a complex of the glucocorticoid receptor (GR) or NF- κ B with its respective DBS has a half-life of 108 minutes or 45 minutes respectively (Perlmann et al., 1990; Zabel and Baeuerle, 1990). The vast majority of TFs in vitro form long-lived complexes with their cognate DBSs. Such observations founded the notion that upon activation, TFs stably bound DNA and resided at a promoter for the duration of transcriptional activation (reviewed in Hager et al., 2006). It was therefore surprising when the occupancy of the oestrogen receptor- α (ER α) was observed at a promoter in vivo using ChIP. Using this technique the occupancy of ER α was observed to cyclically rise and fall in a pattern that periodically repeated every 80 minutes (Shang et al., 2000). The rise and fall in occupancy of both ER α and co-activators within this period was interpreted to represent a single binding event, indicating that the in vivo half life of ER α at a DBS was only around 20 minutes (see Fig. 1.7).

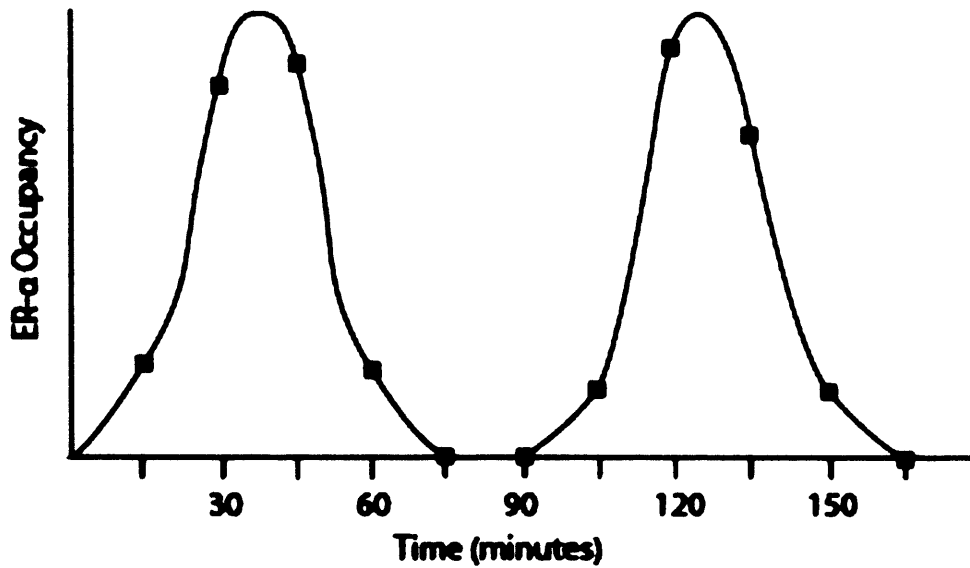


Figure 1.7. Graphical representation of the occupancy of ER α at the captheysin D promoter following addition of estradiol. ChIP results were presented in (Shang et al., 2000).

Whilst the data produced by Shang et al. (2000) was correct, the interpretation is likely flawed. The mistake made was to assume that the changes seen were directly representing the *in vivo* DNA binding kinetics of ER α . At a similar time to this publication, a study using live-cell imagery demonstrated the remarkable observation that the *in vivo* half-life of the GR at a promoter was of the order of a few seconds (McNally et al., 2000a). The rapid exchange of a TF with its promoter *in vivo* was later also observed for ER α , and has been made for all nuclear hormone receptors tested (Klokk et al., 2007; Rayasam et al., 2005; Sharp et al., 2006). These observations quickly altered the models derived from ChIP experiments, and, for some TFs including ER α , the oscillations in occupancy are now believed to reflect gradual changes in the chromatin environment that alter the accessibility of TF DBSs (and thus TF occupancy) over time (Hager et al., 2009; Karpova et al., 2008). Collectively this work demonstrates that a far more powerful appreciation of *in vivo* DNA binding by TFs is provided through studies that complement ChIP with techniques that analyse DNA binding kinetics. Secondly, this demonstrates that ChIP is not well suited for the analysis of DNA binding kinetics (discussed below).

Whilst the exploration of nuclear dynamics has become facile with the use of live-cell imaging, the analysis of site specific DNA binding kinetics (as opposed to generic DNA or chromatin binding) *in vivo* has remained very limited due to the vast technical difficulties in acquiring such information. Rapid exchange of DNA binding

proteins is clearly not always observed in vivo; histones H3 and H4 remain bound within chromatin for several cell generations in HeLa cells, whilst different populations of H2B show variable half-lives ranging from 6 minutes to 8.5 hours (Kimura, 2005). In addition to the nuclear hormone receptors, two site specific DNA binding TFs, NF- κ B and Ace1 (in *S. cerevisiae*) have been demonstrated to rapidly exchange at a promoter in vivo (Bosisio et al., 2006; Karpova et al., 2008). The prevalence of these examples is currently unknown; these studies typically investigate only a single cognate promoter bound by the TF using low resolution analysis. In contrast, under inducing conditions three TFs have been shown to reside at a cognate DBS/promoter in vivo with a half-life of at least 20 minutes; Gal4 (from *S. cerevisiae*), HSF (from *D. Melongaster*), and HIF-1 (from mammals) (Nalley et al., 2006; Yao et al., 2006; Yu and Kodadek, 2007). However, a recent publication has indicated that the stable binding of Gal4 observed at a promoter may result from an artefact of the experimental conditions employed and thus not reflect the wild type behaviour of the protein (Collins et al., 2009). Lastly, nuclear foci of the TF RUNX2, which represent regions of RNAPII mediated transcription, contain a mixed population of both rapid and slow exchanging proteins (Pockwinse et al., 2011). Although limited, the wide variance in the results obtained to date likely reflect that mechanisms that regulate DNA binding kinetics of TFs are both complex and diverse. Therefore, future studies will need to expand the repertoire of TF DNA binding kinetics analysed and include multiple chromosomal locations in order to substantiate how this property is regulated in vivo, and its resultant physiological consequences.

1.6.3 The regulation of DNA binding kinetics

The stark contrast in the lifetime of a DNA bound complex of GR or NF- κ B with its cognate DBS in vitro, compared in vivo, suggests that exogenous factors must function to disrupt (or 'turnover'; a term used here, not to be confused with proteolytic turnover) DNA bound protein complexes within the cell. In support of this, addition of nuclear extracts function to dissociate TF:DBS complexes in vitro (Fletcher et al., 2000; Fletcher et al., 2002; Rayasam et al., 2005). ATP depletion immobilises a fraction of GRs at a promoter array in vivo, suggesting that such activities require energy (Agresti et al., 2005; Stavreva et al., 2004). Furthermore, in situ depletion of soluble nuclear factors inhibit the nuclear mobility of the GR (Elbi et al., 2004). One complication with the latter observation is that the GR has been

suggested to be sequestered at the nuclear scaffold (Stenoien et al., 2001). However, it is generally agreed that a significant fraction of GR is chromatin bound and thus nuclear factors must be important for turnover of chromatin bound GR, and presumably also site-specific DNA bound GR (Agresti et al., 2005; Hager et al., 2009).

To date two classes of proteins have been demonstrated to actively turnover TF:DBS complexes in vitro. The first class of these are molecular chaperones. For example, p23 functions to disrupt thyroid receptor (TR) binding at a DBS in vitro (Freeman et al., 2000; Freeman and Yamamoto, 2002). This activity seems to have a physiological consequence in vivo since artificially tethering p23 proximal to a DBS functions to reduce transactivation by GR, TR, AP1 and NF- κ B. The same effect was also observed for the molecular chaperone Hsp90 (Freeman and Yamamoto, 2002). It was also shown in situ, that the loss of GR mobility due to nuclear factor depletion (as discussed above) could be restored through the addition of a cocktail of seven chaperones/co-chaperones (Elbi et al., 2004). The second class of proteins include members of the Snf2 family of ATPase chromatin remodellers. In vitro, SWI/SNF has been demonstrated to displace DBS binding by the androgen receptor (AR) and GR (Fletcher et al., 2002; Klock et al., 2007). Interestingly, and in complete contrast to the above experiments for p23, displacement of protein binding strictly depended upon a chromatin template since identical experimental procedures using a naked DNA template did not result in TF turnover. This strongly suggests that the activity of chromatin remodelling is required, and a role for chromatin remodellers in regulating DNA binding by altering the accessibility of a DBS within chromatin has been proposed (Karpova et al., 2008; Nagaich et al., 2004). In this regard, SWI/SNF may parallel the activity of another Snf2 member Isw2. This has been demonstrated to displace DNA binding of the artificial activator Gal4 DBD-VP16 AD by sliding a nucleosome into the vicinity of a Gal4 DBS (Kassabov et al., 2002). As a final example, turnover of Acl on chromatin was demonstrated to be accelerated by Rsc2, however the results were concerned only with non-specific chromatin interactions, and have not been tested at a DBS (Karpova et al., 2004).

Accumulating evidence suggests that for some TFs there exists an intimate link between transcription and proteolytic turnover. For example, many ADs contain degrons, a TF's stability is often inversely proportional to its transactivation potential and in some cases, inactivation of the proteasome completely inhibits functional

transcription (Collins and Tansey, 2006). These data suggest that proteolytic turnover of some TFs is necessary for functional transcription. Furthermore, given that the proteasome is recruited to many promoters and that inhibition of transcription often leads to stabilisation of a TF, it is commonly proposed that proteolytic degradation of a TF occurs whilst DNA bound at a promoter and is mechanistically coupled to functional transcription (Kodadek et al., 2006; Morris et al., 2003; Reid et al., 2003; Sikder et al., 2006; Zhu et al., 2007). This model therefore describes a third mechanism by which the cell may function to regulate the turnover of a DNA binding protein at a DBS. Innumerable papers imply proteolytic turnover of a TF at a promoter; for example, in response to galactose only the transcriptionally active pool of Gal4 is rapidly degraded, whilst the remaining pool is stable (Muratani et al., 2005). However, only a handful of examples directly demonstrate a role for proteolytic turnover at the DBS. Occupancy of HIF-1 α at a promoter is negatively regulated by the proteasome, and given that the protein stably binds a promoter in vivo, this activity is likely to occur whilst chromatin bound (Yu and Kodadek, 2007). Live cell imagery has demonstrated a slower exchange of both the GR and NF- κ B at a promoter in response to proteasome inhibition or mutation of a degron respectively (Bosisio et al., 2006; Stavreva et al., 2004). Furthermore, SREBP1 is phosphorylated and ubiquitylated in response to binding a promoter and inhibition of the proteasome results in a rapid accumulation of phosphorylated SREBP1 at a promoter, without a concurrent cellular accumulation of the phosphorylated species, directly demonstrating the protein is proteolytically turned over whilst bound at a promoter (Punga et al., 2006).

1.6.4 Regulation of DNA binding kinetics by the 19S sub-particle of the proteasome

Perhaps the best characterised regulator of TF DNA binding kinetics at a DBS is an apparent activity within the 19S sub-particle of the proteasome (Ferdous et al., 2007). Here the authors demonstrated that the 19S is able to dissociate a stable interaction between a TF and its cognate DBS in vitro. As with p23, this activity was detectable using naked DNA templates. The activity does not prevent the TF from reassociating to a DBS suggesting that it does not involve proteolytic degradation or denaturation of the protein. Furthermore, the activity required a physical interaction between the 19S and a TF AD, and required ATP, and is thus likely to be a function

of the chaperone activity of the 19S AAA ATPases. The second seminal finding of the paper was that monoubiquitylation of a TF functioned to attenuate this activity. It was later determined that the ubiquitin moiety interacts with the 19S subunits Rpt1 and Rpn1, and as such is believed to allosterically inhibit a 19S interaction with an AD (Archer et al., 2008a). As with the 19S interaction, monoubiquitylation required the presence of an AD. Collectively, these data demonstrate that post-translational monoubiquitylation of a protein may function to regulate the lifetime of TF:DBS interactions.

Whilst these observations are very interesting, are they physiologically relevant *in vivo*? A derivative of Gal4, termed Gal4D, which lacks a region of the C-terminal AD necessary for monoubiquitylation, cannot efficiently occupy a cognate promoter *in vivo* or activate transcription (Archer et al., 2008b). However, *in vitro* the ability of Gal4D to bind DNA is not compromised (Wu et al., 1996). If the loss of DNA occupancy *in vivo* was due to 19S mediated disruption of TF:DBS complexes then inactivation of the 19S activity or artificially tethering ubiquitin to Gal4D should restore promoter occupancy; indeed this is the case for both (Archer et al., 2008b). Under certain experimental conditions, the turnover of Gal4 at a promoter is far more rapid under non-inducing conditions than inducing conditions for transcriptional activation (Nalley et al., 2006). This observation has led the authors to propose that, under inducing conditions, Gal4 monoubiquitylation functions to antagonise the destabilisation activity of the 19S resulting in stable, long lived, Gal4-DBS complexes (Ferdous et al., 2007). Indeed, indirect evidence has been provided for this ubiquitylation event under inducing conditions at a Gal4-binding promoter (Archer et al., 2008b). Whilst Gal4D cannot efficiently occupy a cognate promoter *in vivo*, a further deletion of Gal4D, which removes the 19S interaction module, seems to restore the ability of Gal4 to occupy its binding site *in vivo* (Nalley et al., 2006). However, the truncated protein does not retain kinetic stability on DNA under inducing conditions; it possesses a shorter half-life at a DBS when compared with the full length protein. Thus via a mechanism independent to monoubiquitylation, the ability to drive transcription also seems to stabilise the DNA binding kinetics of Gal4; an observation previously made for other TFs (Klokk et al., 2007; Reid et al., 2003; Stavreva et al., 2004; Yu and Kodadek, 2007).

Whilst the physiological relevance of 19S regulated DNA binding kinetics has only been demonstrated *in vivo* for Gal4, a variety of evidence indicates this

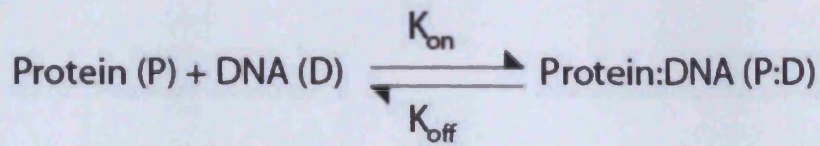
phenomenon may be utilised for many TFs within the eukaryotic cell. Firstly, in vitro it was shown that DBS binding by Pho4 and p53 is also disrupted by the 19S, indicating that any protein that directly interacts with the 19S may be susceptible to the activity (Ferdous et al., 2007; Kim et al., 2009). Secondly, monoubiquitylation has been demonstrated to stimulate the occupancy and transactivation potential of multiple TFs (Brès et al., 2003; Greer et al., 2003; Le Cam et al., 2006; Salghetti et al., 2001). Lastly, the activity of the 19S has also been demonstrated to disrupt both site specific and generic DNA binding of p53; in vivo p53 recruits the 19S to a promoter and inhibition of the 19S both increases promoter occupancy and gene transcription (Kim et al., 2009).

1.6.5 Is there a physiological rationale in regulating DNA binding kinetics?

Whilst it has become apparent that mechanisms exist within the cell that alter the DNA binding kinetics of proteins in vivo, is this property important for the regulation of cellular metabolism or just a consequence of such activity? It is intuitive to suppose that, given the presence of a TF often promotes gene expression, changes that function to increase the occupancy of a TF (or K_a , see Fig. 1.8) should function to increase the transactivation potential. But does it matter how long it resides at a DBS? This topic is a matter of hot debate, but two studies have indicated the answer may well be yes (Brady et al., 2005; Yang et al., 2002a). In both examples a TF was isolated with DBD point mutations that failed to substantially alter the K_a of the protein at a DBS in vitro, but significantly altered the rate at which the protein bound and dissociated from the DBS (the K_{on} and K_{off} rates respectively). In both cases, the TF derivative which stably bound a DBS attained a far greater transactivation potential than that which was kinetically labile. These studies illustrate two important points. Firstly, they demonstrate that altering the lifetime of TF:DBS complexes may provide the cell with an elegant mechanism for the regulation of the physiological function of such proteins, a concept now receiving considerably support (Hager et al., 2009). This correlates well with the observations that mono-ubiquitylation functions as a licensing factor for TFs, and stabilises their turnover at a DBS in vitro. It also correlates with two studies that have demonstrated the TFs Gal4 and HSF to be kinetically stabilised at a promoter in response to environmental cues that activate transcription (Nalley et al., 2006; Yao et al., 2006). Secondly, they demonstrate that technologies designed to measure DNA binding such as EMSA or ChIP, which

measure a protein's occupancy at a DBS (or K_a), will not necessarily observe changes in the DNA binding kinetics. This is because these techniques analyse the relative equilibrium between protein-bound and free DBSs, but do not measure the flux of the equilibrium. If a change in flux results in a change in the equilibrium then this is detected, however, flux can alter without detectable changes in the equilibrium, as demonstrated by the above references (see also Fig. 1.8).

A.



$$K_a = \frac{[\text{Protein:DNA}]}{[\text{Protein}][\text{DNA}]}$$

$$K_a = \frac{k_{\text{on}}}{k_{\text{off}}}$$

B.

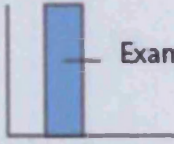


Example	Equation	Association Constant	ChIP graph
1.	$\text{P + D} \xrightleftharpoons[k_{\text{off}} = 1]{k_{\text{on}} = 1} \text{P:D}$	$K_a = \frac{1}{1} = 1$	 <p>Example 1</p>
2.	$\text{P + D} \xrightleftharpoons[k_{\text{off}} = 5]{k_{\text{on}} = 1} \text{P:D}$	$K_a = \frac{1}{5} = 0.2$	 <p>Example 2</p>
3.	$\text{P + D} \xrightleftharpoons[k_{\text{off}} = 5]{k_{\text{on}} = 5} \text{P:D}$	$K_a = \frac{5}{5} = 1$	 <p>Example 3</p>

Figure 1.8. A. Standard equation representing the equilibrium between DNA bound and free protein. The K_a represents the affinity of a protein for its DBS, which is a function of its DNA binding kinetics. B. Examples of how changes in kinetics are represented by technologies such as ChIP that measure the K_a of a protein. In example 3, the rate of protein turnover as a DBS is 5x faster than in example 1, however because the ratio of $K_{\text{on}}/K_{\text{off}}$ is maintained, the increase in turnover is not detected by ChIP.

1.7 Aim of the current study

As described in 1.4.4, Abf1 is part of a heterotrimeric complex with Rad7 and Rad16 termed the GGR complex. Rad7 and Rad16 are generally essential for GGR in vivo, the mechanism of which has been partially characterised. Rad16 is able to induce superhelical torsion in the DNA molecule necessary for oligonucleotide extrusion in vitro. Rad7 and Rad16 have also recently been demonstrated to promote histone H3 K9K14 acetylation and remodel chromatin in vivo, the activities of which are necessary for efficient GGR (further discussed in Chapter 4). As discussed in 1.5.5, the ability of Abf1 to promote GGR correlates with its site specific DNA binding activity. The protein is hypothesised to function by promoting binding of Rad7/Rad16 to domains in the genome in which their biochemical activities promote efficient GGR. The aim of the current study is to further characterise the Abf1 and Rad16 proteins using ChIP coupled to microarrays (ChIP-on-chip). In Chapter 3, Abf1 ChIP-on-chip is performed both in the absence and presence of UV damage. In Chapter 4, Rad16 ChIP-on-chip is similarly performed both in the absence and presence of UV damage. How GGR is organised in relation to the genome-wide distribution of both Abf1 and Rad16 is investigated using global datasets for both histone H3 K9K14 acetylation and CPD repair.

As discussed in Chapter 1.6, the DNA binding kinetics of TFs is an emerging field of research. Numerous studies have indicated that there exists an intimate link between the DNA binding kinetics of TFs and transcriptional activation. Abf1 is structurally homologous to canonical TFs (see Chapter 5.1), and in many circumstances functions as a transcriptional activator (Chapter 1.5.2). The cell appears to have many mechanisms that function to regulate the DNA binding kinetics of a TF in vivo including ubiquitylation and chromatin remodelling by Snf2 protein family ATPases. The GGR complex has both an E3 ubiquitin ligase activity and Rad16 is a member of the Snf2 protein family. Given the structural and functional similarities between Abf1 and other TFs, and that the GGR complex has two activities that could regulate DNA binding kinetics, this study aimed to investigate if changes in Abf1 DNA binding kinetics were mechanistically linked to GGR. In Chapter 5, tools necessary for analysing Abf1 DNA binding kinetics in vivo using the ChIP-on-chip technology are created and optimised. The aim of chapter 6 is then to use these tools to measure the genome-wide DNA binding kinetics of Abf1 both in the presence and absence of UV damage, as a complementary study to Chapter 3.

2. Materials and Methods

This chapter describes the molecular biological techniques employed in this study. Whilst the majority of solutions are described within the text, some solutions have been named but their contents not described; these descriptions may be found in Appendix I.

2.1 Strains, growth and storage

For the short term storage of strains, cell culture was streaked upon either YPD/synthetic drop out media agar plates and incubated at the appropriate temperature (30°C unless otherwise stated) in a LEEC compact incubator until colonies had formed (typically 2 days). Plates were stored at 4°C. For long term storage, cell cultures were grown in exponential phase, glycerol was added to a final concentration of 30% and cells were frozen at -70°C.

For the growth of cells, a single colony was picked from a plate, inoculated in fresh liquid media and maintained in exponential phase. This preculture was then used to inoculate large volumes of liquid media. Liquid cultures were incubated at the appropriate temperature (30°C unless otherwise stated) in an Infors HT multitron standard at 180rpm. Cell cultures taken from frozen stocks were first streaked onto plates, and colonies allowed to grow before proceeding with the above protocol.

For nearly all experimental purposes cell culture was grown to a density of 2×10^7 cells/ml. This density was calculated in two manners. Firstly, 1ml of cell culture was measured at 595nm with a Jenway 6300 Spectrophotometer, blanked against liquid media without cell culture. Cells were grown to a typical OD value of 0.6. Secondly, cell density was calculated using an Improved Neubauer BS748 2 cell counting chamber (Hawksley).

2.2 UV damage

Yeast cells were collected by centrifugation and resuspended in chilled PBS (4°C) to a density of 2×10^7 cells/ml. 50ml of resuspended culture was poured into a Pyrex dish with a diameter of 15cm and exposed to 100J of UV light at 254nm from a germicidal lamp at a fluence of 10W/m^2 . This was repeated 50ml at a time until all culture had received 100J of UV light. Yeast cells were subsequently collected and

resuspended in liquid media for all downstream applications including crosslinking by formaldehyde. All cultures compared with UV treated cells were resuspended in PBS in an identical manner to that of UV treated cells.

2.3 DNA manipulations

2.3.1 DNA gel electrophoresis

Gel electrophoresis of DNA was routinely used for multiple applications including inspecting the success of PCR reactions or plasmid preparations, resolving restriction digestions, observing the uniformity of sonicated DNA samples, and the separation and isolation of DNA fragments for downstream cloning applications.

1. Various agarose concentrations were prepared depending on the downstream application. Typically, if DNA was to be purified from the gel, 0.7% agarose was used, otherwise a 1.0% agarose gel was prepared. Agarose was added to TAE buffer (40mM Tris-Acetate, 1mM ethylenediamine tetraacetic acid (EDTA), pH8.0) and heated in a microwave to dissolve.

2. Agarose solution was cooled to ~50°C. To 100ml of agarose solution, 1µl of 10mg/ml ethidium bromide was added and mixed well. Gels were either cast in a Horizon 58 (Life Technologies) or a Mini-Sub cell GT (Bio-Rad) and left to cool for one hour at room temperature.

3. 50-200ng of DNA was mixed with water to a total of 10µl, to which 2µl of 6x MassRuler loading dye (Fermentas) was added. To DNA samples with a large volume more loading dye was added. Gel tanks were filled with TAE buffer and samples were loaded into the wells. To one well a DNA ladder was loaded; either GeneRuler 1kb DNA ladder or FastRuler low range DNA ladder (Fermentas). Gels were run at 75V on a power-pac 200 (BioRad) at room temperature.

4. Following electrophoresis DNA was visualised using a BioDoc-It Imaging system (UVP) at 302nm. If DNA was to be purified following electrophoresis then it was visualised at 365nm to minimise UV damage, and excised from the gel with a scalpel. DNA was purified from excised gel samples using the PureLink quick gel extraction

kit (Invitrogen) according to the manufacturer's protocol. DNA was purified to 30µl of water.

2.3.2 Polymerase Chain Reaction (PCR)

Unless otherwise stated all PCR reactions were performed using the Expand High fidelity PCR system (Roche). Typically PCR was performed in a total reaction volume of 50µl. If larger quantities of DNA were required multiple 50µl reactions were performed and pooled together during purification.

1. To a 0.2ml PCR tube on ice, the following were added:

10x buffer with magnesium chloride (Roche)	10µl
dNTP mix 10mM (Fermentas)	1 µl
Forward primer (10µM)	0.8 µl
Reverse primer (10 µM)	0.8 µl
25mM Magnesium chloride (Roche)	2 µl
DNA template	1-10ng plasmid, 100-500ng genomic DNA
Water	Up to a total volume of 49.3 µl

2. To this 0.7µl of polymerase enzyme (Roche) was added and the tube was immediately vortex mixed, spun down and run on a PTC-200 PCR machine (MJ Research) with the following conditions:

1. 95.0°C for 4:00 minutes
2. 94.0°C for 0:30 minutes
3. AT°C for 0:30 minutes
4. 72.0°C for ET minutes
5. Go to 2. x30 times
6. 72.0°C for 10:00 minutes
7. End

AT (the annealing temperature) was calculated as five degrees Celsius lower than the lowest primer T_m. ET (extension time) was calculated as 1:00 minutes per kb of DNA to be amplified.

3. Fusion PCR: For fusion PCR the above protocol was also used with a single modification. DNA fragments to be fused were added to the reaction in equimolar concentrations to a total of 50-100ng of DNA.

4. All PCR products were purified into water using the QIAquick PCR purification kit (Qiagen) according to the manufacturer's instructions.

2.3.3 Cloning

Extensive DNA manipulations were performed for a wide variety of cloning purposes presented in subsequent chapters. Such manipulations included DNA restriction and DNA ligation. In these circumstances all enzymes used to perform these manipulations were from New England Biolabs. The following account outlines the common strategies employed for the production of a novel plasmid.

1. All DNA used for recombinant manipulations was purified into either water or 10mM Tris-Hcl pH8.0 and quantified using a Nanodrop 1000 spectrophotometer (ThermoScientific) according to manufacturer's instructions.

2. For DNA restrictions: All restriction digestions were performed in a total volume of 40µl. 1500ng of DNA was combined with water to a total volume of 34 µl for single enzyme digests, or 32 µl for double enzyme digests. To this 4 µl of enzyme buffer was added. 1 µl of each enzyme (at a starting concentration of 10,000 or 20,000 units/ml) to be used was added to this and the reaction was incubated at 37°C for 90 minutes. The reaction was briefly spun to collect condensation and a further 1 µl of each restriction enzyme was added. This was incubated at 37°C for a further 90 minutes. DNA was either directly purified with the QIAquick PCR purification kit (Qiagen) to 30µl water or purified following gel electrophoresis as described above.

3. DNA ligation and cloning: DNA samples were combined with water to total a volume of 18µl consisting of ~200ng of DNA. Typically a single insert: vector ratio of 3:1 was used. For three fragment ligations insert: insert: vector ratios were altered according to size, where smaller fragments were added in a larger molar ratio. For example a 1kb:3kb:5kb (vector) ligation would typically have a 5:3:1 molar ratio respectively. To the DNA solution 2µl of 10x T4 DNA ligase reaction buffer and 1µl of T4 DNA ligase (400,000 cohesive end units/ml; NEB) was added. Reactions were incubated at 16°C for 2-3 hours or at 4°C overnight. 100µl of Library efficient DH5α chemically competent cells (Invitrogen) were subsequently transformed with 10µl of

the ligation reaction according to the manufacturer's protocol. All plasmids in the current study used ampicillin as a selection marker. Treated cells were plated onto LB plates supplemented with 100µg/ml ampicillin and left overnight to grow at 37°C.

Single *E. coli* colonies were tested for the transformation of the correct plasmid by colony PCR (see below). Positive colonies were subsequently picked and grown overnight in LB supplemented with 100µg/ml ampicillin at 37°C, 225 rpm in a Multitron standard incubation shaker (Infors AG). For mini-preps, 5ml of culture was purified to 50µl of EB buffer with the QIAprep spin miniprep kit (Qiagen). For midi-preps 50ml of culture was purified to 1ml of elution buffer with the GenElute HP plasmid midiprep kit (Sigma Aldrich). Plasmid preparations were analysed by restriction digestion using half of the reaction volume to that stated above (20µl in total) and incubated at 37°C for one hour. Following this 3µl of 6x MassRuler loading dye (Fermentas) was added and the samples were run on a 1% agarose TAE gel. Positive plasmid preparations were finally selected for sequencing to confirm the correct clone had been isolated.

2.3.4 DNA sequencing

All sequencing reactions were performed using the BigDye terminator v3.1 cycle sequencing kit (Applied Biosystems).

1. A PCR reaction was prepared in a 0.5ml polypropylene tube on ice with the following:

Template DNA	2-3µg genomic DNA 3-10ng for 200-500bp PCR product 5-20ng for >500bp PCR or plasmid DNA
Primer	0.32µl of 10µM stock
Ready reaction premix	4µl
BigDye sequencing buffer	2µl
Water	Up to a total of 20µl

2. A PCR reaction was performed on a PTC-200 PCR machine (MJ Research) with the following conditions:

1. 96.0°C for 1:00 minutes
2. 96.0°C for 0:10 minutes
3. 50°C for 0:05 minutes
4. 60.0°C for 4:00 minutes
5. Go to 2. X25 times
6. End

3. Precipitation: To each PCR reaction 5µl of EDTA and 60µl of absolute ethanol were added. Samples were centrifuged at 13000 rpm for 20 minutes in a Beckman Coulter Microfuge 22R centrifuge at 4°C. The supernatant was removed and the pellet was washed with 60µl of 70% ethanol. A second centrifugation was performed for 5 minutes as above. The supernatant was again removed and pellets were air dried for 15 minutes.

4. DNA pellets were submitted to Central Biotechnology Services (Cardiff University) for analysis.

2.4 Yeast transformation

The protocol was regularly used for the transformation of plasmids and stable integration of DNA via recombination.

1. 50ml of cell culture was grown to an OD600 of 0.6-0.8.
2. Cells were collected by spinning at 3600 rpm for 5 minutes in an Eppendorf centrifuge 5810R at room temperature. The pelleted cells were washed once in 20ml of water and collected as before.
3. Cells were resuspended in 15ml of lithium acetate solution (100mM lithium acetate, 10mM Tris base, 1mM EDTA, pH7.5) and left at room temperature for one hour.

4. Once permeabilised, cells were collected as before and resuspended in 500µl lithium acetate solution. For each transformation the following was added to a 1.5ml polypropylene tube:

50% Polyethylene glycol 3800, 100mM lithium acetate, 10mM Tris base, 1mM EDTA, pH7.5	300µl
Cells in lithium acetate solution	50-100µl
Denatured UltraPure salmon sperm DNA solution 10mg/ml (Invitrogen)	15µl
DNA to be transformed (plasmid ~30ng, integrating DNA ~1-10µg)	1-5µl

5. Solutions were incubated on a Mini Labroller rotator (Labnet) at room temperature for 30 minutes and then transferred into a water bath set at 42°C for 15 minutes. After 15 minutes the cells were placed on ice for 3 minutes.

6. To precipitate the cells 1ml of water was added to each tube, the solution was spun at 3600 rpm for 5minutes in an eppendorf centrifuge 5414D and the supernatant discarded. Cells were resuspended in 100µl of water and plated on selective media plates as undiluted, 1:10 diluted and 1:100 diluted cell solutions. Occasionally, to increase the efficiency of transformation, cells were resuspended in YPD and incubated for one hour in a Multitron standard incubation shaker (Infors AG) prior to plating.

7. Plates were incubated at a controlled temperature until visible colonies had formed. Transformation of the correct DNA was initially confirmed by colony PCR, and ultimately by DNA sequencing and/or confirmation of protein expression by western blot.

2.5 Colony PCR

Colony PCR was performed to check the correct integration of exogenous DNA into both *E. coli* and *S. cerevisiae* cells.

1. Cell colonies were numbered on the plate as a reference. A P10 pipette tip was used to touch each colony on the plate. Each tip was then placed into 11.5µl of water within a 0.2ml PCR tube. Tips were left for 5 minutes to allow cells to transit into solution, removed and the PCR tubes were closed and micro-waved at full power (800W) for 2 minutes. To each tube, 0.5µl of a forward and reverse primer (at a starting concentration of 10µM) were added, followed by 12.5µl of 2x ReddyMix PCR master Mix (ThermoScientific).

2. PCR reactions were vortex mixed, spun down and run on a PTC-200 PCR machine (MJ Research) with the following conditions:

1. 95.0°C for 4:00 minutes
2. 94.0°C for 0:40 minutes
3. 55.0°C for 0:50 minutes
4. 72.0°C for 1:00 minutes
5. Go to 2. +3 sec/cycle x30 times
6. 72.0°C for 10:00 minutes
7. End

3. For each sample 7µl of the PCR mix was loaded onto a 1% agarose TAE gel with a ladder to check for production of the correct product.

2.6 Protein work

2.6.1 Yeast whole protein lysates

The following protocol was performed for the isolation of the soluble protein fraction from yeast cell lysates.

1. 50ml of cell culture was grown to an OD600 of 0.6-0.8.
2. Cells were collected by spinning at 3600 rpm for 5 minutes in an Eppendorf centrifuge 5810R at room temperature.

3. Pelleted cells were resuspended in 500µl of cold yeast dialysis buffer (20mM HEPES-KOH pH7.6, 10mM magnesium sulphate, 10mM ethylene glycol tetraacetic acid, 20% glycerol) supplemented with 5µl of 100x proteinase inhibitors (1mg/ml pepstatin, 1mg/ml leupeptin, 1mg/ml chymostatin, 1mg/ml antipain, 250mM benzamide, 100mM phenylmethylsulfonyl fluoride in ethanol) and transferred to a 1.5ml polypropylene tube.

4. 500µl of acid washed glass beads (Sigma Aldrich) were added to each sample. Cells were lysed by vortexing on a Vortex Genie 2 (Scientific Industries) at the highest setting. Tubes were vortexed for 2 minutes at 4°C and then transferred to ice for 1 minute. This was repeated four times in total.

5. Lysed cells were spun for 15 minutes at 13000 rpm in a Beckman Coulter Microfuge 22R at 4°C to collect cell debris. The supernatant was transferred to a new 1.5ml tube. Protein lysates were quantified using the Bradford assay (see below), aliquoted, frozen in liquid nitrogen and stored at -80 °C.

2.6.2 Bradford Assay

The Bradford Assay was performed for the quantification of protein content. This had various applications including quantification of yeast whole protein lysates and whole cell extracts from ChIP.

1. A dye solution was prepared by diluting protein assay dye reagent concentrate (Bio-Rad) five fold in water. A series of standards and samples were then prepared in duplicate; for both standards and samples 1ml of diluted protein assay concentrate was added to a 1.6ml polystyrene cuvette (Fisher Scientific). For standards, 1.38mg/ml lyophilised bovine serum albumin (Bio-Rad) was added to produce a linear range of five standards. Typically this range lay between 2-20 µg/ml. For samples, 1µl of protein was added to the cuvette.

2. All cuvettes were mixed by brief vortexing. Standards and samples were measured for absorbance at 595nm on a Beckman Coulter DU 800 spectrophotometer. Protein concentrations of unknown samples were calculated using the systems and applications software for DU 800 UV/visible spectrophotometer (Version 2.0, Beckman Coulter), calibrated against the standard's linear range of absorbance.

2.6.3 Western blotting

All western blots were performed using the Bio-Rad Mini-PROTEAN 3. Gel electrophoresis and protein transfer were performed as described in the Mini-PROTEAN 3 instruction manual (Bio-Rad). The following account does not reiterate the entire protocol but instead includes details necessary for an exact reproduction of the work entailed.

All electrophoresis gels performed were 1.5mm thick. All stacking gels were set using the 1.5mm 10 slot combs (Bio-Rad).

1. Two western gels were always prepared at one time using the reagents listed below in table 2.1. Gel solutions were not degassed under vacuum. Ammonium persulphate (APS) and N,N,N',N'-Tetramethylethylenediamine (TEMED) were added last to prevent polymerisation prior to pouring the gel solutions. 1ml of water was added to the surface of the resolving gel prior to its polymerisation.

20ml Resolving gel – 7.5% acrylamide	20ml Resolving gel – 5% acrylamide
3.75ml 40% acrylamide/bisacrylamide 19:1 (Bio-Rad)	2.5ml 40% acrylamide/bisacrylamide 19:1 (Bio-Rad)
5.00ml 1.5M Tris-Hcl (pH8.8)	5.00ml 1.5M Tris-Hcl (pH8.8)
10.90ml H ₂ O	12.15ml H ₂ O
200µl 10% sodium dodecyl sulphate	200µl 10% sodium dodecyl sulphate
100µl 10% APS	100µl 10% APS
16µl TEMED (Sigma Aldrich)	16µl TEMED (Sigma Aldrich)
8ml Stacking gel – 4% acrylamide	
800µl 40% acrylamide/bisacrylamide 19:1 (Bio-Rad)	
5.00ml 1M Tris-Hcl (pH6.8)	
6.1ml H ₂ O	
80µl 10% sodium dodecyl sulphate	
40µl 10% APS	
8µl TEMED	

Table 2.1. Recipes used for western blot resolving and stacking gels.

2. 15µg of protein from yeast whole protein lysates were combined with water to a total of 10µl. To this 10µl of 2x SDS loading buffer (100mM Tris base, 4% sodium dodecyl sulphate (SDS), 0.2% bromophenol blue, 20% glycerol, 20mM dithiothreitol, pH6.8) was added. Protein samples were subsequently heated to 95°C for 10 minutes.

3. Each 20µl sample was subsequently loaded to the polyacrylamide gel. Each gel included one lane loaded with 10µl of Kaleidoscope Precision Plus protein standards (Bio-Rad).

4. Polyacrylamide gels were run using 1x SDS-PAGE running buffer (25mM Tris base, 250mM glycine, 0.1% SDS, pH8.3) at 100V on a power-pac 300 (Bio-Rad) for 60 to 180 minutes at 4°C.

5. Proteins were transferred from the gel to Immuno-Blot PVDF 0.2µm for protein blotting (Bio-Rad). PVDF membranes were cut to the same size as the gel, submerged in methanol and then water prior to loading to a cassette. Transfer was performed using Western transfer buffer (25mM Tris-base, 150mM glycine, 20% methanol, 0.015% SDS) at 4°C, 100V for 90 minutes.

6. Following transfer membranes were air dried for 40 minutes, submerged in methanol, and then water and transferred to a plastic tank. Membranes were blocked in 2% ECL advance blocking reagent (GE Healthcare) TBST (150mM sodium chloride, 10mM Tris-HCl pH 8.0, 0.05% TWEEN 20 (Sigma Aldrich)) overnight at 4°C. Membrane tanks were rocked at 20 rev/min on a Stuart Scientific platform shaker STR6.

7. In the morning membranes were prepared for chemiluminescent detection. The entire procedure was performed at room temperature on the platform shaker at 20 rev/min. Membranes were first washed in 20ml TBST for 5 minutes. A primary antibody was diluted in 10ml 2% ECL advance blocking reagent TBST. Membranes were incubated with the primary antibody for one hour. Then three washes of 20ml TBST for 10 minutes were performed. A secondary antibody was diluted in 10ml 2%

ECL advance blocking reagent TBST. Membranes were incubated with the secondary antibody for one hour. A final three washes of TBST for 10 minutes were performed.

8. Chemiluminescent antibodies bound to the membranes were detected using ECL advance solution (GE Healthcare). Membranes were removed from TBST and blotted dry using tissue paper at the membrane edge. 1.5ml of development solution (solution A and B mixed) was applied to the membrane surface and left for 5 minutes. Membranes were subsequently blotted dry as before and applied to a plastic sheet for detection.

9. Chemiluminescence was detected with the AutoChemi BioImaging system (UVP) and images were captured using Labworks (Version 4.6.00.0, UVP). Typically images were exposed for 1 minutes 30 seconds, and re-exposed up to 9 times.

10. Reprobing membranes: Membranes were incubated with 100ml stripping buffer (62.5mM Tris-HCl pH6.7, 2% SDS, 100mM 2-mercaptoethanol) for 30 minutes at 50°C with moderate shaking on a Hybaid Maxi 14 hybridization oven (ThermoScientific). Stripped membranes were washed for 5 minutes in TBST and blocked for one hour in 2% ECL advance blocking reagent TBST. The protocol was then resumed from step7.

2.7 Chromatin immunoprecipitation (ChIP)

ChIP was performed in a similar manner to that previously detailed (Yu et al., 2009).

1. 100ml cell samples were grown either in YPD or selective media to a density 2×10^7 cells/ml.

2. To crosslink cells, 2.8ml of 36.5% formaldehyde (Sigma) was added to the medium. Cell samples were left to crosslink for 20 minutes during which time, samples were mixed every 5 minutes by swirling by hand.

3. After 20 minutes, 5.5ml of 2.5M glycine was added and left at room temperature for 5 minutes. Subsequently, each cell sample was equally divided into two 50ml polypropylene conical tubes (Falcon).

4. Cells were pelleted by centrifugation at 4000rpm for 5minutes at 4°C in an Eppendorf centrifuge 5810R. Cells were resuspended in 20ml of TBS (25 mM Tris, 150 mM NaCl, 2 mM KCl, pH 7.4) at 4°C and pelleted by centrifugation as before. Each sample was combined from the two conical tubes by resuspending the pellets in 500µl TBS (4°C) and transferring both cell solutions to a single 1.5ml polypropylene tube. Cells were pelleted by centrifugation at 4000rpm for 5minutes at 4°C in a Beckman Coulter Microfuge 22R centrifuge, resuspended in 1ml lysis buffer (50mM HEPES-KOH pH7.4, 140mM NaCl, 1mM EDTA, 0.5% Igepal CA-630, 0.5% sodium deoxycholate), and pelleted once more as before. The mass of each cell pellet was measured using a Sarorius CP 124 S scale. These were flash frozen in liquid nitrogen and stored overnight at -80°C.

5. Cell pellets were thawed, and resuspended in 500µl of lysis buffer supplemented with 5µl 100x proteinase inhibitors. To this 500µl of acid washed glass beads (Sigma) were added. Cells were lysed by vortexing the tubes on a Vortex genie 2 on the highest setting for 15 minutes at 4°C.

6. The cell lysate was separated from glass beads as shown in Fig. 2.1. A 25G needle was heated under a Bunsen burner and used to make a small hole in the base of the 1.5ml tube. These were subsequently placed into 2ml polypropylene tubes. Cell lysate was collected by a short centrifugation at 2000rpm, 4°C. 200µl lysis buffer/1x proteinase inhibitors was added to the glass beads to wash away remaining lysate and collected as before.

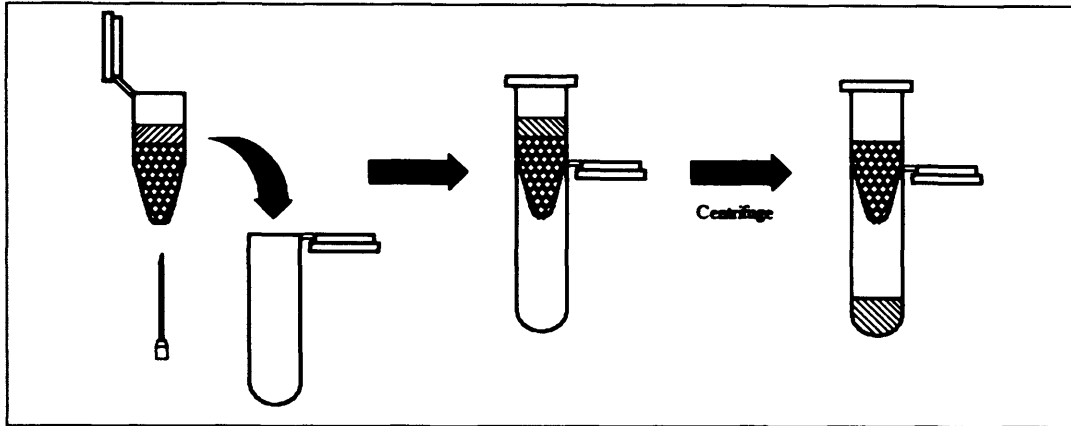


Figure 2.1. Cartoon representing the separation of cell lysate from glass beads.

7. The cell lysate was centrifuged at 13,000rpm for 15 minutes at 4°C in a Beckman Coulter Microfuge 22R. The supernatant was decanted to remove the soluble protein fraction. Cell pellets were resuspended according to their mass; 100µl lysis buffer/1x proteinase inhibitors was added per 0.01g of cell pellet.

8. For sonication 0.5-1ml of cell lysate was pipetted into 15ml centrifuge tubes (Corning). Using a Bioruptor (Diagenode) three cell lysate samples were sonicated at a time with amplification poles for six cycles of 30 seconds on/ 30 seconds off at highest setting (200W), 4°C. This typically sheared DNA to an average length of 200-800bp (see Fig. 2.2A).

9. To pellet cell debris, sonicated samples were transferred to a 1.5ml polypropylene tube and centrifuged at 13,000rpm for 20 minutes at 4°C in an Eppendorf centrifuge 5810R. The supernatant was collected, aliquoted and flash frozen in liquid nitrogen. In addition, protein was quantified using the Bradford assay. For all immunoprecipitation and input samples an identical volume was aliquoted totalling ~300µg of protein.

2.7.1 Immunoprecipitation (IP)

10. Immunoprecipitated antibody-antigen complexes were isolated using Protein G sepharose 4 fastflow (GE healthcare). Sepharose beads were twice washed in 1ml lysis buffer and collected by centrifugation at 3000rpm for 2 minutes on an Eppendorf

centrifuge 5810R. Beads were equilibrated by incubating in 1ml lysis buffer/400µg/ml single stranded salmon sperm DNA (Sigma)/10µg/ml BSA (NEB) for one hour at 4°C on a Mini Labroller rotator (Labnet). Finally beads were washed twice in 1ml lysis buffer as above and resuspended with lysis buffer to make a 50% bead slurry (v/v).

11. To each immunoprecipitation sample lysis buffer/0.25% SDS/1x proteinase inhibitors was added to total volume of 500µl. To clear the solution of non-specific interactions 20µl of beads slurry was added and incubated at 4°C on a Mini Labroller rotator (Labnet) for 2-3 hours at 4°. Following this, beads were collected as above and the solution transferred to a fresh 1.5ml tube.

12. Antibody was added to each sample and left to incubate overnight at 4°C on a Mini Labroller rotator (Labnet). Antibody necessary for maximal chromatin immunoprecipitation was determined empirically by titrating the concentration and calculating DNA content by qPCR (see below). Antibody-antigen complexes were captured by adding 40µl of bead slurry the next morning and incubation was continued for 3 hours at 4°C.

13. To remove non-specific interactions, beads were sequentially washed with the four buffers below. All washes were incubated at room temperature for 10 minutes on a Mini Labroller rotator (Labnet). Beads were collected by centrifugation (2000rpm, 2minutes, Eppendorf 5415D centrifuge) and the supernatant aspirated through a 25G microlance needle to avoid removing beads.

Wash 1. Lysis buffer

Wash 2. Lysis buffer with an increased NaCl concentration of 500mM.

Wash 3. LiCl buffer (10mM Tris-HCl, 250mM LiCl, 1mM EDTA, 0.5% Igepal CA-630, 0.5% sodium deoxycholate)

Wash 4. TE buffer (10mM Tris-Cl, pH7.5, 1mM EDTA)

2.7.2 Preparation of DNA from immunoprecipitated and input samples

14. **Input samples:** Input solution volume was adjusted to 80µl with lysis buffer to which 20µl of 5x pronase buffer (125mM Tris-HCl pH7.5, 25mM EDTA, 2.5% SDS) and 6µl of 20mg/ml pronase (Roche) was added.

Immunoprecipitation samples: Following aspiration of the TE wash, beads were resuspended into 110µl 1x pronase buffer (25mM Tris-Cl pH7.5, 5mM EDTA, 0.5% SDS) and heated at 65°C on a Thermomixer comfort (Eppendorf) with shaking at 1400rpm for 15 minutes to interrupt protein-protein interactions. Samples were centrifuged at 13,000 rpm for 2 minutes on an Eppendorf 5415D centrifuge and 100µl of the solution was transferred to a fresh 1.5ml polypropylene tube. 6µl of 20mg/ml pronase (Roche) was added.

15. **For all samples:** Protein was digested by incubating the solutions at 65°C overnight. In the morning, 1ml of 10mg/ml RNase A (Sigma) was added and left to incubate at 37°C for 30 minutes.

16. Each sample DNA was purified to 30µl EB buffer using the QIAquick PCR purification kit (Qiagen) according to the manufacturer's instructions.

17. To ensure that sonicated DNA samples were evenly sheared and to an appropriate length (~200-800bp), 10µl of each input DNA was run on a 1.5% TAE agarose gel alongside 5µl of FastRuler low range DNA ladder (Fermentas). A gel typical of sheared DNA appropriate for chromatin immunoprecipitation is shown in Fig. 2.2A.

2.7.3 Quantification of DNA by qPCR

1. All DNA samples were quantified by quantitative PCR (qPCR) using SYBR green I. Typically, one input sample was diluted into water to prepare a 10-fold dilution range from 10^{-1} down to 10^{-5} . This range was used as a reference for relative DNA quantification between samples. For quantification, all input samples were diluted 1000-fold in water and all immunoprecipitation samples were diluted 4-fold in water.

2. All qPCR reactions were performed in 96 well PCR plates (Type: LW2215, Alpha Laboratories) and each reaction was prepared with the reagents listed in the below table. A mastermix of all reagents excluding the DNA sample to be quantified was prepared and 18µl aliquots were dispensed into wells using an Eppendorf multipette stream.

qPCR wells each contained:

2x iQ SYBR Green Supermix (Biorad)	10µl
Primer 1 (100µM)	0.06µl
Primer 2 (100µM)	0.06µl
H ₂ O	7.88µl
DNA to be quantified	2µl
Total	20µl

3. All PCR reactions to be quantified were repeated in triplicate including the dilution range. Plates were film sealed and DNA was quantified using an icycler thermal cycler (Bio-Rad) coupled to a My iQ optics module (BioRad). qPCR reactions were performed under the following conditions:

1. 95°C for 3 minutes
2. 95°C for 0:15 minutes
3. 55°C for 0:20 minutes
4. 55°C for 0:10 minutes – followed by optical image
5. Go to 2. x44 times
6. 95°C for 1:00 minutes
7. 55°C for 0:30 minutes
8. Melt curve from 55°C

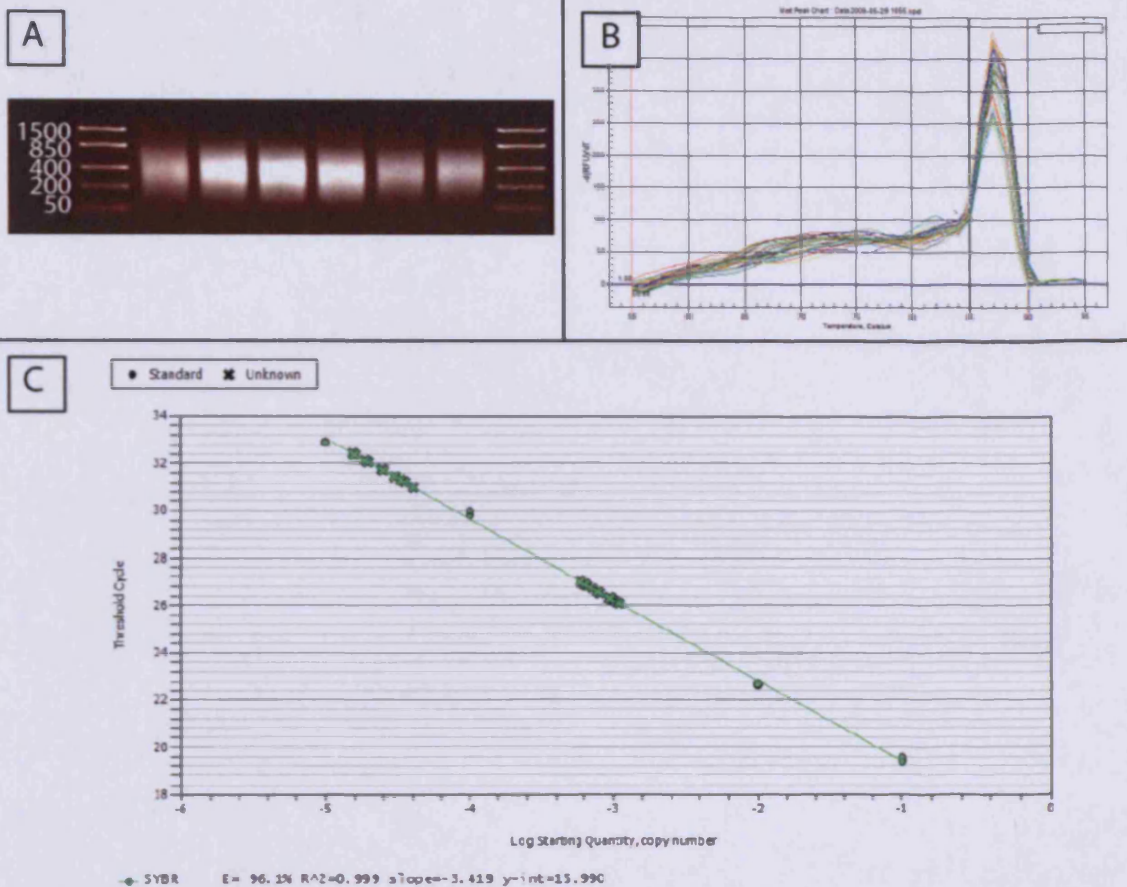


Figure 2.2. A. Gel of typical input samples. The size in bp of the ladder references is given to the left. B. Example of an acceptable qPCR melt curve demonstrating amplification of a single product. C. Graphical representation of the qPCR results. Standards are shown as green circles, unknown samples green crosses. In the example, all unknown samples lie within the linear range of quantification.

2.7.4 Quantifying the relative occupancy of protein-chromatin binding

1. All qPCRs were analysed using the Bio-Rad iQ5 software. Prior to quantification the data was scrutinised to determine whether the reaction had suitably proceeded. The following criteria were evaluated. Firstly, any qPCR reaction that showed a marked variation from 100% efficiency was disregarded. Secondly, any reaction that did not display a single uniform peak on a melt curve was disregarded (Fig. 2.1). Thirdly, all unknown DNA samples had to be quantified within the linear range. iQ5 graphically displays the Ct value of the standard dilution range combined with unknown samples (see Fig 2.1). Only unknown samples in which the Ct value lay within the linear range of quantification were accepted. Lastly, each data triplicate was visually inspected to confirm that all three repeats gave a reproducible Ct value, and single errors were deleted.

2. All data was exported from iQ5 in excel format. The occupancy of immunoprecipitated DNA at given genetic locus was calculated as follows:

$$\text{DNA occupancy} = \frac{\text{Starting quantity (SQ) mean of immunoprecipitated sample (IP)}}{\text{Starting quantity (SQ) mean of input sample (Input)}}$$

2.8 ChIP-on-chip

ChIP samples were prepared for microarray analysis using a similar protocol to that previously detailed (Teng et al., 2010). The protocol first repairs DNA damage and then amplifies DNA using ligation mediated PCR. Amplified DNA is labelled by Cy5 and Cy3 dyes and subsequently applied to microarrays.

1. Following the ChIP protocol, 20-40µl of IP or 1µl of input purified DNA was diluted with water to a total volume of 40µl. DNA damage within each sample was repaired using the PreCR repair mix (NEB). To each sample 10µl of repair mix was added and incubated for 20 minutes at 37°C. Repaired DNA was purified to 50µl EB buffer by the QIAquick PCR purification kit (Qiagen).

Repair mix

dNTP (10mM)	0.5 µl
10xThermoPol buffer	5 µl
100xNAD ⁺	0.5 µl
PreCR repair mix	1 µl
Water	3 µl
Total	10µl

2. To each sample 70µl of blunt end mix was added and incubated for 20 minutes at 12°C. Following this incubation, 11.5µl of 3M NaAc (pH5.2) and 0.5µl glycogen (20mg/ml) were added and mixed by pipette. Then 120µl of phenol:chloroform:isoamly alcohol 25:24:1 (10mM Tris, pH8.0, 1mM EDTA) was added and samples were mixed by vortex, and subsequently centrifuged at 13000 rpm for 5 minutes in an Eppendorf centrifuge 5415D. The upper phase of each sample was transferred to a new tube and DNA was precipitated with 230µl absolute ethanol by centrifugation at 13000 rpm for 15 minutes at 4°C in a Beckman Coulter Microfuge

22R. The supernatant was removed and the pellet was washed with 500µl of 75% ethanol and centrifuged as before for 5 minutes. Following this the wash was discarded and pellets were dried for 10 minutes in an ISS110 SpeedVac system (ThermoSavant) on the medium setting.

Blunt end mix

T4 DNA polymerase buffer	11 µl
BSA (10mg/ml)	0.5 µl
dNTP (10mM)	1 µl
T4 DNA polymerase (NEB #M0203S)	0.2 µl
Water	57.8 µl
Total	70 µl

3. Pellets were resuspended in 25µl of water to which 25µl of ligation mix was added and left overnight at 16°C.

Ligation mix

DNA ligase buffer	5 µl
Linker hybrid DNA	6.7 µl
T4 DNA ligase (NEB #M0202S)	0.5 µl
Water	13 µl
Total	25 µl

4. In the morning 6µl of NaAC (3M) was added to each sample. To this 130µl of ethanol was added and DNA was subsequently precipitated in an identical fashion to that detailed in step 2. Pellets were resuspended in 25µl of water to which 15µl of PCR mix A was added and the solution was transferred to 0.5ml PCR tubes. Each sample was heated in a PCR block for 2 minutes at 55°C (PTC-200 PCR machine (MJ Research)), after which 10µl of PCR mix B was added. PCR was performed with the conditions shown below.

PCR mix A

5xHF Buffer (Finnzymes #F-518)	8 µl
dNTP (10mM)	1.25 µl
Oligo 102 (40µM)	1.25 µl
Water	4.5 µl
Total	15 µl

PCR mix B

5xHF Buffer (Finnzymes #F-518)	2 µl
Phusion DNA polymerase (Finnzymes #F-530)	1 µl
Water	7 µl
Total	10 µl

PCR conditions:

1. 55.0°C for 2:00 minutes
2. 72.0°C for 3:00 minutes
3. 98.0°C for 1:00 minutes
4. 55.0°C for 0:30 minutes
5. 72.0°C for 1:00 minutes
6. Go to 3. X14 times
7. 72.0°C for 5:00 minutes
8. End

5. Following the PCR reaction, 450µl of water was added to each sample and a second PCR amplification was performed with 5µl of the diluted DNA in combination with 45µl of PCR mix 2 and using steps 3 to 8 of the above PCR conditions.

PCR mix 2

5xHF Buffer (Finnzymes #F-518)	10 µl
NTP (10mM)	1.25 µl
Oligo 102 (40µM)	1.25 µl
Phusion DNA polymerase (Finnzymes #F-530)	0.5 µl
Water	32 µl
Total	45 µl

6. These PCR reactions were precipitated by adding 25µl of Ammonium acetate (7.5M) and 225µl of absolute ethanol and preceded in a similar fashion to that stated in step 2. DNA pellets were resuspended in 13µl of water and DNA concentration was quantified using a Nanodrop 1000 spectrophotometer (ThermoScientific). DNA concentrations were adjusted to 150ng/µl with water.

7. DNA was labelled using the BioPrime total genomic labelling system (Invitrogen) by combining the following:

Labelling reaction

DNA sample in water (150ng/μl)	10.5 μl
EDTA (5mM)	2.5 μl
Alexa Fluor Cy3 or Cy5 reaction mix	15 μl
Water	10 μl
Total	22 μl

Typically IP samples were labelled with Cy5 and input samples were labelled with Cy3.

8. Reaction mixes were incubated at 95°C for 5 minutes in a PCR block (PTC-200 PCR machine (MJ Research)). Each sample was subsequently put on ice for 5 minutes and 2μl of Exo-Klenow fragment was added. Samples were returned to the PCR block at 37°C for 2 hours.

8. Labelled DNA was purified to 51.5μl buffer E1 using Invitrogen columns according to the manufacturer's protocol. Purified DNA (1.5μl) was measured using the Nanodrop 1000 spectrophotometer (ThermoScientific), according to manufacturer's protocol.

9. Corresponding IP and input samples were combined to give a total solution volume of 100μl, to which 12μl of NaAc (3M) and 5μl Polyacrylamide (2.5μg/ml) was added. DNA was precipitated with 290μl of absolute ethanol in an identical fashion to that detailed in step 2.

10. Pellets were resuspended in 39μl of water, and to each sample the following were added in order:

Human Cot-1 DNA (1.0mg/ml) (Invitrogen)	5 μl
10x Blocking agent (Agilent)	11 μl
2x Hybridisation buffer (Agilent)	55 μl

11. Samples were mixed and heated at 95°C for 3 minutes in a PCR block. Following this, samples were immediately transferred to another PCR block at 37°C and incubated for 30 minutes.

12. Each 110µl sample was loaded onto one of four arrays on a yeast whole genome ChIP-on-chip microarray 4x44K (Agilent, #G4493A). Slides were transferred to an Agilent Hybridization oven (G2545A) set at 65°C and the maximal rotation speed (20) and left to incubate for ~24 hours.

13. Following hybridisation, slides were washed in ChIP wash buffer I and then ChIP wash buffer II for 5 minutes each according to the manufacturer's protocol (Agilent).

14. Features were extracted using an Agilent microarray scanner (G2505B, Agilent technologies) according to the manufacturer's instructions with the following settings:

Scan region	61 x 21.6 mm
Scan resolution	5µm
5µm scanning mode	Single pass
eXtended dynamic range	Selected
Dye channel	Red & Green
Green PMT	XDR Hi 100%, XDR Lo 10%
Red PMT	XDR Hi 100%, XDR Lo 10%

15. TIFF files of the scanned slides were analysed using Agilent feature extraction software (version 10.10.1.1) and the protocol ChIP_1010_Sep10 according to the manufacturer's instructions. Data was exported as a tab delimited text file (.tab). Data under the column titles 'Row', 'Col', 'ProbeUID', 'ControlType', 'ProbeName', 'GeneName', 'SystematicName', 'Description', 'rBGSubSignal' and 'gBGSubSignal' were extracted from the text files and imported into the statistical open source software language 'R' as an RGList using the bioconductor package Limma (M. Bennet; unpublished results, Gentleman, 2005; Team, 2010). 'gBGSubSignal' represents the quantification of Cy3 labelled DNA hybridisation, which is referred to as 'Green channel' or G. 'rBGSubSignal' represents the quantification of Cy5 labelled DNA hybridisation, which is referred to as 'Red channel' or R. All subsequent data analysis was performed in R using custom scripts written by Mark Bennett (unpublished results, Team, 2010). The binding profile for ChIP-on-chip experiments was calculated as R/G.

3. Mapping the genome-wide localisation of Abf1 in the absence and presence of UV damage

3.1 Introduction

Since the development of microarrays and other high throughput technologies, an ever increasing wealth of genome-wide datasets are becoming available and rapidly driving a new era of scientific discovery. Of these technologies, the use of ChIP followed by hybridisation to microarrays (ChIP-on-chip) has proven to be a powerful technique for mapping the genome-wide localisation of a variety of features including protein-chromatin interactions (Venters et al., 2011), histones and histone modifications (Pokholok et al., 2005) and even direct DNA damage (Teng et al., 2010). The relative ease of growing large cell numbers, genetically epitope tagging proteins and mapping the small genome of *S. cerevisiae* has consequently resulted in the vast majority of studies in this field to adopt this organism. Furthermore, a wide variety of other genome-wide studies (such as differential expression profiles) are available for *S. cerevisiae*, providing a platform for correlative studies.

One field with which ChIP-on-chip has significantly contributed is in examining how TFs are organised throughout the genome. A large body of evidence indicates that TFs function in complex and diverse manners. This is best exemplified by two fundamental studies that have examined the localisation of nearly all ~200 TFs encoded in the yeast genome (Harbison et al., 2004; Lee et al., 2002b). These studies demonstrated not only a wide variance in the numbers of genes bound by a TF but also that many genes are frequently bound by numerous TFs or even multiple times by the same TF. In addition, by re-examining the localisation of many TFs in response to various environmental stresses, the latter study further demonstrated TFs are often redistributed in response to external stimuli (Harbison et al., 2004). Other studies have similarly demonstrated the relocation of TFs by ChIP-on-chip in response to glucose depletion, galactose, pheromones, DNA damage, heat and osmotic shock (Buck and Lieb, 2006; Ni et al., 2009; Ren et al., 2000; Tan et al., 2008; Zanton and Pugh, 2006). Four patterns of binding behaviour have been categorised in response to an environmental stress; condition invariant (does not change localisation), condition enabled (binding activated), condition expanded (target gene number increases) and condition altered (target gene preferences change) (Harbison et al., 2004). These data

suggest that the DNA binding of many TFs is regulated necessary for transcriptional responses to environmental stress.

Abf1 itself has been the subject of numerous genome-wide studies. The first gene expression profiling study that attempted to identify genes regulated by Abf1 genome-wide, compared wild type strains to those expressing the temperature sensitive DNA binding mutant *abf1-1* at both the permissive and restrictive temperature (Miyake et al., 2004). This study identified 86 genes differentially regulated (>1.8 fold change, $p<0.001$) due to the loss of Abf1 binding in the temperature sensitive mutant. Of these, 50 were positively regulated by Abf1, and 36 negatively regulated. A second study, using a similar strategy identified 235 genes that were differentially expressed in the *abf1-1* strain (Yarragudi et al., 2007). Whilst these two studies demonstrate Abf1 clearly influences the transcription of a large number of gene targets, the estimations are likely to be under representative; for example, one or more Abf1 consensus DNA binding sequences have been identified in 1049 promoters (Schlecht et al., 2008). Indeed, a third study using the *abf1-1* mutant and less stringent selection criteria identified 3214 genes potentially regulated by Abf1 (Schlecht et al., 2008). One fundamental difference in this study was that differential gene expression was sampled during three environmental conditions; fermentation, respiration and sporulation. For each condition a subset of genes was observed to be uniquely differentially expressed; 626 genes during fermentation, 966 genes during respiration and 627 genes during sporulation. This suggests that the activities of Abf1 can target different genes in response to an environmental stimulus. One difficulty presented within all three studies, was correlating gene expression targets with the physical location of Abf1. In all cases, the presence of Abf1 at gene promoters from ChIP-on-chip studies (discussed below) was evident for less than 50% of the targets identified. One possible explanation for these observations is that previous studies that have mapped Abf1 binding have failed to sensitively assay all Abf1 binding sites within the genome.

To date, three studies have examined the global localisation of Abf1 using ChIP-on-chip technology. The first two studies analysed the occupancy of a large number of yeast TFs by Myc epitope tagging the proteins and limiting their analysis to intergenic regions of the yeast genome. Lee et al. identified 462 Abf1 binding sites ($P<0.005$), whilst Harbison et al. identified 458 Abf1 binding sites ($P<0.005$) (Harbison et al., 2004; Lee et al., 2002b). The latter study also included how the

location of TFs changed in response to different environmental stresses. Whilst this analysis did not include Abf1, it did demonstrate that other GRFs such as Rap1 and Reb1 dynamically change their genome-wide distribution in response to environmental stresses such as DNA damage and heat shock. When the data from Lee et al. was combined with expression studies under a variety of environmental stresses, a subset of Abf1 bound genes were differentially expressed in all conditions tested, whilst other subsets were found to be differentially regulated under only one specific condition (Luscombe et al., 2004). This was interpreted to mean that Abf1 dynamically interacts with a subset of its target genes according to environmental stresses, whilst consistently maintaining the regulation of other gene subsets (likely housekeeping genes). This idea is further supported by the study of Schlecht et al during fermentation, respiration and sporulation (Schlecht et al., 2008). The authors included a ChIP-on-chip analysis of Abf1 binding at both intergenic and genic regions, identifying 1689 genes potentially bound by the protein (using non-stringent selection criteria). Of these, 387 genes were also identified by Harbison et al (2004). Whilst 1169 genes were bound in all three conditions, Abf1 was suggested to exclusively occupy 82 novel genes during fermentation, 105 during respiration and 331 during sporulation.

One prominent feature of all three ChIP-on-chip studies described above is that they all predict a remarkably similar consensus DNA binding sequence for Abf1 as that derived from in vitro studies (Mukherjee et al., 2004). This strongly suggests DNA is the predominant determinant of Abf1 binding in vivo. Indeed, the Abf1 DNA binding motifs established by in vitro protein binding microarrays are highly represented at in vivo Abf1 binding peaks (Gordan et al., 2009). In addition, high resolution genome-wide maps of nucleosome occupancy demonstrate that the Abf1 DNA binding consensus sequence is the most commonly found motif in NDRs (Lee et al., 2007b). These NDRs are not inherently encoded within the DNA sequence since in vitro reconstitution of chromatin with purified DNA and histone proteins does not recapitulate the NDRs (Kaplan et al., 2009). Indeed, ectopic addition of an Abf1 binding site into DNA in vivo has been demonstrated to occlude nucleosome occupancy proximal to the insertion (Yarragudi et al., 2004). Furthermore, a study that analysed nucleosome occupancy on chromosome III demonstrated a loss of 9% of promoter NDRs in response to Abf1 depletion (Hartley and Madhani, 2009). The majority of NDRs in yeast are found within gene promoters (Lee et al., 2007b). The

high association of an Abf1 consensus DBS with NDRs has provided a novel method for mapping Abf1 genome-wide DNA binding in vivo (and other TFs) by using a DNaseI footprint assay coupled to massively parallel DNA sequencing (Hesselberth et al., 2009). By identifying short nucleotide regions within NDRs that are protected and map to a DNA binding consensus sequence, the location of various DNA binding proteins can be estimated. Using this assay, 536 sites were identified that contained a signature pattern of DNaseI protection over the Abf1 consensus DNA binding sequence. These sites were observed to typically occupy a region ~100bp upstream of a transcription start site (TSS). The frequent occupancy of Abf1 within this region of a promoter has similarly been discerned by other authors (Ganapathi et al., 2010; Lee et al., 2007b; Yarragudi et al., 2007). Collectively, these data strongly suggest the vast majority of interactions between Abf1 and chromatin occur through direct protein-DNA interactions.

Abf1 forms a stable heterotrimeric complex with Rad7 and Rad16 termed the GGR complex (Yu et al., 2004). Rad7 and Rad16 are necessary for the majority of GGR in vivo (Teng et al., 1997; Verhage et al., 1994). The mechanism through which Rad7/Rad16 promotes GGR in vivo has long been considered to include chromatin remodelling, and recent evidence has demonstrated that this is significantly promoted by Rad16 dependent histone H3 K9K14 hyperacetylation after UV (see Chapter 1.4.4 and 4.1 for further discussion, Teng et al., 2008; Yu et al., 2011). Currently, the precise role of Abf1 in the GGR complex is less well understood. Previous studies with strains expressing temperature sensitive mutants of Abf1 demonstrated a correlation between the ability of Abf1 to bind DNA and the proficient repair of UV induced DNA lesions in vivo (Reed et al., 1999). It was subsequently shown that the Abf1 DBS within the *HMLα* I-silencer positively regulated the kinetics of CPD repair at a domain extending ~400bp from the binding site (Yu et al., 2009). This suggests that the site specific DNA binding activity of Abf1 promotes efficient binding of the GGR complex and consequently repair at regions of the genome to which it binds (see Chapter 1.5.5 for further discussion). Efficient repair at the *HMLα* I-silencer was observed to occur concurrent with changes in the occupancy of Abf1. However, it was not established whether the initial increase, nor subsequent decrease in Abf1 occupancy after UV was related to its role in promoting GGR. Interestingly though, these changes in occupancy may suggest a dynamic relocalisation of Abf1 occurs in response to UV, a phenotype observed for many TFs in response to various

environmental stresses (discussed above). The present study investigates the relationship between GGR and Abf1 DNA binding in vivo using ChIP-on-chip studies. The genome-wide localisation of Abf1 is mapped both before and after UV to investigate how changes in Abf1 binding may be related to the molecular mechanism of GGR. In addition, both histone H3 K9K14 acetylation and CPD repair are examined at Abf1 binding sites to investigate how GGR is organised in relation to Abf1 binding.

3.2 Materials and Methods**Strains used in this study:**

Strain	Genotype	Source
BY4742	MAT α , his3 Δ 1 leu2 Δ 0 lys2 Δ 0 ura3 Δ 0	Euroscarf

ChIP-on-chip/ChIP

BY4742 was grown in YPD at 30°C up to a density of 2×10^7 cells/ml and UV irradiated as described in Chapter 2.2. ChIP was performed as detailed in Chapter 2.7. For IP samples, 100 μ l of WCE was immunoprecipitated with 20 μ l α -Abf1 antibody (yC-20, #sc-6679, Santa Cruz Biotechnology). Input samples were purified from 50 μ l of WCE. ChIP samples were prepared for ChIP-on-chip analysis as described in 2.8.

Data values of microarray quantification in Fig. 3.7 and 3.8 are available in appendix II.

ChIP-on-chip chromosomal maps

Chromosomal maps of the averaged traces of ChIP-on-chip data for all Abf1 datasets are available on the accompanying DVD (D:/Chapter 3/ChIPchip).

Primers used for qPCR:

prRPL24A:

Forward: 5' – TTGGTGTCTTGCTTAACTTGG

Reverse: 5' – ACGGGAGGAAATACACACA

Corresponding microrray probe: A_75_P01412828

ARS231:

Forward: 5' – CCCGTCTCTCCGGTCATATT

Reverse: 5' – GCATAGCTTGCTCAATACGC

Corresponding microrray probe: A_75_P01042310

NAT4:

Forward: 5' – TATATGAGGCGCTTGGGTTC

Reverse: 5' – GTCGGAGTCAAGGATTCGAG

Corresponding microrray probe: A_75_P01862612

HML- α I-silencer:

Forward: 5' – CAACATGAAAGCCCGACGTTTG

Reverse: 5' – TTTGATTTTTTCACCCAGAACCCCA

Corresponding microarray probe: A_75_P01104456

Data values of qPCR quantification are available in appendix II. Error bars represent the standard deviation of replicates.

Data normalisation and statistical analysis

All ChIP-on-chip data was exported into 'R' as background subtracted values (see Chapter 2.8). R is an open source software language used for the statistical analysis of data and graphical representation (R Development Core Team, 2010). All probes for mitochondrial DNA and deleted genes (markers) were removed from datasets prior to data analysis. Both quantile normalisation, and shift by mode data manipulations on R/G signals, as well as the peak detection algorithm were performed in R using custom scripts by M.Bennet (unpublished results, R Development CoreTeam, 2010). Averaged datasets were produced using the mean of three normalised biological repeats. Linear chromosomal maps of ChIP-on-chip enrichment were plotted in R using custom scripts by M.Bennett (unpublished results, R Development CoreTeam, 2010). All linear correlations were analysed in R using standard pearson correlation analysis, while all non-linear correlation analysis used standard spearman methods. T-tests were performed in R using a two sided independent samples t-test ($p < 0.05$) assuming non-equal variance. All scatter graphs and box plots were produced in R.

Composite profiles

In this study composite profiles are defined as graphs which repeatedly plot and superimpose ChIP-on-chip data over a range of 4kb. The data is centred at either Abf1 binding peaks or intergenic regions in this chapter, and at Abf1 or Rad16 binding peaks in Chapter 4. An example is given for Abf1 binding in Fig. 3.1. In this circumstance, for every Abf1 binding peak, the composite profile plots 4kb of Abf1 ChIP-on-chip data with the peak position itself at the centre of the graph (a profile). This is repeated for every Abf1 binding peak, and all the profiles are superimposed (composite profile). When this is complete a trendline, which represents the mean

pattern formed by all the profiles is displayed. Composite profiles used in this study were performed in R using custom scripts by M.Bennett (unpublished results, R Development CoreTeam, 2010). All composite profiles in this study used averaged datasets. The trendline represents the mean of the plotted data (50 means are taken along the course of the composite profile).

For scaled chromosomal position (SCP) composite plots, data is centred at intergenic regions between genes (rather than Abf1 binding sites), the borders of which are defined by annotation data from SGD (<http://www.yeastgenome.org/>). All SCP composite profiles exclusively plot intergenic regions of at least 300bp in length, and include 1kb of an ORF either side, unless the ORF is less than 1kb in length. SCP functions to scale profiles such that all intergenic regions are the same length, this scaling applies both to the intergenic and ORF profiles plotted (see Fig. 3.1 D and E). All SCP composite plots that include promoters function to exclude intergenic regions classified as 'downstream'; see Fig.3.6 for a picture of this classification.

Note for Fig. 3.12C

The Rad16 dependent repair rate was calculated by subtracting the *rad16Δ* CPD repair rate (Red channel/Green channel) from the wild type CPD repair rate (Red channel/Green channel) at each position on the yeast microarray. A constant was added to the resultant repair rate at every probe so that every value was a positive number. This does not function to skew the data, nor affect the distributions presented in these figure but does result in higher arbitrary values than those seen in other figures. For graphical representation the Rad16 dependent repair rate was converted to log₂.

Other ChIP-on-chip datasets used in this study

The CPD repair and histone H3 K9K14 acetylation datasets used in this study were kindly provided by K.Evans and Y.Teng (unpublished results, Teng et al., 2010).

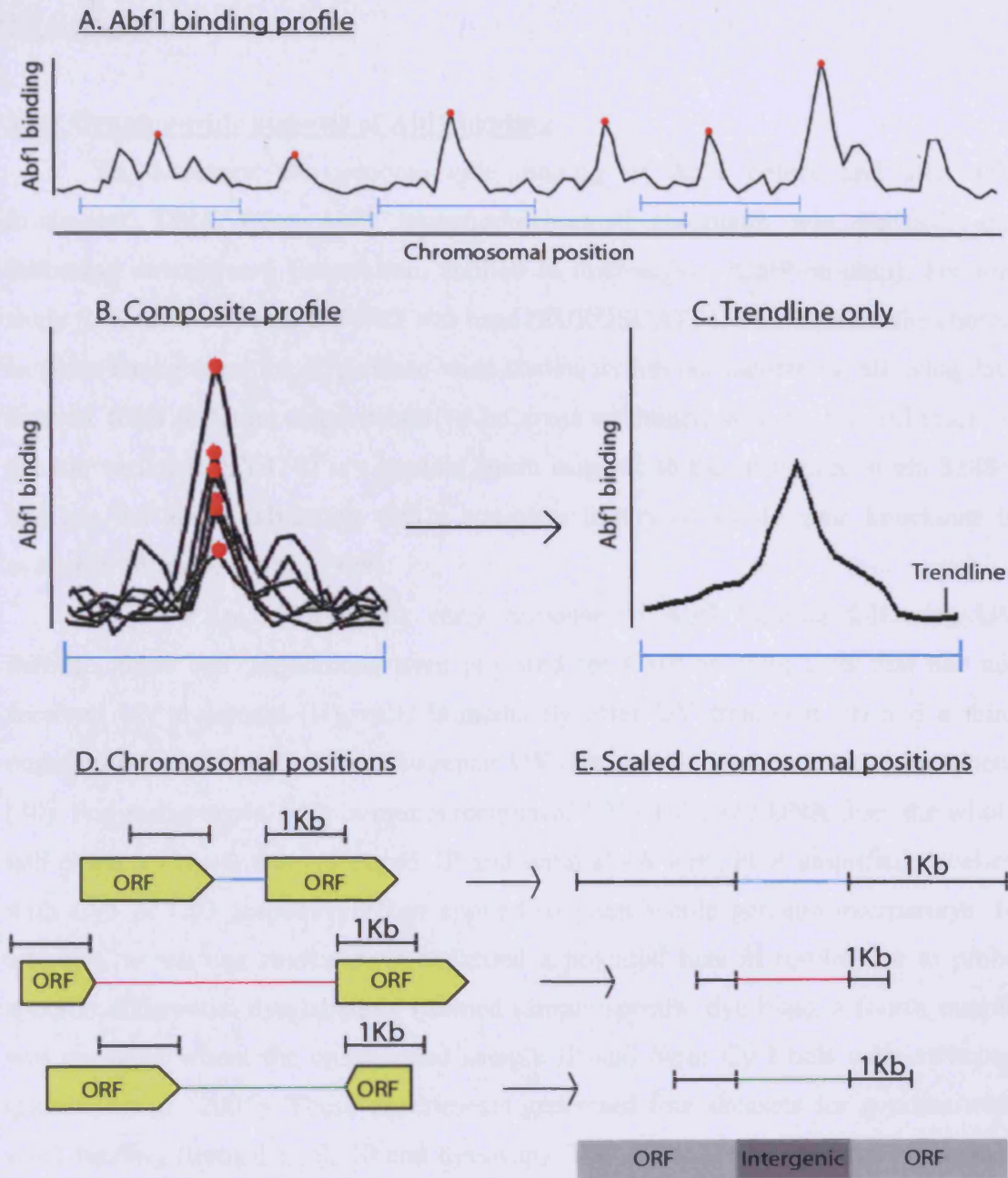


Figure 3.1. How composite profiles function to display Abf1 ChIP-on-chip data. A. Example of an Abf1 binding profile; the red dots in this graph represent Abf1 binding peaks, the blue bars below represent a 4kb range with the Abf1 binding peak at the centre. B. Example of a composite profile. The trace from A is repeatedly plotted centred at the Abf1 binding peak. For each peak, a range of 4kb is plotted. C. A trendline represents the repeated plots shown in B. D. Examples of data with an intergenic region and an ORF either side. E. Example of how data plotted at these sites would be scaled during a SCP composite profile.

3.3 Results**3.3.1 Genome-wide analysis of Abf1 binding**

To determine the genome-wide binding of Abf1 before and after UV irradiation, DNA from Abf1 immunoprecipitated chromatin was purified, and following downstream preparation, applied to microarrays (ChIP-on-chip). For this study *S. cerevisiae* strain BY4742 was used (EUROSCARF). This strain is the chosen isogenic background for all genome-wide studies within our laboratory, allowing data derived from different experiments to be cross examined without the influence of genetic variation. BY4742 is a haploid strain isogenic to the sequenced strain S288c, and has the added advantage that a complete library of viable gene knockouts is available (Winzeler et al., 1999).

In order to delineate the early response of Abf1 binding following UV damage, three cell populations were prepared for ChIP-on-chip; cells that had not received UV treatment (U), cells immediately after UV treatment (0) and a third population which was incubated to repair UV damage for 30 minutes after treatment (30). For each sample, both immunoprecipitated DNA (IP), and DNA from the whole cell extracts (input) were prepared. IP and input DNA were PCR amplified, labelled with Cy5 or Cy3 respectively and applied to yeast whole genome microarrays. In addition, as various studies have indicated a potential bias in results due to probe specific differential dye labelling (termed sample specific dye bias), a fourth sample was prepared where the unirradiated sample IP and input Cy labels were switched (Dobbin et al., 2005). These experiments generated four datasets for genome-wide Abf1 binding (termed U, 0, 30 and dyeswap). The protocol was repeated twice such that each dataset had results from three biological repeats. A diagram summarising the overall protocol is shown in Fig. 3.2.

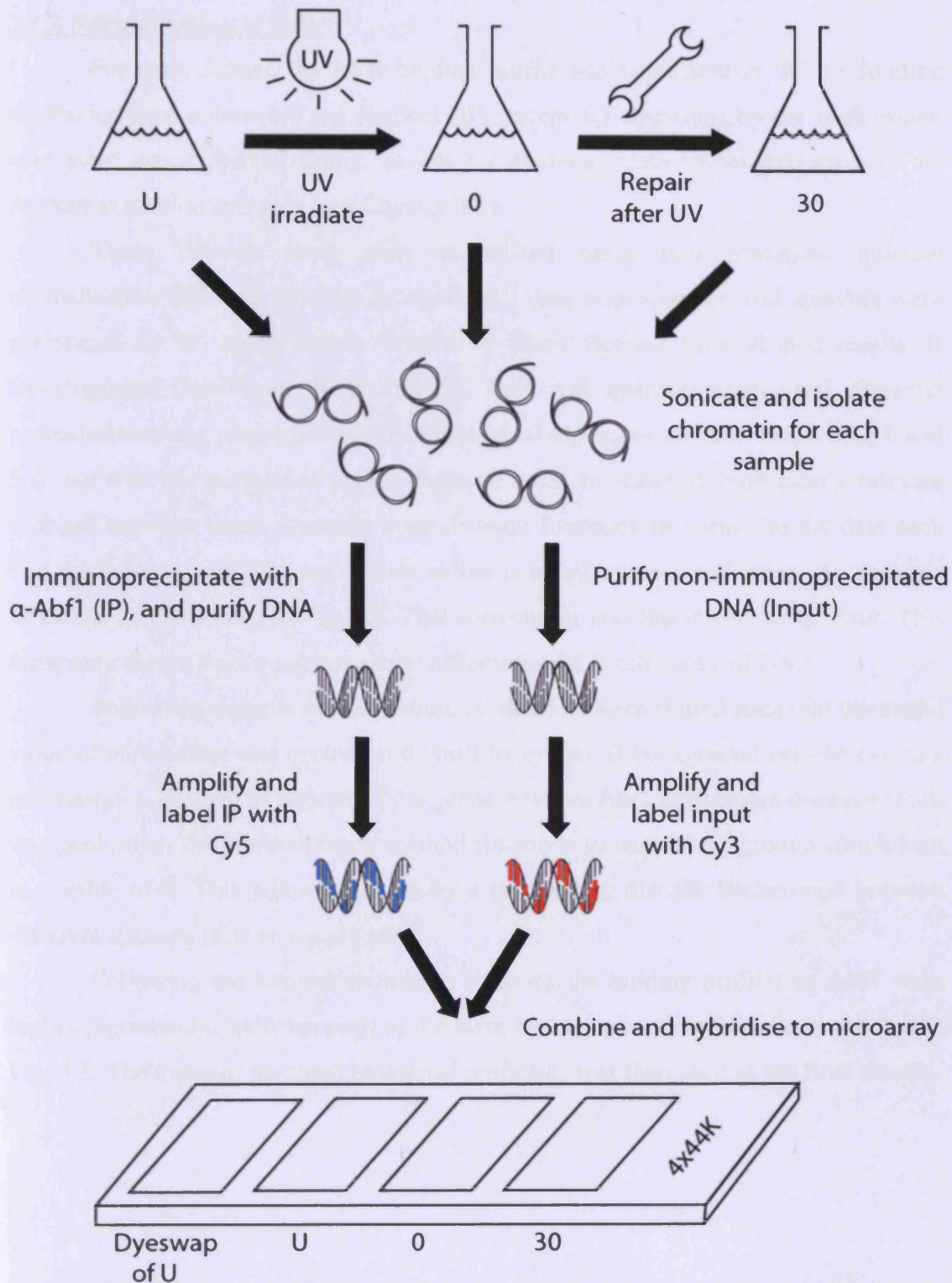


Figure 3.2. Cartoon detailing the various stages necessary for Abf1 ChIP-on-chip.

3.3.2 Normalisation of data

For each dataset, the Abf1 binding profile was calculated in 'R' by dividing the background subtracted red channel (IP, except for dyeswap) by the background subtracted green channel (input, except for dyeswap) data values extracted by the Agilent extraction software (see Chapter 2.8).

These datasets were then normalised using two strategies; quantile normalisation followed by shift by mode. All data normalisation and analyses were performed in 'R' using scripts written by Mark Bennett (unpublished results, R Development CoreTeam, 2010). Firstly, data was quantile normalised. Quantile normalisation was performed between biological replicates for each dataset (U, 0 and 30), but was not performed across datasets, so as to maintain biologically relevant changes between these. Quantile normalisation functions to normalise the data such that the empirical distribution of data values is equal between replicates. An example of its use is also shown in Fig. 3.3. This corrects for non-linear systematic error. This error may derive from sources such as differential PCR efficiency of DNA.

Following quantile normalisation, all datasets were shifted such that the modal value of enrichment was centred at 0 (shift by mode). If background enrichment on a microarray is defined as regions of the genome where Abf1 enrichment does not result in a peak, then this normalisation method functions to centre background enrichment at a value of 0. This adjusts datasets by a constant so that the background between different datasets is of an equal value.

Following the two normalisation methods the binding profiles of Abf1 were highly reproducible between each of the three biological replicates as demonstrated in Fig. 3.3. The mean of the three biological replicates was then used as the final dataset.

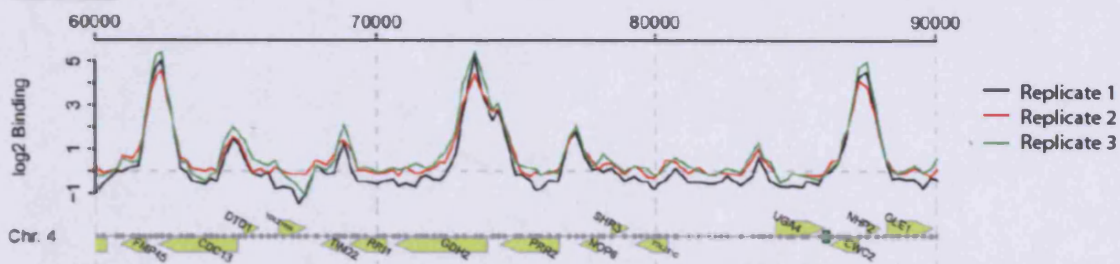
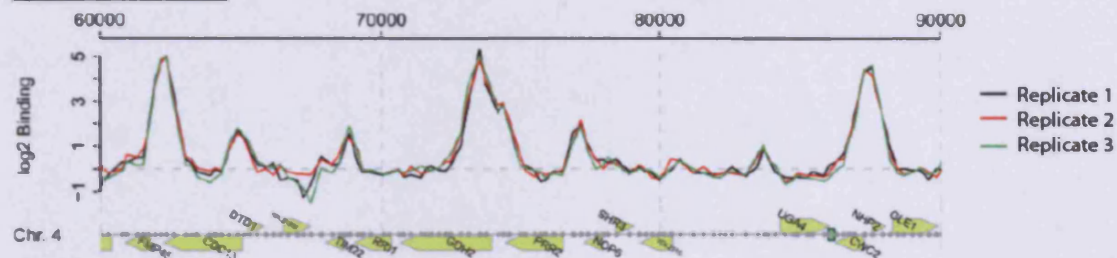
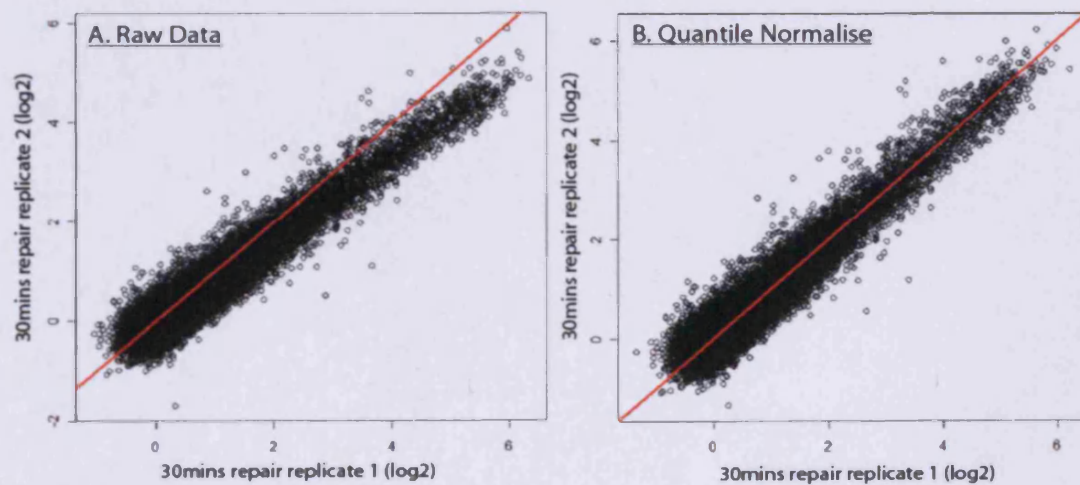
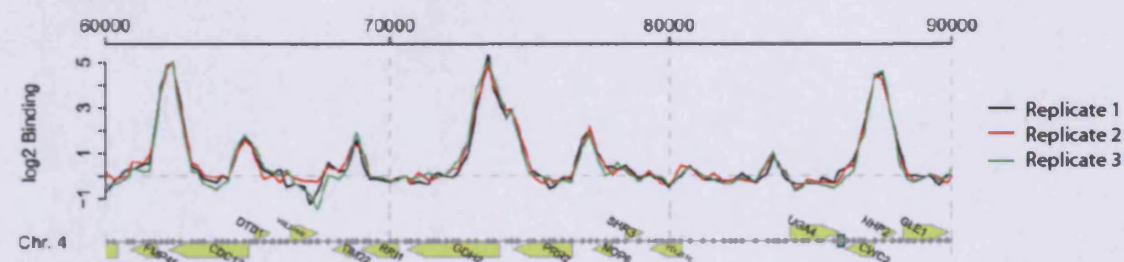
Raw Data**Quantile Normalise****Shift by Mode**

Figure 3.3. Above: Examples of how raw data changed during the normalisation procedure. Below: Relative distribution of data values for two biological replicates before (A) and after (B) quantile normalisation.

3.3.3 Investigating the effect of dye bias

Prior to data analysis, it was necessary to determine if Cy5 IP labelling conferred a dye bias. To examine this, the average of the two normalised datasets taken for Abf1 binding in the absence of UV irradiation, but alternatively Cy labelled (Cy5 IP/Cy3 input vs Cy3IP/Cy5 input), were directly compared. As shown in Fig. 3.4, the two datasets are virtually analogous, with an almost perfect linear relationship. Importantly, this demonstrates that the use of Cy5 labelling for an IP sample, combined with Cy3 labelling for an input sample neither creates false positive Abf1 binding peaks nor alters the relative pattern of peak height when compared to results using opposing labelling. Therefore, data analysis was exclusively performed with the three datasets without the need to correct for gene specific dye bias (Dobbin et al., 2005).

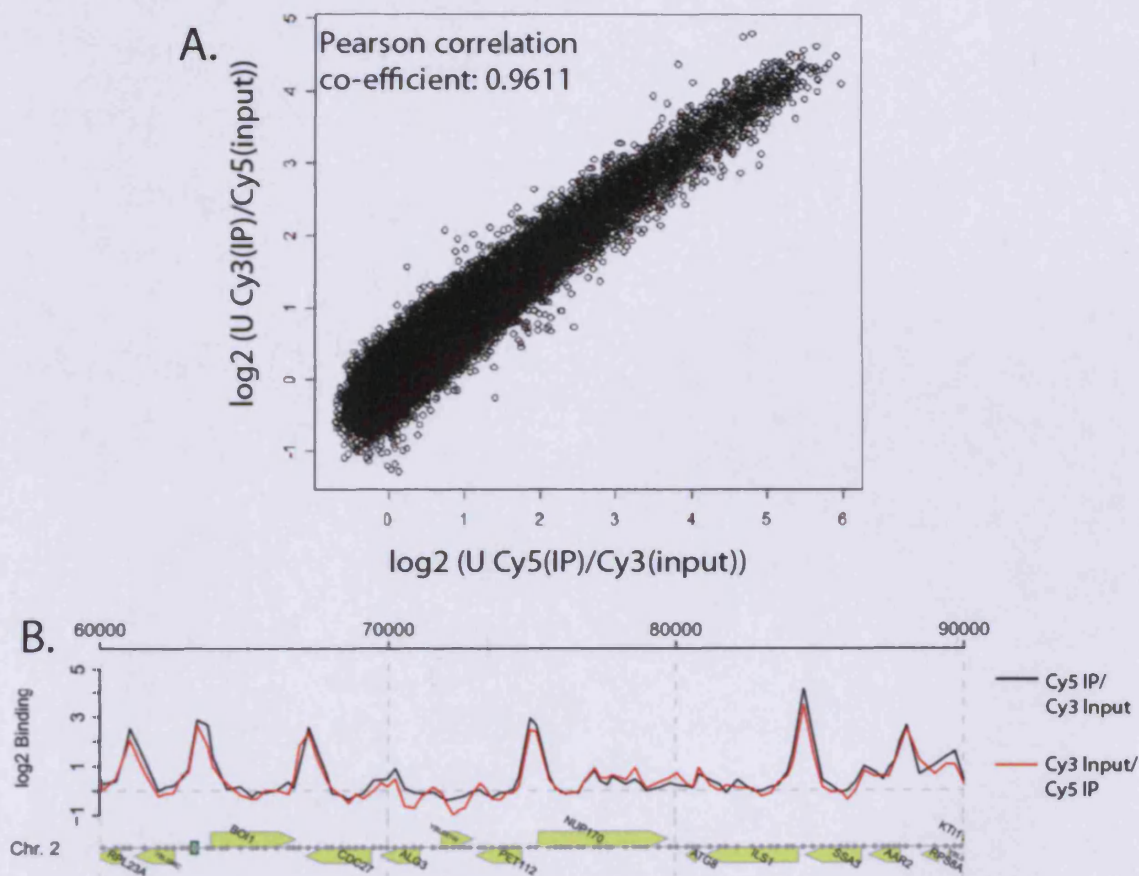


Figure 3.4. A. Scatter graph of the averaged U dataset plotted against the averaged dyeswap dataset. A Pearson correlation coefficient is given in the top left of the graph. B. Example of the data maps for the averaged datasets plotted in A. at chromosome 2. The genome-wide map of B. is available on the accompanying DVD (D:/Chapter3/ChIPchip).

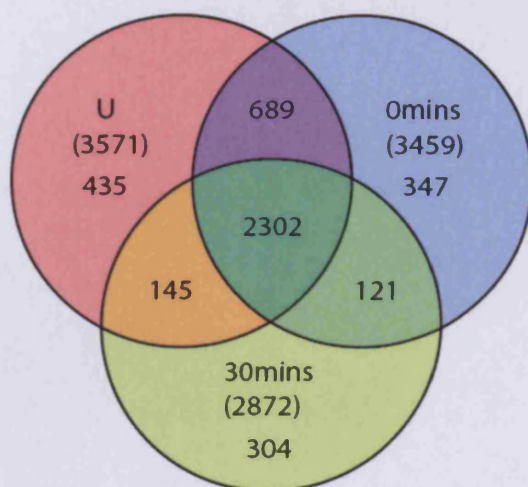
3.3.4 Mapping Abf1 binding peaks

To investigate the genome-wide localisation of Abf1 in response to UV damage, a peak detection algorithm was performed on datasets U, 0 and 30. Statistically significant Abf1 binding peaks ($p < 0.01$) were identified in the U, 0 and 30 datasets to give 3571, 3459 and 2872 peaks respectively (Fig. 3.5A). The majority of the Abf1 binding peaks in each dataset overlap, and careful examination of the chromosomal maps demonstrates that Abf1 binding does not relocate in response to UV irradiation (available on the accompanying DVD, D:/Chapter3/ChIPchip). Abf1 binding peaks that did not overlap in all three datasets were further investigated and the vast majority were not found to represent regions where Abf1 is relocated. Of the non-overlapping peaks detected, roughly one third were found to be the result of the peak shifting by a single probe on the microarray (Fig. 3.5C). Due to the high resolution of the microarrays, this shift in the peak position is likely to be within the error of the system, rather than representing a genuine relocation of Abf1 binding. In support of this, 39% of non-overlapping peaks characterised as unique to U when compared with the dyeswap were also due to this occurrence. In addition, only one third of the peaks that had shifted by one probe were common when comparing datasets U and 0 with U and 30.

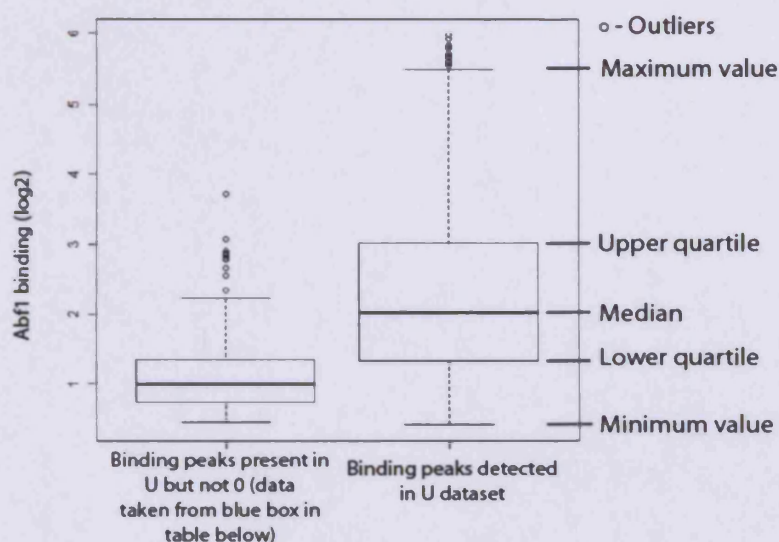
A second common cause of non-overlapping peaks was found to occur at regions of low enrichment, in which the Abf1 binding peak was considered statistically significant in one dataset but not the other. As shown in Fig. 3.5B, a box plot of enrichment for all peaks detected in U and those detected in U but not 0, demonstrates the binding level of the peaks from the latter is significantly lower. To discount peaks of this nature, student t-tests were performed between datasets at non-overlapping peak positions that had not shifted by one probe (Fig. 3.5C). This vastly reduced the number of non-overlapping peaks.

By filtering non-overlapping peaks by discounting those that had shifted by one probe, and those whose height had not significantly changed between the datasets, non-overlapping peaks were not detected when comparing the U and 0 datasets. Under the same criteria, only 4 peaks were detected in 30 that were absent in U. Approximately 100 peaks were detected in U or 0 that were not identified in 30, indicating that following 30 minutes repair after UV damage the occupancy of Abf1 is lost at a very small subset of binding peaks. Therefore, the localisation of Abf1 binding is the same both before and after UV irradiation.

A. Abf1 binding peaks



B. Box plot of detected binding peaks



C. Table categorising non-overlapping Abf1 binding peaks

Peaks found in	Peaks absent from	Quantity	Peaks moved by one probe	Remaining	Remaining peaks statistically different ($p < 0.05$)
U	0	580	239	341	0
0	U	468	239	229	0
U	30	1124	254	870	95
30	U	425	254	171	4
0	30	1036	264	772	98
30	0	449	264	185	0

Figure 3.5. A. Venn diagram representing the number of peaks detected in each Abf1 dataset that are present at identical probes on the microarray. Numbers in brackets represent the total number of peaks identified in each dataset. B. Box plot comparing the range of enrichment for peaks identified in U that were not present in 0 versus all peaks identified in U. C. Summary of the non-overlapping peaks identified in each dataset.

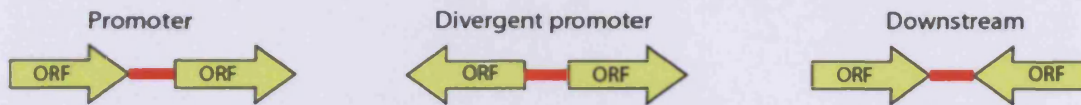
Given the absence of novel Abf1 binding peaks in response to UV irradiation, the Abf1 peaks defined in U represent an appropriate approximation of the distribution of Abf1 binding both before and after UV irradiation. Therefore, unless otherwise stated, the positional data of Abf1 binding peaks defined in U was used for all subsequent data analysis.

3.3.5. Abf1 preferentially binds promoter regions of the genome

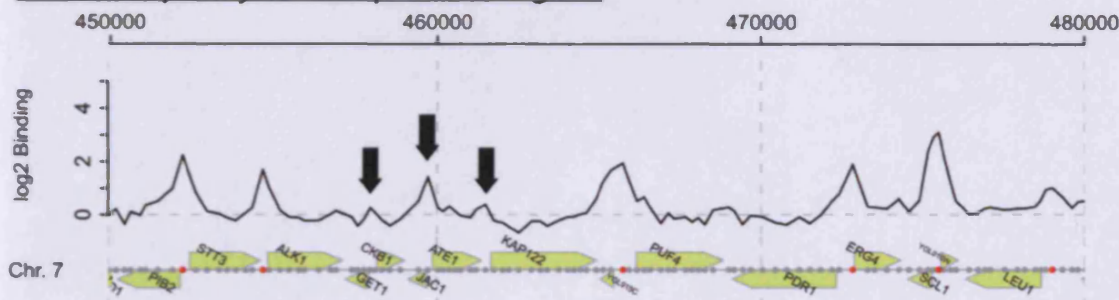
Having identified the relative position of Abf1 binding genome-wide, the peaks were categorised according to their location in the genome. The data was split into 5 categories; intragenic, promoter, divergent promoter, downstream or unknown according to the microarray probe classifications (see Fig. 3.6A). These are provided under the column heading of 'Description' in the exported data files following feature extraction (see Chapter 2.8). As shown in Fig. 3.6A, Abf1 binding peaks are highly over represented at both promoters and divergent promoters but highly under-represented at intragenic regions, relative to the number of probes on the microarray in each category. This suggests Abf1 preferentially binds chromatin at promoter regions. Upon analysis of the genome-wide chromosomal maps it was apparent that a peak of Abf1 binding can be observed upstream of nearly all promoter regions (an example is given in Fig. 3.6B). However, statistically significant binding peaks are only identified at ~40% of yeast promoters. Therefore Abf1 may bind many promoters at a low level that is not statistically significant. To test this possibility a composite profile of Abf1 binding was plotted at intergenic regions with a promoter where Abf1 was identified to bind by statistical analysis and compared against a plot where Abf1 binding was not statistically significant (Fig. 3.6C and D). As shown in Fig. 3.6D, when promoter regions where Abf1 is not identified to bind at statistically significant levels are collectively plotted, a moderate enrichment of chromatin is observed relative to intragenic chromatin. This demonstrates that the location of low level Abf1 binding is non-random (and thus unlikely to be an experimental error) and at promoter regions. This corresponds to the same preferential localisation as statistically significant peaks of Abf1 binding. This suggests that a significant proportion of these promoter regions are occupied by low level binding (LLB) of Abf1, whilst regions with statistically significant peaks represent high level binding (HLB) of Abf1.

A. Location of Abf1 binding peaks

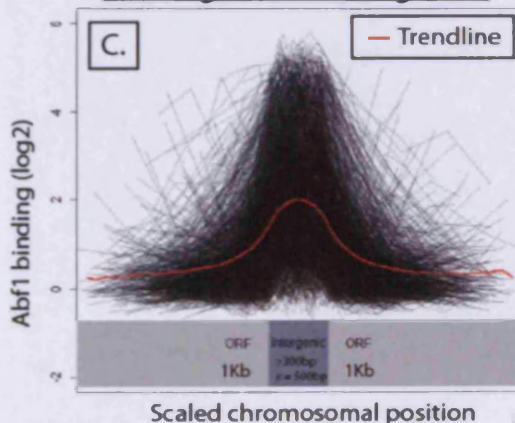
Abf1 peak position	Number of peaks	% of peaks	% of probes on array	% peaks/%probes
Intragenic	977	27	73	0.37
Intergenic	2594	73	27	2.70
-Promoter	1419	40	14	2.86
-Divergent promoter	913	26	8	3.25
-Downstream	252	7	5	1.4
-Unknown	10	0.2	0.3	0.67
Total	3571	100	100	N/A



B. Abf1 frequently binds at promoter regions



Abf1 high level binding (HLB)



Abf1 low level binding (LLB)

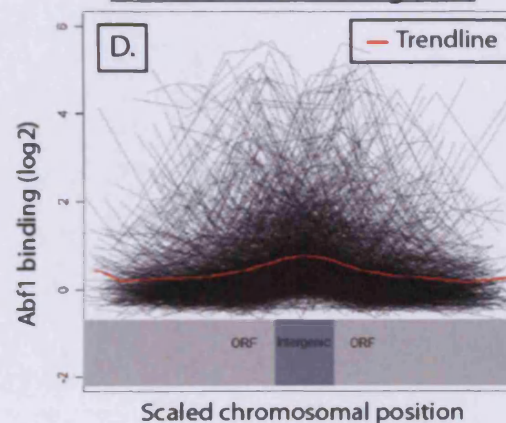


Figure 3.6. A. Location of Abf1 binding peaks. ‘% of probes on array’ represents the percentage of the total probes on each microarray that are classified according to each category under ‘Abf1 peak position’. Intergenic probes are a total of all probes that are not classified as intragenic. An example of a promoter, divergent promoter and downstream region (shown in red) is given below. B. Chromosomal map of Abf1 binding from the U dataset. Red dots are shown below statistically significant Abf1 binding peaks. Black arrows represent Abf1 binding peaks at promoters that are not assigned as statistically significant. C. A composite profile of Abf1 binding centred at intergenic regions with a promoter that contains a statistically significant peak (2332 regions from A). The trace maps the averaged binding data of U for the intergenic region and both the upstream and downstream gene. This trace is repeated for each of the 2332 intergenic regions. The data is scaled such that all data from intergenic regions and ORFs are mapped according to the grey bars shown. A trendline is given in red. D. The composite plot is of the same format as C., but instead plots intergenic regions that do not contain a statistically significant Abf1 binding peak.

3.3.6 UV dependent changes in Abf1 occupancy

Mutation of the Abf1 binding site at the *HML α* I-silencer was previously shown to inhibit efficient GGR (Yu et al., 2009). In addition, the occupancy of Abf1 was observed to alter at the wild type *HML α* I-silencer in response to UV irradiation. Using ChIP, it was shown that the occupancy of Abf1 initially increased following UV, but subsequently decreased at various time points analysed following repair. The significance of these changes was unknown, but the data suggests that alterations in Abf1 occupancy could be mechanistically important for GGR. Recently, our laboratory has utilised ChIP-on-chip technology for the analysis of CPD incidence (and repair) in chromatin following UV irradiation (Fig. 3.7A, Teng et al., 2010). The high correlation between the predicted and experimentally established profile of CPD incidence, demonstrates that the technology provides accurate quantitative information regarding the presence of CPD damage throughout the genome. As a consequence, the Abf1 ChIP-on-chip datasets were examined to determine the change in Abf1 occupancy in response to UV genome-wide.

In order to validate the Abf1 ChIP-on-chip data, the changes in Abf1 binding after UV were quantified by quantitative PCR (qPCR) at a number of loci and compared to the changes in Abf1 binding as quantified by the microarray datasets. qPCR was performed using primers that amplified regions of the genome where a peak of Abf1 binding was observed by ChIP-on-chip. Both the qPCR and ChIP-on-chip datasets used the same DNA sample purified from chromatin. As shown in Fig. 3.7B, when quantified by qPCR, binding of Abf1 at the *HML α* I-silencer follows an identical pattern to that originally described; a UV dependent increase in occupancy, followed by a decrease after 30 minutes repair (Yu et al., 2009). In contrast, the microarray data instead predicts a small loss in Abf1 occupancy immediately after UV. A second example of Abf1 binding is shown at *NAT4*. In this example, both the qPCR and microarray data indicate the same pattern of Abf1 occupancy. Therefore, in some examples there are discrepancies between changes in Abf1 occupancy as quantified by qPCR and microarray methodologies.

To visualise the genome-wide changes in Abf1 occupancy in response to UV, histograms examining the change in Abf1 binding were plotted comparing the U dataset with 0 and the 0 dataset with 30. As shown in Fig. 3.8A, relatively few Abf1 binding peaks demonstrated large changes in Abf1 occupancy (>20%) directly after

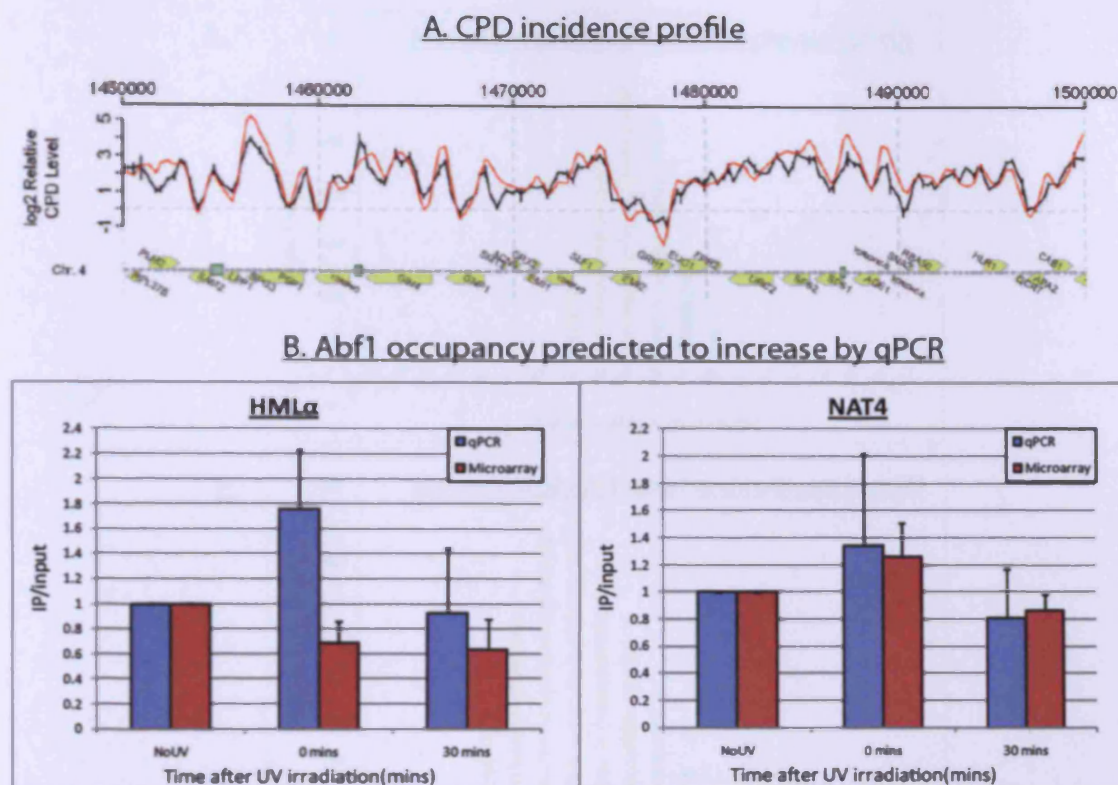


Figure 3.7. A. Example of the quantitative nature of the ChIP-on-chip strategy employed within the laboratory. The experimentally determined CPD incidence, as identified by using an antibody raised against the CPD damage (black line), correlates with a theoretical profile of CPD damage based upon sequence data and the known ratios of CPD incidence between dipyrimidines (red line). B. Comparison of changes in Abf1 binding peaks as quantified by qPCR and microarray.

UV irradiation. However, following 30 minutes repair of UV damage, the occupancy of Abf1 at a large proportion (>50%) of binding peaks is found to decrease (>20%) (Fig. 3.8B). Therefore the predominant UV response of Abf1 after 30 minutes repair results in a loss of occupancy at binding sites. Two of the loci which were found to have a statistically significant loss in Abf1 occupancy ($p < 0.05$) between the datasets U and 30 were selected for quantification by qPCR. As shown in Fig. 3.8C, the qPCR data corresponds well with the prediction by the microarray data demonstrating a significant loss of Abf1 occupancy following 30 minutes repair. Whilst the loss of Abf1 binding was investigated in relation to CPD repair rates (Teng et al., 2010), neither Pearson nor Spearman correlation analysis identified a correlation between the changes in Abf1 binding and efficient CPD repair.

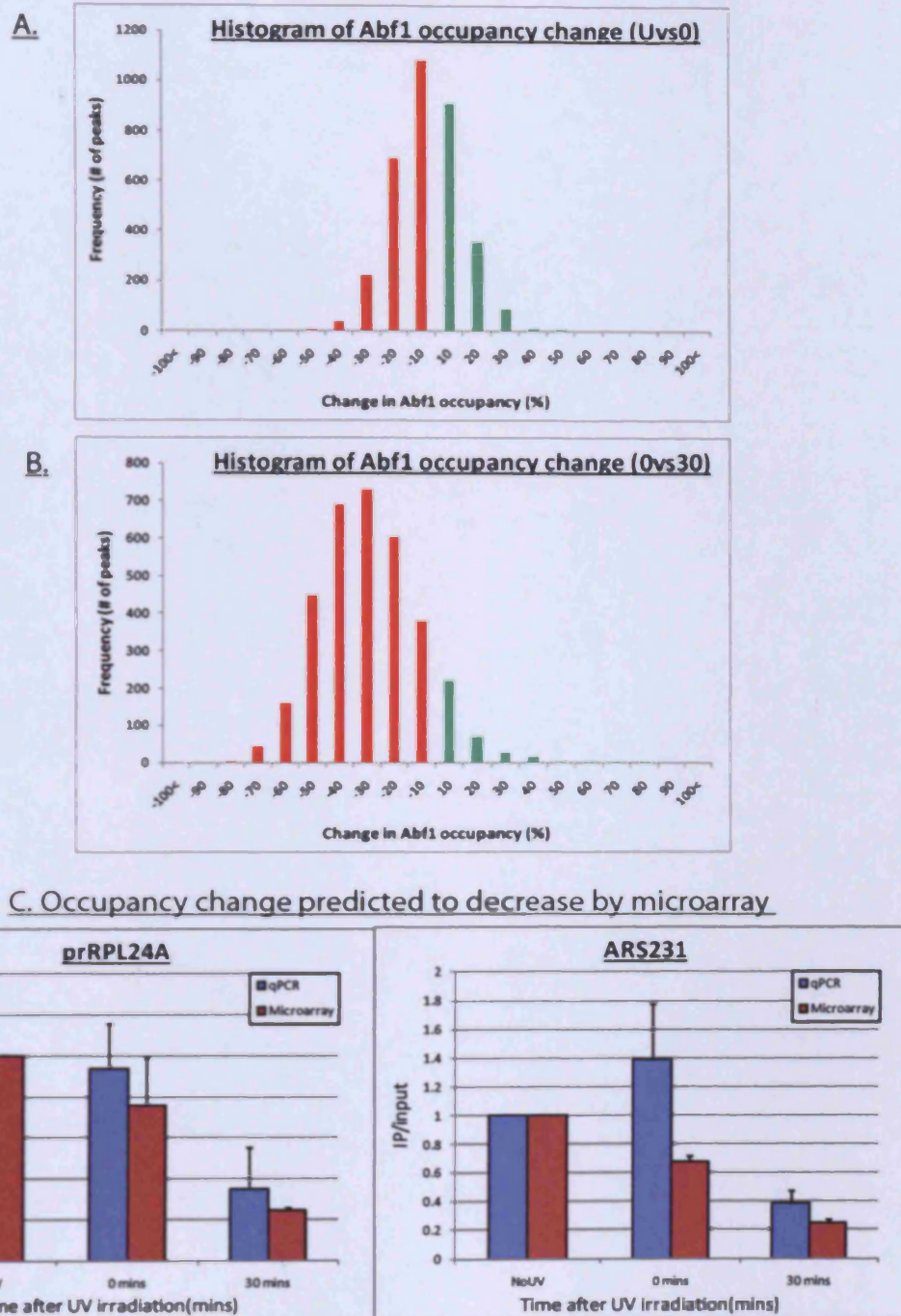


Figure 3.8. A. Histogram of the relative change in Abf1 occupancy (as a % of the original peak height) when comparing the U dataset with the 0 dataset. B. Identical format as A. comparing the 0 dataset with the 30 dataset. Both A. and B. compare peaks identified in the U dataset. C. Comparison of two Abf1 binding peaks predicted to fall in response to UV after 30 minutes repair, as quantified by qPCR and microarray.

3.3.7 Investigating histone H3 K9K14 hyperacetylation at Abf1 binding peaks

As previously discussed in the introduction, the Rad7/Rad16 components of the GGR complex promote histone H3 K9K14 hyperacetylation after UV and GGR (see Chapters 1.4.4 and 4.1, Teng et al., 2008; Verhage et al., 1994). Given that Abf1 binding is believed to promote efficient binding of the GGR complex to domains throughout the genome, this suggests that Abf1 binding may co-ordinate the localisation of Rad16 dependent acetylation and GGR (see Chapter 1.5.5 and introduction for further discussion, Yu et al., 2009). Our lab has recently mapped the genome-wide UV response of histone H3 K9K14 acetylation and CPD DNA repair using the ChIP-on-chip strategy described above (K.Evans, Y.Teng, unpublished data, Teng et al., 2010). This has been performed in both wild type and *rad16Δ* strains of BY4742. These datasets were plotted at Abf1 binding sites to investigate how histone H3 K9K14 acetylation and CPD repair are organised in relation to Abf1 binding.

When the acetylation data was plotted at Abf1 binding peaks as a composite profile, a trendline of two peaks of hyperacetylation either side of the Abf1 binding position was identified (Fig. 3.9). This suggests that Abf1 binding may regulate the distribution of histone H3 K9K14 hyperacetylation. It was previously observed in *S. cerevisiae* that both histone H3 K9 and H3 K14 acetylation, peaks at the TSS of genes (Pokholok et al., 2005). This suggested that histone hyperacetylation at Abf1 binding sites may occur at promoter regions, which as previously shown, is where Abf1 is predominantly localised (Fig. 3.6). To investigate this, composite profiles of histone H3 K9K14 acetylation were plotted in relation to Abf1 binding peaks classified according to their genomic location, as described in Fig. 3.6A (Fig. 3.10). As shown in Fig. 3.10, when plotted in this manner, histone H3 K9K14 hyperacetylation peaks are only found at Abf1 binding sites within both classes of promoter regions. Interestingly however, a low level peak of acetylation is found centred at intragenic Abf1 binding peaks, suggesting that Abf1 binding might promote low level acetylation in these regions. Collectively, these data suggest that histone H3 K9K14 hyperacetylation is organised at the Abf1 binding sites of promoter regions.

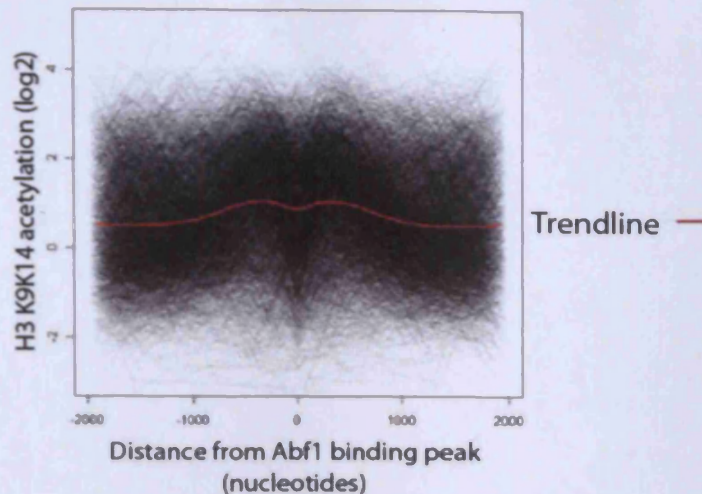


Figure 3.9. Composite profile of histone H3 K9K14 acetylation data. 4000 nucleotides of acetylation data (from unirradiated cells) is plotted such the centre of this plot colocalises at an Abf1 binding peak defined in U. This plot is repeated and superimposed for each of the 3571 Abf1 binding peaks.

To further investigate how histone H3 K9K14 acetylation is organised at Abf1 binding sites, composite profiles of the acetylation data were plotted in relation to Abf1 binding peaks both before and after UV irradiation using the wild type and *rad16Δ* datasets (Fig. 3.10). As observed in the absence of UV damage, peaks of post-UV histone H3 K9K14 hyperacetylation only occur proximal to Abf1 binding sites at promoter regions. In response to UV, the distribution of acetylation is similar to that observed before UV damage at the Abf1 binding sites of all genomic locations. However, the greatest differences in the distribution of acetylation occur at promoters, where the hyperacetylation peaks before UV are accentuated. In the absence of Rad16, the distribution of acetylation is significantly altered at the Abf1 binding sites of promoters; in the absence of UV damage, acetylation is diminished at regions proximal to the Abf1 binding site and the peaks of hyperacetylation are significantly reduced. Interestingly, in response to UV the altered distribution of acetylation at promoters is maintained. This suggests that Rad16 regulates the distribution of histone acetylation at promoters in a similar manner both before and after UV irradiation. These data show that Rad16 is important in regulating the distribution of histone H3 K9K14 acetylation at Abf1 binding sites in promoter regions.

Wild type

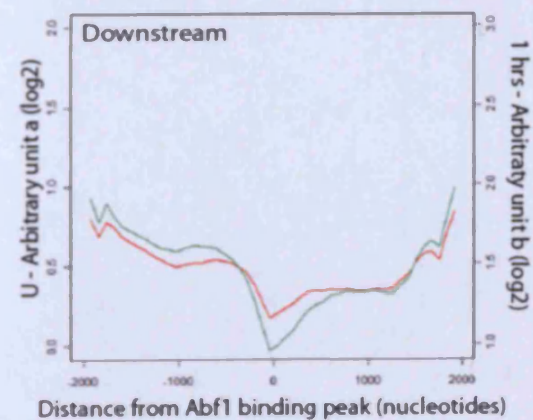
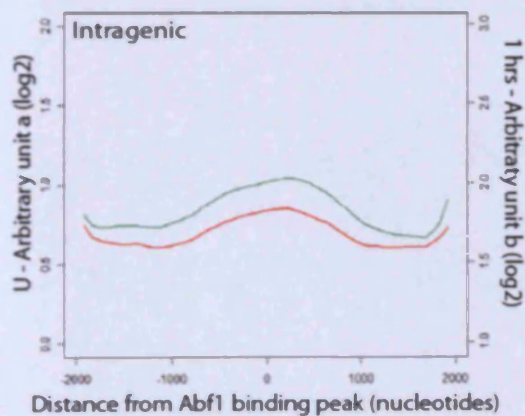
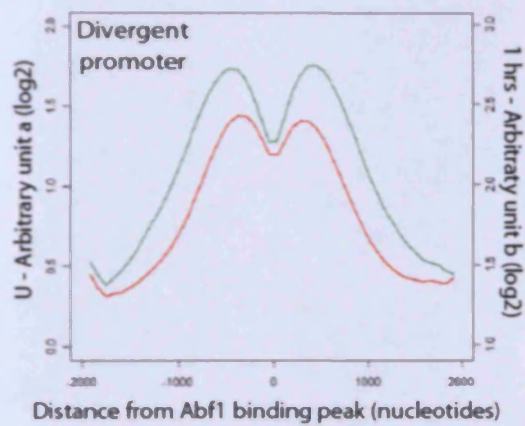
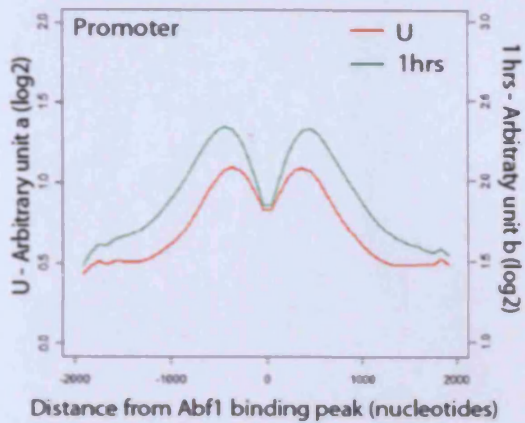
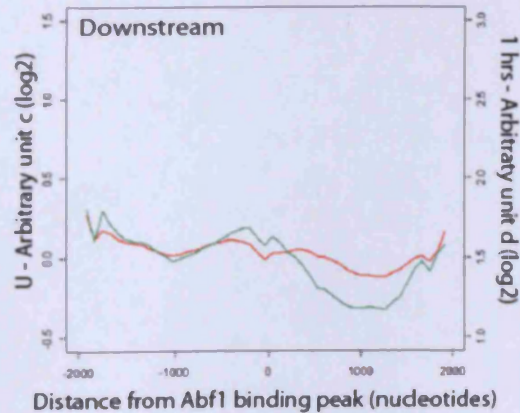
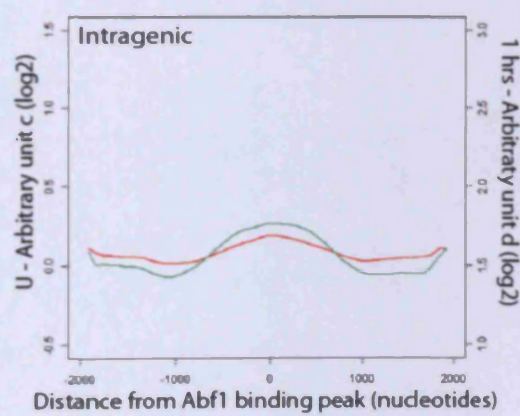
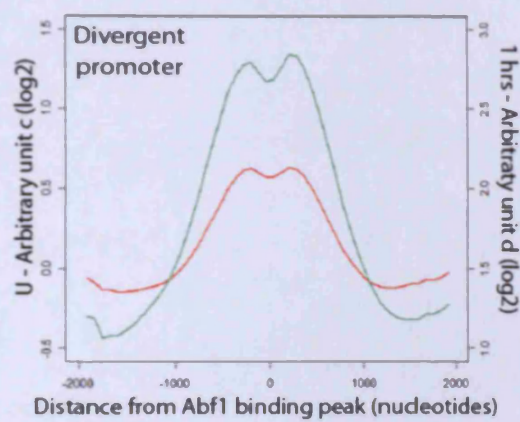
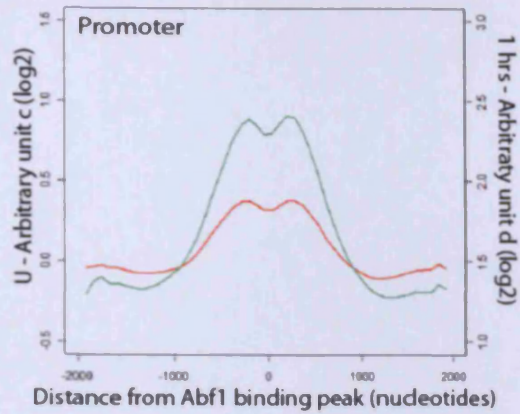
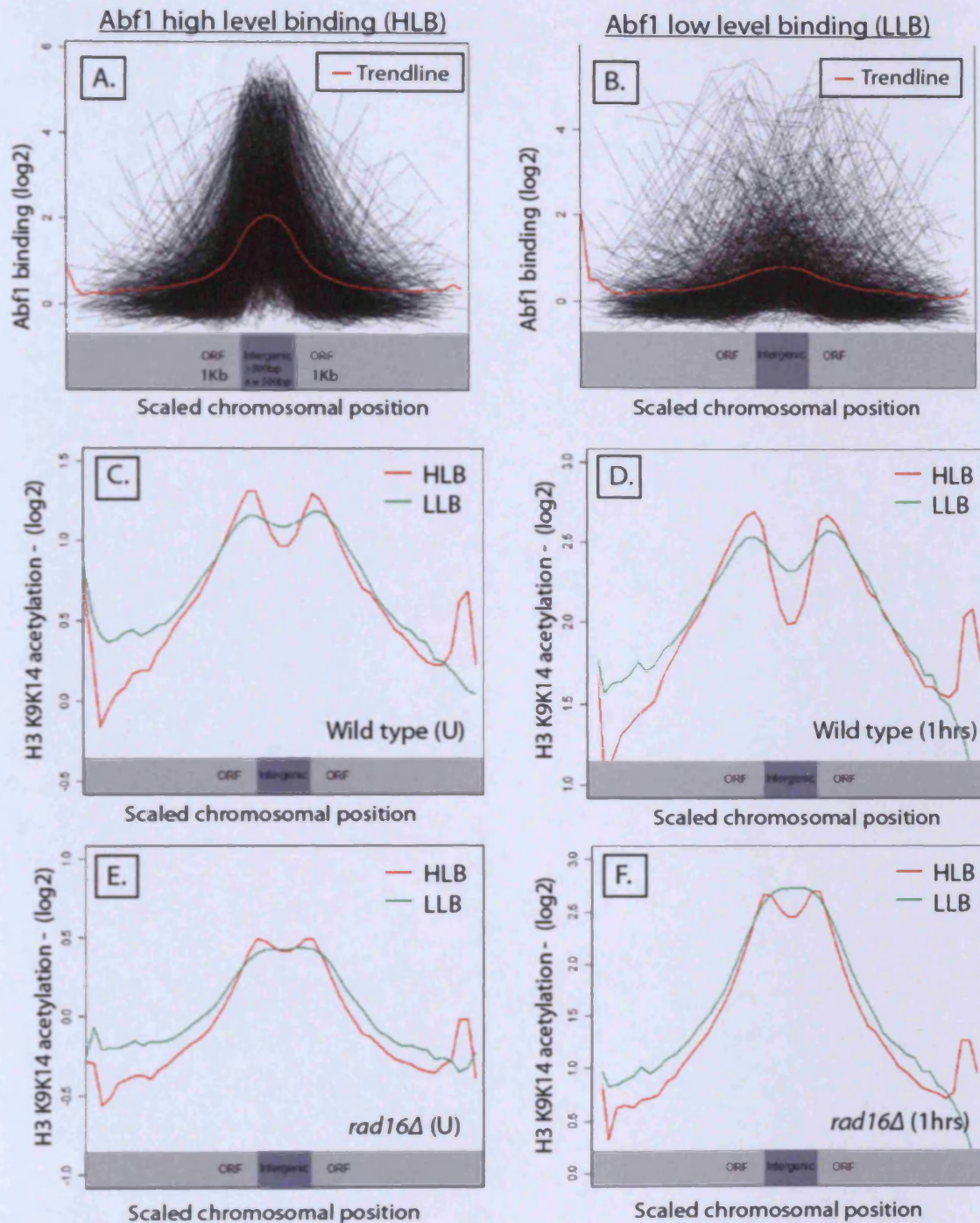
*rad16Δ*

Figure 3.10.(Above) Composite profiles of histone H3 K9K14 acetylation data both before (U – red lines) and one hours after (1hrs – green line) UV irradiation at Abf1 binding peaks. Abf1 binding peaks from the U dataset were categorised according to their location and plotted as four separate graphs. The title in the top left of each plot represents which location the Abf1 binding peaks used to produce the graph are located at. All Abf1 binding peaks for each location were included. Only the trendline of each plot is shown. All graphs on the left represent data from wild type cells. All graphs on the right represent data from *rad16Δ* cells. NB. Scales are non-equivalent between wild type and *Δrad16* datasets. Scales are also non-equivalent between U and 1hrs datasets.

Histone H3 K9K14 acetylation at promoters that were not bound by Abf1 could not be investigated because promoters that do not contain a statistically significant Abf1 binding peak do not accurately represent regions of the genome where Abf1 is not observed to bind (Fig. 3.6). Consequently, a role for Abf1 binding in regulating the distribution of histone H3 K9K14 acetylation at promoters was investigated by comparing promoters with HLB of Abf1 to promoters with LLB of Abf1 (Fig. 3.11). Histone H3 K9K14 hyperacetylation data was plotted at intergenic regions with a promoter and classified into two composite profiles according to whether the intergenic regions contained HLB of Abf1 (statistically significant peak) or LLB of Abf1 (statistically insignificant peak). As shown in Fig. 3.11, peaks of hyperacetylation were centred at promoter regions with HLB and LLB of Abf1 (Fig. 3.11 C. and D.). This suggests that the level of Abf1 binding at a promoter does not regulate histone hyperacetylation. As previously discussed for promoters with HLB of Abf1, the pattern of hyperacetylation is not significantly altered in response to UV at promoters with LLB of Abf1.

It was speculated that if HLB of Abf1 is necessary for the localisation of the Rad16 dependent distribution of histone H3 K9K14 acetylation at promoters, then acetylation at promoters with LLB of Abf1 might be unaffected in a *rad16Δ* strain. To test this possibility, the intergenic composite profiles of acetylation at promoters classified according to HLB or LLB of Abf1, were repeated for the *rad16Δ* dataset (Fig 3.11 E. and F.). In the absence of Rad16 the distribution of acetylation at promoters with HLB and LLB of Abf1 are significantly altered in both cases (compare Fig. 3.11 C with E and 3.11D with F). Therefore, Rad16 regulates the wild type distribution of histone H3 K9K14 acetylation at promoters in a manner independent of the level of Abf1 binding.



- Peaks of histone H3 K9K14 acetylation are found near the TSS of genes with HLB of Abf1 in their promoter or LLB.
- Rad16 is necessary for wild type acetylation patterns at promoters with HLB of Abf1 and LLB of Abf1.

Figure 3.11 (above). A. and B; Composite profiles of Abf1 binding at intergenic regions that contain a promoter using the scaled chromosomal position strategy as described in Fig. 3.6C. Data is classified into intergenic regions with HLB of Abf1 (statistically significant peaks) (A.) or those with LLB of Abf1 (statistically insignificant peaks) (B.). C. and D; Composite profiles of histone H3 K9K14 acetylation from BY4742 before (C) and 1hrs after (D) UV irradiation, centred at intergenic regions which contain a promoter. The data is classified according to intergenic regions with HLB or LLB of Abf1 as seen in A. and B. Only the trendline of the plots is shown. E and F; Identical to that of C. and D. except that the acetylation data is derived from strain *rad16Δ* BY4742. E. is before UV and F. 1hrs after. NB: Data from C., D., E. and F. plots use non-equivalent arbitrary units/scales. (Below) Summary of conclusions.

3.3.8 Investing GGR at Abf1 binding peaks

Abf1 binding sites were previously suggested to promote domains of efficient GGR (see Chapter 1.5.5, Yu et al., 2009). To investigate CPD repair at Abf1 binding sites a composite profile of wild type CPD repair rates was plotted in relation to Abf1 binding peaks. A domain of rapid repair in the vicinity of Abf1 binding was not observed (Fig. 3.12A). Therefore in wild type cells, rapid CPD repair does not occur at domains proximal to Abf1 binding peaks. However, in the absence of Rad16, CPD repair is slowest at regions of the genome centred at Abf1 binding peaks (Fig. 3.12A). To further investigate this observation, composite profiles were plotted according to the genomic location of the Abf1 binding peak. As shown in Fig. 3.12C, the largest differences between the wild type and *rad16Δ* mutant repair rates occur at Abf1 binding peaks situated at promoters. The relative pattern of CPD repair at Abf1 binding peaks that are intragenic is unaffected by the loss of Rad16 likely reflecting the predominance of the TCR pathway in these regions. Remarkably, regions bound by Abf1 downstream of genes are significantly repair defective in wild type cells. This phenotype was observed to be a general trend of regions downstream of a gene (Fig. 3.12B). However, in the absence of Rad16 a domain of deficient repair downstream of genes is not observed. Collectively these results suggest that efficient Rad16 dependent GGR is organised at the Abf1 binding peaks of promoter regions.

To test whether efficient Rad16 dependent GGR colocalised at promoters with HLB of Abf1, CPD repair rates were plotted using composite profiles at intergenic regions which contained a promoter and the data was analysed according to whether the promoter contained HLB or LLB of Abf1. As shown in Fig. 3.13, when plotted in this manner the slowest rates of repair in a *rad16Δ* mutant occur at promoter regions for both classes of Abf1 binding, however, repair rates are slower at promoters with HLB of Abf1. In the presence of Rad16, repair rates remain slowest at promoters with HLB of Abf1. Given that the repair rates are not equal in the absence of Rad16

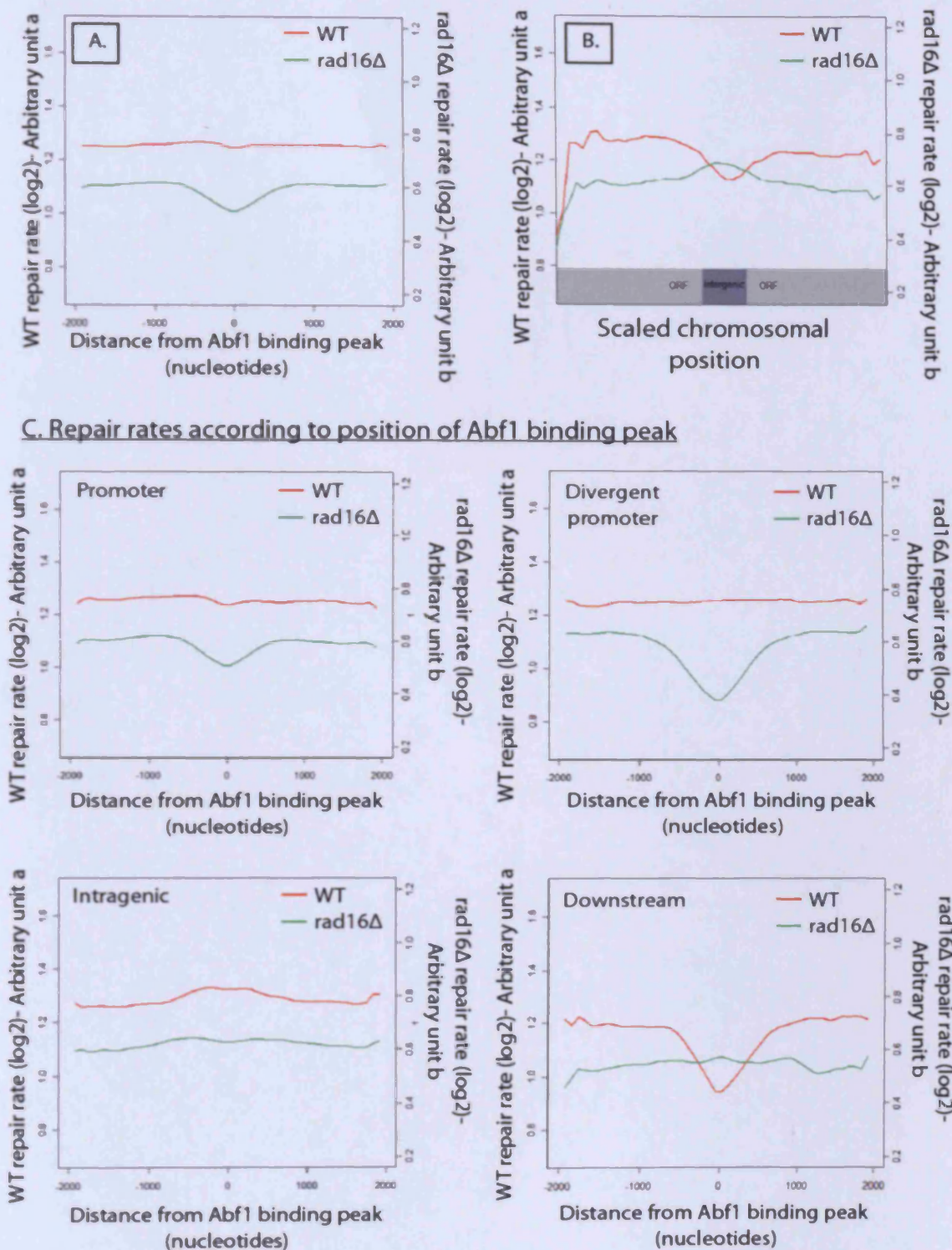


Figure 3.12. A. Composite profile of wild type (red line) and *rad16Δ* (green line) repair rates plotted at Abf1 binding peaks. Only the trendlines are shown. B. Composite profile of repair centred at intergenic regions downstream of a gene (both gene ORFs terminate at the intergenic region, hence a promoter is never present) that do not contain a statistically significant Abf1 binding peak. The trendline of the data is given for wild type repair rates (red) and *rad16Δ* repair rates (green). C. Composite profiles of an identical format as Fig. 3.10 but plotting wild type (red) and *rad16Δ* (green) repair rates. NB. Scales are non-equivalent between wild type and *Δrad16* datasets.

between the two classes of Abf1 binding, Rad16 dependent GGR was estimated by subtracting the *Rad16* CPD repair rate from wild type CPD repair rate. When these data are plotted, little difference in Rad16 dependent GGR rates is observed between promoters with HLB and LLB of Abf1. Collectively these data suggest that there is no correlation between the Abf1 binding level and the rate of Rad16 dependent GGR at promoter regions.

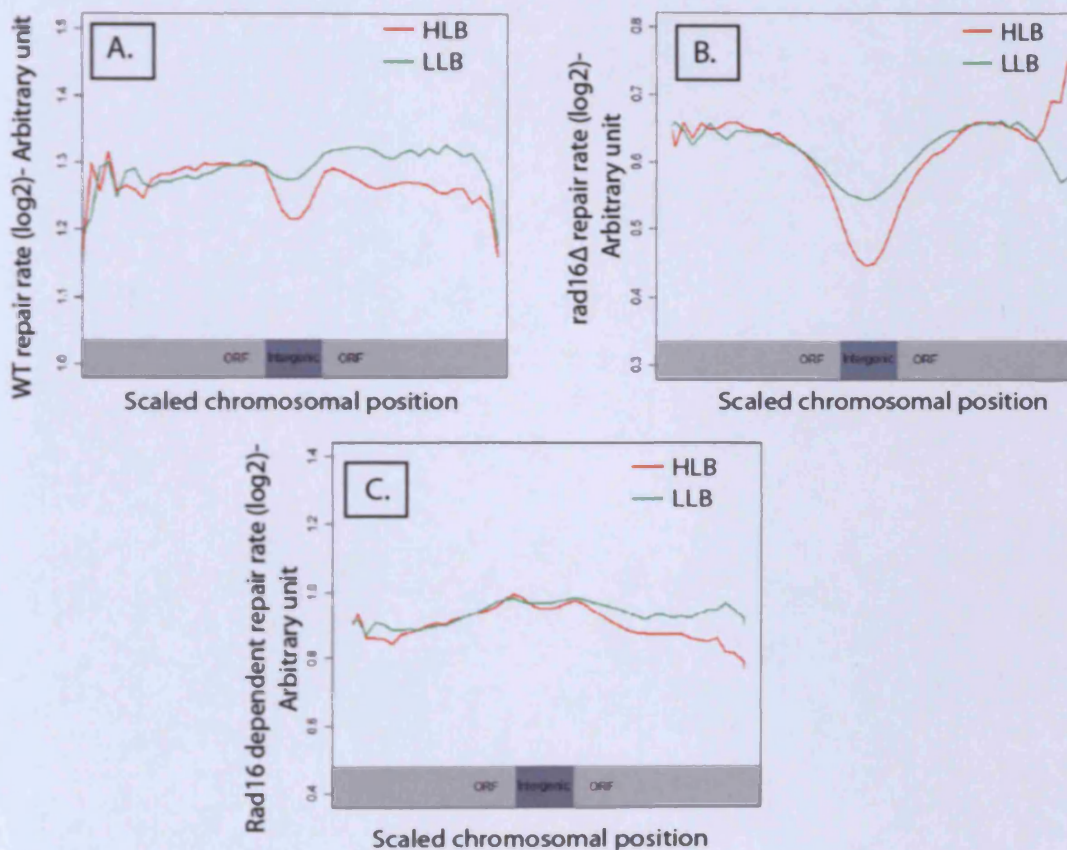


Figure 3.13. A-C. Composite profile of CPD repair at intergenic regions that contain a promoter using the scaled chromosomal position strategy as Fig. 3.6C. Data is classified into intergenic regions with HLB of Abf1 (statistically significant peaks) or those with LLB of Abf1 (statistically insignificant peaks). Only trendlines are shown. A. Wild type CPD repair. B. *rad16Δ* CPD repair. C. Rad16 dependent CPD repair (wild type – *rad16Δ* CPD repair). NB: Data from A., B., and C. plots use non-equivalent arbitrary units/scales.

3.4 Discussion

The aim of the current study was to map the genome-wide localisation of Abf1 before and after UV damage using ChIP-on-chip, to investigate how the protein responds to UV damage as part of the molecular mechanism of GGR. Furthermore, the distribution of Rad16 dependent histone acetylation and GGR were investigated in relation to Abf1 binding sites. Abf1 is observed to bind the genome at a high frequency, and is preferentially localised at promoter regions. In contrast to many TFs, Abf1 is not observed to relocalise its distribution in response to UV damage, however the level of Abf1 binding is significantly reduced at many sites following 30 minutes repair. Abf1, Rad7 and Rad16 form the GGR complex and Rad7/16 promote UV induced histone H3 K9K14 hyperacetylation and CPD repair. Rad16 regulates the distribution of histone H3 K9K14 acetylation at Abf1 binding sites within promoter regions. In addition, efficient GGR is organised at Abf1 binding sites in promoter regions. This suggests that Abf1 binding targets the GGR complex and thus organises GGR at promoter regions. To investigate if Abf1 binding is necessary for efficient Rad16 dependent histone acetylation and efficient GGR at promoter regions, the promoter regions were classified according to whether they contained a statistically significant Abf1 binding peak or not. In this study, Abf1 is observed to bind a very high frequency of promoter regions in vivo, and promoters that do not contain statistically significant binding peaks of Abf1 are observed to contain LLB of Abf1, rather than an absence of Abf1 binding. When the data is classified into promoter regions with HLB or LLB of Abf1, neither the distribution of acetylation nor CPD repair rates are significantly different between the two classes. This suggests that the level of Abf1 binding is not related to acetylation nor CPD repair rates at promoter regions.

Under the current experimental conditions employed, over 3500 statistically significant peaks of Abf1 binding ($p < 0.01$) are observed in the absence of UV irradiation (Fig. 3.5A). This is considerably higher than the number of sites Abf1 is predicted to bind the genome from previous ChIP-on-chip studies (Harbison et al., 2004; Lee et al., 2002b; Schlecht et al., 2008). However, other investigators have indicated that the number of TF interactions estimated in these early studies were low due to the statistical models employed (Workman et al., 2006). Importantly, the studies presented here employ microarrays with a far higher resolution than previously used (4-8 fold higher depending upon the study being compared), which

includes intragenic regions (not analysed in Lee et al., 2002 or Harbison et al., 2004). This not only provides a greater coverage of the yeast genome, but allows more accurate estimations of binding peaks as previously described (Pokholok et al., 2005). This suggests that previous studies have underestimated the true number of Abf1 binding sites *in vivo*.

Comparison of the location of Abf1 binding peaks suggest that Abf1 is predominantly located within intergenic regions, primarily situated at promoters (Fig. 3.6A). Indeed, Abf1 has previously been observed to preferentially bind upstream of genes (Schlecht et al., 2008). This correlates with the preferential location of the Abf1 DNA binding consensus sequence found ~100bp upstream of a TSS (Schlecht et al., 2008). Interestingly this location maps to the preferential position of a promoter NDR, and as previously discussed Abf1 is known to promote NDRs (Hartley and Madhani, 2009; Lee et al., 2007b; Yarragudi et al., 2004). The consensus DNA binding sequence of Abf1 was previously mapped to ~500 promoters at NDRs, however the studies presented here suggest that Abf1 in fact binds at a much larger number of promoters. This likely reflects the fact that Abf1 is not exclusively found at NDRs, nor its consensus DNA binding sequence (Ganapathi et al., 2010; Schroeder and Weil, 1998). Indeed, of the 3571 Abf1 binding peaks identified in this study only ~1000 are observed to contain an Abf1 consensus DNA binding sequence (M. Bennett, unpublished results). The results presented here also suggest that the 2332 promoters identified to be bound by Abf1 may be a conservative estimation, as statistically insignificant LLB peaks of Abf1 are found at many other promoter regions (Fig. 3.6C). A recent study that analysed nucleosome occupancy genome-wide, demonstrated that a strain expressing the DNA binding temperature sensitive mutant *abf1-1* at the restrictive temperature, displayed higher levels of nucleosome occupancy at NDRs when compared with the wild type strain (Ganapathi et al., 2010). Whilst they detected changes at 444 NDRs that were considered statistically significant ($p < 0.05$), 4478 loci were observed to change. Interestingly, the statistical significance for changes in nucleosome occupancy correlated well with that for Abf1 occupancy at values far below $p < 0.05$. This suggests that many of the enriched sites ($p < 0.05$) in both microarray studies genuinely represent Abf1 binding sites despite a lack of statistical significance at the level of probability selected. These observations are in good agreement with the conclusions presented in this study; that Abf1 binds at thousands of sites throughout the genome, that Abf1 is preferentially localised at

promoter regions (where NDRs are primarily found) and that many regions of Abf1 binding that are not statistically significant likely represent true binding sites that are biologically relevant. Therefore, promoter regions with statistically insignificant Abf1 binding peaks identified in this study (Fig. 3.6), as a population, are more appropriately considered to represent regions of LLB for Abf1 rather than regions not bound by the protein. Furthermore, given that the cell populations used in these studies were heterogeneous, LLB of Abf1 may also represent binding sites that are differentially bound at different phases of the cell cycle.

Immediately after UV irradiation the genome-wide localisation of Abf1 was not observed to change significantly, however, following 30 minutes repair, the occupancy of Abf1 is found to fall at a large proportion of Abf1 binding peaks (Fig. 3.5 and 3.8). Therefore the recruitment of Abf1 to numerous novel genomic loci does not occur as part of the early DNA damage response. These observations suggest that the GGR complex may bind Abf1 binding sites in the absence of DNA damage, rather than being recruited to binding sites in response to UV. Alternatively, a dynamic exchange of Abf1 for the GGR complex at Abf1 binding sites could occur after UV; this might not be detected using the current experimental strategy. The data suggests that Abf1 is a condition invariant DNA binding protein, in contrast to other GRFs such as Reb1 and Rap1 (Harbison et al., 2004). Induced binding of Abf1 to a small subset of genes has previously been observed under conditions promoting fermentation, respiration or sporulation (Schlecht et al., 2008). However, the authors noted that the majority of Abf1 binding targets remained the same in all conditions. It is noteworthy that this study also suggested that a proportion of Abf1 binding targets were different in response to UV irradiation (Fig. 3.5A), however, after careful analysis these results were discovered to be false positives. The cause of this was either due to the peak position shifting by a single probe or where low binding peaks were not statistically significant either before and after UV despite little change in the level of binding. Therefore, the small subsets of differential Abf1 binding targets identified by Schlecht et al. could potentially represent false positives due to the same causes described in this study. As previously shown at the *HML α* I-silencer, the occupancy of Abf1 is lower at many Abf1 binding sites in response to UV damage (Fig. 3.8B, Yu et al., 2009). However, when Abf1 binding is quantified by qPCR directly after UV damage some loci show increased levels of occupancy that is not reflected in the microarray data (Fig. 3.7B, Fig. 3.8C). Whilst the reasons for these

discrepancies are unknown, the collective data suggests that the predominant loss of Abf1 occupancy correlates with the onset of DNA repair following UV damage. However correlations were not observed between changes in the level of Abf1 binding and CPD repair rates. This is further discussed in Chapter 7.

Abf1 promotes binding of the GGR complex to an Abf1 consensus DBS *in vitro*, suggesting that Rad7/Rad16 may be targeted to domains bound by Abf1 *in vivo* (Yu et al., 2009). This may function to co-ordinate Rad16 dependent histone H3 K9K14 acetylation and GGR at domains bound by Abf1. Using composite profiles, histone H3 K9K14 hyperacetylation peaks were observed proximal to Abf1 binding sites within promoter regions (Fig. 3.10). In these regions, a peak of acetylation is situated either side of the Abf1 binding sites. Given that both K9 and K14 hyperacetylation peaks have previously been suggested to be orientated at TSSs, this double peak pattern may represent the distribution of TSSs either side of Abf1 binding sites in promoters (Pokholok et al., 2005). However, when acetylation is plotted at Abf1 binding sites where a TSS is strictly orientated to one side of the binding site, two peaks are still observed (see appendix II). Given that Abf1 is known to promote NDRs at promoters (Hartley and Madhani, 2009; Yarragudi et al., 2004), an alternative explanation for the distribution of histone acetylation at the Abf1 binding sites is that an NDR functions to lower the level of acetylation by reducing the target substrate itself (ie. a nucleosome). Indeed, preliminary data from our lab has suggested that when histone acetylation is normalised relative to histone occupancy a single peak of histone H3 K9K14 acetylation is found centred at the Abf1 binding site (K. Evans, unpublished data). This suggests that Abf1 binding may have a functional role in regulating the distribution of histone H3 K9K14 acetylation at promoters.

In response to UV damage the distribution of histone H3 K9K14 acetylation at Abf1 binding sites is not significantly altered (Fig. 3.10). These observations also hold true at promoter regions with LLB of Abf1 (Fig. 3.11). It was previously shown that the genome-wide levels of histone H3 K9K14 acetylation significantly rise in response to UV damage (Teng et al., 2008; Yu et al., 2005). Collectively these data suggest that regions of hyperacetylation prior to UV are maintained after UV. Indeed, a very strong correlation is observed between the distribution of histone H3 K9K14 acetylation before and after UV (K. Evans, unpublished data). This suggests that mechanisms which regulate the distribution of histone H3 K9K14 acetylation prior to UV are likely to be functional in the UV responsive pathway. In support of this idea,

it is interesting to note that the loss of Rad16 significantly affects the distribution of histone acetylation at promoters both before and after UV (Fig. 3.10 and 3.11). This demonstrates that Rad16 has a functional role in histone acetylation in the absence of UV damage, in addition to its previously noted role after UV (Yu et al., 2005). Rad16 functions to promote the distribution of acetylation at regions proximal to Abf1 binding sites in promoter regions (Fig. 3.10 and 3.11). This effect is profound and likely occurs at a large majority of promoters. In response to UV irradiation, the distorted distribution of acetylation at promoters in the *rad16Δ* mutant is maintained (Fig. 3.10). These data again support the hypothesis that similar mechanisms regulate the distribution of acetylation in the absence and presence of UV damage. This suggests that the activities of Rad16 necessary for histone acetylation are upregulated, rather than activated, in response to UV.

Abf1 preferentially binds at promoter regions and Rad16 functions to promote the distribution of histone H3 K9K14 hyperacetylation at Abf1 binding sites in promoter regions, suggesting that Abf1 functions to target Rad16 dependent histone acetylation to these sites. To investigate whether Abf1 binding is necessary for histone hyperacetylation at promoters, histone H3 K9K14 acetylation was plotted at promoters that do not contain a statistically significant Abf1 binding peak (Fig. 3.11 C and D). These regions of the genome were predicted to be absent of histone H3 K9K14 hyperacetylation peaks if Abf1 binding was necessary for the acetylation pattern. Although such promoters still demonstrate typical hyperacetylation peaks, these regions more accurately represent domains of LLB rather than domains not bound by Abf1 (Fig. 3.6). Therefore, using the current experimental data it is unclear whether Abf1 binding is necessary for or promotes histone H3 K9K14 hyperacetylation at promoter regions. The same conclusion may also be made for Rad16 dependent acetylation and GGR. By comparing promoter regions with statistically significant Abf1 binding peaks (HLB) to those that do not contain a statistically significant Abf1 binding peak (LLB), it was shown that Rad16 dependent acetylation is not restricted to promoter regions with HLB of Abf1 (Fig. 3.11 E. and F.). These data demonstrate that the level of Abf1 binding is not important for promoting Rad16 dependent acetylation at promoters. Indeed, pearson/spearman correlation analysis did not observe a correlation between the level of Abf1 binding and either wild type nor *rad16Δ* acetylation levels. This is further discussed in Chapter 7.

When the Abf1 DNA consensus binding site was mutated at the *HML α* 1-silencer a ~400bp domain of reduced GGR was observed extending in one direction from the binding site (Yu et al., 2009). This demonstrates that Abf1 binding can promote GRR within a proximal domain. At the genomic level rapid CPD repair rates do not colocalise with Abf1 binding (Fig. 3.12). This demonstrates that other factors promote rapid CPD repair rates in vivo. One such factor is likely to be the presence of genes, which would be preferentially repaired on the TS by TCR; this is known to repair CPDs faster than GGR (Mellon et al., 1987). Therefore, analysing GGR rates in the absence of TCR may be more suitable to investigate how Abf1 binding influences CPD repair genome-wide. Relative to the wild type repair rates, the largest defects in CPD repair in a *rad16 Δ* mutant are observed at Abf1 binding sites in promoter regions (Fig. 3.12). This demonstrates that efficient Rad16 dependent GGR is organised at Abf1 binding sites in promoter regions, which correlates with the location of Rad16 dependent histone acetylation. The large defect in repair in a *rad16 Δ* mutant at promoters likely reflects the fact that TCR does not significantly function to contribute to repair in these regions of the genome and thus most CPD repair here requires GGR and thus Rad16 (Hanawalt and Spivak, 2008). Therefore, in the absence of a Rad16 dependent CPD repair profile, promoter regions may represent the most suitable regions of the genome for analysing GGR. As with acetylation, distinguishing HLB and LLB of Abf1 at promoters demonstrates that there is not a correlation between the level of Abf1 binding and Rad16 dependent GGR (Fig 3.13).

The current study demonstrates that Abf1 binds the genome at a high frequency, and is predominantly situated within promoter regions. In response to UV, Abf1 does not relocalise but the global occupancy of Abf1 binding on chromatin is reduced at a proportion of its binding sites. This suggests that the GGR complex may bind at Abf1 binding sites in the absence of UV damage. Rad16 has a global role in regulating the distribution of histone H3 K9K14 acetylation at promoters both before and after UV. It is also at these regions that efficient Rad16 dependent GGR is localised. The correlation between Abf1 binding at promoters and the organisation of Rad16 dependent histone H3 K9K14 acetylation and efficient GGR in these regions

strongly suggests that Abf1 binding targets the GGR complex and thus organises GGR from promoter regions of the genome.

As a complementary study to the current chapter, the proceeding chapter investigates the genome-wide localisation of the GGR complex by analysing the distribution of Rad16 binding using a similar ChIP-on-chip strategy.

4. Mapping the genome-wide localisation of Rad16 in the absence and presence of UV damage

4.1 Introduction

To date, the current understanding of the molecular mechanism of NER has been significantly determined using biochemical in vitro assays that have studied the repair of naked DNA. However, within the cell DNA is packaged into a structural fibre of nucleosomal DNA termed chromatin. The nucleosome consists of a protein octamer of two copies of histones H2A, H2B, H3 and H4. This core particle also includes ~147bp of DNA which wraps around the histone octamer. This primary structure is the predominant form in which DNA exists within the cell, and therefore this poses the fundamental question as to how NER operates during repair of this substrate.

In vitro, reconstitution of naked DNA into chromatin inhibits the efficient excision of NER substrates such as (6-4)PPs, when combined with the core NER factors necessary for efficient repair of naked DNA (Hara and Sancar, 2002, 2003; Ura et al., 2001). These observations suggest that additional factors exist within the cell to permit efficient repair of chromatin in vivo. The original observation that repair of UV damage is concurrent with the relaxation of chromatin founded the long standing model whereby chromatin is remodelled to permit efficient NER, and then restored to its original structure; this is termed the access, repair, restore (ARR) model (Green and Almouzni, 2002; Smerdon and Lieberman, 1978). Chromatin remodelling is considered to occur by three principle activities; exchange of core histones with histone variants, covalent modification of histone tails and alterations in histone-DNA interactions (Saha et al., 2006). The latter of these activities is catalysed by the Snf2 protein family of ATPases (Clapier and Cairns, 2009; Flauss et al., 2006). These activities are believed to modulate the accessibility of DNA within the nucleosome thereby facilitating DNA dependent interactions/reactions with chromatin modifying factors.

Recent evidence has implicated a variety of chromatin remodellers and modifications to be related to UV damage and NER in vivo (Palomera-Sanchez and Zurita, 2011; Zhang et al., 2009). In *S. cerevisiae*, an interaction between Rad4-Rad23 and the Snf2 chromatin remodeller SWI/SNF is stimulated upon UV irradiation (Gong

et al., 2006). Deletion of Snf6, a subunit of the SWI/SNF complex necessary for functional activity, inhibits both UV dependent chromatin remodelling and efficient GGR in vivo. Knockdown of Brg1, the catalytic subunit of hSWI/SNF, similarly inhibits efficient UV dependent chromatin remodelling and CPD repair in human cells (Zhao et al., 2009). A UV inducible interaction between Rad4-Rad23 and the Snf2 chromatin remodeller Ino80 complex has also been recently observed (Sarkar et al., 2010). In mammals, the INO80 complex interacts with DDB1, and whilst in both yeast and mammalian cells INO80 is observed to promote repair of UV damaged DNA, the stage at which this protein promotes NER is unresolved (Jiang et al., 2010). The UV-DDB complex is also part of an E3 ubiquitin ligase which has been demonstrated to ubiquitylate histones H2A, H2B, H3 and H4 in vitro (Wang et al., 2006). Interestingly, both histone H2A, H3 and H4 ubiquitylation has been demonstrated to be upregulated in response to UV, implicating that these modifications could occur by UV-DDB to remodel chromatin during GGR (Bergink et al., 2006; Kapetanaki et al., 2006; Wang et al., 2006). The UV-DDB complex has also been shown to interact with the histone acetyl transferases (HATs) CBP, STAGA and p300 suggesting that histone acetylation may also be important for UV dependent chromatin remodelling (Datta et al., 2001; Martinez et al., 2001; Ropic-Otrin et al., 2002). Recently, the catalytic component of STAGA, GCN5, was demonstrated to be recruited to UV damaged chromatin in an E2F1 dependent manner (Guo et al., 2010a; Guo et al., 2010b). E2F1 is a TF that is also known to interact with UV-DDB (Hayes et al., 1998). Importantly, GCN5 is necessary for UV dependent histone H3 K9 acetylation at sites of DNA damage. Knockdown of GCN5 inhibited this UV dependent acetylation event and significantly reduced the repair rates of both (6-4)PPs and CPDs. Collectively these data strongly suggest that chromatin remodelling is necessary for the efficient repair of DNA damage by NER in vivo.

As previously described in Chapter 1.4.4, Rad16 is a member of the Snf2 family of ATPases, suggesting that the protein may play a fundamental role in chromatin remodelling. As with other members of the Snf2 family, Rad16 is able to induce superhelical torsion in DNA, likely through the activity of DNA translocation (Flaus et al., 2006; Yu et al., 2004; Yu et al., 2009). DNA translocation (and torsion) by Snf2 members is thought to disrupt histone-DNA interactions which can result in a variety of chromatin remodelling outcomes including the ejection of the nucleosome, nucleosome sliding, unwrapping of DNA at the nucleosome and histone variant

exchange (Clapier and Cairns, 2009). In vitro, Rad16, as part of the GGR complex, was not observed to promote nucleosome sliding (Yu et al., 2009). In addition, the RING domain of Rad16, in combination with Rad7, Cul3 and Elc1 functions as an E3 ubiquitin ligase (Gillette et al., 2006; Ramsey et al., 2004). As discussed above, the activities of either of these functions may promote chromatin remodelling in response to UV damage.

Gcn5 was originally demonstrated to be necessary for the efficient in vivo repair of CPDs in *S. cerevisiae* (Teng et al., 2002; Yu et al., 2005). UV irradiation stimulates large increases in histone H3 K9K14 acetylation levels, concurrent with increases in chromatin accessibility (Yu et al., 2005). This hyperacetylation event requires Gcn5, demonstrating that HATs catalyse UV dependent histone hyperacetylation in both yeast and humans. Interestingly, whilst UV dependent histone H3 K9K14 hyperacetylation can occur in the absence of Rad4 or Rad14 and thus functional NER, Rad16 is strictly required (Teng et al., 2008; Yu et al., 2005). At the *MFA2* promoter, deletion of *TUP1* suppresses the requirement of Rad16 for functional GGR (Teng et al., 2008). Deletion of *TUP1* also induces histone H3 K9K14 hyperacetylation. These observations suggested that Rad16 might function to promote UV dependent histone H3 K9K14 hyperacetylation prior to repair, which is necessary for efficient GGR in vivo. This hypothesis has recently been tested at the *MFA2* locus (Yu et al., 2011). Using this model gene locus, it was shown that both Rad7 and Rad16 are required for UV dependent increases in the level of Gcn5 binding, subsequent histone H3 K9K14 acetylation and increases in chromatin accessibility. In the absence of Tup1 and Rad16, histone H3 K9K14 hyperacetylation at *MFA2* is abrogated when Gcn5 is deleted. In addition to the loss of hyperacetylation, the triple mutant also showed a significant decrease in chromatin accessibility and GGR. This demonstrates that a significant proportion of Rad16 independent GGR in *TUP1Δ* is due to histone H3 K9K14 hyperacetylation. Therefore, Rad7/Rad16 regulates the occupancy of Gcn5 and histone H3 K9K14 acetylation that mediates chromatin remodelling necessary for efficient GGR in vivo. Interestingly, mutating either the ATPase domain or RING domain of Rad16 alone partly inhibits efficient GGR but mutating both domains was necessary to inhibit UV dependent increases in Gcn5 occupancy and histone H3 hyperacetylation. These observations demonstrate that both the ATPase and E3 ligase activities of Rad16 contribute to regulating Gcn5 occupancy and histone acetylation. They also suggest that histone H3

hyperacetylation might not be the only chromatin remodelling activity that Rad7/Rad16 promotes necessary for efficient GGR in vivo. Other chromatin remodelling activities could include histone ubiquitylation and the induction of superhelical torsion by Rad16 dependent translocation.

Site specific DNA binding by Abf1 promotes efficient DNA binding of the GGR complex in vitro and efficient GGR at a proximal domain in vivo (Yu et al., 2009). Efficient binding of Rad7 and Rad16 at Abf1 binding sites is hypothesised to promote domains of efficient GGR (see Chapter 1.5.5, Chapter 3). In the previous chapter, both histone H3 K9K14 acetylation and CPD repair was investigated in relation to Abf1 binding (Chapter 3). A correlation was observed between Abf1 binding at promoter regions, Rad16 dependent histone acetylation and efficient GGR suggesting that Abf1 binding targets the GGR complex to promoter regions. In response to UV, unidirectional translocation by Rad16 from the Abf1 binding site (see Chapter 1.5.5), in addition to the E3 ligase of the GGR complex, is modelled to promote histone hyperacetylation and remodel chromatin (see above). These activities subsequently promote efficient GGR. It was also suggested that Rad16 regulates the distribution of histone acetylation at promoters in a similar manner both before and after UV (Chapter 3). Therefore the E3 ligase/DNA translocation by the GGR complex may also be actively promoting acetylation in the absence of damage, and this is upregulated in response to UV. Finally, it was shown that the genome-wide localisation of Abf1 does not change in response to UV damage; this was interpreted to suggest that the GGR complex functions to bind chromatin in the absence of UV. The present study aims to further extrapolate upon these conclusions by investigating the global role of the GGR complex by performing Rad16 ChIP-on-chip in both the presence and absence of UV damage. Using these datasets, Rad16 binding is then correlated with both acetylation and CPD repair in the context of Abf1 DNA binding sites at promoters.

4.2 Materials and Methods

Strains used in this study:

Strain	Genotype	Source
BY4742	MAT α , his3 Δ 1 leu2 Δ 0 lys2 Δ 0 ura3 Δ 0	Euroscarf
BY4742 (Rad16-Myc)	BY4742, <i>RAD16::18xMyc-URA3</i>	S.Yu (unpublished)

ChIP-on-chip/ChIP

BY4742 (or BY4742 (Rad16-Myc)) was grown in YPD at 30°C up to a density of 2×10^7 cells/ml and UV irradiated as described in Chapter 2.2. ChIP was performed as detailed in Chapter 2.7 with the following modifications. Cells were crosslinked for 40 minutes. Cells were lysed by vortexing with glass beads for 30 minutes. IPs were performed using Dynabeads pan mouse IgG (Invitrogen, #110.41). Beads were washed three times in 500 μ l of PBS (BSA 1mg/ml) and resuspended in an equal volume of PBS (BSA 1mg/ml) to that originally taken. α -Myc antibody (9B11 mAB#2276, Cell Signalling Technology) was added at a concentration of 4 μ l per 100 μ l of bead suspension and left to incubate at 30°C and 1300rpm on an eppendorf thermomixer comfort for 30 minutes. Bead suspension was subsequently washed three times and resuspended as before. For IP samples, 200 μ l of WCE was diluted with 100 μ l of bead suspension and BSA was added to a final concentration of 1mg/ml. IP samples were incubated at 21°C and 1300rpm on an eppendorf thermomixer comfort for 3 hours. Beads were subsequently washed and immunoprecipitated chromatin was purified to DNA as described in Chapter 2.7. Input samples were purified from 50 μ l of WCE. ChIP samples were prepared for ChIP-on-chip analysis as described in Chapter 2.8.

ChIP-on-chip chromosomal maps

Chromosomal maps of the averaged traces of ChIP-on-chip data for both Rad16 datasets are available on the accompanying DVD (D:/Chapter 4/ChIPchip).

Primers used for qPCR:

IRC5:

Forward: 5' – AGTCGGGGCAGATACAGTTG

Reverse: 5' – GGCCGCTCTGGTCAATATAA

prRAD23:

Forward: 5' – TAGCAAGCTTGTCTGCGAAC

Reverse: 5' – AGGCAAGAAATAGCGACAGC

prMFA2:

Forward: 5' – AAAAGCATGTATTTACCTATTCG

Reverse: 5' – TATATACAAAATTACGTGGTAATGC

Data values of qPCR quantification are available in appendix III. Error bars represent the standard deviation of replicates.

Data normalisation and statistical analysis

All data normalisation, manipulations and statistical analysis were performed in 'R' as described in Chapter 3.2.

Note for Fig. 4.4B and C

The fold change in Abf1 enrichment after UV was calculated as $\log_2(\text{Red channel/Green channel})_{30} - \log_2(\text{Red channel/Green channel})_U$ using the averaged Abf1 binding datasets. The data values of $\log_2(\text{Red channel/Green channel})_{30} - \log_2(\text{Red channel/Green channel})_U$ at Abf1 binding peaks that co-localised with Rad16 binding peaks were ranked and sorted from largest increases to largest decreases. These sorted values were equally divided into 5 groups of ~200 values. The corresponding probes from these values were then used in 5 individual composite profiles for each of the trendlines given in Fig. 4.4B. The fold change in Rad16 enrichment after UV was calculated as $\log_2(\text{Red channel/Green channel})_{30} - \log_2(\text{Red channel/Green channel})_U$ using the averaged Rad16 binding datasets. The same 5 groups of probes identified for fold changes in Abf1 binding defined the composite profiles for the trendlines of Rad16 binding fold change given in Fig. 4.4C.

Note for Fig. 4.6, 4.7 and 4.8

As described in the legend above Fig. 4.6, 4.7 and 4.8 also use a ranking system to graphically display correlations. The data plotted at these graphs is limited

to sites where a Rad16 binding peak colocalises at an Abf1 binding peak, and this is found within a promoter region. In all three figures the level of Rad16 binding in the absence of UV is ranked from highest to lowest and the sorted values are split into 5 groups ~150 values. The trendlines of these groups are then plotted on the composite profiles. All other datasets are split into the same 5 groups as defined by the Rad16 binding rank and the corresponding trendlines are plotted.

Note for Fig. 4.8.

Rad16 dependent histone H3 K9K14 acetylation was calculated as (Red channel/Green channel) U wild type – (Red channel/Green channel)U *rad16Δ*. The Rad16 dependent repair rate was calculated as (Red channel/Green channel) wild type CPD repair rate – (Red channel/Green channel) *rad16Δ* CPD repair rate using the averaged datasets. For graphical representation these calculations were converted to \log_2 . Because some R/G values were negative (which cannot be logged) in these datasets, a constant was added to these R/G datasets to remove these. This does not function to skew the data, nor affect the patterns presented in these figures but does result in higher arbitrary values than those seen in other figures.

Other ChIP-on-chip datasets used in this study

The CPD repair and histone H3 K9K14 acetylation datasets used in this study were kindly provided by K.Evans and Y.Teng (unpublished results, Teng et al., 2010).

4.3 Results

4.3.1 Genome-wide analysis of Rad16 binding

In order to delineate the global distribution of Rad16 before and after UV irradiation, a similar strategy was used to that previously described for Abf1 (see Chapter 3.3). For these experiments BY4742 harbouring an endogenous copy of Rad16 with an 18xMyc tag at its C-terminal was used. This strain is known to possess a wild type UV sensitivity, demonstrating that the tag does not alter the functionality of the protein (S.Yu, unpublished results). Rad16 was immunoprecipitated from chromatin that had not received UV irradiation (U) and from a sample allowed to repair UV damage for 30 minutes following UV irradiation (30). IP and input DNA was labelled with Cy5 and Cy3 respectively and applied to yeast whole genome microarrays. These experiments were repeated to provide three biological replicates of the data. Raw data was quantile normalised and shifted by mode between each of the three biological replicates as previously described for Abf1 ChIP-on-chip (Chapter 3.3.2).

As seen with Abf1, following data normalisation each of the replicates presented highly reproducible results (Fig. 4.1A). In contrast to Abf1, the genome-wide distribution of Rad16 both before and after UV irradiation presented peaks with low levels of enrichment above background (2-4 fold) (the averaged datasets are available on the accompanying DVD, D:/Chapter 4/ChIPchip). In further contrast to the Abf1 datasets, Rad16 peaks are not detected as discrete peaks in some instances; instead, a broad range of enrichment is observed over many kilobases (Fig. 4.1A). These observations suggested that Rad16 may be capable of binding throughout the entire genome but is preferentially localised to certain regions where peaks are observed. To test this possibility, ChIP enrichment of Rad16 with the C-terminal Myc tag was compared against an isogenic strain without the tag (negative control) at numerous loci where Rad16 binding was not observed to peak from the genome-wide data. As shown in Fig. 4.1B, when ChIP is performed upon both strains using an α -Myc antibody, the strain expressing Myc tagged Rad16 immunoprecipitates higher levels of chromatin than the negative control at all regions tested. This is true both in the absence and presence of UV damage. These results demonstrate that Rad16 interacts with chromatin throughout the entire genome both before and after UV damage.

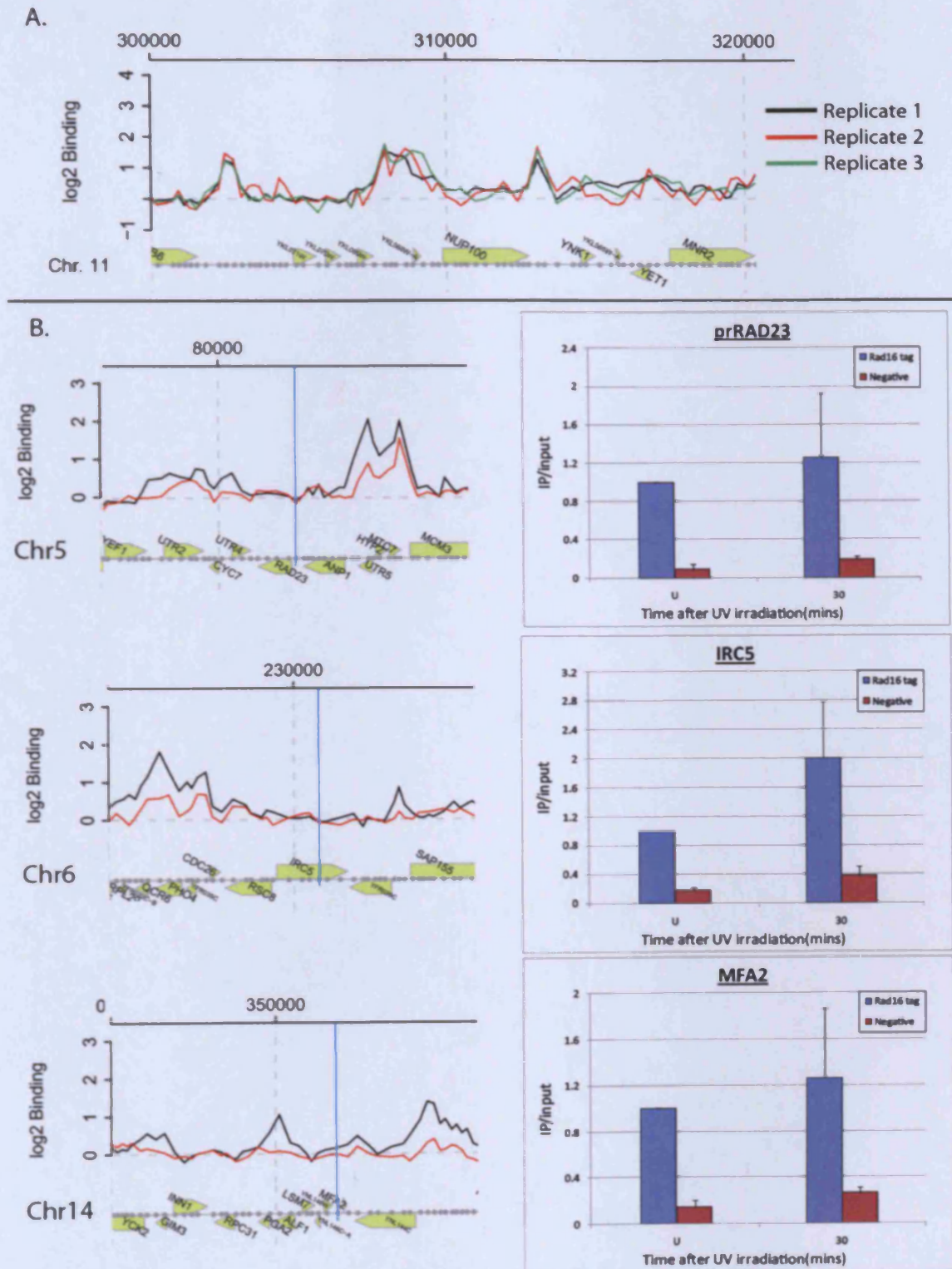


Figure 4.1. A. Example of the Rad16 binding datasets at chromosome 11 following normalisation. B. Rad16 ChIP at three sites where a peak of enrichment is not observed in the genome-wide datasets. Left hand graphs represent the averaged datasets of Rad16 enrichment in the unirradiated condition (black line) and 30 minutes following repair (red line). The blue line represents the region analysed using qPCR. Right hand graphs show the quantification of Rad16 binding for a positive (Myc tagged) and negative (non-tagged) control strain at the loci represented at the blue lines.

4.3.2 The distribution of Rad16 before and after UV irradiation

The peak detection strategy previously applied to the Abf1 datasets was also utilised for Rad16 binding (Fig. 4.2A). In the absence of UV irradiation a total of 1479 peaks were detected ($p < 0.01$), which dropped to 728 peaks after UV. Of these peaks, 384 overlapped within a single probe of each other between the two datasets. As previously noted with the Abf1 datasets, all non-overlapping peaks detected in the Rad16 dataset after UV were not statistically different in height from the equivalent probes in the U dataset, suggesting that these peaks represent false positives. However, of the 1095 peaks present in the U dataset but absent in the 30 dataset, 653 were significantly lower following 30 minutes repair ($p < 0.05$). These data suggest that following UV, peaks of Rad16 binding are lost or diminished (Fig. 4.2C and D). Given that this does not represent loss of Rad16 chromatin binding (Fig 4.1B), this indicates that the genome-wide localisation of Rad16 is more evenly distributed in response to UV damage. These observations are consistent with a model in which UV damage upregulates the DNA translocase activity of Rad16, resulting in the more uniform distribution of Rad16 binding observed (see discussion). The genome-wide loss of Rad16 binding peaks after UV correlates with the onset of histone H3 K9K14 hyperacetylation (Teng et al., 2008; Yu et al., 2005). When composite profiles of Rad16 binding are compared at the 1479 binding sites defined in U, the loss of Rad16 peaks is clearly apparent (compare Fig. 4.2C and D). The Rad16 peaks in U were also categorised into their respective genomic location (Fig. 4.2B). As previously seen with Abf1, Rad16 binding peaks are highly enriched at promoter regions.

A. Rad16 peak detection summary

Dataset	Peaks	Identical peak position	Peaks moved by one probe	Remaining peaks	Remaining peaks statistically different ($p < 0.05$)
U	1479	284	100	1095	653
30	728	284	100	344	0

B. Location of Rad16 binding peaks

Rad16 peak position	Number of peaks	% of peaks	% of probes on array	%peaks/%probes
Intragenic	420	28	73	0.38
Intergenic	1059	72	27	2.67
-Promoter	554	37	14	2.64
-Divergent promoter	395	27	8	3.38
-Downstream	106	7	5	1.40
-Unknown	4	0.2	0.3	0.67
-Total	1479	100	100	N/A

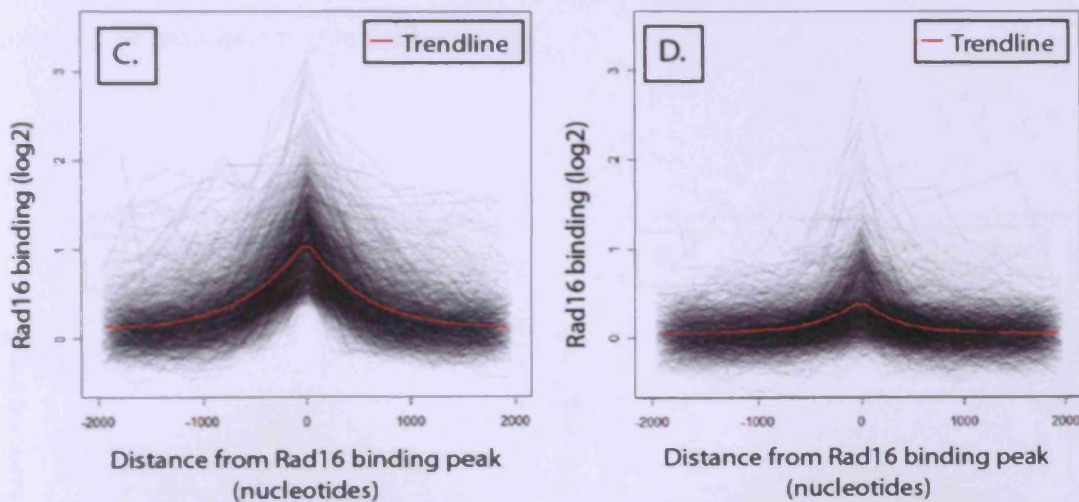
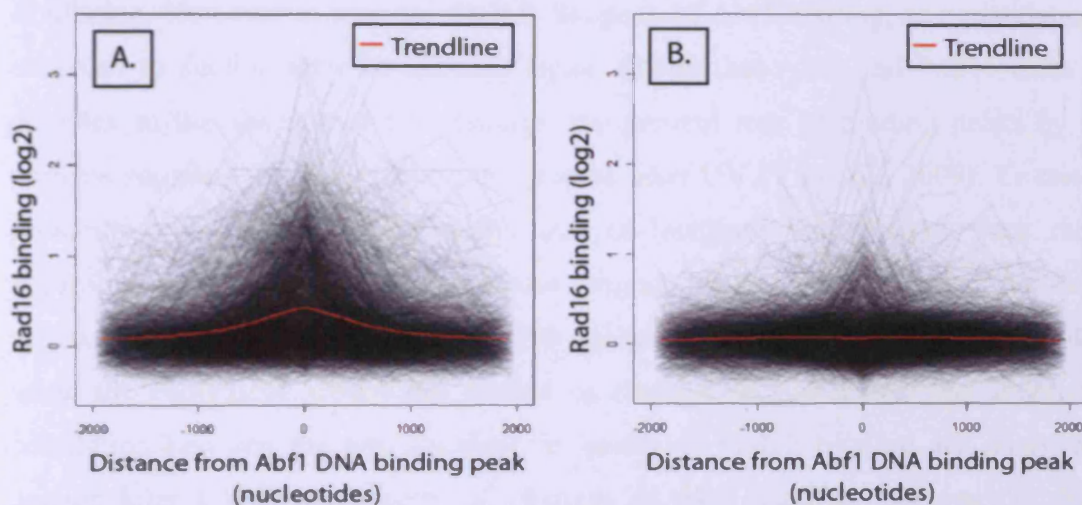


Figure 4.2. A. Table summarising peaks detected in the Rad16 datasets. B. Table summarising the location of the Rad16 peaks detected in the U dataset. C. Composite profile of Rad16 binding at the peaks identified in the U dataset. D. Composite profile using the same peak positions as C. but data shows Rad16 binding after UV irradiation (30).

4.3.3 Rad16 binding colocalises with Abf1 binding in vivo

Abf1 binding by the GGR complex has been previously demonstrated to target Rad7/Rad16 to a consensus binding site in vitro in the absence of UV damage, but due to technical limitations at the time, this was not demonstrated in vivo (Yu et al., 2009). To investigate whether Abf1 functions to localise Rad16 to regions of the genome to which it efficiently binds, the co-localisation of the two proteins was examined. When the U Rad16 dataset is plotted at the statistically significant Abf1 binding peaks identified in the respective U dataset (Chapter 3), a clear co-localisation is observed (Fig. 4.3A). Indeed, of the 1479 Rad16 peaks detected in the U dataset, 519 of these intersect with an Abf1 binding peak whilst a further 450 co-localise

within one probe on the microarray. Furthermore, of the Rad16 peaks in promoters that do not co-localise with Abf1, ~50% of these are present at the same gene promoters as statistically significant Abf1 binding peaks (data not shown). This demonstrates that the majority of Rad16 peaks colocalise with Abf1 binding peaks, strongly supporting the hypothesis that Abf1 functions to promote binding of the GGR complex to its cognate binding sites in vivo. In accordance with the above results, peaks of Rad16 binding at Abf1 binding peaks is lost after UV irradiation (Fig. 4.3B). The genomic position of Rad16 colocalisation with Abf1 binding was also examined (Fig. 4.3C). Interestingly, ~80% of sites of colocalisation occur at promoter regions further supporting the hypothesis that Abf1 binding targets the GGR complex to promoter regions (Chapter 3).



C. Relative distribution of Abf1/Rad16 colocalisation

Rad16 peak position	Independent of Abf1 peak	Colocalise with Abf1	% of peaks that colocalise	% of Abf1 peaks	%peaks colocalise /% Abf1 peaks
Intragenic	279	141	15	27	0.56
Intergenic	231	828	85	73	1.16
-Promoter	120	434	45	40	1.13
-Divergent promoter	81	314	32	26	1.23
-Downstream	30	76	8	7	1.14
-Unknown	0	4	0.4	0.2	2.00
-Total	510	969	100	100	N/A

Figure 4.3. A. Composite profile of Rad16 binding data (U) plotted at Abf1 binding peaks identified in U. B. As A. but plots the Rad16 binding data after UV irradiation (30). C. Table summarising the location of Rad16 peaks (U) in relation to Abf1 binding peaks (U).

4.3.4 The UV responsive changes in GGR complex chromatin binding

In response to UV, the GGR complex was previously suggested to promote domains of superhelical torsion necessary for GGR in vivo by unidirectional translocation initiated at an Abf1 DBS (Yu et al., 2009). The UV dependent loss of Rad16 enrichment at Abf1 binding peaks is consistent with the translocation of Rad16 after UV (Fig. 4.3A and B). This view would be further substantiated if the localisation of the GGR complex was observed to redistribute itself distal to an Abf1 binding peak at an intermediate timepoint between the unirradiated condition and 30 minutes after UV. Therefore, composite profiles of Abf1 binding were plotted at the 916 sites where Rad16 and Abf1 were observed to co-localise and examined for the U, 0 and 30 datasets. As shown in Fig. 4.4A, the distribution of Abf1 binding does not relocate distal to the binding site neither immediately nor 30 minutes after UV irradiation. However as seen for Rad16, the peak of Abf1 binding, as a population, is observed to decline after 30 minutes repair. Given that Abf1 and Rad16 exist as a complex in the absence of UV damage, the general loss of binding peaks by both proteins suggests that they remain in complex after UV (Yu et al., 2009). To test this possibility, the Abf1 binding peaks that co-localised with Rad16 were ranked according to their UV response (from largest decline in enrichment to largest increase) and plotted as 5 groups of ~200 probes (Fig. 4.4B). As shown in Fig. 4.4C, when the equivalent groups are plotted as changes in Rad16 binding, there is no correlation between the two datasets; ie. peaks of Rad16 binding are observed to decline after UV independently of changes in Abf1 binding. Pearson correlation analysis did not indicate a correlation between the changes in Rad16 and Abf1 binding after UV. These data suggest that the two proteins might not function as a complex on chromatin after UV irradiation.

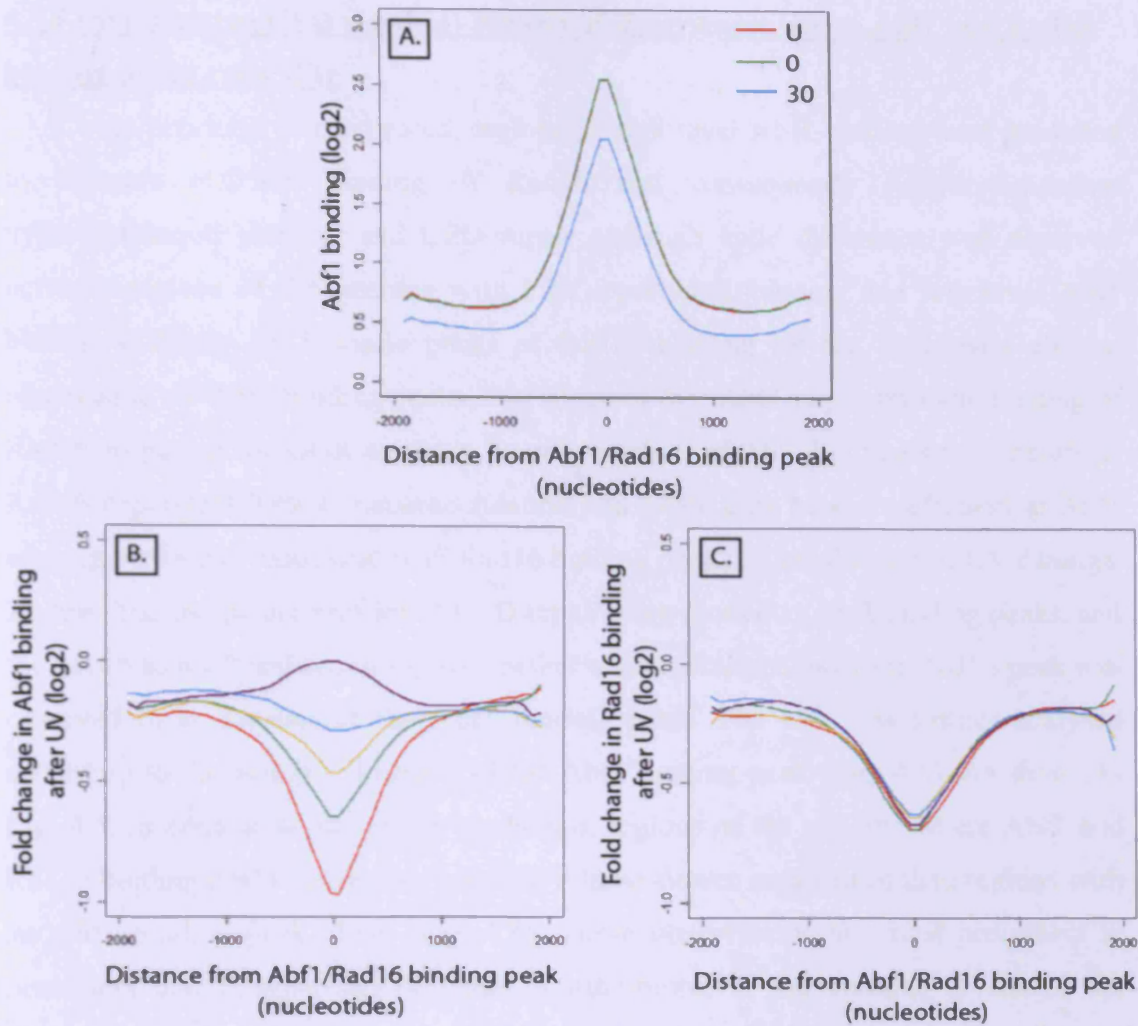


Figure 4.4. A. Composite profile of Abf1 binding for the datasets U (red line), 0 (green line) and 30 (blue line) positioned at Abf1 binding peaks that co-localise with a Rad16 binding peak. Only the trendlines are shown. The red trendline (U) maps exactly to that of the green trendline (0). B. Composite profile of the relative UV responsive changes in Abf1 binding positioned at Abf1 binding peaks that co-localise with a Rad16 binding peak. The data was separated into 5 groups according to the relative change. The trendlines plotted represent the average response for each group. C. As B. but plotting the equivalent UV responsive changes in Rad16 binding.

4.3.5 Investigating CPD repair at regions of the genome where Abf1 and Rad16 binding peaks colocalise

As previously investigated, regions of high level Abf1 binding were predicted to promote efficient binding of Rad16 and consequently Rad16 dependent hyperacetylation patterns and CPD repair although little difference was observed between regions of the genome with high level Abf1 binding and low level Abf1 binding (Chapter 3). Because peaks of Rad16 binding (in the U dataset) are not observed at all Abf1 binding peaks, this suggests that Abf1 might promote binding of Rad16, as part of the GGR complex, to only a subset of Abf1 binding sites. Therefore, Rad16 dependent histone hyperacetylation and GGR may be more efficient at Abf1 binding peaks that colocalise with Rad16 binding peaks in the absence of UV damage. To test this, composite profiles of CPD repair were plotted at Abf1 binding peaks, and the data was analysed according to whether a statistically significant Rad16 peak was observed to co-localise at the Abf1 binding peak. The data was further analysed according to the genomic location of the Abf1 binding peak (Fig. 4.5). As shown in Fig. 4.5, in contrast to the above prediction, regions of the genome where Abf1 and Rad16 binding peaks colocalise before UV have slower repair rates than regions with an Abf1 binding peak alone (Fig. 4.5). These observations are most prominent at promoters and downstream of genes. Furthermore, in the absence of Rad16 the difference in repair rates between the two groups is largely diminished. Therefore the difference in the repair rates between the two groups in wild type cells is likely due to Rad16 dependent GGR. This suggests that the absence of Rad16 binding peaks at Abf1 binding sites is related to rapid GGR.

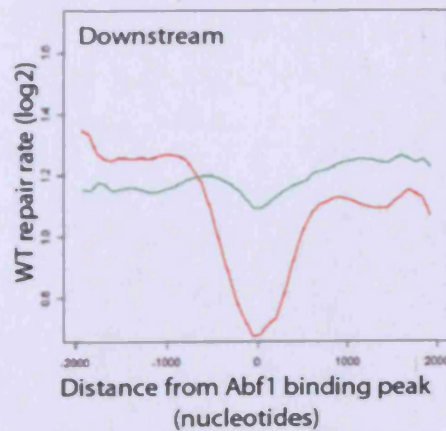
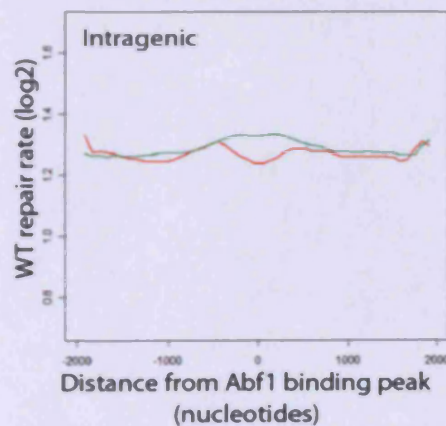
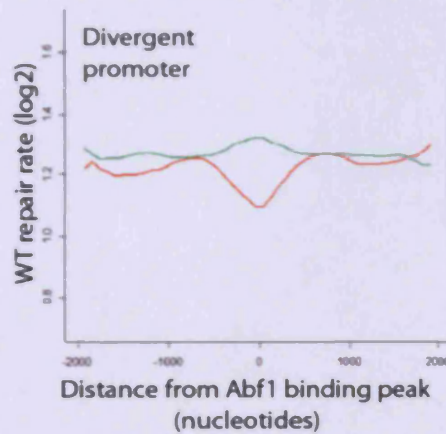
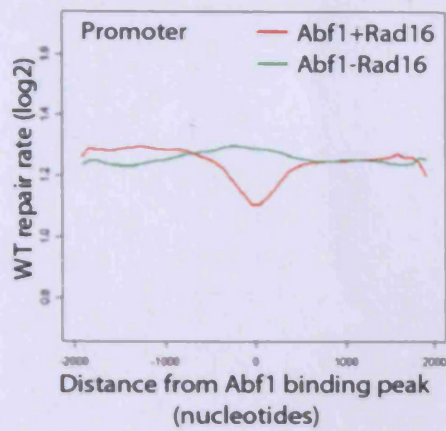
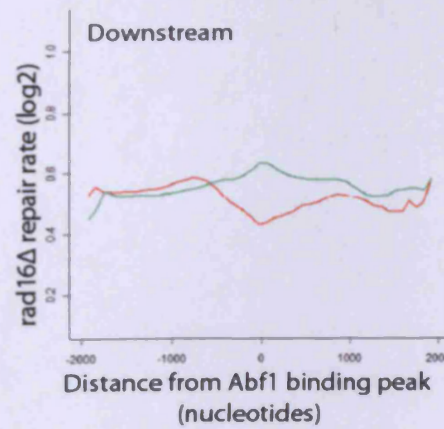
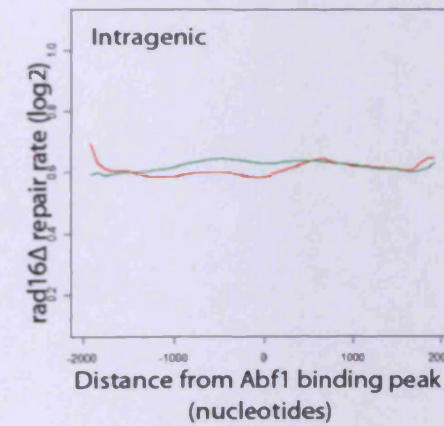
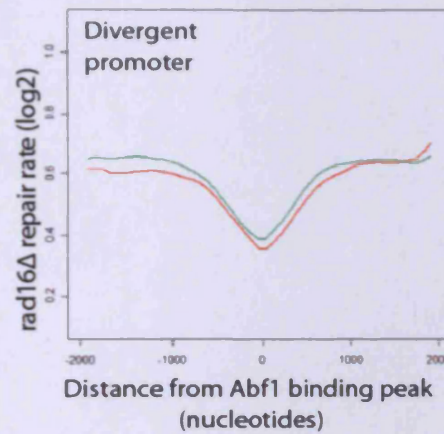
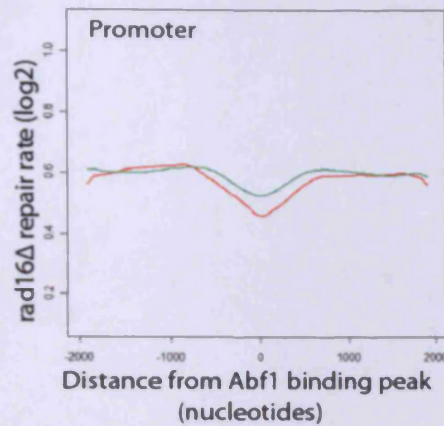
Wild typerad16Δ

Figure 4.5 (Above). Composite profiles of wild type (left hand graphs) and *rad16Δ* (right hand graphs) CPD repair rates. Data is plotted at Abf1 binding peaks that either co-localise with Rad16 binding peaks (red trendline) or do not co-localise (green trendline). Only trendlines are shown. The position of the Abf1 binding peaks is identified in the top left of each plot. NB. Scales are non-equivalent between wild type and *Δrad16* datasets.

4.3.6 Investigating the relationship between Rad16 binding, Rad16 dependent acetylation and CPD repair

The results in 4.3.5 were further investigated exclusively at promoter regions efficiently bound by the GGR complex in the absence of UV (simultaneously analysing promoters and divergent promoters where Abf1 and Rad16 binding peaks colocalise) using ranked composite profiles as adopted in Fig. 4.4. The results in Fig. 4.5 suggested a relationship between the level of Rad16 binding and CPD repair. Given that Rad16 dependent histone H3 K9K14 acetylation has also been recently demonstrated to be necessary for efficient GGR in vivo (Yu et al., 2011), the relationship between Rad16 binding, histone H3 K9K14 acetylation and CPD repair rates was investigated. As shown in Fig. 4.6, an inverse relationship is observed between the level of Rad16 binding and wild type unirradiated acetylation levels at promoters efficiently bound by the GGR complex (Fig. 4.6 A and B). Sites with low level Rad16 binding peaks, have high acetylation levels. The unirradiated acetylation status also positively correlates with the rate of repair (Fig. 4.6 B and C). Rad16 binding and acetylation after UV were also investigated in relation to Rad16 binding before UV. As seen in Fig. 4.6 D and E, Rad16 binding is lost after UV, and this correlates with increased acetylation levels. Furthermore, the relationship between Rad16 binding and acetylation does not change after UV. Therefore, sites with the highest level of Rad16 binding before UV, have the highest level of Rad16 binding after UV, which correlates with the lowest levels of acetylation both before and after UV, and the slowest repair.

The above data suggests that loss of Rad16 binding at Abf1 binding sites positively regulates acetylation, which subsequently promotes efficient repair in promoter regions. When the distribution of hyperacetylation at promoters where Abf1 and Rad16 colocalise in the absence of UV is compared to regions with an Abf1 binding peak alone, the level of histone H3 K9K14 acetylation is higher at a domain proximal to the Abf1 binding site for regions efficiently bound by Abf1 alone (Fig. 4.6 F). This occurs within the same domain where more efficient repair is observed

(Fig. 4.5). This strongly suggests that the differences in the acetylation levels at these regions significantly determine the differences in wild type CPD repair rates.

Composite profiles at promoters where Abf1/Rad16 binding peaks colocalise

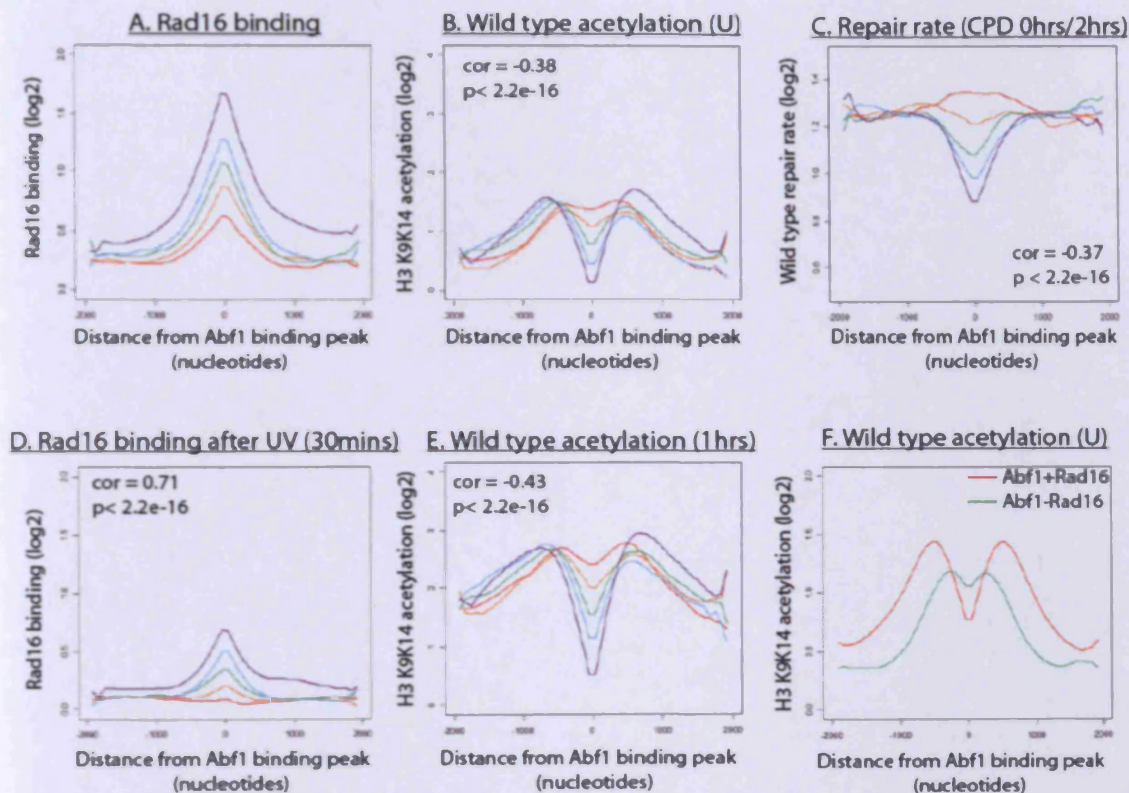


Figure 4.6. A. Rad16 binding peaks that colocalise with Abf1 at a promoter were ranked and reordered according to the peak height. These were split into 5 even groups of ~150 probes, the trendlines of which are shown in A. The data shown in B, C, D and E is ordered into the same groups as A. A Pearson's correlation coefficient is given for the correlation between A and either B, C, D or E at the Abf1 binding peak, in each plot. Only trendlines are shown. F. Composite profile of histone H3 K9K14 acetylation before UV (U) at promoters where Rad16 and Abf1 binding peaks colocalise (red line), or where an Abf1 peak is only observed (green line). NB. F. uses a different scale to that used in B. and E.

To investigate whether the correlation between Rad16 binding levels and the acetylation status is directly related to the presence of Rad16, histone H3 K9K14 acetylation from the *rad16Δ* dataset was compared to the level of Rad16 binding (Fig. 4.7 A and B). An inverse relationship between Rad16 binding and acetylation can still be observed, suggesting that some of the differences in the acetylation levels at sites efficiently bound by the GGR complex occur in a Rad16 independent fashion. However, the presence of Rad16 in wild type cells clearly induces changes in the acetylation patterns (compare Fig. 4.7 B and D).

Composite profiles at promoters where Abf1/Rad16 binding peaks colocalise

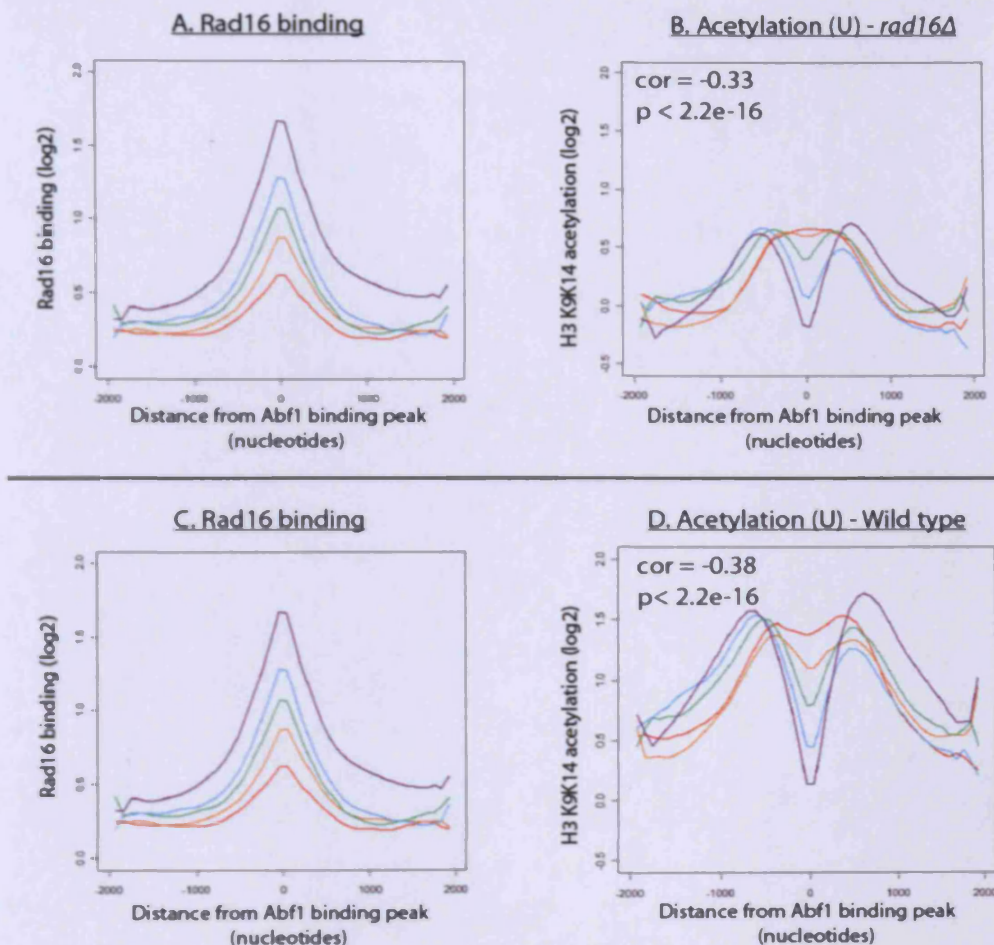


Figure 4.7 A and C. Rad16 binding is ranked and grouped as described in Fig. 4.6A. B. Composite profile of histone H3 K9K14 acetylation in the absence of Rad16, ranked and grouped according to Rad16 binding in A. D. Composite profile of histone H3 K9K14 acetylation in the wild type cells, ranked and grouped according to Rad16 binding in C. E. Composite profile of histone H3 K9K14 acetylation in the absence of Rad16, ranked and grouped according to the level of acetylation at the Abf1 binding site.

Finally, to investigate the effect of Rad16 binding on acetylation and repair, Rad16 independent acetylation and CPD repair was compared against Rad16 dependent acetylation and CPD repair. Rad16 dependent acetylation was calculated by subtracting the *rad16Δ* acetylation pattern from the wild type acetylation pattern. The Rad16 dependent repair rate was calculated by subtracting the *rad16Δ* repair rate from the wild type repair rate. As shown in Fig. 4.8, in the absence of Rad16, the differences in the acetylation levels at promoters ordinarily bound by the GGR complex have a minor effect in promoting CPD repair (Fig. 4.8 A-C). This demonstrates that in this context, differences in acetylation have only a minor role in

promoting Rad16 independent repair. In contrast, when Rad16 dependent acetylation and CPD repair is plotted, a strong correlation is observed between the level of Rad16, Rad16 dependent acetylation and Rad16 dependent CPD repair at the Abf1 binding sites (Fig. 4.8 D-F). This strongly suggests that loss of Rad16 binding functions to positively regulate Rad16 dependent hyperacetylation and CPD repair at regions proximal to an Abf1 binding site. In other words, low level binding of Rad16 promotes high level Rad16 dependent acetylation and rapid Rad16 dependent GGR.

Composite profiles at promoters where Abf1/Rad16 binding peaks colocalise

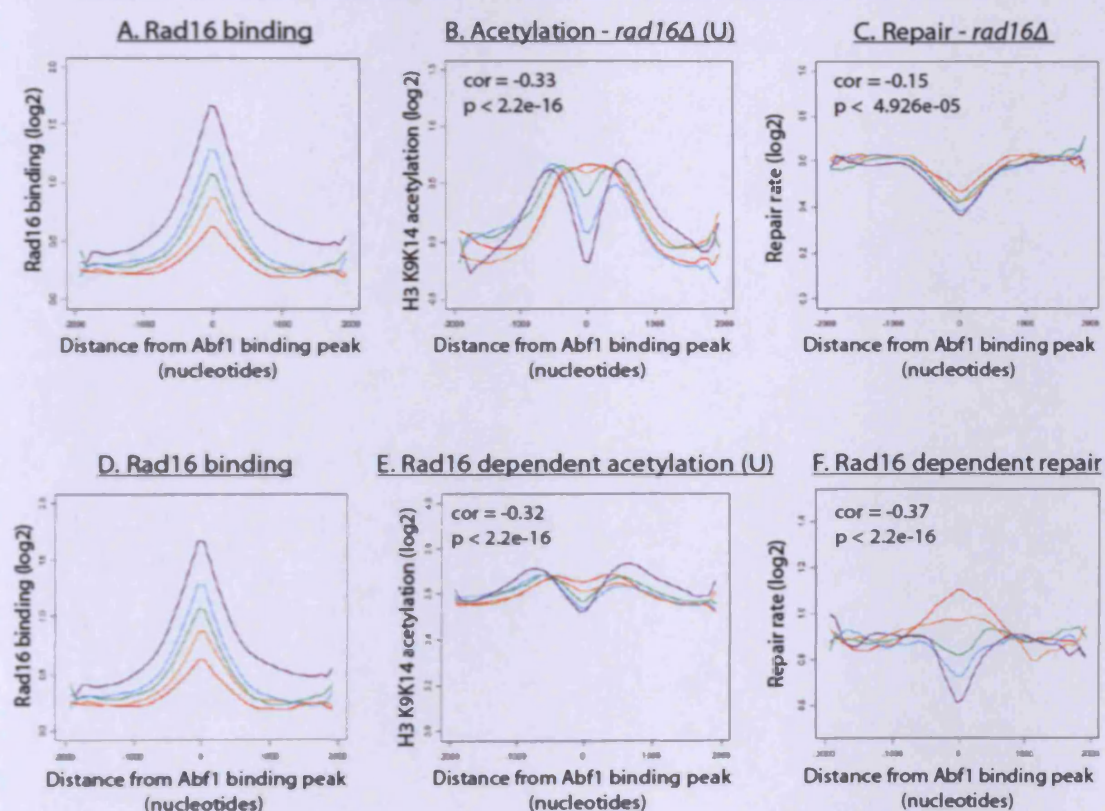


Figure 4.8. A. Rad16 binding is ranked and grouped as Fig. 4.6A. Composite profile of histone H3 K9K14 acetylation in the absence of Rad16, ranked and grouped according to Rad16 binding in A. Composite profile of repair in the absence of Rad16, ranked and grouped according to Rad16 binding in A. D as A. E. Composite profile of Rad16 dependent histone H3 K9K14 acetylation, ranked and grouped according to Rad16 binding in D. F. Composite profile of Rad16 dependent repair, ranked and grouped according to Rad16 binding in D. A pearson correlation coefficient is given in B, C, E and F for the correlations (A and B), (A and C), (D and E) and (D and F). NB: Data from B., C., E. and F. plots use non-equivalent arbitrary units/scales.

4.4 Discussion

By analysing the genome-wide distribution of Rad16 binding, the current study significantly expands our understanding of how Rad16 interacts with chromatin and functions to promote both acetylation and CPD repair genome-wide. Both in the presence and absence of UV damage Rad16 binds throughout the genome, however peaks of high level Rad16 binding are observed in the absence of UV and these predominantly colocalise with Abf1 binding peaks in promoter regions. In response to UV, peaks of Rad16 binding are lost in a manner that appears independent to changes in Abf1 binding. Whilst Rad16 functions to promote acetylation and CPD repair genome-wide, regions of the genome where Abf1 and Rad16 binding peaks colocalise in the absence of UV demonstrate slow repair rates at regions proximal to the Abf1 binding site and this correlates with low histone H3 K9K14 acetylation levels. The ability of Rad16 to promote both acetylation and CPD repair is inversely related to the level of Rad16 binding both before and after UV.

By using a combination of both genome-wide and site specific ChIP analysis, Rad16 was observed to bind throughout the yeast genome both in the absence and presence of UV damage (Fig. 4.1). The universal occupancy of Rad16 on chromatin in the absence of UV damage correlates with the ability of this protein to promote histone H3 acetylation patterns genome-wide before UV irradiation (Chapter 3). These observations are particularly significant as classically NER factors are generally believed to be recruited to chromatin in response to UV damage (Groisman et al., 2003; Houtsmuller et al., 1999; Zotter et al., 2006). However, some factors such as TFIIH, CSA and XPC have previously been observed to interact with chromatin in the absence of UV damage (Groisman et al., 2003; Hoogstraten et al., 2008; Hoogstraten et al., 2002). In addition, it was recently demonstrated that core NER factors are recruited to promoters in a manner necessary for transcriptional activation, but independent to functional NER, in the absence of UV damage (Le May et al., 2010). These observations correlate with the preferential location of Rad16 binding peaks at promoter regions (Fig. 4.2). Therefore, Rad16 may play a functional role in the transcription of genes. However, in contrast to mammalian NER factors, Rad16 is not observed to be recruited to specific promoters as part of a transcriptional response to UV damage (Fig. 4.2). In addition, UV dependent chromatin remodelling at the *MFA2* promoter by Rad16 was previously demonstrated not to induce transcriptional

activation of the gene (Teng et al., 2008). This suggests that the genome-wide localisation of Rad16 is principally related to the mechanism of GGR.

High level binding peaks of Rad16 principally colocalises with Abf1 binding peaks, and these sites of colocalisation are predominantly found at promoter regions (Fig. 4.3). This strongly suggests that Abf1 binding functions to promote efficient binding of the GGR complex *in vivo*. These observations also provide further support of a model in which Abf1 binding targets the location of the GGR complex and thus organises GGR from promoter regions. High level Rad16 binding peaks are restricted to roughly one third of Abf1 binding peaks, therefore, other factors independent of Abf1 binding must influence the binding level of Rad16 at these sites *in vivo* (see below). In response to UV damage, peaks of high level Rad16 binding are diminished (Fig. 4.2). As previously discussed, Rad16 is a Snf2 family ATPase which can translocate along DNA and induce superhelical torsion *in vitro* (Yu et al., 2004; Yu et al., 2009). These activities are suggested to promote histone hyperacetylation and chromatin remodelling necessary for efficient GGR (see introduction). The loss of high level Rad16 binding does not reflect dissociation of Rad16 from chromatin but instead a redistribution of the protein (Fig. 4.1). These observations are in strong support of a model whereby in response to UV damage, the translocation of Rad16 is upregulated at Abf1 binding sites, as part of the response to promote GGR. The global interaction of Rad16 with chromatin in the absence of UV, also suggests that Rad16 may translocate from an Abf1 binding site in the absence of DNA lesions. This proposition is consistent with the observation that Rad16 binding peaks are not exclusively found at Abf1 binding peaks (Fig. 4.3). Therefore, the activity of Rad16 translocation may also function to influence the binding level of Rad16 at Abf1 binding sites in the absence of UV, in which low level Rad16 binding is indicative of high level DNA translocase activity.

At sites where Abf1 and Rad16 colocalise, the loss of Rad16 binding in response to UV does not correlate with changes in the levels of Abf1 binding (Fig. 4.4). This suggests that the two proteins may not function in complex after UV. DNA translocation by Rad16 could conceivably transition the dissociation from Abf1. In relation to above discussions, this transition may also occur in the absence of UV damage. However, it is noted that Abf1 is a highly abundant protein, and that a large fraction (~70%) of this protein is not found in complex with Rad16 (Reed et al., 1999). Therefore, the discordance between Abf1 binding and Rad16 binding in

response to UV may result from a predominant fraction of Abf1 at sites of colocalisation functioning independently of Rad16. This model is not favoured as the presence of Rad16 peaks that do not colocalise with Abf1 demonstrates that Rad16 can interact with chromatin independent of an interaction with Abf1 (Fig. 4.3).

Regions of the genome where Abf1 and Rad16 binding peaks colocalise in the absence of UV damage have slower CPD repair rates *in vivo* relative to regions of the genome with high level Abf1 binding alone (Fig. 4.5). Given that DNA translocation by Rad16 is hypothesised to promote GGR, I speculated that the loss of Rad16 from Abf1 binding sites promotes rapid CPD repair. This was investigated by examining the relationship between Rad16 binding, histone H3 K9K14 acetylation and CPD repair at promoter regions where Abf1 and Rad16 binding peaks colocalise. Interestingly, an inverse relationship is found between the level of Rad16 binding and histone H3 K9K14 acetylation or CPD repair rates (Fig. 4.6). Low level binding of Rad16 correlates with high level acetylation and rapid CPD repair (Fig. 4.6 A-C). Furthermore, in response to UV, lower levels of Rad16 binding correlate with higher levels of acetylation (Fig. 4.6 D and E). A strong correlation exists between Rad16 binding and acetylation before UV and Rad16 binding and acetylation after UV, further supporting a model in which Rad16 functions to promote the distribution of acetylation both before and after UV in a similar manner (Fig. 4.6 D. and E., see also Chapter 3.4). These observations are consistent with a model in which the level of Rad16 binding at Abf1 binding sites is inversely proportional to the level of DNA translocase activity (as discussed above). I suggest that low level binding of Rad16 reflects regions of the genome where Rad16 efficiently translocates from the Abf1 binding site. As previously discussed, the ATPase motors of Rad16, necessary for DNA translocation, are suggested to function to promote histone H3 K9K14 hyperacetylation and efficient GGR (see introduction). Therefore low levels of Rad16 binding that represent efficient translocation, would correlate with high level acetylation and rapid CPD repair at the Abf1 binding site, as observed (Fig. 4.6 and 4.8, Yu et al., 2011). This model may also predict that Abf1 binding sites where Rad16 peaks are not observed to colocalise could reflect regions of the genome where efficient Rad16 translocation also occurs, and thus subsequent high level acetylation and GGR at the Abf1 binding site. This phenotype was observed to be true at promoter regions (Fig. 4.5 and 4.6). However, it is not expected that all Abf1 binding sites that do not colocalise with Rad16 would necessarily demonstrate this

relationship. As previously discussed Abf1 binding appears to primarily organise GGR at promoter regions, therefore the relationship may be restricted to these sites (Chapter 3). The details of this model are shown in Fig. 4.9. An alternative interpretation of these data is that efficient binding of the GGR complex colocalises with regions of the genome that are refractory to histone hyperacetylation and efficient CPD repair, and thus efficient binding of the GGR complex functions to promote these activities.

Histone H3 K9K14 acetylation levels in a *rad16Δ* mutant also correlate with Rad16 binding levels at promoters where Abf1 and Rad16 binding peaks colocalise (Fig. 4.7). This demonstrates that Rad16 is not the only determinant of acetylation levels/(distribution) at these sites. Interestingly, even in the absence of Rad16 there is a weak correlation between histone H3 K9K14 acetylation and CPD repair rates (Fig. 4.8C). This is found at regions proximal to the Abf1 binding site within a promoter. This likely represents regions of the genome where TCR is unable to repair (see Chapter 3.4), strongly suggesting that this is Rad16 independent GGR occurring in a similar fashion to that described at *MFA2* in *TUP1Δ* mutant cells (Yu et al., 2011). Importantly though, only low level repair rates are observed. However, when the Rad16 dependent increase in histone H3 K9K14 acetylation is plotted at promoters a robust correlation is found with the promotion of Rad16 dependent GGR. This strongly suggests that Rad16 dependent histone acetylation promotes the GGR rates in these regions, which correlates with the recent observations reported at the *MFA2* locus (Yu et al., 2011). The level of Rad16 dependent acetylation and GGR has an inverse relationship to the level of Rad16 binding (Fig. 4.9). In reference to the model above, this suggests that the activity of the Rad16 DNA translocase promotes Rad16 dependent acetylation and GGR.

Finally, it may be observed that wild type CPD repair rates at regions distal to the Abf1 binding sites of promoters do not correlate with either Rad16 dependent or Rad16 independent histone H3 K9K14 acetylation (Fig. 4.6 and 4.8). Given that these sections predominantly represent genic regions this suggests that the TCR pathway predominately dictates the ultimate repair rate in these regions and that this is not as significantly influenced by histone H3 K9K14 acetylation levels as GGR (Fig. 4.6, Yu et al., 2011).

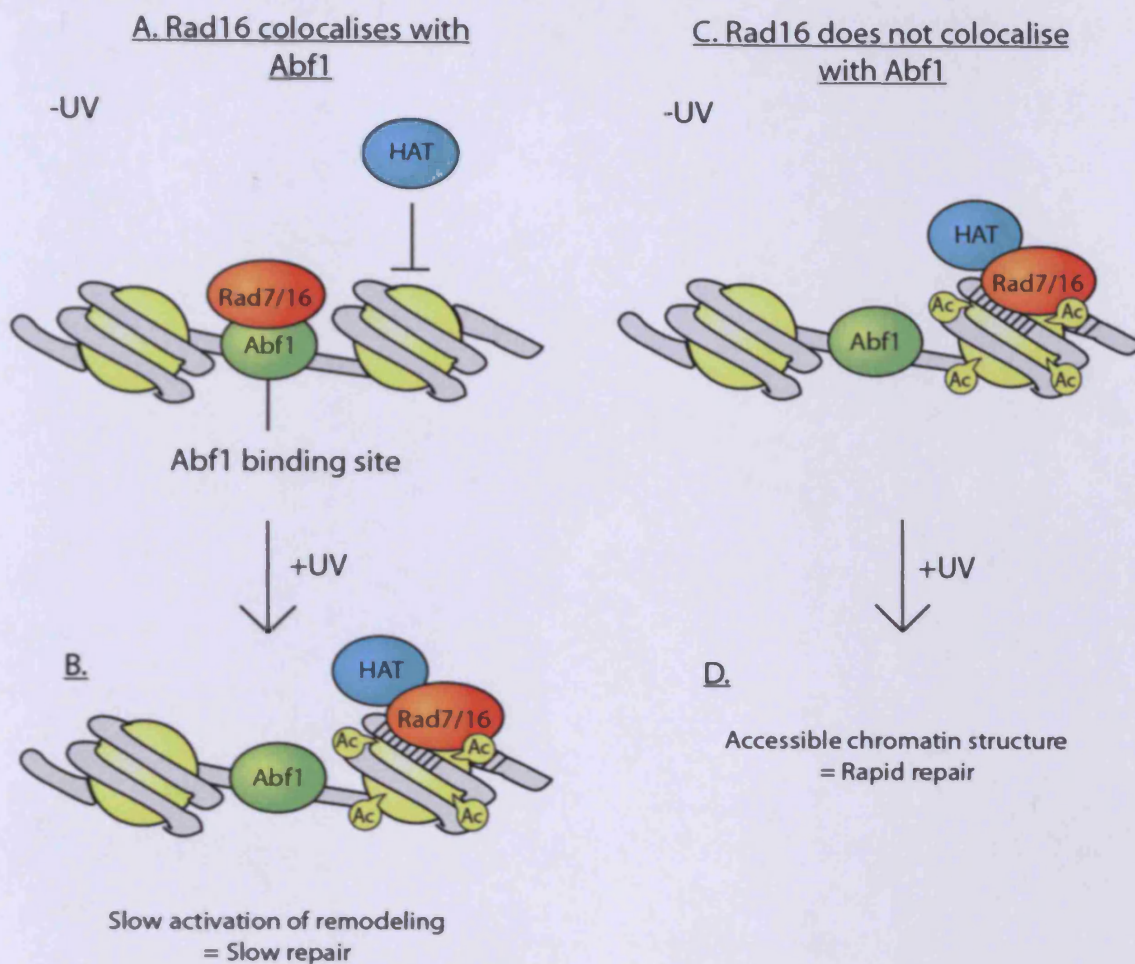


Figure 4.9. A. In promoter regions of the genome where Abf1 and Rad16 colocalise, Rad16 fails to efficiently translocate from the Abf1 binding site and thus functional recruitment of HATs such as Gcn5 does not occur. This results in low level acetylation at the Abf1 binding site and a chromatin structure refractory to efficient GGR. B. In response to UV irradiation the dissociation of Rad16 and subsequent translocation is upregulated from Abf1 binding sites promoting the recruitment of HATs, chromatin remodelling and GGR. C. At promoter regions of the genome where Abf1 does not colocalise with Rad16, Rad16 dependent chromatin remodelling as described in B occurs at high levels in the absence of UV irradiation. D. The upregulation of chromatin remodelling is not required in these regions (or is more rapidly activated) permitting efficient GGR to occur and thus CPD repair is faster.

As explained in the aims of the study, several lines of evidence suggest that the GGR complex could function to regulate the DNA binding kinetics of Abf1 (see Chapters 1.7, 5 and 6.1). Therefore, I wished to investigate if, as recently seen for transcription, changes in Abf1 DNA binding kinetics are mechanistically linked to GGR. As a complementary study to the steady state occupancy of Abf1 binding as reported in Chapter 3, the proceeding chapters aim to investigate Abf1 DNA binding kinetics in the presence and absence of UV using a novel variant of the ChIP-on-chip strategy.

5. Developing tools for the in vivo analysis of Abf1 DNA binding kinetics

5.1 Introduction

The site specific DNA binding activity of Abf1 is important for the ability of the protein to promote GGR (see Chapter 1.5.5, Reed et al., 1999; Yu et al., 2009). Given these observations, ChIP-on-chip studies were performed both in the absence and presence of UV damage to investigate how changes in the level of Abf1 DNA binding are linked to the protein's role in GGR (Chapter 3). Interestingly, Abf1 does not relocalise in response to UV damage. The absence of relocalisation is surprising given that this is often observed for TFs in response to different environmental stimuli (Harbison et al., 2004). These results suggest that neither DNA damage response regulatory pathways upstream of Abf1 nor the biochemical activities of the GGR complex itself function to alter the localisation of Abf1 DNA binding in response to UV, despite the fact that the binding of Abf1 itself is important for efficient GGR. One property that standard ChIP studies fail to accurately measure is the DNA binding kinetics of a protein (Brady et al., 2005; Hager et al., 2009; Yang et al., 2002a). Consequently the following studies aimed to investigate if the DNA binding kinetics of Abf1 provide a more informative view of both how and where Abf1 DNA binding is related to promoting efficient GGR.

TFs are critical determinants for the regulation of RNAPII gene transcription (see Chapter 1.6.1 for the definition of a TF in this study). DNA sequences within the promoters (and beyond) of genes are bound by TFs which function to control the activities of RNAPII mediated transcription. TFs are typically modular in nature and may consist of a variety of interchangeable domains, but fundamentally include a DBD and a domain which functions to promote transcription termed an activation domain (AD) (Kadonaga, 2004). The modular structure of the proto-typical TF Gal4 is shown in Fig. 5.2. Some TFs target the recruitment of co-activators to genes which function to promote transcription. The activities of such co-activators include chromatin remodelling by covalent histone modification or ATP dependent nucleosome remodelling (Weake and Workman, 2010).

The molecular mechanisms through which TFs function to promote transcription are at least partially conserved, given that the ectopic recruitment of ADs

to promoters from proteins including Gal4 or herpes simplex virus protein VP16 function to promote gene transcription in a wide variety of eukaryotic hosts (Ptashne, 1988). Furthermore, TFs have also been shown to promote the activity of other processes including DNA replication, meiotic recombination and DNA repair, and in all cases this has been correlated with the ability of these factors to promote chromatin remodelling (Frit et al., 2002; Kohzaki and Murakami, 2005; Nicolas, 1998). The ability of TFs to promote numerous pathways in chromatin metabolism is reminiscent of the multiple regulatory functions of Abf1 (Yarragudi and Morse, 2006). As with other TFs, Abf1 is modular consisting of two N-terminal DBDs and a C-terminal AD that has been subcategorised into two regions termed CS1 and CS2 (Fig. 5.2) (Miyake et al., 2002). Interestingly, with respect to ARS1 dependent DNA replication, the stimulatory role of Abf1 can be functionally substituted by other TFs such as Gal4, VP16 and p53 (Li et al., 1998). Collectively, these observations suggest that whilst TFs are tailored to individual roles within the cell, many of the molecular mechanisms employed by these proteins share common origins.

As discussed in Chapter 1.6, the DNA binding kinetics of TFs *in vivo* has become a recent area of active research. Interestingly, a number of studies have demonstrated a correlation between the DNA binding kinetics of a TF at a promoter, and transactivation of a gene (Brady et al., 2005; Klok et al., 2007; Nalley et al., 2006; Reid et al., 2003; Stavreva et al., 2004; Yang et al., 2002a; Yao et al., 2006). In all of these examples, the stabilisation of a TF:DBS interaction correlates with the onset of efficient transcriptional activation. The cell appears to contain a diverse range of mechanisms which may function to regulate DNA binding kinetics *in vivo* (Ferdous et al., 2007; Freeman and Yamamoto, 2002; Yu and Kodadek, 2007). At present it remains unclear whether changes in TF DNA binding kinetics at promoters are necessary for the regulation of transcription or a consequence of such activity (Hager et al., 2009; Kodadek et al., 2006). However, importantly these data demonstrate that changes in TF DNA binding kinetics are mechanistically coupled to the activity of transcriptional regulation. Given that Abf1 is structurally homologous to canonical TFs, and in some contexts functions as a TF, the following studies aimed to investigate whether, as discussed above for transcription, changes in Abf1 DNA binding kinetics are mechanistically coupled to GGR. The current chapter describes the creation of the tools necessary for the analysis of Abf1 DNA binding kinetics *in vivo*, which are utilised in the proceeding chapter.

5.1.1 Molecular biological techniques for the study of DNA binding kinetics in vivo

The kinetics of protein-DNA (or chromatin) interactions in vivo can be studied through the genetic fusion of the protein of interest to a fluorescent molecule; most commonly green fluorescent protein (GFP) (Voss and Hager, 2008). Provided the fusion protein retains its biological function in vivo, this can then be readily visualised using fluorescence microscopy. Protein DNA binding kinetics are measured using a technique termed fluorescent recovery after photobleaching (FRAP) (Fig. 5.1A) (Hager et al., 2009). The technique uses a high intensity laser to photobleach the GFP fusions in a partial area of a nucleus without destroying the protein's biological function. Three derivatives of this technique are used for the quantitative measurement of protein-DBS interactions (Fig. 5.1A). The first method bleaches a large area of the nucleus and then monitors the rate at which both the bleached and non-bleached areas resolve to a uniform fluorescence (Phair et al., 2004). Models of protein binding kinetics are then formulated to fit the experimental data (Phair et al., 2004). For a TF, this technique often predicts two (or more) populations; one which has a short residence time on a substrate, and one a long residence time. These are predicted to indicate chromatin binding and site specific DNA interactions, but the genuine substrates are not known. Furthermore, kinetic predictions are only validated by the fact that the models predict an outcome that mimics the experimental findings, therefore, the results are highly sensitive to the model used, and differing models can shift estimates by at least three orders of magnitude (Mueller et al., 2010). Alternatively, direct measurements of residence times at specific sites on chromatin may be quantified by FRAP or FLIP (fluorescence loss in photobleaching). For a TF, for example, either the GFP fusion at the promoter is photobleached (FRAP), or the entire nucleus except for the promoter is photobleached (FLIP). The time taken for the difference in fluorescence between the nucleus and the promoter to resolve indicates the rate of protein exchange.

Although FRAP and FLIP are very powerful techniques, when this method is specifically applied to monitor site specific DNA binding kinetics in vivo the principle limitation is the spatial resolution of the technique. Whilst microscopy is able to detect single GFP molecules, it is currently very difficult to distinguish a single DBS bound molecule amongst thousands of proximal non-bound molecules

(Baldini et al., 2005; Hager et al., 2006). Whilst this has been achieved, it is yet to be widely applied to DNA binding kinetic studies (Elf et al., 2007). Furthermore, there are no generally applicable methods for the identification of chromosomal positions/promoters that are compatible with live cell imagery. These practical issues have been circumvented by the artificial incorporation of a gene array into the genome, providing hundreds of proximal DBSs, which, if bound by the tagged TF, produces a spot of intense fluorescence (McNally et al., 2000b). This unambiguously

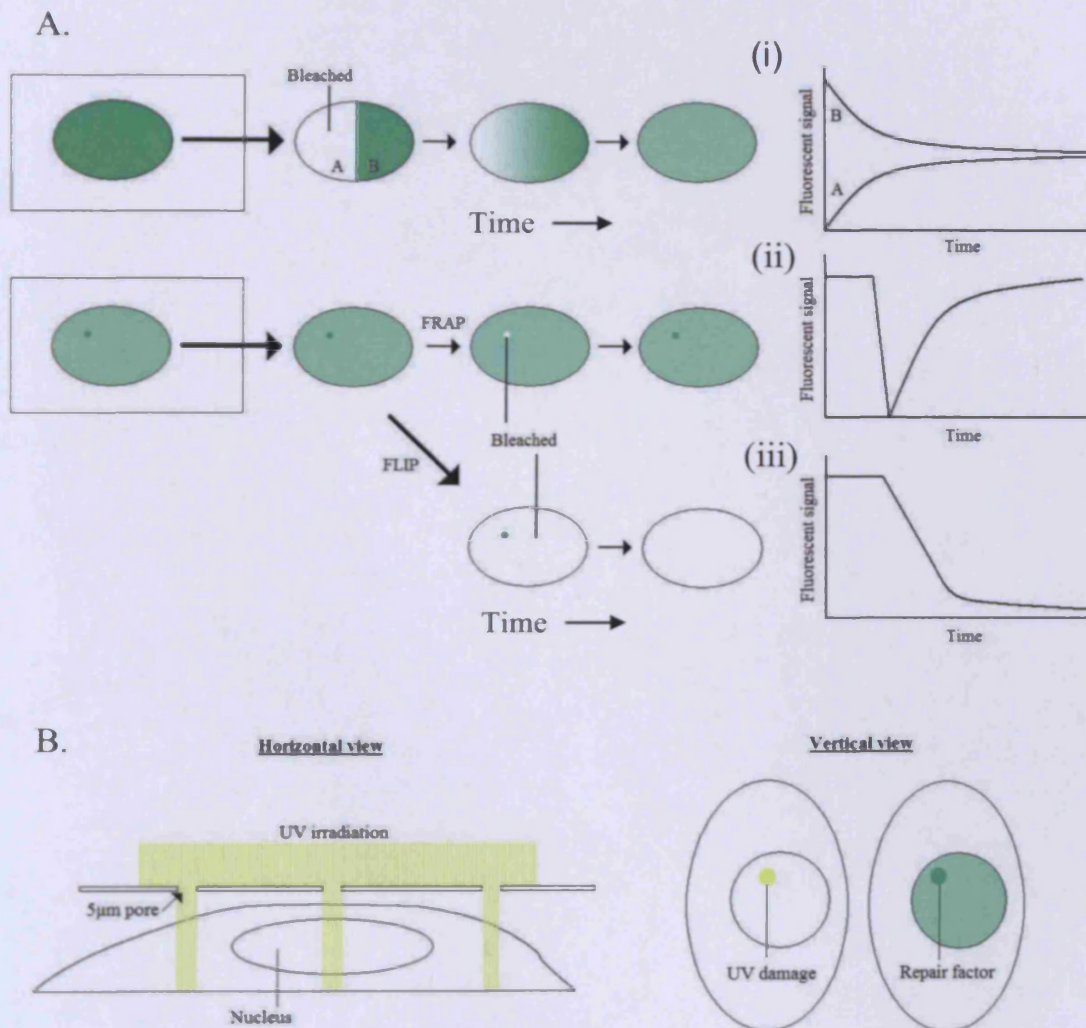


Figure 5.1. **A.** Pictorial representation, and concurrent graphical output of the data provided from a nuclear localised protein fused to GFP under microscopic investigations; using three techniques: **(i)** The protein does not accumulate to form a dot. A region of the nucleus is bleached and the rate of exchange of the GFP signal between bleached and non-bleached is measured. **(ii)** The protein accumulates at a nuclear structure forming a dot, this is bleached in FRAP. **(iii)** All regions except the dot are bleached in FLIP. In both **(ii)** and **(iii)** fluorescence is monitored at the dot. **B.** Cells UV irradiated through a porous filter create 'spots' of localised UV damage, which may be subsequently studied using techniques such as FRAP and derivatives.

identifies both chromosomal location, and the chromatin bound tagged proteins. In rare examples artificial gene arrays are not required when a protein naturally accumulates to a site in the genome, provided this location can be unambiguously identified in each nucleus (Karpova et al., 2008; Yao et al., 2006).

Fluorescently tagged proteins have also been extensively used for the study of mammalian NER. To date, published studies have used fluorescent tagged versions of NER factors DDB2 (Alekseev et al., 2008; Luijsterburg et al., 2007), DDB1 (Alekseev et al., 2008), XPC (Hoogstraten et al., 2008), ERCC1 (Houtsmuller et al., 1999), XPG (Zotter et al., 2006), XPB (Hoogstraten et al., 2002), XPA (Rademakers et al., 2003), CSB (van den Boom et al., 2004) and PCNA (Essers et al., 2005). The technology has been used to provide a wealth of information including protein cellular localisation, whether NER factors diffuse as singular molecules or combined as preassembled complexes, the order of factor assembly at a damage site and kinetics. In order to study kinetics and circumvent microscopy resolution limitations, cell nuclei are damaged in one small region by virtue of passing UV light through a polycarbonate filter with 5 μ M pores (Rademakers et al., 2003). This localises the tagged NER factors to this area causing a spot of intense fluorescence (Fig. 5.1B). The reaction rate for the spot fluorescence to plateau indicates the damage binding kinetics, or in other words, the rate at which the protein associates to a damage site. The mean residence time of a protein at a damage site is also measured using FRAP and FLIP (Zotter et al., 2006).

Despite the widespread applications of fluorescence microscopy, its use for measuring DNA binding kinetics at a DBS still has some large drawbacks. The protein of interest must be tagged with a large fluorescent protein and is usually overexpressed (Phair et al., 2004). As discussed, the cell line hosting this recombinant protein must also have an artificial gene array integrated. Even if these technical requirements are established, it remains unknown how any of these artificial alterations might affect *in vivo* kinetics. Furthermore, the analysis remains limited to one chromosomal location.

5.1.2 Competitive ChIP; a novel technique for the analysis of DNA binding kinetics in vivo

An alternative to fluorescence microscopy for the analysis of DNA binding kinetics in vivo has been to use a technique termed competitive ChIP. In one derivative of this technique, the protein of interest is expressed in two formats, one of which is constitutively expressed, and the other of which is inducibly overexpressed (relative to the first) (Dion et al., 2007; van Werven et al., 2009). Both versions of the protein are distinguished by different epitope tags. Following induction the large molar excess of the induced protein functions to replace the occupancy of the constitutive protein on chromatin. ChIP is performed at various time points to follow the rate of exchange. Since the constitutively expressed protein must dissociate from chromatin for the induced protein to bind, regions of the genome where the constitutive protein are rapidly replaced demonstrate shorter residence times on chromatin than those which are slowly replaced. This technique vastly improves the spatial resolution of analysing DNA binding kinetics, however, because the technique requires 30-45 minutes for the induced protein to accumulate, it cannot analyse the kinetics of DNA binding proteins with short half-lives on chromatin. It also requires a system where transcription is not inhibited (not compatible for UV damaged cells as general transcription is inhibited by this damage (Reagan and Friedberg, 1997)).

A second variant of competitive ChIP also exists. This strategy has previously been used for the study of DNA binding kinetics with Gal4 in yeast and HIF1 α in mammalian cells (Nalley et al., 2006; Yu and Kodadek, 2007). Using the Gal4 system as an example, the principle behind this concept is outlined in Fig. 5.2. The strategy requires the expression of a novel protein termed the competitor. The structure of the Gal4 competitor is given in Fig. 5.2A. The competitor is a recombinant protein containing the Gal4 DBD which functions to bind DNA at a Gal4 DBS. However, the competitor's DNA binding activity is tightly regulated through fusion to a hormone binding domain (HBD), which functions as an autonomous regulatory cassette subjecting the competitor to hormonal control. Following hormonal activation, the large molar excess of the competitor functions to replace endogenous Gal4 at a DBS. This is monitored by ChIP in the same manner as above. This technique is advantageous compared with the former derivative of competitive ChIP since post-translational activation of the competitor is more rapid than transcriptional activation, and the endogenous protein does not require an epitope tag. However, it has been

noted that this technique is also limited, and cannot resolve the kinetics of proteins with a half-life on chromatin of less than ~5 minutes (Yu and Kodadek, 2007).

The structure of the Gal4 competitor used by Nalley and co-workers is shown in Fig. 5.2A. The protein's N-terminal contains a single Myc tag which was used to immunoprecipitate the competitor. This is followed by the Gal4 DBD. Hormonal control of DNA binding is achieved by fusion of the Gal4 DBD to the oestrogen-receptor α ligand binding domain (ER α LBD). The heterologous fusion of a wide variety of proteins to steroid receptor LBDs has been demonstrated to subject their activity to hormonal control (Picard, 2000). Steroid receptors LBDs form high affinity complexes with the molecular chaperone Hsp90 and this complex is believed to maintain the apo-protein in an inactive state (Picard, 2006). Addition of a reciprocal hormone causes ligand binding and release of Hsp90 from the LBD (Fig. 5.2B). It is believed that the Hsp90-LBD functions to inhibit macromolecular interactions through steric hindrance. The system allows constitutive expression of the Gal4 competitor with rapid activation following addition of the ligand 17 β -oestradiol.

The final two domains of the Gal4 competitor are the acidic AD of the herpes simplex virus protein VP16 (VP16 AD) and a C-terminal FLAG tag. Under conditions in which Gal4 promotes transcription, Nalley et al. demonstrated the competitor was unable to occupy Gal4 responsive gene promoters within 60 minutes after hormonal activation. However, under non-inducing conditions the competitor rapidly replaced the occupancy of Gal4. Furthermore, the authors also showed that a derivative of Gal4 deleted of its C-terminal AD was also rapidly replaced by the competitor even under inducing conditions. The interpretation of these data was that activation of transcription functions to stabilise a Gal4:DBS interaction (Nalley et al., 2006). These observations may explain why the competitor needs the VP16AD, since in its absence the recombinant protein is not an effective competitor of Gal4 occupancy at a gene promoter (T. Kodadek, personal communication). Presumably a Gal4 competitor absent of the VP16 AD, which is unable to activate transcription, cannot form a stable complex at a DBS and effectively compete with Gal4 for promoter occupancy (Louvion et al., 1993).

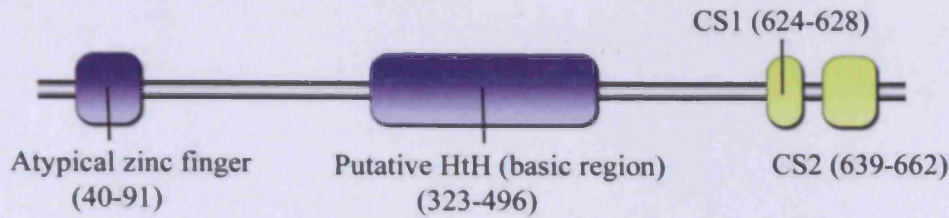
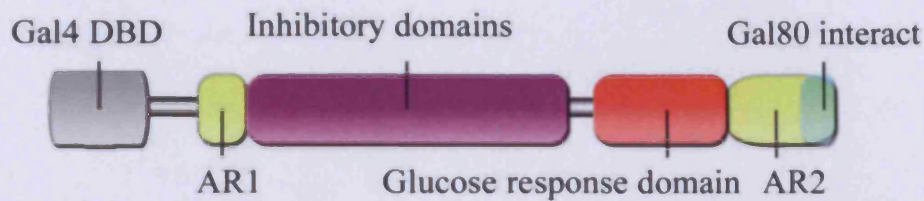
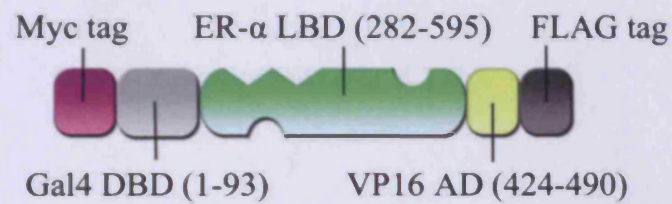
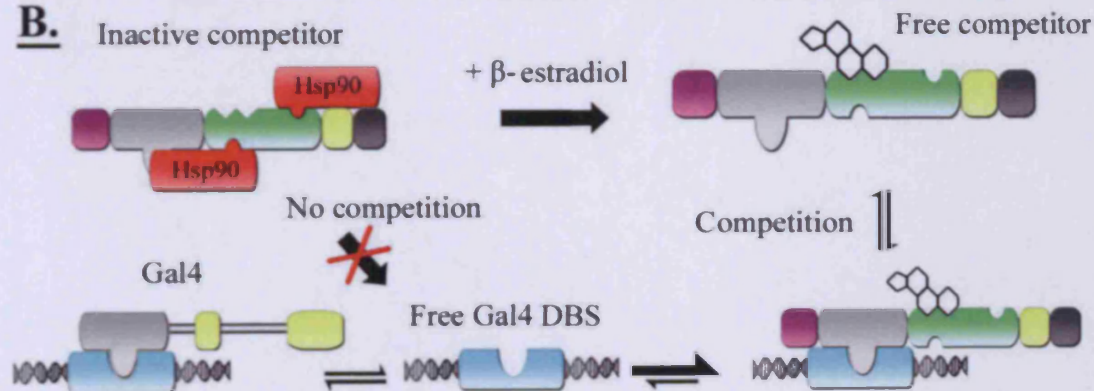
A.Abf1Gal4Gal4 competitor**B.**

Figure 5.2. A. Structure of Abf1, Gal4 and the Gal4 competitor. B. Cartoon representing the molecular mechanism of Gal4 competitive ChIP. Note that when Gal4 occupies a DBS, the competitor would be unable to bind until the protein has dissociated.

The aim of this chapter is to adapt the Gal4 competitor for the subsequent use of the reagent to analyse Abf1 DNA binding kinetics. In order to establish an 'Abf1 competitor' a variety of criteria had to be fulfilled. As with the Gal4 competitor, an Abf1 competitor must:

- Be immunologically distinguishable from the endogenous protein
- Function to bind DNA in the same site specific manner as the endogenous protein
- Be dormant in the absence of hormonal activation
- Bind DNA(/chromatin) in the presence of hormonal activation

Creation of a fully functional Abf1 competitor required extensive DNA manipulations, parameter optimisations and the design of novel experiments to test such parameters. The following chapter describes the design, practical implementation and results of this work in chronological order. This organisation best explains why and how the final design of the Abf1 competitor was determined.

5.2 Materials and Methods

Strains used in this study

Strain	Genotype	Source
SX46a	MATa, ade2 his3-532 trp1-289 ura3-52	(Reed et al., 1999)
SX46a pRS314	SX46a, pRS314 (TRP)	Commercial plasmid
JCA30	MATa, trp1A his3A200 ura3-52 lys2-801 ade2-1 gal ABF1 HIS3a	(Rhode et al., 1992)
JCA31	MATa, trp1A his3A200 ura3-52 lys2-801 ade2-1 gal abf1-1 HIS3a	(Rhode et al., 1992)
JCA30 pRS314	JCA30 pRS314 (TRP)	Commercial plasmid
JCA31 pRS314	JCA31 pRS314 (TRP)	Commercial plasmid
SX46a pCCA114	SX46a pRS314-prADH1-Abf:aa19-523-ERαLBD	This study
SX46a pCCA214	SX46a pRS314-prADH1-Abf:aa19-523-ERαLBD-VP16AD	This study
SX46a pCCA314	SX46a pRS314-prADH1-Abf:aa1-530-ERαLBD	This study
SX46a pCCT114	SX46a pRS314-prTDH3-Abf:aa19-523-ERαLBD	This study
SX46a pCCT314	SX46a pRS314-prTEF2-Abf:aa1-530-ERαLBD	This study
SX46a pCCG114	SX46a pRS314-prTDH3-Abf:aa19-523-ERαLBD	This study
SX46a pCCG314	SX46a pRS314-prTDH3-Abf:aa1-530-ERαLBD	This study
JCA31 pCCA114	JCA31 pRS314-prADH1-Abf:aa19-523-ERαLBD	This study
JCA31 pCCA314	JCA31 pRS314-prADH1-Abf:aa1-530-ERαLBD	This study
JCA31 pCCT114	JCA31 pRS314-prTDH3-Abf:aa19-523-ERαLBD	This study
JCA31 pCCT314	JCA31 pRS314-prTEF2-Abf:aa1-530-ERαLBD	This study
JCA31 pCCT414	JCA31 pRS314-prTEF2-Abf:aa1-530-ERαLBD-VP16AD	This study
JCA31 pCCG114	JCA31 pRS314-prTDH3-Abf:aa19-523-ERαLBD	This study
JCA31 pCCG314	JCA31 pRS314-prTDH3-Abf:aa1-530-ERαLBD	This study
JCA31 pCCG514	JCA31 pRS314-prTDH3- ERαLBD-Abf:aa1-530-ERαLBD	This study
JCA31 pCCG614	JCA31 pRS314-prTDH3- ERαLBD-Abf:aa1-530-ERαLBD-VP16AD	This study

Western blotting

Western blots were performed as described in Chapter 2.6.3 using yeast whole protein lysates (Chapter 2.6.1). The Abf1 competitor was detected using α -Myc antibody (9B11 mAB#2276, Cell Signalling Technology) 1:2000 dilution, and secondary antibody goat- α -Mouse IgG (H+L) HRP #NA931VS (Amersham) 1:30,000 dilution. Abf1 was detected with α -Abf1 antibody (yC-20 #sc-6679 Santa Cruz Biotechnology) 1:1000 dilution, and secondary antibody donkey- α -goat IgG-HRP (#sc-2020 Santa Cruz) 1:30,000 dilution. Tubulin (α subunit) was detected with α -Tubulin antibody (YL1/2 GTX76511, Genetex) 1:2000 dilution, and secondary antibody rabbit- α -rat(ab6734-1, abcam) 1:30,000 dilution.

Cloning

The extensive cloning described in this chapter required a large number of strategies, including fusion PCR, to successfully construct the various recombinant proteins described. All primer names end in either suffix F or suffix R. F, or forward primers are always complementary to the antisense strand of the ORF, whilst R, or reverse primers are always complementary to the sense strand of an ORF. A complete list of primers used for the PCRs described below are given in appendix IV. All plasmids were sequenced, and if necessary, subcloned to remove point mutations (these frequently occurred during fusion PCR reactions). All PCR conditions, restriction assays and cloning techniques are described in Chapter 2.3.

pCCA114: (For graphical representation of this method, see Fig. 5.4)

The 5' PCR consisting of the ADH1 promoter and Myc epitope was amplified from pTK513 using primers ADH1_F and ADH1_R. ADH1_F introduces a 5' BamHI restriction site, whilst ADH1_R introduces the first fifty nucleotides of the ABF1 ORF starting at +55 (amino acid 19) downstream of the Myc tag. The ABF1 DBD was PCR amplified from genomic DNA (strain BY4742) using primers ABF1_55F and ABF1_1569R. The 3' PCR was amplified from pTK513 using primers ER_F and ER_R. ER_F introduces the last fifty nucleotides of ABF1 DBD finishing at +1569 5' to the ER α LBD primer. ER_R introduces the large T antigen NLS, followed by two STOP codons and an XhoI restriction site after the ER α LBD. The three PCRs were combined by fusion PCR using the primers ADH1_F#2 and ER_R#3. The PCR product was subsequently cloned as a BamHI/XhoI fragment into PRS314.

pCCA214:

The 5' PCR and ABF1 DBD PCR performed above were included in the fusion PCR. The 3' PCR was amplified from pTK513 using primers ER_F and ER_R#2. ER_R#2 introduces the large T antigen NLS, followed by two STOP codons and an XhoI restriction site after the VP16 AD. The three PCR products were fused in an identical fashion to that as stated above using the primers ADH1_F#2 and ER_R#3. The PCR product was subsequently cloned as a BamHI/XhoI fragment into PRS314.

pCCA314 and pCCA414:

The ABF1 DBD (nucleotides +1 to +1590) was amplified from genomic DNA (strain BY4742) using the primers ABF1_1F and ABF1_1590R. ABF1_1F introduces an Aval site 5' to the ABF1 DBD; this restriction site is also located at the 3' of the competitor Myc tag ORF (see Fig. 5.3). The competitor ORF downstream of the ABF1 DBD was amplified from pCCA114 or pCCA214 with the primers ER_fus_F and ER_R#3. ER_fus_F introduces the last fifty nucleotides of the ABF1 DBD finishing at +1590 5' to the ER α LBD primer. The Abf1 DBD (+1-1590) was fused to the ORF PCR of pCCA114 or pCCA214 by fusion PCR using the primers ABF1_1F#2 and ER_R#3. pCCA114 was restricted with Aval, and the ORF was removed by gel purification. The fusion PCRs were subsequently cloned into the cleaved plasmid as an Aval restricted fragment to replace the ORF (for visual aid, see Fig. 5.3).

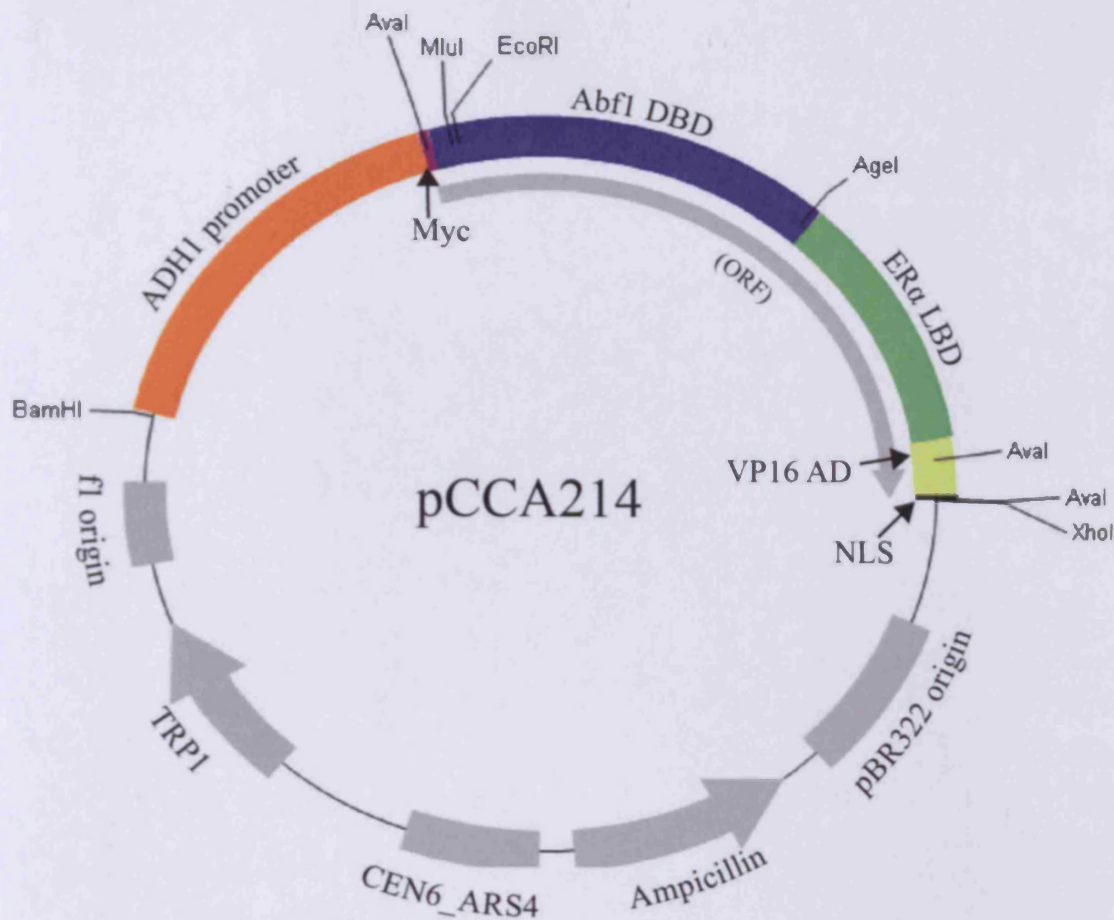


Figure 5.3. A restriction map of pCCA214. All restriction sites shown are unique except *AvaI*. A total of three *AvaI* sites are found within pCCA214 (or two in pCCA114).

Altering the promoter:

TEF2: The TEF2 promoter (nucleotides -402 to -1) was amplified from genomic DNA (strain BY4742) using the primers TEF2_-402F and TEF2_-1R. TEF2_-402F introduces a *Bam*HI site 5' to the promoter, whilst TEF2_-1R introduces the first 36 nucleotides of the Myc tag downstream of the promoter (this region contains the *AvaI* restriction site). pCCA114 was restricted with *Bam*HI and *AvaI*, and the promoter was removed by gel purification. The TEF2 promoter PCR was subsequently cloned into this cleaved plasmid as a *Bam*HI/*AvaI* restricted fragment to produce pCCT114.

TDH3: The TDH3 promoter (-690 to -3) was amplified from genomic DNA (strain BY4742) using the primers TDH_F and TDH_R. The competitor ORF was amplified from pCCA114 using the primers ORF_F and ORF_R. ORF_F introduces the last 53 nucleotides of the TDH3 promoter upstream of the competitor ORF. The

TDH3 promoter PCR was fused to the ORF PCR of pCCA114 by fusion PCR using the primers TDH_F#2 and ER_R#3. TDH_F#2 introduces a BamHI restriction site 5' to the TDH3 promoter. The fusion PCR was cloned into pRS314 as a BamHI/XhoI restricted fragment to give pCCG114.

Exchanging domains:

The remaining plasmids shown in Fig. 5.10 were constructed by exchanging domains between two plasmids. In each case, a plasmid was restricted at two sites and the fragment was removed from the plasmid by gel purification. This was replaced by the same restricted fragment from a second plasmid. The details of such exchanges are given in Table 5.1.

Plasmid created	Domain exchanged	Removed from	Replaced with same domain from	Alteration made
pCCT214	AgeI/XhoI	pCCT114	pCCA214	+VP16 AD
pCCT314	AvaI/AvaI	pCCT114	pCCA314	+(aa1-530) DBD
pCCT414	AgeI/XhoI	pCCT314	pCCA414	+VP16 AD
pCCG214	AgeI/XhoI	pCCG114	pCCA214	+VP16 AD
pCCG314	AvaI/AvaI	pCCG114	pCCA314	+(aa1-530) DBD
pCCG414	AgeI/XhoI	pCCG314	pCCA414	+VP16 AD

Table 5.1. The exchanged domains, shown as restriction fragments, of the competitor plasmids used to create new variants.

pCCG514 and pCCG614

The ER α LBD was amplified from pTK513 using the primers ER_F#2 and ER_fus_R. ER_fus_R introduces the first fifty nucleotides of Abf1 3' to the ER α -LBD ORF. ABF1 (+1-180) was amplified from pCCA314 using the primers ABF1_1F#3 and ABF1_60R. The ER α LBD was fused upstream of the first 180nt of ABF1 with the primers ER_F#3 and ABF1_60R. ER_F#3 introduces an AvaI site 5' to the ER α LBD. The fused PCR product was inserted into pCCG314 or pCCG414 as an AvaI/MluI restricted fragment to give pCCG514 and pCCG614 respectively.

pCCG714

The N-terminal ER α LBD and Abf1 DBD were amplified from pCCG514 using the primers Myc_F and ABF1_1590R#2. ABF1_1590R#2 introduces a NLS,

two STOP codons and an XhoI restriction site 3' to the Abf1 DBD. The PCR product was inserted into pCCG114 as an Aval restricted fragment to give pCCG714.

The sequences of all the plasmids created in this study are available on the accompanying DVD (D:/Plasmids).

Yeast transformation

Strains were transformed with the plasmids described in this study as detailed in Chapter 2.4.

Competitive ChIP

Strains were grown in synthetic dropout media (-Trp) at 30°C up to a density of 2×10^7 cells/ml. ChIP was performed as detailed in Chapter 2.7. Competitive ChIP was activated by 1 μ M β -oestradiol (Sigma-Aldrich, E8875) using a stock of 1mM β -oestradiol in ethanol. After β -oestradiol addition, cells were returned to an incubator with shaking for the timepoints indicated. For each ~300 μ g protein sample (50 μ l of WCE), Abf1 was immunoprecipitated with 12 μ l of α -Abf1 (yC-20 Santa Cruz Biotechnology) and the competitor was immunoprecipitated with 4 μ l of α -Myc (mAB 2276, Cell signalling technology).

Primers used for qPCR:

HML- α I-silencer:

Forward: 5' – CAACATGAAAGCCCGACGTTTG

Reverse: 5' – TTTGATTTTTTTCACCCAGAACCCCA

ARS121:

Forward: 5' – TCATGTTGCGGGTTGGTAT

Reverse: 5' – CGCCGAAATGGGTAAATAAGT

Negative Primers (IRC5)

Forward: 5' – AGTCGGGGCAGATACAGTTG

Reverse: 5' – GGCCGCTCTGGTCAATATAA

NAT4:

Forward: 5' – TATATGAGGCGCTTGGGTTC

Reverse: 5' – GTCGGAGTCAAGGATTCGAG

Data values of qPCR quantification are available in appendix IV. Error bars represent the standard deviation of replicates.

abf1-1 Competitive ChIP

Strains were grown in synthetic dropout media (-Trp) at 25°C and then subsequently incubated at the semi-permissive temperature (32°C) for three hours, to a density of 2×10^7 cells/ml. Incubations following addition of β -oestradiol were performed at 32°C. All further experimental conditions were performed as described above (Competitive ChIP).

5.3 Results

5.3.1 Designing an Abf1 competitor

The Gal4 competitor was constitutively expressed under the *ADHI* promoter from the centromeric plasmid pTK513. Therefore, appropriate alterations were made to pTK513 to produce the Abf1 competitor.

Abf1 contains two DBDs; an atypical zinc finger situated between aa40-91 and a putative helix-turn-helix (HtH) motif situated between aa323-496 (Fig. 5.2) (Cho et al., 1995). Both domains are required for DNA binding, whilst the C-terminal of the protein is not (Cho et al., 1995; Miyake et al., 2002). Therefore Abf1 aa19-523 was selected to replace the Gal4 DBD of pTK513.

To date, hormone activated competitive ChIP has successfully been employed for the study of two TFs; Gal4 in yeast and HIF-1 α in human cells (Nalley et al., 2006; Yu and Kodadek, 2007). As previously detailed, a Gal4 competitor devoid of an AD could not function to replace endogenous Gal4. Conversely, a HIF-1 α competitor absent of an AD has been demonstrated to successfully compete for promoter occupancy with the endogenous TF. As a consequence the necessity to include the VP16 AD within the Abf1 competitor was unknown. Recently, the 19S proteasome has been demonstrated to reversibly disrupt TF:DBS complexes and tethering the Gal4 DBD to the VP16 AD (which physically interacts with 19S subunit Sug1) results in 19S dependent destabilisation of DNA binding in vitro (Ferdous et al., 2007; Lee et al., 1995). Therefore, the VP16 AD had the potential to both stabilise or destabilise the DNA binding activity of an Abf1 competitor. Consequently two versions of the construct were made, one of which kept the VP16AD of pTK513, the other did not.

A final consideration for the Abf1 competitor was the intracellular localisation of the protein. Clearly for efficient and rapid competition following hormone induction the competitor needed to be localised in the nucleus prior to hormone activation. Unfortunately, HBDs other than the glucocorticoid receptor are not efficient at regulating nuclear localisation (Picard, 2000). In addition, since a nuclear localisation signal (NLS) is known to be found within the Gal4 DBD (amino acids 1-74), deleting this domain for the Abf1 competitor may have resulted in cytoplasmic localisation (Nelson and Silver, 1989). The NLS necessary and sufficient for Abf1 nuclear localisation lies within the AD (aa604-662) (Loch et al., 2004). Loch and co-workers demonstrated that a K625I mutation of Abf1 aa1-662 (the minimal domain of

Abf1 necessary to support cell growth (Miyake et al., 2002)) abolished nuclear localisation. However addition of the SV40 large T antigen NLS (PKKKRKV) at the C-terminus of this mutant fully restored nuclear localisation. Therefore, the SV40 NLS was also incorporated at the C-terminal of the Abf1 competitor.

Given these considerations two competitors were designed as shown in Fig. 5.4.

5.3.2 Construction and expression of an Abf1 competitor

The two variants of the Abf1 competitor were constructed using a fusion PCR strategy, whereby three separate PCR products were fused together in a final PCR reaction. The strategy employed is outlined in Fig. 5.4. The first PCR product, containing the *ADH1* promoter and a Myc tag was amplified from pTK513. Using 5' primer overhangs a BamHI restriction site was introduced 5' to the *ADH1* promoter, and fifty bases homologous to the Abf1 DBD (beginning at nucleotide +54) was introduced in frame 3' to the Myc tag. The second PCR product amplified the Abf1 DBD (nt +54-1569) from *S. cerevisiae* genomic DNA. Oligo (Molecular Biology Insights, Inc) primer design designated favourable priming sites within a DBD spanning Abf1 aa19-523 (nt +54 – 1569), which included both the Abf1 zinc finger and putative HtH domain (see above). The final PCR product, which contained the ER α LBD either with or without a VP16AD was amplified from pTK513. Using 5' primer overhangs fifty bases homologous to the Abf1 DBD (ending at nucleotide +1569) was introduced in frame 5' to the ER α LBD, whilst to the 3' of both PCR products the large T antigen NLS, two STOP codons and an XhoI restriction site were added respectively. Three separate PCR products were combined in a final fusion PCR for each of the variant constructs, which were subsequently inserted into pRS314.

prADH1- Myc-Abf1 DBD(aa19-523)- ER α LBD- NLS was inserted into pRS314 to give pCCA114 (plasmid Competitive Chip *ADH1*14).

prADH1- Myc- Abf1 DBD(aa19-523)- ER α LBD- VP16 AD- NLS was inserted into pRS314 to give pCCA214.

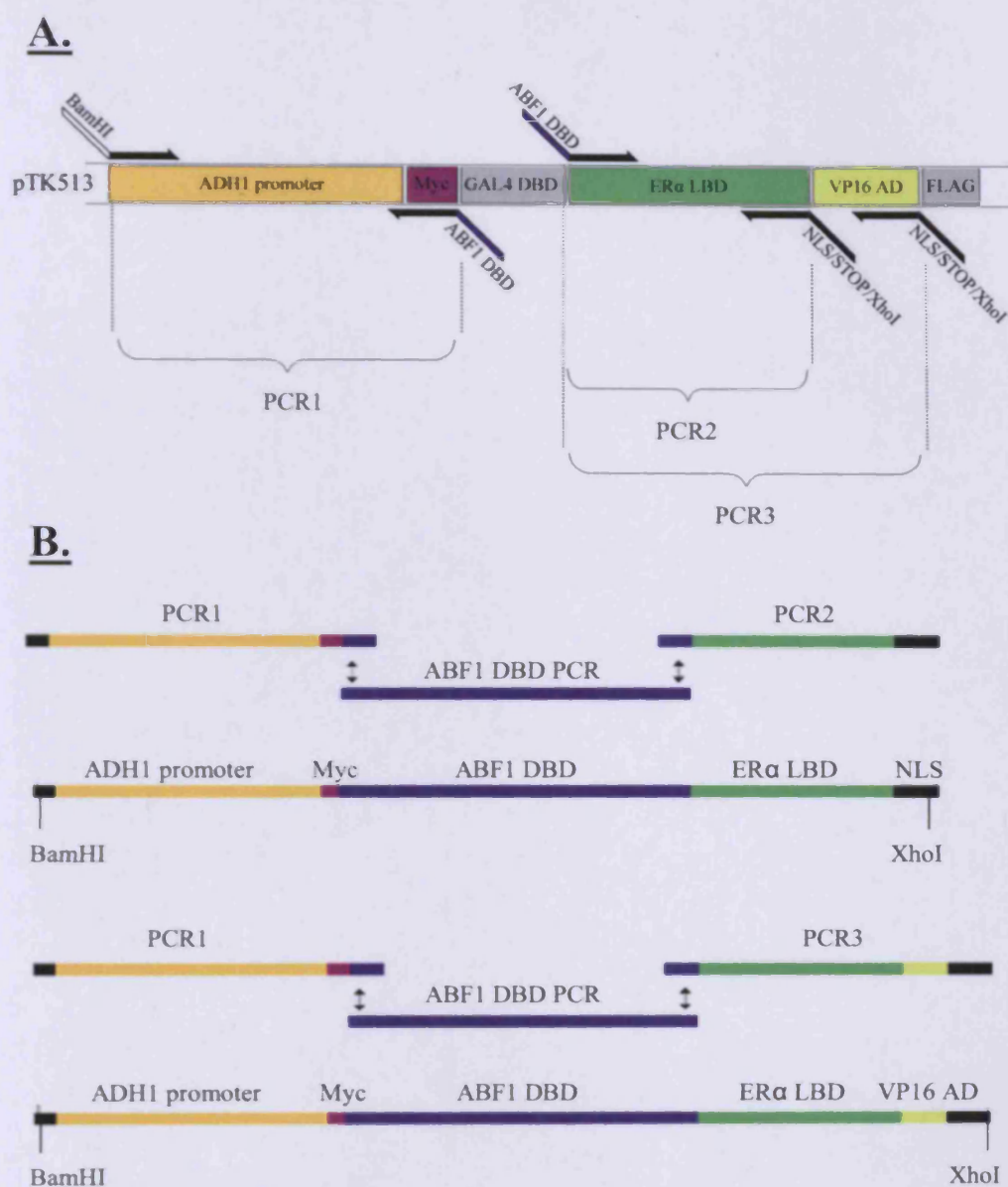


Figure 5.4. A. Domain structure of the Gal4 competitor of pTK513 with a representation of the position of the primers used to replicate the domains necessary for the Abf1 competitor, and resultant PCR products. Angular writing describes 5' sequences added to each primer. B. Graphical representation of the three PCR products used for each final construct and the resultant fusion PCR product. Double headed arrows indicate regions of homology.

pCCA114 and pCCA214 were transformed into SX46a. Western blots of protein whole cell extract from these strains were performed to test for the stable expression of the competitor, and to ascertain that the competitor was immunologically distinguishable from endogenous Abf1. As shown in Fig. 5.5, stable expression of the Abf1 competitor was confirmed from whole cell extract by western

blot using an α -Myc antibody. This demonstrates that under the conditions tested, the α -Myc antibody binds the Abf1 competitor without a detectable ability to bind endogenous Abf1. In addition, Fig. 5.5 shows the same membrane reprobed with an α -Abf1 antibody. Equally this demonstrates that α -Abf1 can only detect the endogenous protein, not the competitor.

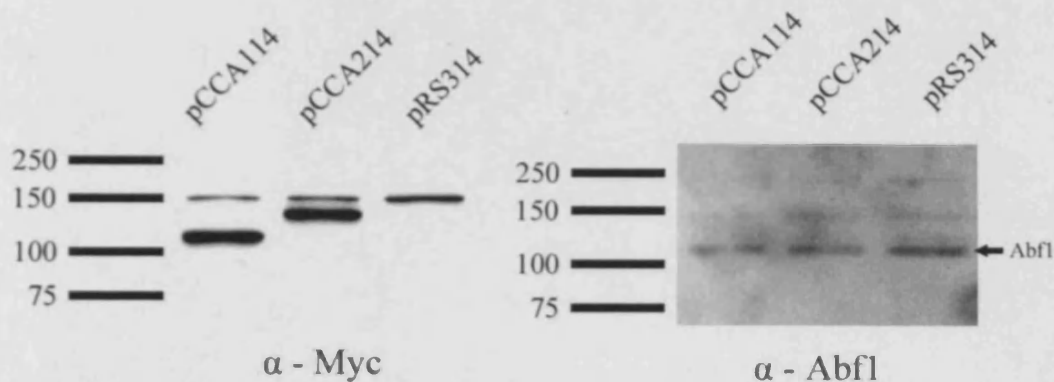


Figure 5.5. Western blot of SX46a transformed with either pCCA114, pCCA214 or PRS314 (empty vector). Ladder indicates approximate positioning of molecular weight. The left blot is developed using α -Myc, and the right picture indicates the same blot reprobed for with α -Abf1. A negative control for the Abf1 protein is not shown because the protein is essential. However, the antibody detecting Abf1 was well characterised and therefore there is a high confidence the band indicating Abf1 is correct (see appendix IV for antibody characterisation).

5.3.3 Abf1 competitive ChIP

Given that both strains stably expressed the individual Abf1 competitors and that both Abf1 and the competitor could be immunologically distinguished, the two strains were tested to see if the competition assay was functional. Competitive ChIP was performed in a similar manner to that previously described (Nalley et al., 2006). Both Abf1 and competitor were immunoprecipitated with the same antibodies as used for the western blot in Fig. 5.5. As shown in Fig. 5.6, the occupancy of both Abf1 and the competitor were compared at timepoints -1, 30 and 60 minutes after hormone activation by addition of β -oestradiol. The DNA binding occupancy was analysed at two established Abf1 binding sites; the I-silencer of *HML- α* and the B3 element of *ARS121* (Francesconi and Eisenberg, 1989; Harbison et al., 2004; Yu et al., 2009). These sites were compared to a negative control where Abf1 does not bind (*IRC5*, taken from Chapter 3 data, see appendix IV). As shown in Fig. 5.6, under all conditions tested, immunoprecipitation of the competitor was not observed to enrich

chromatin to a level higher than a negative control. This demonstrates that DNA binding of the competitor to *ARS121* or *HML α* could not be detected. In contrast, endogenous Abf1 DNA binding was readily detected at both genomic loci.

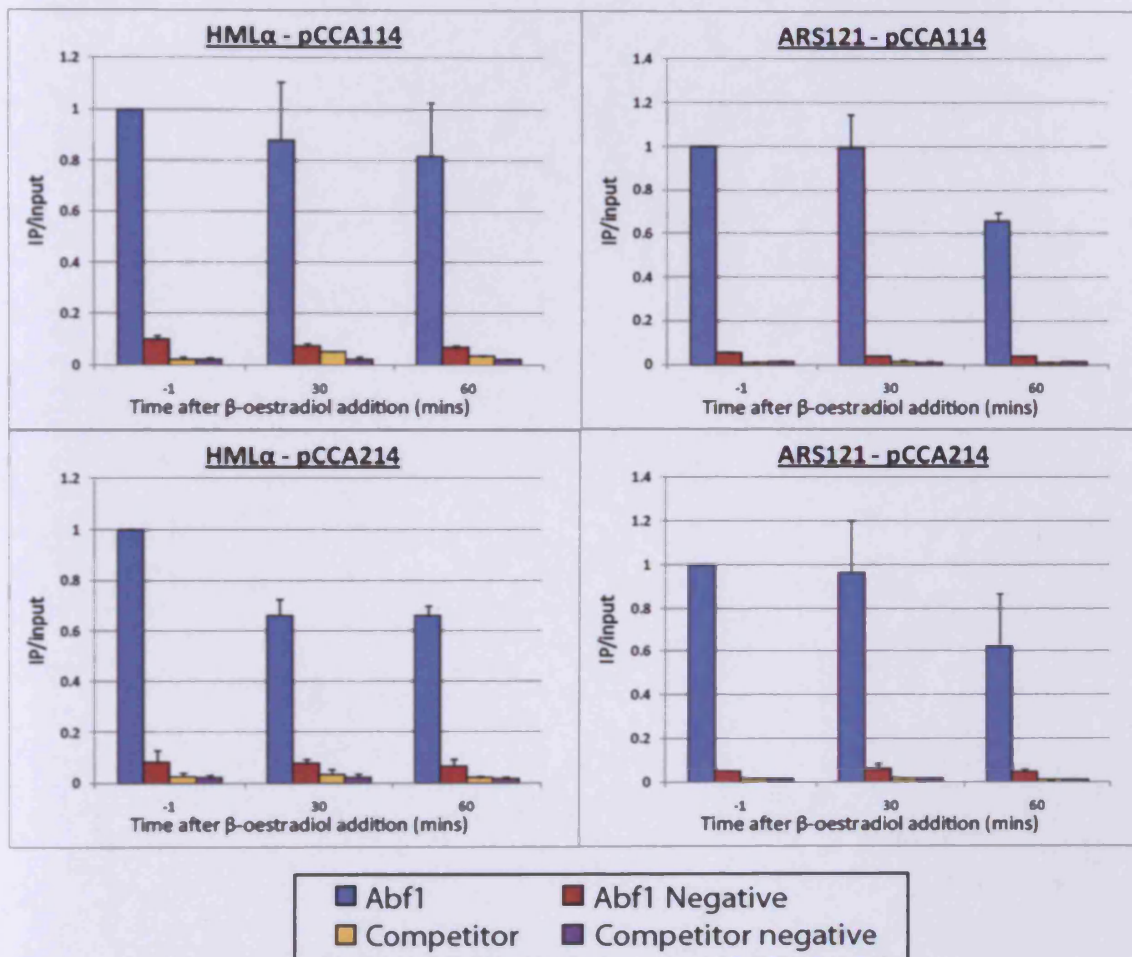


Figure 5.6. Graphs representing the occupancy of Abf1 and the competitor (pCCA114) or (pCCA214) by ChIP, before and after β -oestradiol addition. Two genomic loci were observed – the I-silencer of *HML α* and *ARS121*. The bars indicated as ‘negative’ represent a region of the genome (*IRC5*) where Abf1 does not bind.

The failure to detect DNA binding of the competitor in vivo could be potentially attributed to a number of difficulties. An insufficient β -oestradiol concentration could fail to activate the competitor. This was considered unlikely given that the transactivation potential of the Gal4 competitor expressed under the *ADHI* promoter is saturated at 0.1 μ M β -oestradiol (Louvion et al., 1993). The Abf1 competitor was induced at a ten-fold higher concentration to this (1 μ M); as previously

described for Gal4 competitive ChIP (Nalley et al., 2006). Alternatively, the Myc-ChIP may have failed. This was also deemed an unlikely cause, given that, under identical conditions the Abf1 ChIP was successful and that the α -Myc antibody used to IP the competitor has been successfully used for Myc-ChIP both in our lab and others (Fox and Good, 2008; Kibe et al., 2007; Lee et al., 2007a; Ono et al., 2003; Ueno et al., 2004, unpublished results; Dr. Y.Yu). Therefore, the most likely cause of an inability to ChIP the competitor was considered to be one of two causes. Firstly, if Abf1 were to stably bind at the DBS, then this would function to sterically inhibit DNA binding of the competitor. Alternatively, the design of the Abf1 competitor may have been flawed.

5.3.4 Testing the ability of the competitor to bind chromatin in the absence of Abf1 binding

It has previously been suggested that Abf1 fully occupies its binding sites in vivo (Schroeder and Weil, 1998). Therefore, if Abf1 does this in a kinetically stable manner, with a half-life in the range of hours, then the competitor would be unable to occupy chromatin under the conditions tested in 5.3.3. Therefore, designing an assay that eliminated endogenous Abf1 binding, whilst maintaining the Abf1 DBS would circumvent this issue. Abf1 is an essential gene and as such a null mutant is inviable, therefore a temperature sensitive DNA binding mutant of Abf1, termed *abf1-1*, was used (Rhode et al., 1992; Rhode et al., 1989). By comparing genome-wide ChIP data for Abf1 (strain JCA30) with *abf1-1* (strain JCA31) in cells grown under the semi-permissive temperature (32°C), a genomic locus was chosen with exceptionally reduced Abf1 occupancy (unpublished results; Dr Y.Teng, Dr S.Yu). As shown in Fig. 5.7, when JCA30 and JCA31 are grown at the restrictive temperature for three hours, the occupancy of *abf1-1* is significantly reduced (relative to Abf1) at the gene *NAT4*. Furthermore, in response to addition of β -oestradiol the occupancy of *abf1-1* remains very low after 30 minutes.

To test the competitor at an endogenous Abf1 DBS in the absence of Abf1 occupancy, JCA31 was transformed with pCCA114 and pCCA214. These strains were subsequently grown under the semi-permissive temperature and were incubated with β -oestradiol for 30 minutes, a timepoint previously shown to be sufficient for maximal competitor activation (Nalley et al., 2006; Yu and Kodadek, 2007). Both

competitor and Abf1 ChIP were performed. Neither competitor was found to bind *NAT4* under these conditions (data not shown). The competitor was subsequently redesigned (discussed below) and placed under the strongest constitutive yeast promoter known, *prTDH3* (Mumberg et al., 1995; Velculescu et al., 1997). As shown in Fig. 5.7B, when the Abf1 competitor without an AD is expressed under *prTDH3* (expressed on pCCG114) in JCA31 (abf1-1), binding at *NAT4* cannot be detected 30 minutes after β -oestradiol addition. The results are not expected to differ for a competitor with the VP16AD (not tested, see below). Collectively these data demonstrates that in the absence of Abf1 binding, the competitor remained unable to bind at an Abf1 DBS following hormonal activation.

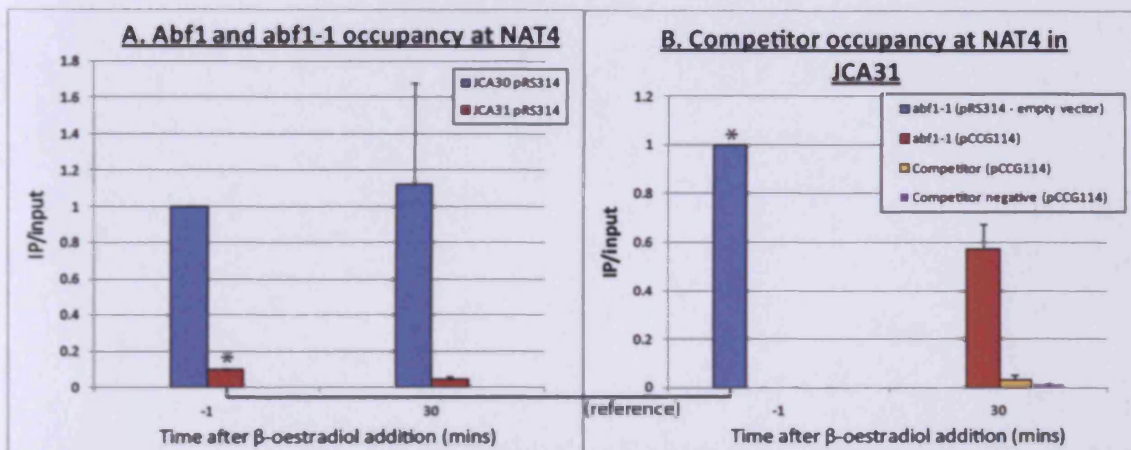


Figure 5.7. A. ChIP occupancy of Abf1 (JCA30) and abf1-1 (JCA31) grown under the semi-permissive temperature, before and after β -oestradiol addition. B. ChIP occupancy of abf1-1 (red bar) and the competitor (yellow bar) in JCA31 cells expressing pCCG114 (Myc-Abf1 DBD (19-523)- ER α LBD) 30 minutes after β -oestradiol addition. The enrichment of the competitor at *IRC5* (purple bar) functions as a negative control. NB- the blue bar at -1mins in graph B functions as a reference – this represents the occupancy of abf1-1 in JCA31 cells expressing an empty vector. As can be seen, the occupancy of abf1-1 in JCA31 expressing pCCG114, remains very low relative to the occupancy of Abf1 in JCA30 cells.

5.3.5 Redesigning the Abf1 competitor

Given the results in Fig. 5.7 it was considered possible that the design of the Abf1 competitor was flawed, thus inhibiting it from binding DNA. Three potential flaws were identified. Firstly, the competitor may not be nuclear localised. This was considered very unlikely given that the large T antigen NLS is known to be a powerful nuclear import signal with the ability to ectopically import recombinant proteins in excess of 100kDa into the yeast nucleus, and as such was not investigated (Nelson and Silver, 1989). Secondly, the competitor expression level may have been

too low to significantly bind the thousands of Abf1 binding sites within the genome (see Chapter 3). Thirdly, the Abf1 DBD selected for the competitor may have been non-functional.

Re-examining the expression level of the competitor

The expression of Abf1 is considered to be significantly higher than that of other stereotypical TFs such as Gal4 or Gcn4 (Arndt and Fink, 1986; Bram and Kornberg, 1985; Dorsman et al., 1988). As a consequence, whilst the *ADH1* promoter may have been suitable to express a sufficient concentration of Gal4 competitor, the same may not be true of Abf1. To directly assess if the Abf1 competitor was sufficiently expressed required a means to compare the stable expression level of both Abf1 and competitor. Since there was no facile way of achieving this, and since it was impossible to predict the level of expression required to successfully compete with Abf1 for DNA occupancy, the promoter of the Abf1 competitor was chosen to be altered such that a range of expression levels could be achieved. This was accomplished by replacing the *ADH1* promoter with either the *TEF2* promoter or *TDH3* promoter. When these promoters are fused to an ORF on a centromeric plasmid (as used in this study) they are predicted to increase protein levels ~17-fold higher (*pr TEF2*) or ~72-fold higher (*pr TDH3*) than the *ADH1* promoter (Mumberg et al., 1995). Fig. 5.8 shows three independent clones of SX46a expressing Myc-Abf1 DBD (aa19-523)-ER α LBD under the *ADH1*, *TEF2* or *TDH3* promoter. In good agreement with Mumberg et al (1995) this successfully achieves a range of increasing expression levels.

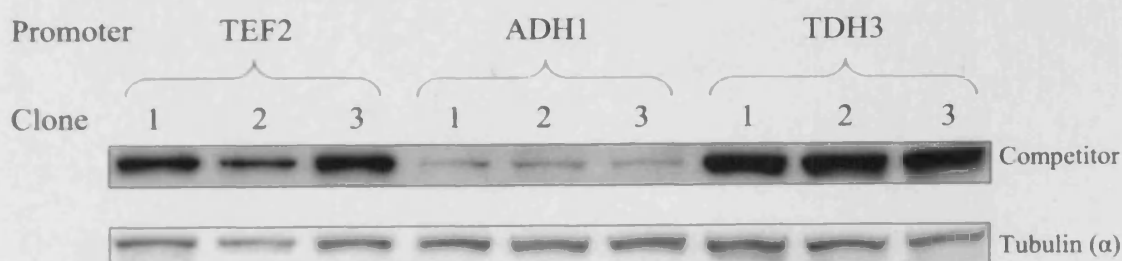


Figure 5.8. Western blot of three different SX46a clones, expressing Myc-Abf1 DBD (aa19-523)-ER α LBD under the control of the promoter from *ADH1*, *TEF2* or *TDH3*. The competitor blot was developed with α -Myc. As a loading control, the blot was reprobed with α -Tubulin.

Re-examining the Abf1 DBD

Whilst the two domains attributed to Abf1 DNA binding are stated to lie between aa40-496, it was plausible that aa19-523 of Abf1 within the competitor was not sufficient for DNA binding in vivo (Miyake et al., 2002; Yarragudi and Morse, 2006). Two Abf1 homologues, both of which can substitute for the essential functions of Abf1 in *S. cerevisiae*, have been identified in *Kluyveromyces lactis* and *Kluyveromyces marxianus* (Goncalves et al., 1992; Obery et al., 1993 respectively). A sequence alignment of the three homologues is given in Fig. 5.9. Interestingly the three homologues have two areas of high homology that approximately map to the two predicted DBDs in Abf1. These two domains correspond to Abf1 aa6-81 and aa323-441. Since the conservation of these residues may indicate that these are necessary for protein functionality, it is possible that residues N-terminal to aa19 of Abf1 are necessary for functional DNA binding in vivo. To date the minimum DBD sufficient for Abf1 binding in vivo has been demonstrated to be aa1-577 (Miyake et al., 2002). However, an Abf1 DBD of aa1-530 has been demonstrated to bind an Abf1 DNA binding consensus sequence in vitro (Halfter et al., 1989). Given that the domain of aa1-530 included both regions of homology shown in Fig.5.9, this was chosen to replace the competitor Abf1 DBD of aa19-523.

By changing both the promoter of the competitor and the Abf1 DBD, a series of novel Abf1 competitors were created and cloned into pRS314. Various domains were constructed and exchanged by both fusion PCR and standard cloning techniques. The details of this, along with a restriction map of one of the competitors in pRS314 are described in Chapter 5.2. This resulted in a total of 12 variations of the Abf1 competitor, the structures of which, and the nomenclature used for the plasmids, are provided in Fig. 5.10. Strains SX46a (Abf1) and JCA31 (abf1-1) were subsequently transformed with each of the 12 Abf1 competitor plasmids to test the competition assay in the presence of Abf1 or abf1-1, respectively. During the transformations, it was observed that there was a considerable contrast in the transformation efficiency and cell growth rates between the various transformants. These observations are summarized in Fig. 5.10. Plasmids containing the VP16 AD gave indistinguishable results from their counterparts without an AD (data not shown). Essentially all plasmids containing the *TEF2* promoter gave similar results to those with the *ADHI* promoter. Plasmids with the *TDH3* (strongest) promoter clearly showed a reduction in

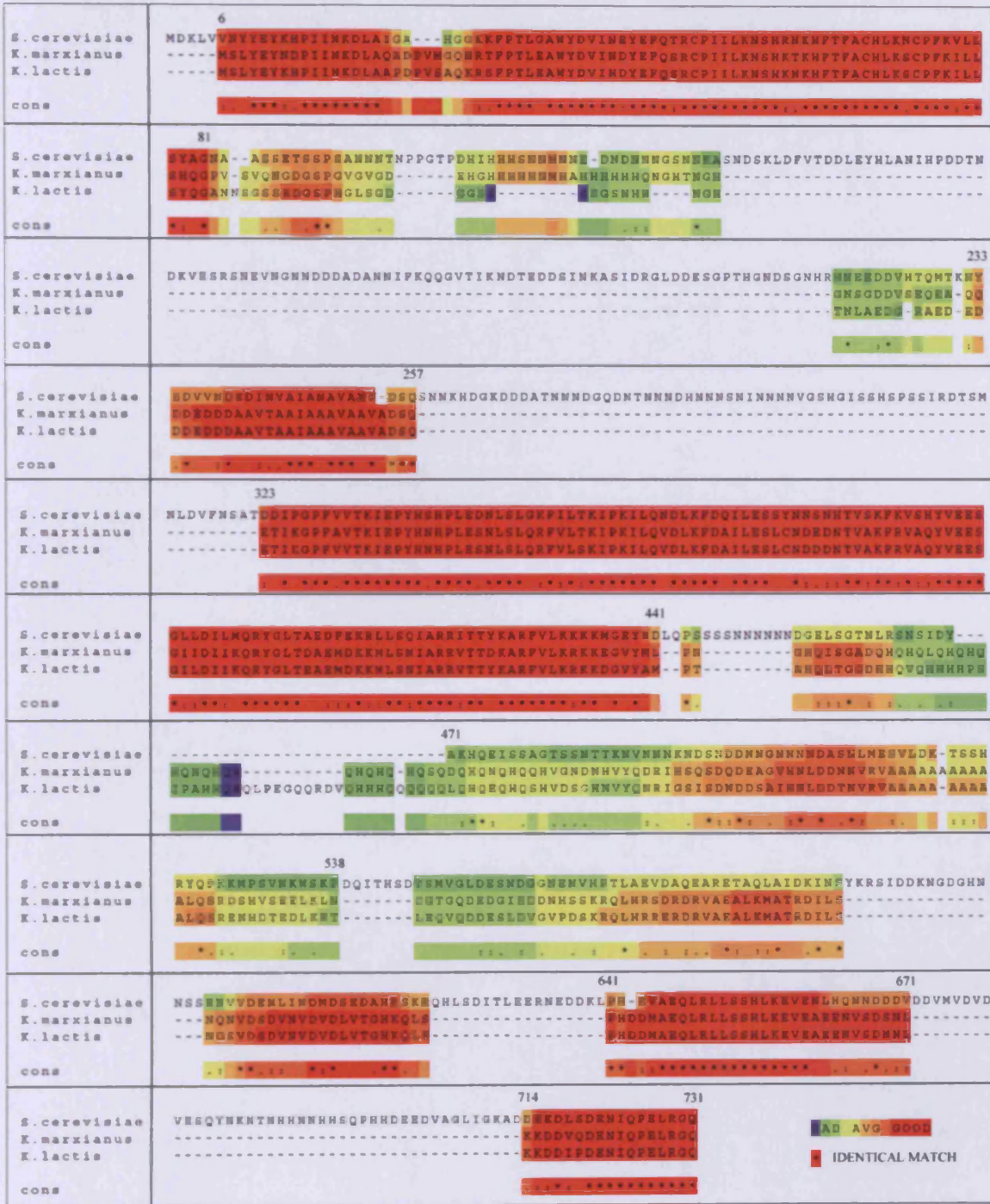


Figure 5.9. Sequence alignment of Abf1 homologues from *Saccharomyces cerevisiae*, *Kluyveromyces marxianus* and *Kluyveromyces lactis*. Numbers above borders of high homology represent the aa position of Abf1 from *S. cerevisiae*. Alignment was produced using tcoffee (<http://tcoffee.vital-it.ch/cgi-bin/Tcoffee/tcoffee.cgi/index.cgi>).

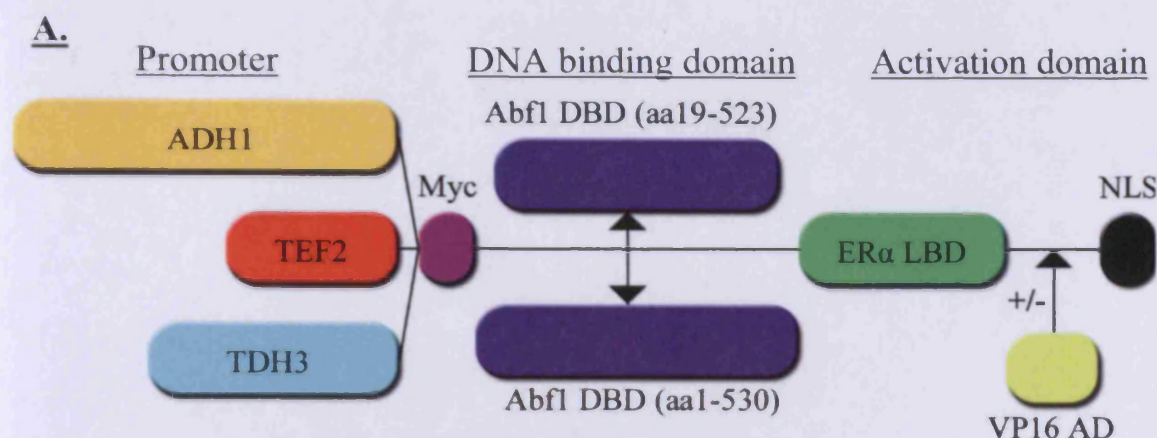


Table B. – Nomenclature used for Abf1 competitors cloned into pRS314

Nomenclature	Abf1 DBD (aa19-523)		Abf1 DBD (aa1-530)	
Promoter	No AD	With VP16 AD	No AD	With VP16 AD
ADH1 (pCCA)	pCCA114	pCCA214	pCCA314	pCCA414
TEF2 (pCCT)	pCCT114	pCCT214	pCCT314	pCCT414
TDH3 (pCCG)	pCCG114	pCCG214	pCCG314	pCCG414

Table C.

Strain (Genotype)	Plasmid	Transformation efficiency	Colony Growth	Protein expression of the competitor
SX46a (Abf1)	pCCA114	++++	++++	Stable
SX46a (Abf1)	pCCT114	++++	++++	Stable
SX46a (Abf1)	pCCG114	+++	+++	Stable
SX46a (Abf1)	pCCA314	++++	+++	Stable
SX46a (Abf1)	pCCT314	++++	+++	Stable
SX46a (Abf1)	pCCG314	++	+	Unstable
JCA31 (abf1-1)	pCCA114	++++	++	Stable
JCA31 (abf1-1)	pCCT114	++++	++	Stable
JCA31 (abf1-1)	pCCG114	+++	++	Stable
JCA31 (abf1-1)	pCCA314	++	++	Stable
JCA31 (abf1-1)	pCCT314	++	+	Stable
JCA31 (abf1-1)	pCCG314	-	-	N/A

Figure 5.10. A. Graphic illustrating the exchanged domains (titled above) of the Abf1 competitor. Table B. Listing of the nomenclature for the 16 plasmids created. Table C. Relative transformation efficiency, rate of colony growth and protein expression of strains SX46a and JCA31 following transformation with all Abf1 competitor variants without the VP16 AD. Increasing numbers of '+' indicates either a higher number of transformants per ng of plasmid DNA or faster colony growth. '-' indicates that no transformants could be obtained. For pictorial examples of the data shown in Table C please refer to appendix IV.

transformation efficiency and cell growth. In addition, changing the competitor DBD from aa19-523 to aa1-530 of Abf1 also had a similar effect. Of great interest, when the competitor with the Abf1 DBD 1-530 was expressed under the *TDH3* promoter (on plasmid pCCG314), a very significant defect in transformation efficiency and cell growth rate was observed (see also appendix IV). JCA31 cells (abf1-1) transformed with the plasmid pCCG314 were inviable (data not shown). Although SX46a cells transformed with pCCG314 were viable, cell growth was very slow and a clone that stably expressed the competitor was not isolated (clonal expansion of cells consistently resulted in the loss of competitor expression). Therefore, experiments could not be performed using a competitor with the Abf1 DBD aa1-530 expressed from the *TDH3* promoter.

The above results demonstrate that the additional residues within the Abf1 DBD aa1-530 (relative to aa19-523), render the competitor (or its expression) capable of interfering with efficient cell growth. Since overexpressing Abf1, or expressing C-terminal truncated versions of Abf1 also interfere with cell growth, this phenotype could be due to the competitor emulating Abf1 (or a C-terminal truncated Abf1) (Miyake et al., 2002; Sopko et al., 2006). This was interpreted to mean that the competitor with the DBD aa1-530 was DNA binding competent, whilst the competitor with DBD aa19-523 was not. This was subsequently investigated in 5.3.6 (see below).

5.3.6 The in vivo molecular characteristics of the revised Abf1 competitor

If, as suggested by the results in 5.3.5, the Abf1 competitor with a DBD aa1-530 of Abf1, could bind DNA at Abf1 DBS, and that this functioned to inhibit efficient cell growth, then two other important conclusions may be drawn from the observations in Fig. 5.10. Firstly, the competitor was not under complete hormonal regulation, since the inhibition of cell growth could be observed in the absence of β -oestradiol. Secondly, given that inhibition of cell growth was only prominent when the competitor was expressed from the *TDH3* promoter, this expression level is most likely to be required for strong competition of Abf1 DBSs by the competitor. This second assumption is further supported by the observation that addition of β -oestradiol to cells expressing the competitor under the *TEF2* promoter did not inhibit cell growth (data not shown).

In order to test whether the altered DBD renders the competitor DNA binding competent, competitive ChIP was performed in JCA31 cells (abf1-1) expressing the

Abf1 competitor (DBD aal-530) under the *TEF2* promoter, with the assay established in 5.3.4. The occupancy of abf1-1 and the competitor was measured both before and after β -oestradiol addition at a locus both positive (*NAT4*) and negative (*IRC5*) for Abf1 binding. As shown in Fig. 5.11, the competitor binds at *NAT4* irrespective of whether it possesses the VP16AD or not. Furthermore, the competitor binds at *NAT4* in the absence of β -estradiol, although occupancy is increased in response to hormonal activation. However, the competitor does not bind within a region of the genome to which Abf1 does not bind, demonstrating that the DNA binding capacity of the competitor is specific to Abf1 DBS (Fig. 5.11).

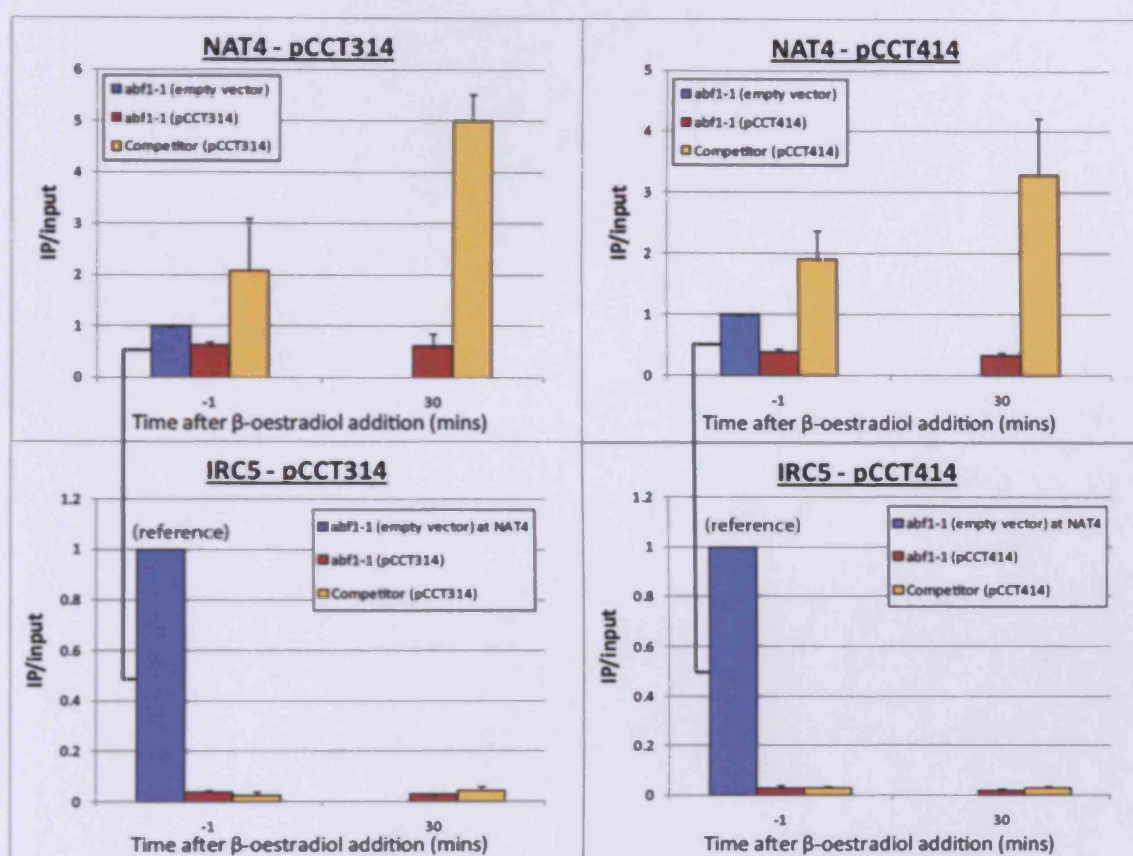


Figure 5.11. ChIP of abf1-1 and the competitor expressed from pCCT314 and pCCT414 at *NAT4* (positive control) and *IRC5* (negative control). At the *IRC5* locus the blue bar represents the equivalent occupancy of abf1-1 at *NAT4*.

5.3.7 Improving the hormonal regulation of the Abf1 competitor

Collectively the results from 5.3.5 and 5.3.6 suggested that an Abf1 competitor (with the DBD aal-530) expressed under the *TDH3* promoter would be optimal if the DNA binding capacity of this competitor was under stricter hormonal control. Previous work with hormone binding domains (HBDs) has suggested that the

proximity of the HBD fusion to the domain to be regulated vastly influences the efficiency of hormone dependent regulation (Nichols et al., 1997; Picard et al., 1988). Therefore, the ~430aa distance between the ER α LBD and the zinc finger of the Abf1 DBD within the competitor seemed a likely cause of incomplete hormonal regulation. To counter this, two new derivatives of the competitor were created. The first version repositioned the ER α LBD N-terminal to the Abf1 DBD so that it is proximal to the atypical zinc finger but distal to the HtH domain. A second version was created that included an ER α LBD both N and C-terminal to the Abf1 DBD. As with all other competitors both a version with and without the VP16 AD were constructed.

Upon transforming cells with the plasmid expressing the N-terminal ER α LBD under the *TDH3* promoter (pCCG714 (without VP16AD)), a similar phenotype was observed to that of transformants with plasmid pCCG314. Since JCA31 cells expressing this competitor could not be obtained, further investigations with this plasmid were not performed. In contrast, cells transformed with the double ER α LBD (pCCG514 (without VP16AD) and pCCG614 (with VP16AD)) showed a transformation efficiency and cell growth phenotype indistinguishable from cells transformed with pCCG114 (DNA binding defective competitor under the *TDH3* promoter). The activity of these two competitors was subsequently tested in JCA31 under identical conditions to that used for the experiments in Fig. 5.7 and Fig. 5.11. As shown in Fig. 5.12, in the absence of β -oestradiol neither competitor can be detected at *NAT4*. However, in the presence of the hormone both competitors bind at the locus, although surprisingly the occupancy of the competitor is considerably lower than that observed for the competitors expressed on pCCT314 and pCCT414 as seen in Fig. 5.11.

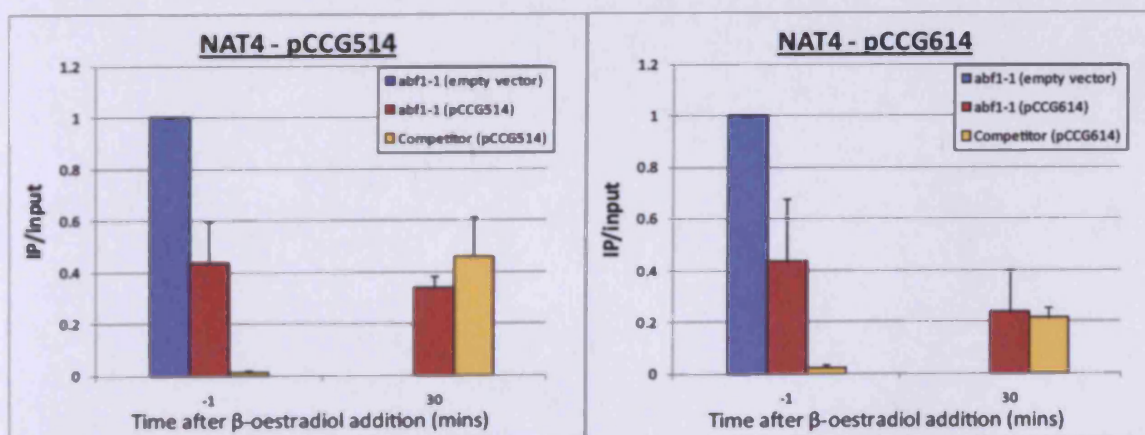


Figure 5.12. ChIP of abf1-1 and the competitor expressed from pCCG514 and pCCG614 at *NAT4*.

5.4 Discussion

The aim of the current study was to adapt a reagent previously used for Gal4 competitive ChIP, so that it may be utilised for Abf1 competitive ChIP. These studies present the successful creation of a recombinant protein that; is immunologically distinguishable from Abf1, can bind at Abf1 DBSs in vivo and ultimately is under strict hormonal regulation, thus fulfilling all the criteria previously considered necessary for a functional Abf1 competitor. The results presented here highlight some of the principle considerations and parameters that must be optimised to establish a functional competitor. These include; identifying a suitable DBD, choosing an appropriate expression level, optimising regulation through HBD fusion and considering the influence of an AD upon DNA binding in vivo.

The original design for an Abf1 competitor included a DBD between aa19-523 of Abf1. This DBD was subsequently shown to be unable to bind a domain bound by endogenous Abf1 at *NAT4* in vivo (Fig. 5.7). *NAT4* contains multiple copies of the Abf1 consensus DBS, and is a high affinity binding domain for Abf1 in vivo (unpublished results, Chapter 3). The N-terminal two thirds of bacterially expressed Abf1 (aa1-530) was previously demonstrated to bind an Abf1 DBS in vitro (Halfter et al., 1989). This domain includes a sequence that loosely resembles a zinc finger DBD predicted to be located between aa40-91 (Cho et al., 1995; Diffley and Stillman, 1989; Halfter et al., 1989; Rhode et al., 1989). Indeed, the protein does require zinc to bind DNA in vitro (Diffley and Stillman, 1989). Zinc fingers are common DNA binding motifs predominantly characterised by the presence of histidine and cysteine residues which function as ligands for the zinc atom (Klug, 2010). Abf1 contains histidine residues at aa57, 61 and 67, and cysteine residues at aa49, 66 and 71. Base substitutions at any of these residues inhibit Abf1 DNA binding in vitro (Cho et al., 1995; Halfter et al., 1989; Rhode et al., 1992). A second domain in Abf1 between aa323-496 is also predicted to function as a putative HtH DBD, and mutations within this region similarly inhibit efficient DNA binding of Abf1 in vitro (Cho et al., 1995).

By switching the Abf1 DBD to aa1-530, the competitor was subsequently demonstrated to bind at *NAT4* in vivo (Fig. 5.11). This suggests that either aa1-19 or aa523-530 are essential for Abf1 DNA binding in vivo, and two lines of evidence suggest the essential residues are found within aa1-19. Firstly, it has been previously demonstrated that deleting the N-terminal 47aa of Abf1 inhibits functional DNA binding in vitro (Halfter et al., 1989). Interestingly, this deletion mutant does not

exclude any of the histidine or cysteine residues predicted to function within the zinc finger, and combined with the studies presented here, may suggest residues upstream of aa19 are necessary for the functional activity of this domain. Secondly, two homologues of Abf1 found in *Kluyveromyces lactis* and *Kluyveromyces marxianus* each contain domains of high homology between aa6-81 of Abf1, but only low homology between aa441-538 (Fig. 5.9). *S. cerevisiae* strains expressing either of these homologues in place of the endogenous protein are viable (Goncalves et al., 1992; Obery et al., 1993). Given that the ability of Abf1 to bind DNA is essential for cell viability, these homologues must possess all residues necessary for DNA binding at an Abf1 DBS in vivo (Rhode et al., 1992). Interestingly this suggests that residues approximately between aa81-323 of Abf1 are dispensable for DNA binding and indeed a deletion mutant of Abf1 ($\Delta 200/265$) retains DNA binding capacity in vitro (Fig. 5.9, Cho et al., 1995)

Relative to the studies performed in vitro, less is known about the residues of Abf1 necessary for DNA binding in vivo. To date, the minimum in vivo DBD has only been ascertained through C-terminal deletions of the protein that maintain cell viability. A deletion mutant of Abf1 (aa1-599) is lethal, however if an AD (devoid of DNA binding activity) of Rap1 is added to this C-terminal, cell viability is restored (Goncalves et al., 1996; Rhode et al., 1992). Interestingly, Miyake and co-workers demonstrated that whilst a deletion mutant of Abf1 (aa1-587) was lethal, a further deletion mutant Abf1 (aa1-577) was viable. However, C-terminal deletions beyond aa577 did not support cell viability. The studies presented here demonstrate for the first time that the minimum in vitro DBD of Abf1 (aa1-530) is sufficient for DNA binding in vivo.

Over expressing a DNA binding competent competitor under limited hormonal regulation reduced cell viability and growth (Fig. 5.8 and 5.10). This phenotype is likely to be the result of the competitor contending against endogenous Abf1 for DBSs in vivo. This conclusion is supported by the observation that over expressing a DNA binding defective competitor (Abf1 DBD aa19-523), does not inhibit viability or cell growth (Fig. 5.7 and 5.10). Furthermore, inhibiting the DBD of the competitor with two ER α LBDs restores viability and cell growth (Fig. 5.12). How might binding of the competitor at Abf1 DBSs reduce the viability of the cell? As explained above, C-terminal truncations of Abf1 similar to that of the competitor (ie beyond aa530) are not viable (Goncalves et al., 1996; Miyake et al., 2002; Rhode et al., 1992). Within

the C-terminal of Abf1 two domains have been characterised, termed CS1 (aa624-628) and CS2 (639-662), which have been demonstrated to be necessary for the roles of Abf1 in transcription, silencing, DNA replication and nucleosome remodelling (Miyake et al., 2002). Therefore, a competitor deleted of this domain of Abf1 is unlikely to perform any of these activities *in vivo*. Interestingly, overexpressing the unregulated competitor with a VP16AD equally causes reduced viability and cell growth (data not shown). As discussed within the introduction, Abf1 may function to mediate both transcription and DNA replication in a similar manner. Indeed, the DBS of Abf1 at ARS1 (on a plasmid) may be functionally substituted for the DBS of a transcriptional activator such as Gal4 or Rap1 (Marahrens and Stillman, 1992). Furthermore, artificially tethering the C-terminus of Abf1 (aa608-731), the Gal4 AD or the VP16AD to the B3 element of ARS1 stabilises autonomous replication of a plasmid deleted of an Abf1 binding site (Li et al., 1998; Marahrens and Stillman, 1992). These domains are also known to function as transcriptional activators (Miyake et al., 2002; Ptashne, 1988). This either suggests the domains promote two biochemical activities, or the same activity stimulates both processes. It also suggests that a competitor with the VP16AD may promote some of the activities of Abf1 *in vivo*. Since overexpression of this construct still reduces viability, the VP16AD may not function to substitute for all essential activities found within the C-terminal of Abf1. To date, the only transactivation domain tested to substitute for the C-terminal of Abf1 is a domain within Rap1, which maintained the viability of the cell (Goncalves et al., 1996). Alternatively, given that over expressing Abf1 is also lethal, overexpression of the competitor may promote this phenotype by emulating the endogenous protein (Sopko et al., 2006).

As previously detailed for the Gal4 and HIF-1 α DBDs, heterologous fusion of the ER α LBD to an Abf1 DBD inhibits DNA binding (Fig. 5.11 and 5.12, Nalley et al., 2006; Yu and Kodadek, 2007). This inhibition by virtue of fusion to a HBD is not limited to DNA binding, and has been shown to regulate a wide variety of activities including kinases, recombinases and enzymes such as β -galactosidase (Picard, 1999). Interestingly, addition of a single ER α LBD to the Abf1 DBD did not fully inhibit DNA binding activity of the competitor (Fig. 5.11). This is in contrast to studies with Gal4 and HIF-1 α , however in these cases the target to be inhibited was far smaller. The Gal4 competitor included just aa1-93 of Gal4 next to the HBD. Although the HIF-1 α competitor included aa1-390, this domain includes both a DBD and a HIF-1 β

interaction domain where inhibition of either inhibits functional DNA binding (the protein binds DNA as a heterodimer with HIF-1 β) (Yu and Kodadek, 2007). Autonomous regulation through HBD fusion is considered to occur through an interaction between the HBD and Hsp90 in the absence of a ligand, which functions to sterically interfere with proximal regulatory domains (Picard, 1999; Picard, 2006). A corollary of this prediction is that domains distal to the HBD will not be under hormonal regulation. In support of this, ER α LBD repression of FLP recombinase (in the absence of a hormone) is stronger when the N-terminal domain of the LBD is deleted thus bringing the recombinase sequence more proximal to the HBD (Nichols et al., 1997). Similarly, fusion of the adenovirus E1A protein to the glucocorticoid receptor LBD confers complete hormonal dependence for transcriptional activation of targets genes (Picard et al., 1988). However if a 500aa intramolecular spacer is added between E1A and the HBD, the repressive activity of the HBD is lost, and even a 100aa spacer causes partial derepression (Picard et al., 1988). The latter result suggests that the ER α LBD C-terminal to the Abf1 DBD (aa1-530) may not have any influence upon the zinc finger of the Abf1 DBD. However, the zinc finger of Abf1 alone is not sufficient for DNA binding both in vitro and in vivo, therefore it is likely that a single C-terminal ER α LBD cannot fully inhibit the activity of the putative HtH motif of the Abf1 DBD either (Cho et al., 1995; Rhode et al., 1992). Over expressing the C-terminal fused ER α LBD competitor reduced cell viability and growth and this correlates with the ability of the competitor to bind DNA in the absence of hormonal activation (see above). Furthermore, it was found that over expressing a competitor with an N-terminal ER α LBD resulted in an identical phenotype and was thus assumed to similarly bind DNA in the absence of hormonal activation (data not shown). However, when a competitor with an ER α LBD both N and C-terminal to the Abf DBD was over expressed, the product neither reduced viability or cell growth, and could only bind DNA at *NAT4* in the presence of β -oestradiol (Fig. 5.12). In the absence of β -oestradiol this construct was unable to bind *NAT4* despite the fact that ~90% of the occupancy of Abf1 was lost from this site under the conditions tested, and therefore could not prevent the competitor binding due to steric hindrance. It is believed that this is the first ever example of using two HBDs to regulate protein function in this way.

When the double ER α LBD competitor was induced by β -oestradiol it was observed to occupy *NAT4* at a far lower level than that of the competitor with only a C-terminal ER α LBD (compare Fig. 5.111 with 5.12). This is despite the fact that the former competitor was expressed under the stronger *TDH3* promoter (Fig. 5.8, Mumberg et al., 1995). Therefore it is possible that the inclusion of a large N-terminal polypeptide (>300aa in total) interferes with the ability of the Abf1 DBD to interact with DNA. However, it is worth noting that the occupancy of the competitor with two ER α LBDs would be expected to be lower than a competitor with one ER α LBD if the concentration of β -oestradiol was limiting, since the former should require at least double the concentration to be fully alleviated of HBD regulation (this is examined in Chapter 6). HBDs are also known to dimerize albeit with a weak interaction, and thus two ER α LBDs may stabilise intermolecular dimerization between the competitor proteins more efficiently than one LBD (Picard, 1999). Furthermore, the double ER α LBD has the potential to form intramolecular dimerization interactions. In either case, this would lower the pool of free competitor proteins to bind DNA.

The results from Fig. 5.11 and 5.12 suggest that the inclusion of the VP16AD has little influence upon the ability of the competitor to bind chromatin in vivo. Nevertheless, these results are obtained in the absence of competition from Abf1. Whilst this does establish that the competitor does not require the VP16 AD for DNA binding in vivo, it does not provide an indication of the efficiency of competition against endogenous Abf1 occupancy.

Within the following chapter the tools constructed here were subsequently used to determine appropriate reaction conditions for Abf1 competitive ChIP and ultimately utilised to explore the in vivo kinetics of Abf1 DNA binding both in the absence and presence of UV damage.

6. Investigating Abf1 DNA binding kinetics using Abf1 competitive ChIP

6.1 Introduction

An accurate description of the molecular mechanism of Abf1, as part of the GGR complex, must include an understanding of DNA binding kinetics since this can significantly alter the interpretations of ChIP data (see Chapter 1.6 and Chapter 5). In addition, several lines of evidence suggest that changes in the DNA binding kinetics of Abf1 may be mechanistically linked to GGR. Firstly, data from our lab has recently identified a physical interaction between Abf1 and the 19S by co-immunoprecipitation (N.Humphryes, Thesis (2010)). To date, site specific DNA binding by three TFs (Gal4 DBD-VP16, Pho4 and p53) has been demonstrated to be displaced from a DBS by an activity within the 19S (Ferdous et al., 2007; Kim et al., 2009). In all cases, a physical interaction between the TF and the 19S was necessary for the displacement from a DBS, and this interaction occurred at the AD for both p53 and Gal4-VP16AD. Therefore, the 19S may function to promote the displacement of Abf1 at DBSs in vivo. Interestingly, both the p53 AD and VP16 AD have been shown to functionally substitute for the Abf1 AD at an origin of replication, potentially indicating that the C-terminal of Abf1 harbours an interaction domain with the 19S (Li et al., 1998). Secondly, monoubiquitylation of a TF functions to allosterically inhibit the 19S and attenuate its capacity to displace TF DBS binding (Archer et al., 2008b; Ferdous et al., 2007). Both Rad7 and Rad16, together with Cul3 and Elc1, are functional members of an ECS type E3 ubiquitin ligase, which has previously been demonstrated to ubiquitylate Rad4 in response to UV (Gillette et al., 2006; Ramsey et al., 2004). Therefore, Abf1, as a part of the GGR complex, physically interacts with members of a UV dependent ubiquitin ligase. This ubiquitin ligase could therefore regulate Abf1 DNA binding kinetics by modulating a functional interaction with the 19S. Alternatively, an ubiquitylation event could initiate proteolytic turnover of Abf1 at a DBS. In either case, this would regulate the half-life of the Abf1:DBS interaction. As previously discussed with transcription, this could potentially regulate the mechanism by which Abf1 promotes efficient GGR (see Chapter 1.6 for discussion).

A second activity within the GGR complex could also mediate changes in Abf1 DNA binding kinetics. As previously discussed, the GGR complex is

hypothesised to translocate from Abf1 binding sites in response to UV as part of the molecular mechanism of GGR (see Chapter 1.5.5 and 4). This process is predicted to be catalytically driven by the known translocase activity of Rad16, which functions to promote superhelical torsion in DNA and has recently been shown to promote chromatin remodeling (see Chapter 4.1, Yu et al., 2004; Yu et al., 2009; Yu et al., 2011). Chromatin remodelling by the Snf2 protein SWI/SNF has previously been demonstrated to displace TF binding of both the androgen receptor and glucocorticoid receptor from a DBS (Fletcher et al., 2002; Klok et al., 2007). A second member of the Snf2 superfamily, Rsc2, has also been shown to increase the kinetics of Acl1 binding *in vivo*; this is also predicted to occur through chromatin remodelling (Karpova et al., 2004). Therefore, the rapid turnover of Abf1 DNA binding at Abf1 binding sites could represent where Rad16 translocates and promotes chromatin remodelling in response to UV.

The aim of the current study is to use Abf1 competitive ChIP for the analysis of Abf1 DNA binding kinetics both in the absence and presence of UV damage. These datasets could then be compared to the Rad16 binding datasets, as well as CPD repair and histone acetylation to investigate the relationship between Abf1 DNA binding kinetics and GGR. The data presented in this study demonstrates that the exchange of the competitor for Abf1 at a DBS is incomplete when the competition reaction is in equilibrium. At least one potential caveat is identified when interpreting data of this nature. The results indicate that at present, the current Abf1 competitor adopted for the analysis of Abf1 DNA binding kinetics may require further optimisation for this investigation.

6.2 Materials and methods

Strains used in this study

Strain	Genotype	Source
BY4742	MAT α , his3 Δ 1 leu2 Δ 0 lys2 Δ 0 ura3 Δ 0	Euroscarf
JCA30	MAT α , trp1A his3A200 ura3-52 lys2-801 ade2-1 gal ABF1 HIS3a	(Rhode et al., 1992)
JCA31	MAT α , trp1A his3A200 ura3-52 lys2-801 ade2-1 gal abf1-1 HIS3a	(Rhode et al., 1992)
SX46a	MAT α , ade2 his3-532 trp1-289 ura3-52	(Reed et al., 1999)
BY4742 pRS316	BY4742 pRS316 (URA)	Commercial plasmid
BY4742 pCCG516	BY4742 pRS316-prTDH3- ER α LBD-Abf:aa1-530-ER α LBD	This study
BY4742 pCCG616	BY4742 pRS316- prTDH3- ER α LBD-Abf:aa1-530-ER α LBD-VP16AD	This study
BY4742 pCCG616A	BY4742 pRS316- prTDH3- ER α LBD-Abf:aa1-530-ER α LBD-Abf1:aa531-680	This study
BY4742 pCCG616R	BY4742 pRS316- prTDH3- ER α LBD-Abf:aa1-530-ER α LBD-Rap1:aa582-692	This study
JCA30 pCCG616	JCA30 pRS316- prTDH3- ER α LBD-Abf:aa1-530-ER α LBD-VP16AD	This study
JCA31 pCCG616	JCA31 pRS316- prTDH3- ER α LBD-Abf:aa1-530-ER α LBD-VP16AD	This study
JCA31 pGMA114	JCA31 pRS314- prTDH3- Myc- Abf1	This study
SX46a pCCT314	SX46a pRS314- prTEF2- Abf:aa1-530-ER α LBD	This study

Cloning

All PCR conditions, restriction assays and cloning techniques are described in Chapter 2.3.

The promoter and ORF of the Abf1 competitor was restricted from pCCG514 or pCCG614 as a BamHI/XhoI fragment and inserted into the multiple cloning site of pRS316 to give pCCG516 and pCCG616 respectively.

To produce the Myc tagged Abf1 protein used in Fig. 6.5, Abf1 was amplified from genomic DNA (BY4742) using the primers ABF1_1MF and ABF1_2924MR with the PCR conditions given in Chapter 2.3.2. ABF1_1MF introduces part of a Myc tag 5' to the Abf1 ORF, which includes an Aval restriction site. ABF1_2924MR introduces two STOP codons and an Aval restriction site 3' to the end of the Abf1 ORF. The PCR was Aval restricted and replaced the Aval enclosed competitor ORF of pCCG314 to give pGMA114.

The incorporation of Abf1 (aa531-680) or Rap1 (aa582-692) to the C-terminal of the Abf1 competitor was achieved using a fusion PCR strategy. Abf1 (aa531-680) was amplified with the primers ABF1_1593F and ABF1_2193R from genomic DNA (BY4742). ABF1_2193R introduces a NLS and two STOP codons 3' to the Abf1 domain. The ER α LBD was amplified from pCCA314 with the primers ABF1_1437F and ABF1_fus_R. ABF1_fus_R introduces the first 50 nucleotides of Abf1 aa531-680 3' to the ER α LBD. The PCRs of the ER α LBD and Abf1 aa531-680 were fused using the primers ABF1_1437F and ER_R#3. The fusion PCR was AgeI/XhoI restricted and replaced an AgeI/XhoI domain within pCCG616 to give pCCG616A. Rap1 (aa582-692) was added with an identical strategy. The Rap1 domain was amplified with the primers RAP1_1746F and RAP1_2076R from genomic DNA (BY4742). The ER α LBD was amplified from pCCA314 with the primers ABF1_1437F and RAP1_fus_R. The two domains were fused using the primers ABF1_1437F and ER_R#3 and the product was inserted as an AgeI/XhoI fragment in pCC616 to give pCCG616R.

All primers described above are listed in appendix V.

The sequences of all the plasmids created in this study are available on the accompanying DVD (D:/Plasmids).

Yeast transformation

Strains were transformed with the plasmids described in this study as detailed in Chapter 2.4.

Western blotting

Western blots were performed as described in Chapter 2.6.3 using yeast whole protein lysates (Chapter 2.6.1) and the conditions detailed in Chapter 5.2. To IP Myc tagged Abf1 from protein lysate of JCA31 expressing pGMA114, 180 μ g of protein was used for an IP as described in Chapter 2.7.1. 5 μ l of α -Myc antibody (9B11 mAB#2276, Cell Signalling Technology) was used to IP Myc tagged Abf1.

Competitive ChIP

Optimisation of hormone: A 1mM stock of β -oestradiol (Sigma-Aldrich, E8875) in ethanol was used to activate the competitor at a final concentration of 1, 10 or 20 μ M β -oestradiol. A 2mM stock of β -oestradiol in dimethyl sulfoxide (DMSO) was used to activate the competitor at a final concentration of 200 μ M.

All other steps in the protocol were performed as detailed in Chapter 5.2. Competitors expressed on pRS316 were selected for using synthetic dropout media (-Ura). ChIP analysed at *NAT4*, *ARS121* and *HML α* used the primers given in Chapter 5.2.

Novel qPCR primers used:

prSRB2:

Forward: 5'- GATAACGCACGCAAAACTCA

Reverse: 5'- GCTGGCTGGAGAACAATAGC

abf1-1 Competitive ChIP

This was performed as described in Chapter 5.2.

Data values of qPCR quantification are available in appendix V.

Competitive ChIP-on-chip

BY4742 pCCG616 was grown in synthetic dropout media (-Ura) at 30°C up to a density of 2×10^7 cells/ml and UV irradiated as described in Chapter 2.2. During the process of (mock/) UV treatment β -oestradiol was added to PBS prior to UV treatment to a final concentration of 20 μ M from a stock of 1mM in ethanol. Following UV treatment cells were resuspended in synthetic dropout media (-Ura) identically supplemented with 20 μ M β -oestradiol. ChIP was performed as detailed in Chapter 2.7, using the conditions given in Chapter 5.2. All ChIP-on-chip datasets were normalised using shift-by-mode only, as described in Chapter 3.

ChIP-on-chip chromosomal maps

Chromosomal maps of the competitive ChIP-on-chip data are available on the accompanying DVD (D:/Chapter 6/ChIPchip).

6.3 Results

Prior to the investigations presented in this chapter, the promoter and ORF of the Abf1 competitors from plasmids pCCG514 and pCCG614 (Chapter 5) were inserted into pRS316 to give the plasmids pCCG516 and pCCG616. These plasmids were transformed into yeast strain BY4742 such that competitive ChIP-on-chip could be performed in an isogenic strain to that of the Abf1/Rad16 ChIP-on-chip studies presented in Chapters 3 and 4.

6.3.1 Optimising hormone concentration for competitive ChIP

As demonstrated in Chapter 5, the Abf1 competitor did not occupy *NAT4* to a high level following hormonal induction, even in the absence of endogenous Abf1 binding when investigated using the abf1-1 mutant (Fig. 5.12). One possible explanation for these observations is that the concentration of β -oestradiol employed in these experiments was insufficient to complete competitor activation when highly expressed. In order to test this possibility, competitive ChIP was activated for 4 hours using a range of β -oestradiol concentration. The subsequent occupancy of Abf1 and the competitor was analysed at *NAT4* and the *HML α* I-silencer (Fig. 6.1). Complicating this experiment is the fact that β -oestradiol has a low solubility in water, estimated to be $\sim 5.5\mu\text{M}$ (Shareef et al., 2006). However, the solubility of β -oestradiol is improved in ethanol and is even higher when dissolved in DMSO for example β -oestradiol has a solubility of $\sim 700\mu\text{M}$ when dissolved in 1:4 DMSO:PBS (see www.caymanchem.com/pdfs/1000631). Competitive ChIP was activated by β -oestradiol dissolved in either ethanol or DMSO, however, in either case the precise concentration of soluble β -oestradiol is unknown (see materials and methods). As shown in Fig. 6.1, increasing the concentration of β -oestradiol from $1\mu\text{M}$ (as used in the experiments in Chapter 5) to $20\mu\text{M}$ effectively increased the occupancy of the competitor at both *NAT4* and the *HML α* I-silencer. This also resulted in a concurrent loss of Abf1 occupancy. However, attempts to further this exchange by adding β -oestradiol at a concentration of $200\mu\text{M}$ in DMSO did not significantly improve the competition reaction beyond that observed for $20\mu\text{M}$ β -oestradiol in ethanol.

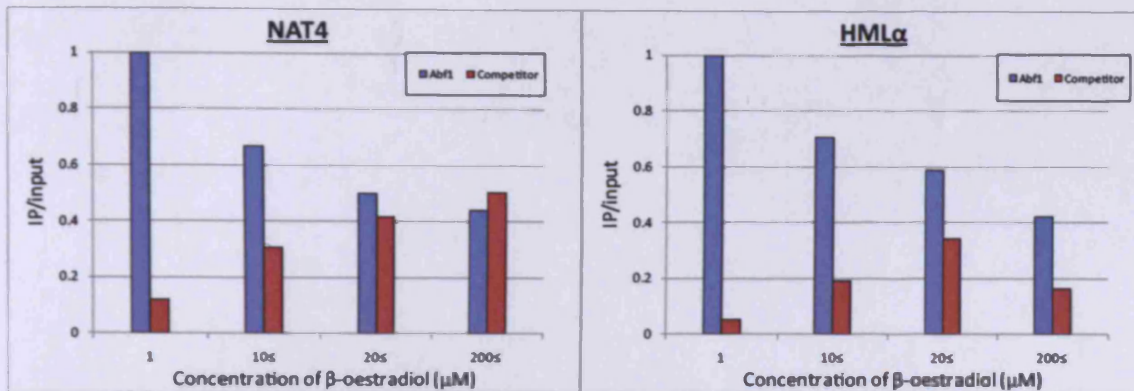


Figure 6.1. The influence of β -oestradiol on Abf1 competitive ChIP at *NAT4* and *HML α* 4 hours after activation. The experiment was performed in BY4742 transformed with pCCG616. The use of ' \leq ' is in reference to the fact that the precise concentration of β -oestradiol used in these experiments is unknown (see text for details).

6.3.2 Examining the efficiency of the competition reaction

Coincident with β -estradiol optimisation, the activity of Abf1 competitive ChIP was studied both one and two hours after hormonal activation. As shown in Fig. 6.2, when the competitor was induced with the optimal concentration of 20 μ M β -oestradiol, the competition reaction reached equilibrium at *NAT4* within one hour (Fig. 6.2B and C). This was also observed to be true at the *HML α* locus (Fig. 6.3C). Therefore, the reaction conditions chosen for β -estradiol optimisation (4 hours following activation), were sufficient for the competition reaction to complete and thus demonstrate that 20 μ M β -estradiol is adequate for maximal activation of the competitor. This concentration was adopted for all subsequent experiments.

Two further experiments were performed under the same experimental conditions as above. Firstly, β -oestradiol was added to a strain transformed with an empty vector (not expressing an Abf1 competitor) (Fig. 6.2A). In this circumstance, β -oestradiol failed to alter the occupancy of Abf1 at *NAT4*. This suggests the hormone has minimal effect upon the endogenous protein's ability to bind DNA. It also demonstrates that the loss of Abf1 must be a direct consequence of competition following hormonal activation in cells expressing the competitor. Secondly, the reaction was performed with cells expressing the competitor devoid of the VP16 AD (Fig. 6.2B). As shown, the competition reaction also reaches equilibrium within one hour at *NAT4*, with indistinguishable exchange to that observed with the competitor with a VP16 AD. Both competitors were also found to be expressed at similar levels (Fig. 6.2D) and thus must have a similar capacity to compete with endogenous Abf1

for occupancy. Consequently, further studies were performed using only the competitor with the VP16 AD.

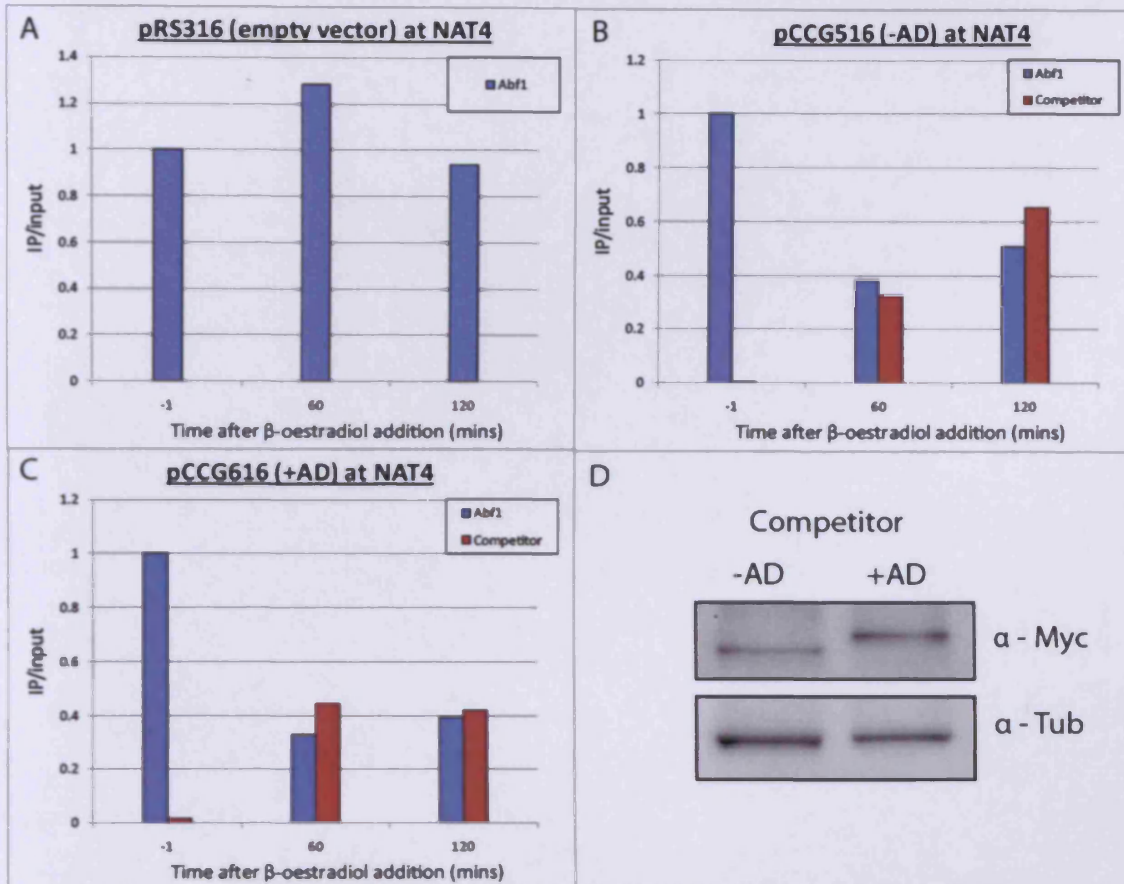


Figure 6.2. A. ChIP of Abf1 performed at *NAT4*. B. Competitive ChIP at *NAT4* using the competitor expressed upon pCCG516 (-AD). C. Competitive ChIP at *NAT4* using the competitor expressed upon pCCG616 (+AD). D. Western blot of the relative expression of the competitor expressed from pCCG516 (-AD) and pCCG616 (+AD). All experiments were performed in BY4742.

An important observation from Fig. 6.2 is that when the competition reaction has reached equilibrium, the exchange of Abf1 occupancy for the competitor is incomplete. It was unknown how common this phenomenon would be at Abf1 binding sites. Furthermore, the rate of exchange between Abf1 and the competitor was unknown. To gain an understanding into both of these considerations, the competition reaction was repeated and analysed 10 minutes, 60 minutes and 120 minutes after activation at a range of Abf1 binding sites. As shown in Fig. 6.3, at all three loci tested, the competition reaction did not reach an equilibrium after 10 minutes following β -estradiol addition. However, by 60 minutes the exchange had reached equilibrium at all loci since little additional exchange between Abf1 and the competitor was observed 120 minutes after activation compared with 60 minutes. As

previously observed, the level of exchange between Abf1 and the competitor was partial for all sites tested. However, the total occupancy replaced by the competitor was different for each example. In contrast to the results presented at *NAT4* (Fig. 6.2C), where the competitor was observed to replace roughly half the occupancy of Abf1, at the loci *ARS121* and *prSRB2* lower levels of exchange between Abf1 and the competitor are observed.

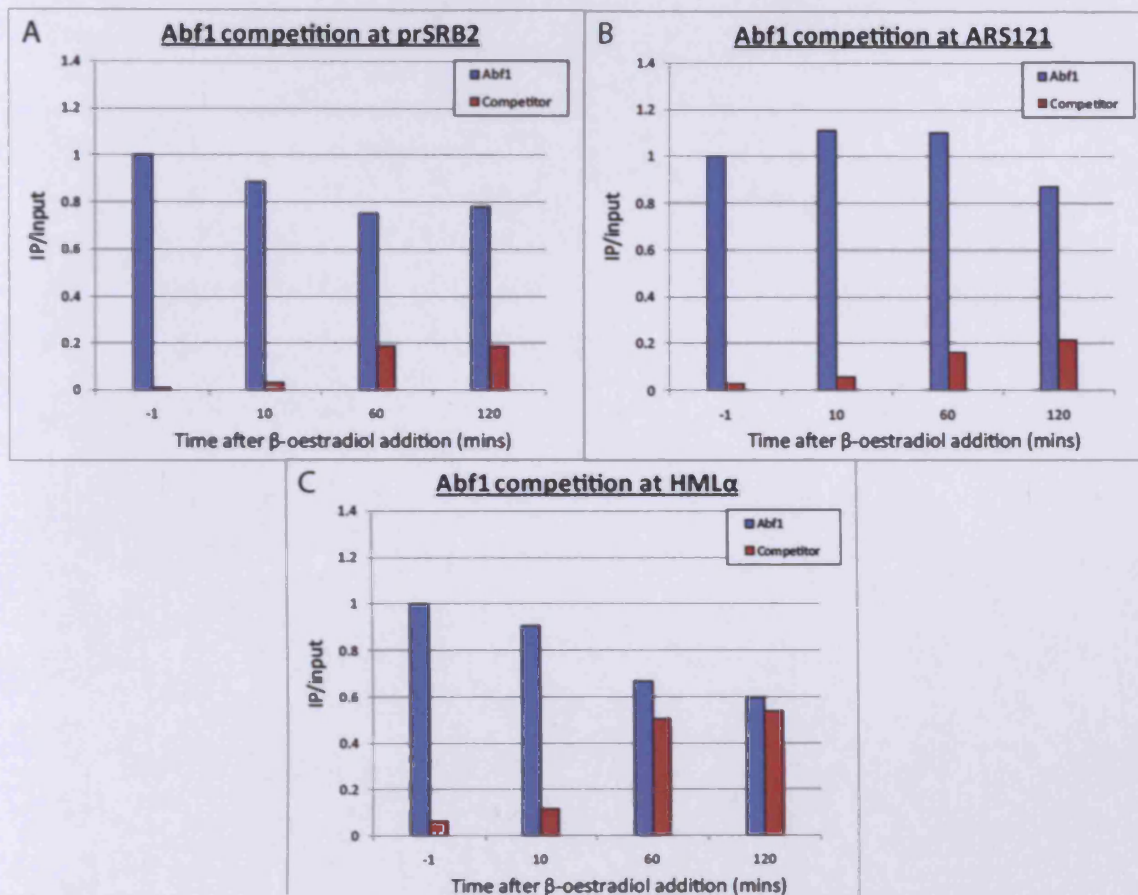


Figure 6.3. Competitive ChIP with BY4742 expressing pCCG616 at the loci prSRB2 (A), ARS121 (B) and the *HML α* I-silencer (C). Experiments were performed in BY4742.

6.3.3 Potential caveats when investigating DNA binding kinetics at sites of incomplete competitor exchange with Abf1

The results shown in Fig. 6.3 could be interpreted to suggest that Abf1 DNA binding kinetics are more rapid at loci where a greater exchange with the competitor has occurred one hour after hormonal activation, than those with little exchange. However, in the current experimental setup, the exchange of Abf1 for the competitor is incomplete when at equilibrium. I hypothesised that the affinity of Abf1 relative to the competitor for any given locus could influence the relative exchange of the two

proteins in a manner independent to Abf1 DNA binding kinetics. For example, if the competitor had a lower affinity for binding at *prSRB2* than *NAT4*, relative to Abf1, then little exchange of the two proteins would occur at *prSRB2* (as observed).

To investigate these two possibilities, the competitor was activated both in the presence and absence of Abf1 binding using the JCA30 (Abf1) and JCA31 (abf1-1) strains. Abf1 DNA binding was diminished by growing cells at the restrictive temperature as previously shown (Chapter 5.3) and competitor binding was observed at the loci *NAT4* and *prSRB2*, as examples of ‘good’ and ‘poor’ competition respectively (Fig. 6.4). Occupancy of Abf1 and the competitor were observed -1, 10 and 20 minutes after hormonal activation. As previously shown (Fig. 6.2C and 6.3A), in the presence of Abf1 binding the efficiency of competition was greater at *NAT4* than *prSRB2*. Interestingly, in both examples the competition reaction 20 minutes after hormonal activation is similar to the reaction at equilibrium described above (Fig. 6.2 and 6.3), suggesting that at both loci the competition reaction completes within ~20 minutes. It should be noted, that both the Gal4 and HIF-1 α competitors required ~20 minutes for full activation to occur in the absence of the endogenous protein (Nalley et al., 2006; Yu and Kodadek, 2007). By significantly reducing the occupancy of Abf1 using the abf1-1 mutant, it can be seen that the activation of the competitor is also incomplete 10 minutes after activation in the absence of Abf1 binding. This strongly suggests that at *NAT4* and *prSRB2*, the competitor requires ~20 minutes for full induction, and at these sites the kinetics of Abf1 binding are rapid such that they do not delay binding of the competitor to the loci (Fig. 6.4B and 6.4D). Furthermore, in the abf1-1 mutant (Fig. 6.4B and 6.4D) the level of competitor binding at *NAT4* is higher than *prSRB2* relative to the wild type levels of Abf1 binding. This explanation is true both 10 minutes (during competition) and 20 minutes (when equilibrium is reached) after hormone activation. This might suggest that the occupancy of the competitor for these two sites is different in a manner independent to endogenous Abf1 binding, and this may influence the exchange of the two proteins, rather than Abf1 DNA binding kinetics. These results demonstrate that the interpretation of competitive ChIP results at loci where protein exchange is incomplete, may not accurately reflect Abf1 DNA binding kinetics.

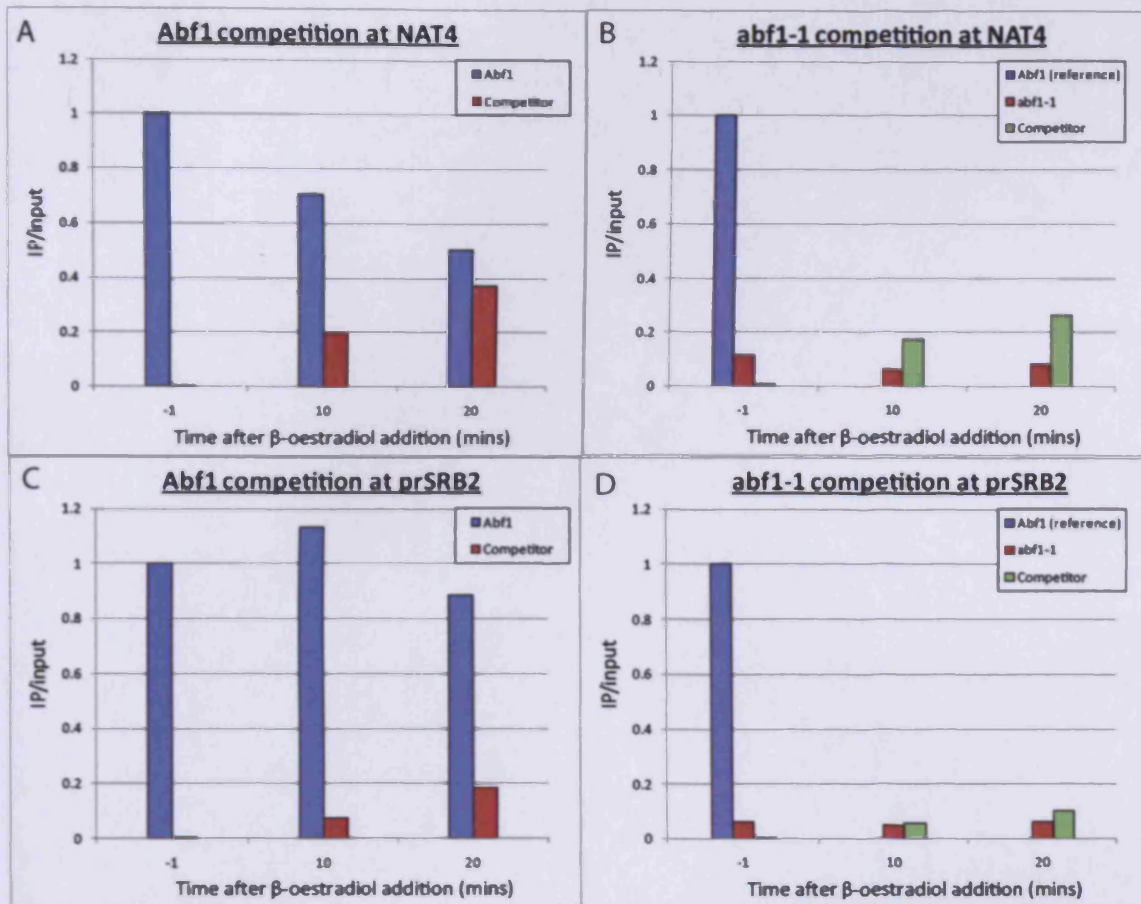


Figure 6.4. Competitive ChIP using pCCG616 expressed in either JCA30 (Abf1 competition) or JCA31 (abf1-1 competition). A and B. compare competition at *NAT4*. C and D. compare competition at *prSRB2*.

6.3.4 Comparing the protein level of the competitor to Abf1 in vivo

The inefficiency of the competition reaction was surprising given that the competitor was expressed under the powerful *TDH3* promoter (see Chapter 5). If the competitor was highly abundant relative to Abf1, it should be expected to effectively compete for Abf1 DBSs. In order to establish whether this was the case, the relative intracellular levels of the two proteins were compared. An effective antibody that could recognise an epitope shared in both the competitor and Abf1 could not be acquired (data not shown). Consequently, several attempts were made to Myc tag the endogenous Abf1 protein. However, this was also an unsuccessful strategy (data not shown). Therefore, the ORF of pCCG314 was altered to give a construct which contained the exact full length ORF of Abf1 with an N-terminal Myc epitope. The protein was expressed in JCA31 (abf1-1), the only strain identified to stably express Myc tagged Abf1. The Myc tagged protein was subsequently isolated by

immunoprecipitation from whole cell extracts. This protein provided a convenient intermediate to directly compare the endogenous levels of Abf1 and the competitor by western blot (see Fig. 6.5 for details). As shown in Fig. 6.5, the competitor is expressed ~4-fold higher than endogenous Abf1.

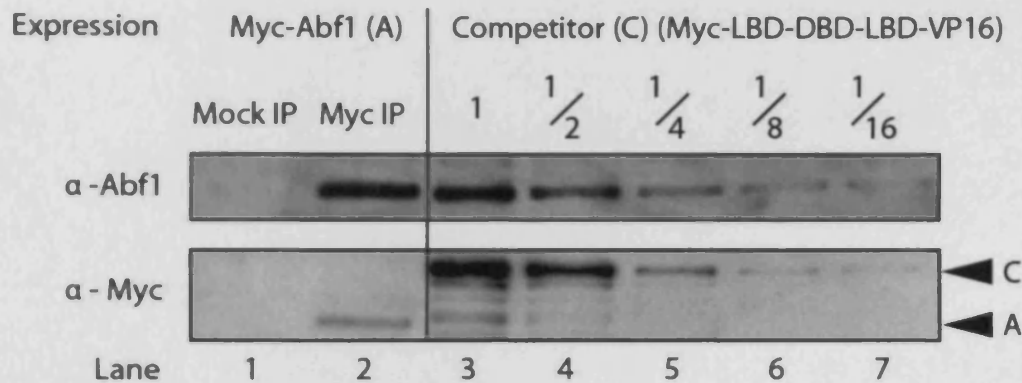


Figure 6.5. Picture shows a single western blot probed with α -Abf1 and then reprobed with α -Myc. Left hand side; Myc tagged Abf1 (A) expressed in JCA31 is isolated by α -Myc IP (Lane 2). The mock IP fails to isolate Abf1 (Lane1) demonstrating all Abf1 in Lane 2 is Myc tagged. Right hand side; Protein WCE from BY4742 expressing the competitor (C) and endogenous non-tagged Abf1. A serial dilution of WCE runs from Lanes 3-7. α -Abf1 developed membrane; Lane 3 demonstrates that BY4742 has equivalent levels of Abf1 to the level of Myc tagged Abf1 loaded in Lane 2. α -Myc developed membrane; Lane5, which has four fold less BY4742 WCE than lane 3, has an equivalent level of competitor to the Myc tagged Abf1 in Lane 2. Thus the competitor expressed in BY4742 is ~4 fold higher than the endogenous Abf1 protein level.

6.3.5 Attempts to further improve the efficiency of Abf1 competitive ChIP

As demonstrated in 6.3.3, the interpretation of Abf1 competitive ChIP is difficult when the exchange of Abf1 and the competitor is incomplete. Therefore, adapting the assay such that the competitor could replace Abf1 occupancy entirely (>90%) was a high priority. Given that the competitor was only in 4-fold molar excess to Abf1, further overexpression of the competitor was attempted by incorporating the construct into the multicopy plasmids pRS426 or YEplac195. However, a strain that stably expressed either competitor (with or without the VP16 AD) could not be isolated.

If one considers that a competitor with aa1-530 of Abf1, expressed 4-fold higher than Abf1, has a much lower affinity for binding in vivo than the endogenous protein, this may suggest that the C-terminal aa531-731 of Abf1 is important for DNA binding in vivo, and that the VP16 AD does not functionally substitute for this activity. To test this hypothesis, the VP16 AD of the competitor was replaced with Abf1 aa531-680. This domain ensured that the competitor remained immunologically

distinguishable from the endogenous protein. In addition, the VP16 AD was substituted for a similar domain from Rap1 (aa582-692) which has been demonstrated to functionally substitute for the Abf1 C-terminal in cell survival assays (Goncalves et al., 1996). Both competitors were activated for 4 hours and tested at the *prSRB2* locus. However, neither proved to be an effective competitor at this site (Fig. 6.6). As a final attempt, the competitor with a single C-terminal ER α LBD (from Chapter 5) was also tested but was observed to be equally ineffective at *prSRB2* (Fig. 6.6).

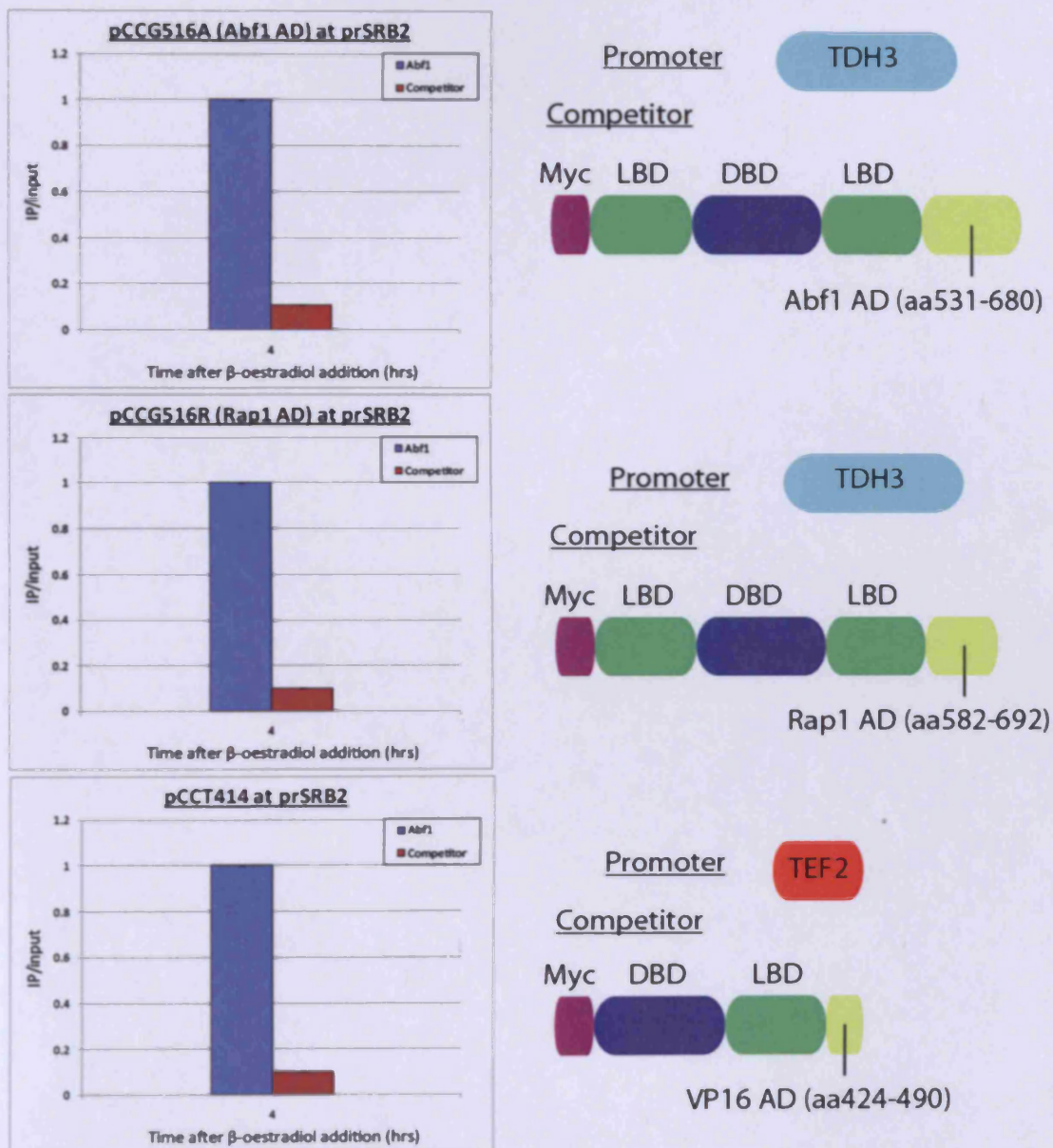


Figure 6.6. Competitive ChIP at *prSRB2* 4 hours following β -oestradiol activation. The competitor constructs are shown on the right, and ChIP results to the left. pCCG516A and pCCG516R were expressed in BY4742. pCCT414 was expressed in SX46a.

6.3.6 Genome-wide analysis of Abf1 competitive ChIP both in the presence and absence of UV damage

Despite the difficulties presented for the Abf1 competition reaction, Abf1 competitive ChIP was performed genome-wide to try and identify regions of the genome in which the competitor provided effective competition with Abf1, and analyse how the kinetics of Abf1 binding might differ in response to UV damage. ChIP-on-chip was performed in a similar manner to that previously described (Chapter 3). Abf1 competitive ChIP was initiated in BY4742 expressing pCCG616 with 20 μ M β -oestradiol. Addition of oestradiol was performed during mock UV (cold PBS only) or UV treatment of cells. Cells were subsequently resuspended in selective media containing 20 μ M β -oestradiol and incubated for one hour. Cells were fixed prior to UV treatment (No treatment), after 10 minutes incubation following UV treatment (10 minutes) and after 60 minutes incubation following UV treatment (60 minutes). Based upon the experiments presented in Fig. 6.3 and Fig. 6.4, these incubations were hypothesised to mostly represent where the competition reaction is in dynamic exchange (10 minutes) and has reached equilibrium (60 minutes). As shown in Fig. 6.7, in the absence of UV damage binding of the competitor at Abf1 binding sites is not observed to occupy at a high level, even following 60 minutes after activation. This suggests that the ability of the competitor to compete with Abf1 binding is limited throughout the genome. An alternative interpretation of these data is that endogenous Abf1 is stably bound at DBSs in the absence of UV.

In response to UV damage, the occupancy of the Abf1 competitor is observed to increase at some Abf1 binding sites to a moderate degree. Binding of the competitor is rapid and occurs within 10 minutes after β -oestradiol addition (Fig. 6.7). One interpretation of these data is that the half live of Abf1 binding at some DBSs is shorter in response to UV irradiation. However as discerned in 6.3.3, the biological significance of partial exchange between the competitor and Abf1 is difficult to interpret. It should be noted that in the absence of UV damage the competitor is not observed to occupy Abf1 binding sites to an equivalent level, even following one hour after activation. This could suggest that the ability of the competitor to bind at these sites is non-equivalent in the presence and absence of UV damage. As previously discussed this might suggest that the levels of competitor binding do not represent differences in Abf1 DNA binding kinetics (6.3.3, see also discussion). These data suggest that the competitor may require further optimisation to improve the

confidence of results obtained using the reagent before biological interpretations of Abf1 DNA binding kinetics can be made.

Finally, whilst the reasons for the differences observed for competitor binding at Abf1 sites in the presence and absence of UV damage were not resolved, I wished to investigate how the competitor behaved after UV damage relative to the location of the Abf1 binding site. Therefore, the binding of the competitor in the presence of UV damage, ten minutes after β -oestradiol, was plotted at the Abf1 binding sites classified according to their genomic location. Interestingly, significant binding by the competitor was only observed at Abf1 binding sites within the promoter regions (Fig. 6.8). These observations correlate with the preferential location the GGR complex and where Rad16 dependent acetylation and efficient GGR appear to be organised from (Chapters 3 and 4). This suggests that this phenotype may be mechanistically related to the activity of GGR.

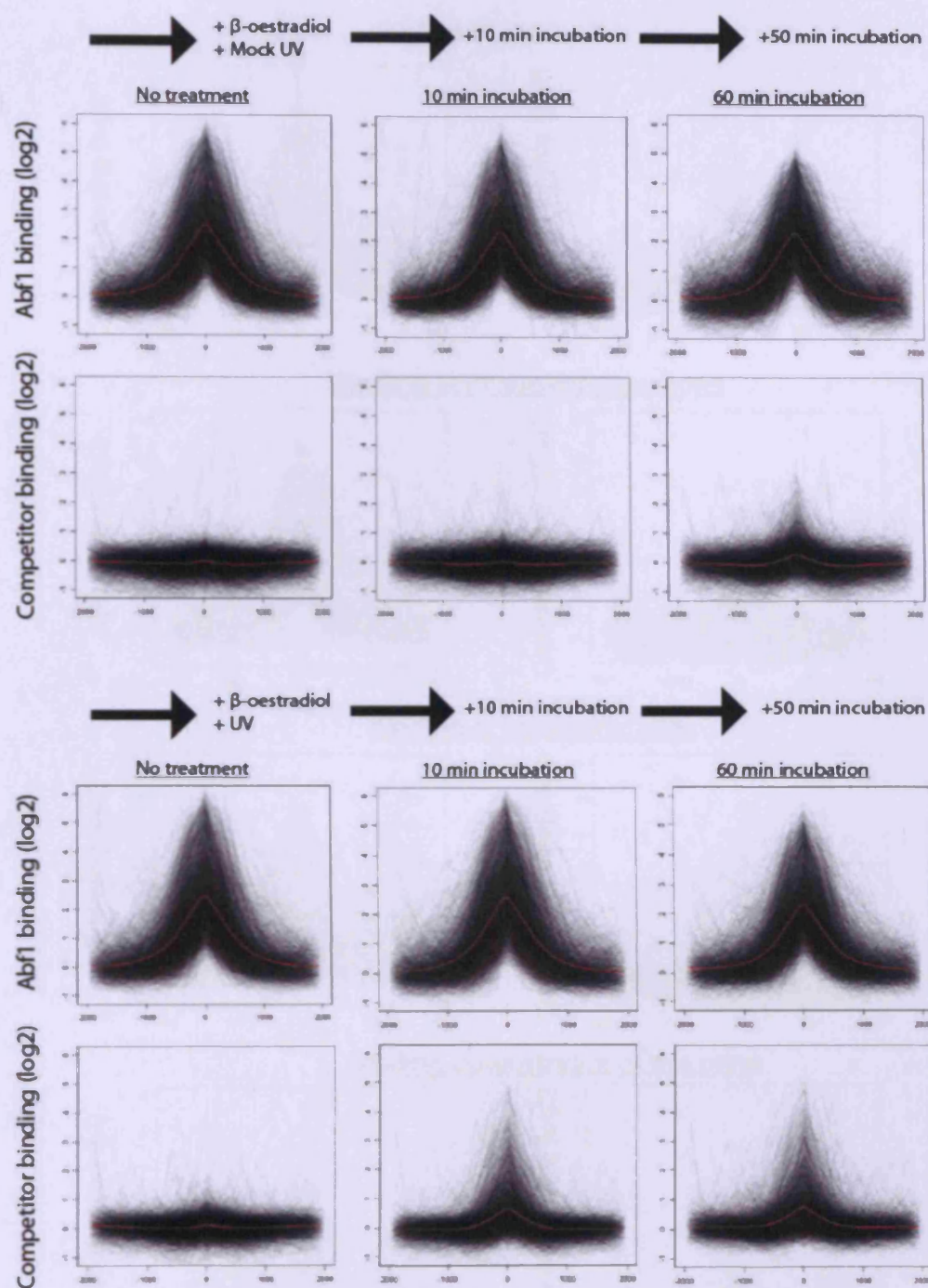


Figure 6.7. Composite profile centred at all Abf1 binding peaks defined in the unirradiated condition (Chapter 3). All x-axes represent distance from an Abf1 binding peak (nucleotides). Above 6 plots represent data taken in the absence of UV irradiation. Blow 6 plots represent data taken in the presence of UV irradiation. Experiments were performed in BY4742.

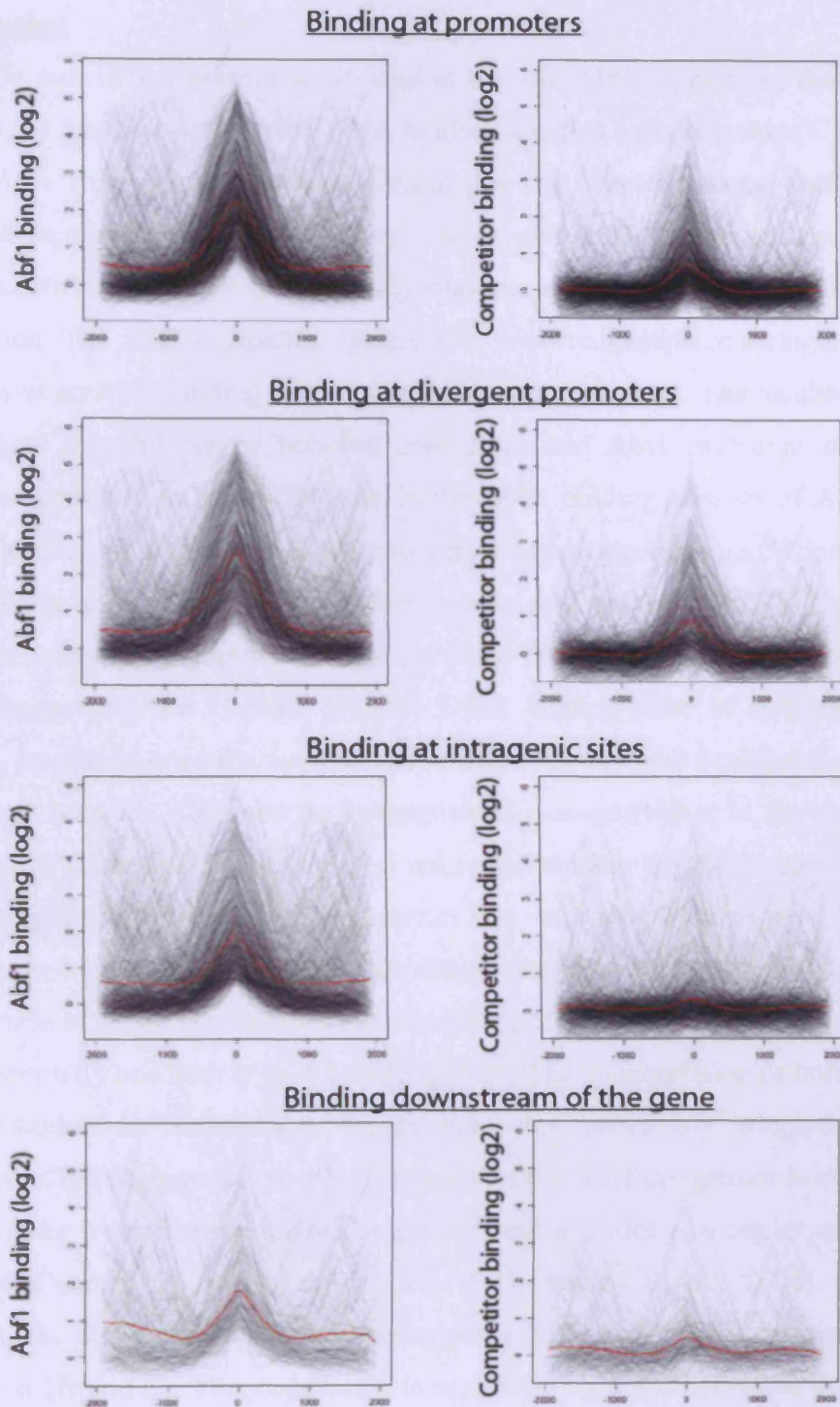


Figure 6.8. Binding of Abf1 (from the U dataset) was plotted using composite profiles, and split according to the genomic location of the Abf1 binding site (left hand graphs). Binding of the competitor in the presence of UV damage, 10 minutes after addition of β -oestradiol was plotted in the same manner (right hand graphs). All x-axes represent distance from an Abf1 binding peak (nucleotides). All Abf1 binding peak positions were derived from classifications determined in Chapter 3.

6.4 Discussion

The aim of the present study was to use the Abf1 competitor developed in Chapter 5 for the analysis of Abf1 DNA binding kinetics by competitive ChIP before and after UV. The preliminary results presented in this chapter indicate that there may exist a link between Abf1 DNA binding kinetics and GGR. However at present, the Abf1 competitors designed in this study may require further optimisation for this investigation. The Abf1 competitor is only able to partially replace endogenous Abf1 occupancy at an Abf1 binding site, this holds true genome-wide. The results presented here suggest that differences between competitor and Abf1 exchange at two loci might not accurately reflect differences in the DNA binding kinetics of Abf1, if the extent of exchange is different at the two sites when at equilibrium. When the Abf1 competition reaction is performed in the absence and presence of UV damage, the competitor is found to rapidly occupy an Abf1 DBS only in the presence of UV damage, suggesting the kinetics of Abf1 DNA binding alter in response to UV. However, it appears once the competition reaction has reached equilibrium, the level of exchange between Abf1 and the competitor is non-equivalent in the absence and presence of UV damage. Therefore, it is unknown whether the differences accurately reflect changes in Abf1 DNA binding kinetics as a result of UV damage.

At the locus *NAT4*, when the competition reaction is activated with the optimal concentration of 20 μ M β -oestradiol the occupancy of the competitor and Abf1 reaches an equilibrium by one hour (Fig. 6.1 and Fig. 6.2). The concentration of hormone used in these studies is considerably higher than that previously adopted for Gal4 competitive ChIP, however it should be noted that the Abf1 competitor is expressed at a much higher level than the Gal4 competitor, and includes two copies of the ER α -LBD (see Chapter 5.3, Mumberg et al., 1995; Nalley et al., 2006). Following activation, the competitor successfully competes with Abf1 for binding at *NAT4* in vivo (Fig. 6.2B and C). This conclusion is supported by the observation that addition of β -oestradiol in the absence of a competitor does not result in a loss of occupancy of Abf1 at *NAT4* (Fig. 6.2A). In the absence of a competitor, addition of β -oestradiol appears to have little effect upon the level of Abf1 binding. This is in contrast to a recent report which demonstrated that the levels of Gal4 binding at the GAL1/10 promoter significantly increase in response to addition of the hormone; this has complicated the interpretations of data using the Gal4 competitor (Collins et al., 2009). The exchange of Abf1 and the competitor one hour after hormone activation

suggests that Abf1 does not stably occupy this locus in vivo with a half life in the range of hours. Although the data is limited, this conclusion appears to be true for a large number of Abf1 binding sites (Fig. 6.3 and 6.7). Interestingly, at both *NAT4* and *prSRB2* the competition reaction completes within ~20 minutes (Fig. 6.4). It was previously shown for both the Gal4 and HIF1 α competitor that in the absence of the endogenous protein, the competitor required ~20 minutes for full occupancy at a locus in vivo (Nalley et al., 2006; Yu and Kodadek, 2007). When Abf1 binding at *NAT4* is diminished using the *abf1-1* temperature sensitive mutant, the competition reaction similarly requires ≥ 20 minutes for full activation (Fig. 6.4A). Therefore, as previously observed for other competitors, the rate of association on chromatin for the Abf1 competitor is limited within this time period, and this could be due to a factor other than Abf1 binding kinetics. Because all three competitors (Abf1, Gal4, HIF1 α) have been shown to be limited in this manner, the mechanism is likely to be the same for all. This could include the rate of hormone diffusion through the cell, the association rate of hormone-LBD complexes or the dissociation rate of LBD-Hsp90 complexes. However, because Abf1 appears to play fundamental roles in the structure of chromatin, the 'slow' activation of the competitor for the results presented in this study could also be due to a fundamental difference in chromatin structure in the *abf1-1* mutant (see Chapter 1.5, Lee et al., 2007b; Yarragudi and Morse, 2006). These data suggest that at *NAT4* and *prSRB2* the kinetics of Abf1 DNA binding are rapid such that the association rate of the competitor is not restricted by this parameter. This suggests that Abf1 binds at these sites with a short half-life ($t_{1/2} \leq \sim 5$ mins). It is noted that the confidence of these conclusions is very much limited due to the inefficiency of the competition reaction.

At present, the exchange between Abf1 and the competitor is only partial when the reaction is at equilibrium, and at the majority of Abf1 binding sites very little exchange between the two proteins is observed (Fig. 6.2, 6.3, 6.6, 6.7). These observations may not be entirely due to stable binding of Abf1 inhibiting the competitor from binding at DBSs since neither diminishing the occupancy of Abf1 with *abf1-1*, nor allowing the competition reaction to proceed for long periods of time permit high level competitor binding (Fig. 6.2, 6.3, 6.4, 6.6, 6.7). This suggests that the competitor is unable to efficiently bind DNA in vivo, or it is expressed at levels far lower than endogenous Abf1. The latter proposition was investigated and the protein level of the competitor was demonstrated to be ~4 fold higher than the Abf1

protein level (Fig. 6.5). Therefore theoretically if the competitor was equally efficient at binding DNA in vivo, at equilibrium with Abf1 this should occupy ~80% of an Abf1 DBS. This strongly suggests that the competitor cannot efficiently bind DNA in vivo. How might the competitor be restricted in this function? Previous studies have suggested that the AD of a TF functions to stabilise the DNA binding kinetics of a protein in vivo, which can influence the level of protein binding (see Chapter 1.6, Ferdous et al., 2007; Klok et al., 2007; Nalley et al., 2006; Reid et al., 2003; Stavreva et al., 2004; Yu and Kodadek, 2007). However, neither the VP16 AD, Rap1 AD nor the Abf1 AD was observed to improve the efficiency of the competitor to bind DNA in vivo (Fig. 6.2, 6.6). The inclusion of the Abf1 AD (aa 531-680) to the competitor incorporates both the CS1 and CS2 domains of Abf1, known to be important for the protein's function in vivo (Li et al., 1998; Miyake et al., 2002). It was previously shown that cells expressing Abf1 aa1-662 have a growth phenotype indistinguishable from those expressing full length Abf1 (Miyake et al., 2002). The ability of Abf1 to bind DNA in vivo is essential for robust cell growth, strongly suggesting that Abf1 aa1-662 contains all the amino acids necessary for efficient DNA binding in vivo (Rhode et al., 1992). Therefore the inability of the competitor with the Abf1 DBD (aa1-530) and Abf1 AD (aa 530-680) to efficiently bind DNA in vivo suggests that the two ER α LBDs present within this recombinant protein restrict this activity, even in the presence of β -oestradiol. This observation was also proposed in the previous chapter (see Chapter 5.4 for discussion), where it was shown that the addition of a second ER α LBD N-terminal to the Abf1 DBD significantly reduced the capacity of the competitor to occupy an Abf1 DBS in vivo (Fig. 5.11 and 5.12). Given these considerations, the Abf1 competitor with a single ER α LBD (C-terminal to the Abf1 DBD) was tested using the optimal β -oestradiol concentration established in this chapter, however, this competitor was equally inefficient at competing for Abf1 occupancy at *prSRB2* (Fig. 6.6). This likely reflects the fact that this protein is expressed at a much lower level than the other competitors used in the current study, since high level expression of this competitor is lethal (Chapter 5.3).

The experiment designed in Fig. 6.4 investigated whether Abf1 DNA binding kinetics could be compared between different Abf1 binding sites using an incomplete competition reaction. The data demonstrated that the different levels of exchange between Abf1 and the competitor may not be entirely due to differences in the kinetics of Abf1 DNA binding at the different sites. In this example it was suggested

that the affinity of the competitor for a DNA binding site, relative to Abf1, may influence the level of exchange between the two proteins (Fig. 6.4). Therefore, Abf1 DNA binding kinetics at two DBSs may only be comparable if the level of exchange between Abf1 and the competitor is equivalent when the competition reaction is in equilibrium (see Fig. 6.8 for graphical explanation). Practically, this is best achieved by expressing a competitor that functions to replace the occupancy of Abf1 at all DBSs (>90%). In this circumstance, the time taken to reach this equilibrium provides a qualitative measurement of Abf1 DNA binding kinetics.

Despite the partial exchange between the competitor and Abf1 at equilibrium, some preliminary experiments were performed to examine if changes in Abf1 DNA binding kinetics may be mechanistically coupled to GGR. In the presence of UV irradiation, higher levels of competitor binding are observed 10 minutes after activation of the competition reaction, than seen in the absence of UV damage. This could suggest that there is a change in the binding kinetics of Abf1 in the presence of UV damage. For four loci tested, the data suggested that by one hour the competition reaction was in equilibrium in the absence of UV (Fig. 6.2 and 6.3). Therefore, this suggests that for many of the Abf1 DBS, the competition reaction may be at equilibrium one hour following hormonal activation. Given that binding of the competitor is not equivalent by one hour in the presence and absence of UV, an alternative interpretation of the data is that the affinity of the competitor for Abf1 binding sites, relative to Abf1 itself, is not equivalent in the absence and presence of UV damage. Therefore, the difference in the competition reaction experiments may be independent of Abf1 DNA binding kinetics (see above, 6.3.3). Consequently, at present the biological interpretation for the differences in competitor binding in the absence and presence of UV damage is unclear. Interestingly, when the competitor binding in the presence of UV damage is organised according to the location of the Abf1 binding site, competitor binding is specifically enriched at promoter regions (Fig. 6.8). This correlates with the preferential location of the GGR complex (Chapter 4) and is where GGR appears to be organised from (Chapter 3), suggesting that the competition phenotype may be linked to the activity of GGR. This clearly warrants further investigation.

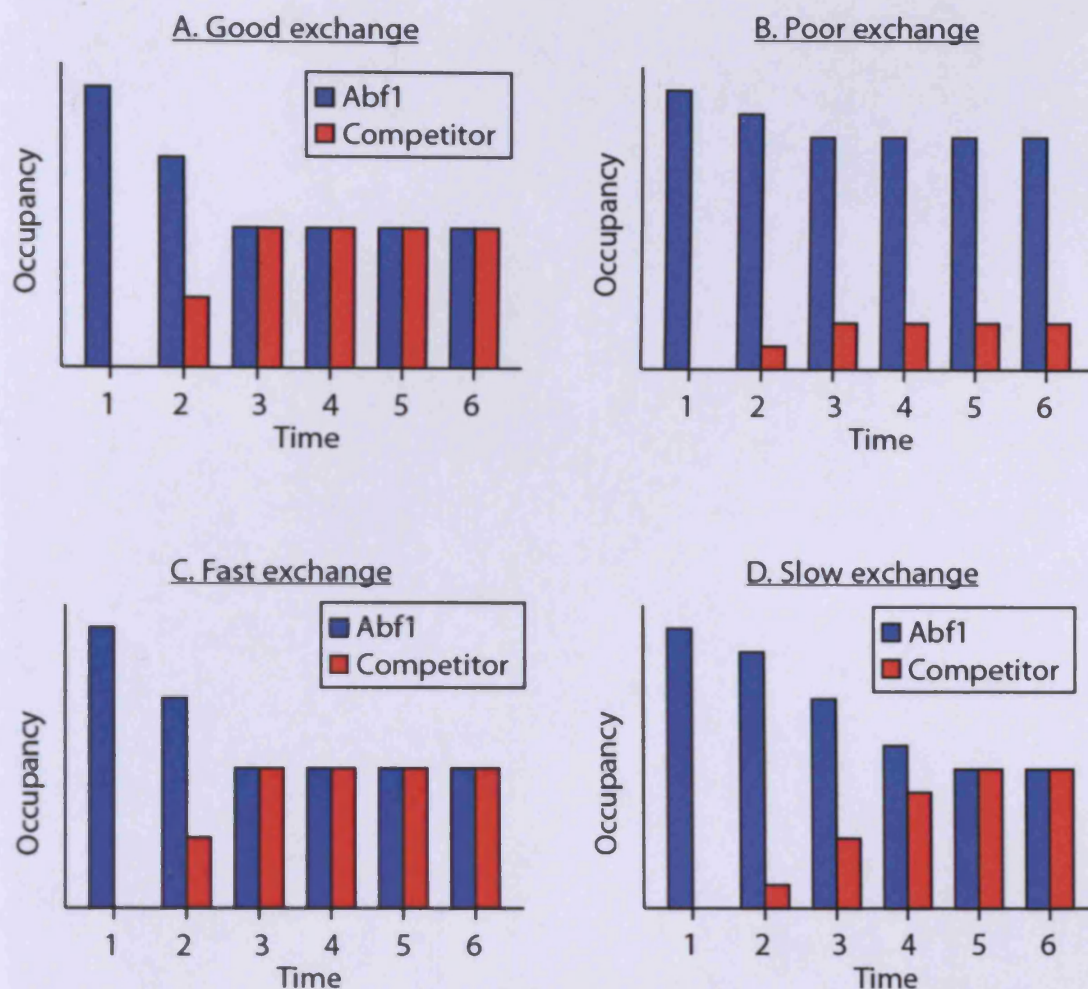


Figure 6.8. Graphical representation of potential caveats when comparing DNA binding kinetics at sites of partial exchange between Abf1 and the competitor. In A, a 50% exchange between Abf1 and the competitor is complete by timepoint 3. In B a 20% exchange between Abf1 and the competitor is complete by timepoint 3. However the dissociation rate of Abf1 is not necessarily faster in A than B since the time taken for the competition reaction to reach equilibrium is the same in both. In D a 50% exchange between Abf1 and the competitor also occurs, but is complete by timepoint 5. A greater confidence in the interpretation of results is provided when comparing the kinetics of C and D. In this example, Abf1 should dissociate faster at C than D since both competition reactions reach an equivalent equilibrium, but C reaches this sooner than D.

7. General conclusions and future experiments

In *S. cerevisiae*, the GGR complex is a heterotrimeric complex of Abf1, Rad7 and Rad16 necessary for UV dependent histone H3 K9K14 hyperacetylation and the efficient repair of UV damage by GGR (Reed et al., 1999; Teng et al., 1997; Teng et al., 2008; Verhage et al., 1994; Yu et al., 2009; Yu et al., 2011). The present study has used the powerful technique of ChIP-on-chip to further characterise both the Abf1 and Rad16 proteins in a genome-wide context in relation to their roles in GGR. The results presented here strongly suggest that GGR is organised by Abf1 binding to domains within the promoter regions of the yeast genome. In addition, a number of characteristics were observed that significantly expand our understanding of how the GGR complex functions in vivo both in the absence and presence of UV damage. In addition to these studies, this investigation reports the development of a novel tool for the analysis of Abf1 DNA binding kinetics in vivo. Preliminary data is reported suggesting that changes in this property might be related to promoting efficient GGR. The work in this study provides numerous avenues for further research, as discussed below.

7.1 Chapter 3. Mapping the genome-wide localisation of Abf1 in the absence and presence of UV damage

The ability of Abf1 to promote GGR correlates with the protein's site specific DNA binding activity (Reed et al., 1999; Yu et al., 2009). In many respects Abf1 is analogous to canonical TFs; it has the ability to both promote and repress transcription and its structure is bipartite, consisting of N-terminal DBDs and a C-terminal AD that has been shown to be functionally redundant with many canonical TFs ADs at an origin of replication (Cho et al., 1995; Li et al., 1998; Marahrens and Stillman, 1992; Miyake et al., 2004). The recent use of ChIP-on-chip for the analysis of genome-wide TF binding has significantly expanded our understanding of how transcription is organised within the cell (Harbison et al., 2004; Lee et al., 2002b). In addition, numerous studies have demonstrated that the DNA binding of many TFs relocates and is thus likely to be regulated in response to environmental stresses such as DNA damage (Harbison et al., 2004; Workman et al., 2006). Therefore, the genome-wide analysis of Abf1 was performed both before and after UV damage to observe whether changes in DNA binding of Abf1 may be related to efficient GGR. A previous study

suggested that the site specific DNA binding activity of Abf1 promotes efficient binding of the GGR complex, and subsequently GGR, at domains within the genome to which the protein binds (Yu et al., 2009). Therefore, both Rad16 dependent histone H3 K9K14 acetylation and GGR were investigated in relation to Abf1 binding.

In Chapter 3, the localisation of Abf1 was observed using ChIP-on-chip both before and after UV irradiation. Abf1 was shown to bind the genome at thousands of sites, and is preferentially localised to promoter regions of the genome. Whilst ~3500 statistically significant ($P < 0.05$) binding peaks were identified, this study suggests that Abf1 binding is localised to the vast majority of promoter regions in the genome, many of which occur at a low level that is not statistically significant. In response to UV, Abf1 was not observed to relocate, although the occupancy of Abf1 binding was observed to fall at a proportion of binding sites. This demonstrates that the GGR complex is not recruited to novel Abf1 binding sites in response to UV damage. This suggested that the GGR complex binds chromatin in the absence of UV damage, which was subsequently demonstrated in the proceeding chapter. Although the loss of Abf1 occupancy at binding sites correlates with the onset of DNA repair, correlations between the level of Abf1 binding (or UV dependent changes) and CPD repair were not observed. Difficulties in correlating TF binding to gene expression studies have also been reported, and in these circumstances numerous potential caveats could preclude identifying correlations, these include; temporal fluctuations in TF occupancy (Karpova et al., 2008; Metivier et al., 2003; Ni et al., 2009), combinatorial regulation by numerous TFs (Harbison et al., 2004; Tan et al., 2008; Wang et al., 2009), positive and negative regulatory activities elicited by the same TF (Ni et al., 2009; Tan et al., 2008) and indirect regulation (Workman et al., 2006). Numerous factors may similarly preclude direct correlations between the level of Abf1 DNA binding and CPD repair despite the fact that Abf1 binding promotes CPD repair (Reed et al., 1999). Firstly, ChIP-on-chip will detect a heterogeneous pool of Abf1, a large proportion of which will not be in complex with Rad7/Rad16 (Reed et al., 1999). Secondly, Abf1 may not promote binding of Rad16 to all sites of the genome with which it binds itself. Thirdly, Abf1 may not promote CPD repair directly at the binding site but instead at a domain proximal to the binding site. Fourthly, a stronger correlation may exist with Abf1 DNA binding kinetics rather than the protein binding level. These parameters may similarly preclude the observation of correlations between the level of Abf1 binding and histone acetylation. It was also noted that the

TCR rate is likely to predominate the ultimate CPD repair rate at genic regions since TCR is known to repair CPDs at a faster rate than GGR (Mellon et al., 1987). This could function to mask a correlation between the level of Abf1 binding and GGR rates. It would therefore be of great interest to experimentally determine the genome-wide repair rates of GGR in the absence of TCR using a *rad26 Δ rpb9 Δ* double mutant (Li et al., 2006b; Li and Smerdon, 2004).

It is also worth noting that Abf1 DNA binding is known to mediate both transcription and DNA replication, the activities of which are regulated in response to UV damage (Friedberg, 2006; Rhode et al., 1992). It is likely therefore, that some of the changes in Abf1 DNA binding observed in response to UV, could reflect the role of Abf1 in pathways other than GGR. Functionally separating DNA repair from other DNA damage responses is difficult as often such pathways are regulated by DNA repair factors. It would be interesting to observe what changes, if any, occur for Abf1 DNA binding in response to UV in the *rad16 Δ* mutant. It has previously been shown that Rad7/Rad16 proteins are not required for the UV dependent activation of G1 and G2 checkpoint responses, although both proteins have been implicated in UV dependent de novo protein synthesis (Giannattasio et al., 2004; Gillette et al., 2006). Therefore, a proportion of the UV DNA damage response should proceed in the absence of Rad16.

When analysed in relation to Abf1 binding, the distribution of Rad16 dependent histone H3 K9K14 acetylation is organised at Abf1 binding sites in promoters. Rad16 is observed to have a global role in promoting acetylation at promoters, and this is observed both in the presence and absence of UV damage. Therefore, Rad16 is important for regulating histone H3 K9K14 acetylation in the absence of UV damage, as well as in response to UV, as previously reported (Yu et al., 2005). This was interpreted to suggest that the activities of Rad16 necessary for histone acetylation are upregulated, rather than activated, in response to UV. In addition to Rad16 dependent acetylation, efficient Rad16 dependent GGR also correlates with Abf1 binding sites in promoter regions. This suggests that Abf1 binding targets the GGR complex to promoter regions, thus organising GGR at these sites. Further investigation of this hypothesis should be performed by genome-wide analysis of both acetylation and CPD repair in the absence of Abf1 binding. Given that Abf1 is an essential gene, this would best be achieved using the *abf1-1* temperature sensitive DNA binding mutant, and repeating the genome-wide

acetylation and CPD repair datasets using this strain (Rhode et al., 1992). An alternative strategy would be to degrade Abf1 in a temperature sensitive manner, using the N-degron strategy previously described (Reed et al., 1999). One difficulty with this experiment is that the degradation of Abf1 also significantly reduces the stability of Rad7 and Rad16 (Reed et al., 1999), therefore these proteins would have to be artificially overexpressed to maintain wild type levels.

7.2 Chapter 4. Mapping the genome-wide localisation of Rad16 in the absence and presence of UV damage

Rad16 is known to possess both an ATPase activity necessary for DNA translocation, and a RING domain which functions with Rad7, Elc1 and Cul3 as an E3 ubiquitin ligase (Gillette et al., 2006; Ramsey et al., 2004; Yu et al., 2009). Both of these activities are necessary for GGR (Ramsey et al., 2004; Yu et al., 2011). In addition, both activities have also been shown to be important for UV dependent increases in both Gcn5 occupancy and histone K9K14 acetylation, which promotes chromatin remodelling necessary for efficient GGR (see Chapter 4.1, Yu et al., 2011). The results from chapter 3 suggested that Abf1 binding functioned to organise these Rad16 dependent activities and subsequently acetylation and GGR at the promoter regions of the yeast genome. It was suggested that the GGR complex was likely to bind chromatin in the absence of UV damage, and that Rad16 functioned in a similar manner both before and after UV to promote histone acetylation, however this is upregulated in response to UV damage. These conclusions were further investigated by analysing the genome-wide distribution of Rad16.

In Chapter 4, the localisation of Rad16 was observed using ChIP-on-chip both before and after UV irradiation. Rad16 was demonstrated to interact with chromatin throughout the entire genome both before and after UV irradiation. These observations correlate with the ability of the protein to regulate the distribution of histone H3 K9K14 from Abf1 binding sites at promoters throughout the entire genome both before and after UV irradiation (Chapter 3). Although Rad16 associates with chromatin genome-wide, peaks of Rad16 binding were observed in unirradiated cells. These were predominantly localised to Abf1 binding sites situated within promoter regions, suggesting that, as previously shown in vitro, Abf1 DNA binding promotes binding of the GGR complex to domains in vivo (Yu et al., 2009). These observations strongly support a model where Abf1 binding targets efficient binding of

the GGR complex to promoter regions thus organising the GGR response from these sites.

In response to UV irradiation, peaks of Rad16 at Abf1 binding sites are lost, resulting in a more uniform distribution of Rad16 throughout the genome. These observations are in strong support of a model in which Rad16 DNA translocation is upregulated from Abf1 binding sites in response to UV. This activity is hypothesised to promote histone hyperacetylation and chromatin remodelling necessary for efficient GGR. A critical experiment to test this hypothesis would be to repeat the Rad16 ChIP-on-chip datasets using a strain expressing ATPase mutated Rad16 (Ramsey et al., 2004; Yu et al., 2011). As observed for many Snf2 family proteins, ATP hydrolysis by Rad16 is necessary for DNA translocation (Flaus et al., 2006; Yu et al., 2009). A previous study demonstrated that a K216A mutation within the walker A domain of Rad16 functions to inhibit the ATPase activity (Ramsey et al., 2004). This mutant was also shown to have a defective GGR capacity and lower UV survival than wild type cells (Yu et al., 2011). Therefore, the UV dependent change in localisation of K216A mutated Rad16 should be determined using ChIP-on-chip. It would also be of interest to examine if the E3 ligase activity of Rad16 mediates the genome-wide localisation of this protein. Similar experiments could therefore be performed using the RING mutated Rad16 protein (C552A,H554A); cells expressing this are also known to have a defective GGR capacity and reduced UV survival (Yu et al., 2011).

At sites where Abf1 and Rad16 binding peaks were found to colocalise, it was observed that the UV dependent changes in Abf1 binding do not correlate with changes in Rad16 binding. This suggests that Abf1 and Rad16 might not remain in complex after UV irradiation. However, because Abf1 is highly abundant within the cell, a large proportion (~70%) of the protein is not found in complex with Rad7/Rad16 (Reed et al., 1999). Therefore a correlation between Abf1 binding and Rad16 binding in response to UV may be masked by the predominant fraction of Abf1 that functions independently of Rad16. A facile method for testing if Abf1 and Rad16 are not in complex after UV would be to co-immunoprecipitate the proteins from protein extracts before and after UV. This experiment was attempted using antibodies against Rad7 and Abf1 however conditions which successfully co-immunoprecipitated the two proteins were not established. An alternative method could be to biochemically purify the GGR complex using His-tagged Rad7 (as originally described (Reed et al., 1999)) in the absence and presence of damage using

a UV mimetic such as 4-nitroquinoline 1-oxide. However, the best strategy for this experiment would probably be to use ChIP-western, in which chromatin WCE is prepared for standard ChIP (see Chapter 2.7), chromatin is immunoprecipitated, crosslinking is reversed and co-immunoprecipitated proteins are analysed by western blotting (Fousteri et al., 2006b). This strategy has the added advantages that chemical crosslinking can capture transient protein-protein interactions, and that the strategy is limited to chromatin bound proteins. The latter advantage is especially useful as Rad16 was suggested to dissociate from Abf1 upon chromatin binding. This was based upon the observation that peaks of Rad16 binding were not exclusively found to colocalise with Abf1 binding peaks prior to UV irradiation. Both before and after UV irradiation, dissociation of Rad16 from Abf1 is suggested to occur by the translocation activity of Rad16. However, the E3 ligase activity of Rad16 may also contribute to this transition. Therefore, depending on the results of the former experiment, it would be of interest to see how mutating either the RING or ATPase domains of Rad16 could modulate an interaction with Abf1 on chromatin.

Regions of the genome in which peaks of Abf1 and Rad16 binding colocalise in the absence of UV damage have significantly slower GGR rates than those bound by Abf1 alone. When these observations were further investigated at promoter regions where Abf1 and Rad16 binding peaks colocalise, an inverse relationship was found between the level of Rad16 binding and the level of Rad16 dependent acetylation in the absence of UV damage. Abf1 binding sites at promoters with low level Rad16 binding peaks, or absent of a Rad16 binding peak, are suggested to represent regions of the genome where there is high level Rad16 DNA translocation activity, which would promote binding of HATs such as Gcn5 and subsequently histone H3 K9K14 hyperacetylation. This hypothesis is based upon the recent observation that the ATPase activity of Rad16 is important for UV dependent increases in Gcn5 occupancy and histone H3 K9K14 acetylation at the *MFA2* locus (Yu et al., 2011). Gcn5 has previously been demonstrated to promote GGR in yeast (Teng et al., 2002; Yu et al., 2005). It has also recently been shown to promote CPD repair in human cells (Guo et al., 2010a; Guo et al., 2010b). Thus, performing Gcn5 ChIP-on-chip would provide further evidence to establish the link between Rad16 binding and acetylation genome-wide. It would also be of great interest to examine the levels of ATPase mutated Rad16 binding in the absence of UV damage to see if the binding levels are considerably higher than the wild type protein. This would strongly suggest

that DNA translocation by Rad16 functions to reduce the binding peak levels. The difference in Rad16 binding levels between wild type and ATPase mutated Rad16 may also indicate the level of DNA translocase activity, which could be correlated to Rad16 dependent acetylation (and Gcn5 occupancy).

ChIP-on-chip of histone H3 K9K14 acetylation (/Gcn5 occupancy) could also be performed in the Rad16 ATPase mutant to investigate how the distribution of Rad16 dependent histone H3 K9K14 acetylation is related to the translocase activity. However, it should be noted that it was previously observed that mutation of either the RING domain or the ATPase domain of Rad16 alone does not inhibit UV dependent increases in Gcn5 occupancy and histone H3 K9K14 acetylation at *MFA2*, whilst mutation of both does (Yu et al., 2011). Therefore, ChIP-on-chip investigations with either the E3 ligase or ATPase mutated Rad16 alone may not demonstrate differences in the occupancy of Gcn5 and histone hyperacetylation. The double mutant might be expected to provide identical results to a *rad16Δ* mutant since it possesses a similar repair defect and UV sensitivity (Yu et al., 2011). The necessity to disable both catalytic activities of Rad16 to inhibit this phenotype suggests that other factors within the cell may functionally substitute for the catalytic activities of Rad16. With respect to the ATPase activity of Rad16, this may have a functional redundancy with other Snf2 family proteins already implicated in NER such as SWI/SNF or the Ino80 complex (Gong et al., 2006; Jiang et al., 2010; Sarkar et al., 2010; Zhao et al., 2009). This in itself is also an interesting topic of research.

Based upon observations in Chapter 3, the mechanism through which Rad16 functions to promote acetylation is suggested to be the same both before and after UV irradiation. In support of this, the same inverse relationship between Rad16 binding and histone acetylation is observed both before and after UV. A strong correlation between the level of histone H3 K9K14 acetylation and CPD repair was observed at Abf1 binding sites in promoters, but not at regions distal to this. This is expected to occur because these regions are mostly genic and TCR is suggested not to be promoted by histone H3 K9K14 acetylation. Therefore, it would be interesting to correlate histone H3 K9K14 acetylation levels to the genome-wide dataset of GGR using the *rad26Arpb9Δ* double mutant (Li et al., 2006b; Li and Smerdon, 2004). Finally, it was suggested that Rad16 promoted an activity necessary for GGR independent of histone H3 K9K14 hyperacetylation (see Chapter 4.1). It would be interesting to identify and characterise further this activity. This might be achieved

using a strain which expresses histone H3 mutated at K9K14 to eliminate post-translational modifications at these sites. Such strains are viable (Jin et al., 2009). This would be predicted to inhibit Rad16 dependent acetylation events that promote GGR. In the absence of this activity, it would then be of interest to see how both the ATPase and RING domains of Rad16 contribute to UV dependent chromatin remodelling and functional GGR.

The genome-wide datasets presented in this study, in combination with future ChIP-on-chip studies such as those discussed above, provide a platform for systems biology based approaches to investigate NER at a global level. In addition to these studies, it is important to appreciate that statistical packages must also be developed for the analysis of these datasets. The current study employed a statistical strategy for the identification of peaks in both the Abf1 and Rad16 datasets (Chapters 3 and 4). Multiple strategies for this type of statistical analysis have been published (Buck et al., 2005; Glynn et al., 2004). However at present numerous conclusions drawn in this study lack statistical inference. These include the low level binding of Abf1 observed at numerous promoter regions (Fig. 3.6), the differences in acetylation patterns observed between wild type and *Δrad16* cells (Fig. 3.10) and the colocalisation of Abf1 and Rad16 binding peaks (Fig. 4.3). Therefore, in future it will be necessary to develop tools for the statistical analysis of these relationships. Previous studies have used statistical strategies for the analysis of protein colocalisation between multiple ChIP-on-chip datasets (Schlecht et al., 2008; Workman et al., 2006). A means to evaluate the statistical significance of the CPD repair rate is also necessary. This will be of paramount importance when comparing repair profiles between different datasets (for example between the wild type and *Δrad16* datasets).

Ultimately, the development of statistical packages as well as other advanced bioinformatic tools will be utilised to incorporate these multiple ChIP-on-chip datasets into networks. The aim of such networks would be to accurately define the functional components that mediate the heterogeneous DNA repair rate in vivo. These advanced strategies are still in their infancy but techniques such as Bayesian network inference are beginning to be employed to produce detailed maps of targeting/functional protein interactions and ultimately how these function to influence transcriptional output (Beyer et al., 2006; van Steensel et al., 2010).

7.3 Chapter 5. Developing tools for the in vivo analysis of Abf1 DNA binding kinetics

Recent studies have suggested that there exists an intimate link between transcriptional regulation and the DNA binding kinetics of TFs (Brady et al., 2005; Klok et al., 2007; Nalley et al., 2006; Reid et al., 2003; Stavreva et al., 2004; Yang et al., 2002a; Yao et al., 2006). These data complement the observations that the cell appears to possess a variety of strategies which can regulate the half-life of TF:DBS interactions (Ferdous et al., 2007; Freeman and Yamamoto, 2002; Yu and Kodadek, 2007). The analysis of DNA binding kinetics provides a more powerful interpretation of steady state binding datasets using studies such as ChIP (Hager et al., 2009; Karpova et al., 2008). Given that Abf1 shares many structural and functional properties with canonical TFs, I wished to investigate if changes in Abf1 DNA binding kinetics were mechanistically coupled to the protein's role in GGR. The study of Abf1 DNA binding kinetics was considered a complementary study to the steady state binding of Abf1 (in Chapter 3) to provide a more powerful appreciation of both how and where Abf1 DNA binding promotes efficient GGR.

In Chapter 5, a tool termed the competitor, previously used for the analysis of Gal4 and HIF-1 α , was adapted for the study of Abf1 DNA binding kinetics (Nalley et al., 2006; Yu and Kodadek, 2007). The competitor is an abundant site specific DNA binding recombinant protein that replaces the occupancy of an endogenous protein at a DBS in response to hormonal activation. Because the competitor can only bind at a DBS when the endogenous protein has dissociated from this site, the rate at which the competitor replaces the occupancy of the endogenous protein, as measured by ChIP, is a qualitative measurement of the rate of dissociation of the endogenous protein from the DBS (Yu and Kodadek, 2007).

Abf1 is considered to have two DBDs both of which are necessary for site specific DNA binding; an atypical zinc finger situated between aa40-91 and a putative helix-turn-helix (HtH) motif situated between aa323-496 (Cho et al., 1995; Miyake et al., 2002; Yarragudi and Morse, 2006). Consequently, the original Abf1 competitor design included a DBD of Abf1 aa19-523. This was subsequently demonstrated to be unable to bind at an Abf1 DBS in vivo. However, when the competitor DBD was changed to aa1-530, the protein acquired a site specific DNA binding capacity in vivo. When Abf1 was aligned with two known homologues in *K. marxianus* and *K. lactis*, two regions of homology were found between these proteins that approximately map

to the DBDs of Abf1. Given these results, it is suggested that the zinc finger domain of Abf1, necessary for site specific DNA binding is found within a domain aa6-81.

When the ER α LBD was fused C-terminally to the Abf1 DBD (aa1-530), the protein was demonstrated not to be under strict hormonal control. This is believed to be related to the size of the Abf1 DBD (see below). Indirect evidence was also provided to suggest that an N-terminal fusion is equally unable to strictly regulate the Abf1 DBD. Interestingly, when these competitors are expressed under the powerful *TDH3* promoter a significant inhibition of cell growth and survival is observed. This phenotype requires the competitor to have a DNA binding capacity. This strongly suggests that DNA binding by the competitor at Abf1 DBSs inhibits cell growth and survival. This observation correlates with the observations that overexpression of Abf1, or expressing C-terminal truncated Abf1 is lethal (Miyake et al., 2002; Sopko et al., 2006). However, when the competitor was expressed from the weaker *TEF2* or *ADH1* promoters cell growth and survival were not inhibited suggesting that the protein level of the competitor was insufficient to effectively compete with endogenous Abf1 binding for a DBS.

To suppress the lethality of overexpressing the Abf1 competitor with a single ER α LBD, a second ER α LBD was added to the construct in an attempt to tighten the hormonal regulation of the competitor. This strategy successfully placed DNA binding of the Abf1 competitor under strict hormonal regulation, however the addition of a second ER α LBD was observed to restrict the ability of the competitor to bind at a DBS in the presence of β -oestradiol.

7.4 Chapter 6. Investigating Abf1 DNA binding kinetics using Abf1 competitive ChIP

In chapter 6, the tools created in chapter 5 were used to perform Abf1 competitive ChIP for the analysis of Abf1 DNA binding kinetics in vivo. At numerous loci including *NAT4*, *HML α* and *SRB2* the competitor was demonstrated to replace occupancy of endogenous Abf1 within one hour. This suggests that Abf1 does not possess a half-life on chromatin in the range of hours. Interestingly, as observed for both the Gal4 and HIF1 α competitors, the Abf1 competition reaction appeared to require ~20 minutes for full activation (Nalley et al., 2006; Yu and Kodadek, 2007). For both *NAT4* and *SRB2* it was shown that the competition reaction had reached equilibrium within this timeframe suggesting that Abf1 interacts with a DBS in these

regions with rapid kinetics (half-life ≤ 5 minutes). However, at all loci tested the competitor was not observed to replace the occupancy of Abf1 when the competition reaction had reached equilibrium, potentially compromising the confidence of the interpretation of these results.

One of the primary difficulties identified in this study in interpreting data for competitive ChIP is when the exchange for the endogenous protein by the competitor is incomplete at equilibrium. If this occurs, then the loss of Abf1 binding from the DBS during the competition reaction is not irreversible. In this circumstance, the rate and level of exchange between Abf1 and the competitor is influenced by the association rate of Abf1. Therefore, the assay does not exclusively measure the dissociation rate of Abf1, complicating data interpretation. This potential caveat has previously been identified (Yu and Kodadek, 2007). Using *NAT4* and *SRB2* as a model it was shown that in the absence of Abf1 binding the relative affinity of the competitor appeared higher for *NAT4* than *SRB2*. Because of this, it was suggested that at these loci, that the differences in the relative exchange between the competitor and Abf1 may occur in a manner independent to Abf1 DNA binding kinetics.

How might the efficiency of the Abf1 competition reaction be improved? In Chapter 5, strong indirect evidence was provided that a competitor with a single ER α LBD, expressed under the *TDH3* promoter, could effectively compete for occupancy at an Abf1 DBS. However, expression of the reagent was lethal to the cell. This was suggested to be a result of the fact that the competitor was not under strict hormonal regulation. Whilst adding a second ER α LBD to the competitor functions to suppress the lethality of expressing the competitor from the *TDH3* promoter, the results in Chapter 6 suggest that this also functions to significantly restrict DNA binding by the Abf1 DBD. These data suggest that an optimal competitor would be expressed under the *TDH3* promoter with a single C-terminal HBD that can strictly regulate DNA binding of the competitor. One method by which the activity of the competitor might be more tightly regulated is through control of the nuclear localisation of the competitor. If in the absence of a hormone the competitor is not nuclear localised then this could not bind DNA. Whilst HBDs are not generally considered to regulate nuclear localisation, the GR has previously been demonstrated to regulate the localisation of the TF E1A (Picard et al., 1990; Picard et al., 1988). Therefore, switching the ER α LBD for the GR LBD may tighten the regulation of the competitor. It has also been suggested that the distance between the HBD and the regulatory target

of the fusion protein can significantly influence the efficiency of hormone regulation (Nichols et al., 1997; Picard, 1999; Picard et al., 1988). This is of interest because the Abf1 DBD is very large, and therefore the distance between the ER α LBD and its regulatory targets is also large. Therefore, minimising the size of the Abf1 DBD may improve the regulation by a single ER α LBD. One strategy to reduce the size of the Abf1 DBD, may be to delete sequences found between the N-terminal zinc finger and the central putative HtH domain (Chapter 5). Indeed, it has previously been shown that deleting aa200-265 (which lies between these domains) of Abf1 does not inhibit DNA binding in vitro (Cho et al., 1995). An alternative strategy may also be to swap the Abf1 DBD for a homologous sequence from either the Abf1 protein homologue of *Kluyveromyces marxianus* or *Kluyveromyces lactis* (Goncalves et al., 1992; Obery et al., 1993). As demonstrated in Chapter 5, both of these proteins have regions of high homology at the zinc finger and putative HtH domain of Abf1. Both of these proteins may also functionally substitute for the essential functions of Abf1 in *S. cerevisiae* and therefore must bind Abf1 DBSs in vivo (Goncalves et al., 1992; Obery et al., 1993; Rhode et al., 1992). Importantly, the protein domain that maps to the Abf1 DBD for either of these homologues is considerably smaller.

Two other parameters may be worth considering to improve the efficiency of the competition reaction. Whilst, a concentration of β -oestradiol above 20 μ M was not observed to significantly improve the competition reaction, this experiment is complicated by the fact that the solubility of β -oestradiol in water is \sim 5.5 μ M (Shareef et al., 2006). Therefore, it is unknown whether the addition of higher concentrations of β -oestradiol actually increases the intracellular concentration of the soluble hormone. An alternative strategy to increase intracellular hormone concentrations would be to genetically cripple ATP binding cassette transporters, which are necessary for the catalytic efflux of toxic compounds in yeast (Paumi et al., 2009). It has previously been shown that mutating the ABC transporter genes *PDR5* and *SNQ2*, can increase intracellular β -oestradiol concentrations by up to \sim 30-fold (Mahe et al., 1996). Finally, further increasing the expression level of the competitor would be expected to improve the efficiency of the competition reaction also, although as discussed in Chapter 6, attempts to express the competitor from a multicopy plasmid were not successful. Expressing a heterologous protein from the *TDH3* promoter on a multicopy plasmid is predicted to increase expression \sim 4 fold relative to expressing it from a centromeric plasmid (Mumberg et al., 1995).

Even in the absence of an optimised protocol, Abf1 competitive ChIP data clearly demonstrated a phenotype when compared in the absence and presence of UV damage. The Abf1 competitor was observed to rapidly bind chromatin at numerous loci in response to UV. This primarily occurred at Abf1 binding sites in promoter regions, which correlates with sites at which GGR appears to be organised from, suggesting that this is somehow mechanistically linked to the process of GGR. Whilst the interpretation of the data is complicated, these observations clearly warrant further investigation. The interpretation of data using the current Abf1 competitive ChIP protocol would be more accurate if the competition reaction is performed at numerous timepoints so that a good approximation of the time taken for the reaction to reach equilibrium can be ascertained. As discussed in Chapter 6, comparing sites where the exchange between Abf1 and the competitor is equivalent is also easier to interpret. Therefore, at present, the genome-wide datasets are most probably best used to identify model genes for further investigation by competitive ChIP.

Appendix I – Liquid and solid media

YPD – 1L

10g Yeast extract

20g Bacto peptone

20g Glucose

Fill to 1L with water. Autoclave at 125°C for 15 minutes.

Synthetic dropout (minimal media) – 1L

6.6g Yeast nitrogen base

20g Glucose

850mg Synthetic complete dropout mix

Fill to 1L with water. Autoclave at 125°C for 15 minutes.

Synthetic complete dropout medium – 36.2g

2g Adenine hemisulphate*

2g Arginine HCl

2g Histidine HCl*

2g Isoleucine

2g Leucine*

2g Lysine HCl*

2g Methionine

3g Phenylalanine

2g Serine

2g Threonine

3g Tryptophan*

2g Tyrosine

1.2g Uracil*

9g Valine

*Appropriate aa were excluded according to selectable marker.

LB Media with ampicillin – 1L

10g Bacto tryptone

5g Bacto yeast extract

5g NaCl

Fill to 1L with water. Autoclave at 125°C for 15 minutes. Allow to cool to 55°C and add ampicillin to a final concentration of 100µg/ml.

YPD/Selective media/LB plates

Media was prepared as above with 2% agar.

PBS

137mM NaCl, 2.7mM KCl, 4.3mM Na₂HPO₄, 1.47mM KH₂PO₄, pH 7.4

Appendix II – Raw data and supplementary information for Chapter 3

ChIP qPCR quantification at HML α (Chapter 3, Fig. 3.7)

Genotype	Timepoint	SQ Mean		IP/input	Normalise to 1	Averaged Dataset	
		Abf IP	Input			Mean	SD
BY4742	NoUV	3.02E-03	9.28E-04	3.25E+00	1.00E+00	1.00E+00	0.00E+00
BY4742	0mins	7.11E-03	1.09E-03	6.51E+00	2.00E+00	1.75E+00	4.78E-01
BY4742	30mins	2.88E-03	1.10E-03	2.61E+00	8.03E-01	9.25E-01	5.15E-01
Repeat 1							
BY4742	NoUV	5.95E-03	1.02E-03	5.82E+00	1.00E+00		
BY4742	0mins	1.06E-02	8.86E-04	1.20E+01	2.05E+00		
BY4742	30mins	5.26E-03	6.06E-04	8.67E+00	1.49E+00		
Repeat 2							
BY4742	NoUV	9.61E-03	1.09E-03	8.80E+00	1.00E+00		
BY4742	0mins	1.43E-02	1.35E-03	1.06E+01	1.20E+00		
BY4742	30mins	5.18E-03	1.22E-03	4.25E+00	4.83E-01		

SD = Standard deviation

Excel files of quantification available on DVD (D:/Chapter 3/Figure 3.7)

ChIP qPCR quantification at NAT4 (Chapter 3, Fig. 3.7)

Genotype	Timepoint	SQ Mean		IP/input	Normalise to 1	Averaged Dataset	
		Abf IP	Input			Mean	SD
BY4742	NoUV	3.28E-02	1.41E-03	2.32E+01	1.00E+00	1.00E+00	0.00E+00
BY4742	0mins	5.05E-02	1.06E-03	4.77E+01	2.05E+00	1.34E+00	6.73E-01
BY4742	30mins	6.22E-02	2.24E-03	2.77E+01	1.19E+00	8.07E-01	3.60E-01
Repeat 1							
BY4742	NoUV	7.31E-02	1.19E-03	6.15E+01	1.00E+00		
BY4742	0mins	1.20E-01	1.53E-03	7.81E+01	1.27E+00		
BY4742	30mins	8.67E-02	1.88E-03	4.60E+01	7.48E-01		
Repeat 2							
BY4742	NoUV	8.50E-02	1.24E-03	6.83E+01	1.00E+00		
BY4742	0mins	1.26E-01	2.59E-03	4.86E+01	7.11E-01		
BY4742	30mins	9.04E-02	2.76E-03	3.28E+01	4.80E-01		

SD = Standard deviation

Excel files of quantification available on DVD (D:/Chapter 3/Figure 3.7)

ChIP qPCR quantification at prRPL24A (Chapter 3, Fig. 3.8)

Genotype	Timepoint	SQ Mean		IP/input	Normalise to 1	Averaged Dataset	
		Abf IP	Input			Mean	SD
BY4742	NoUV	4.14E-03	1.32E-03	3.14E+00	1.00E+00	1.00E+00	0.00E+00
BY4742	0mins	5.17E-03	1.59E-03	3.26E+00	1.04E+00	9.37E-01	2.18E-01
BY4742	30mins	1.62E-03	1.87E-03	8.67E-01	2.76E-01	3.50E-01	2.01E-01
Repeat 1							
BY4742	NoUV	7.59E-03	1.55E-03	4.88E+00	1.00E+00		
BY4742	0mins	6.82E-03	1.29E-03	5.31E+00	1.09E+00		
BY4742	30mins	3.83E-03	1.36E-03	2.82E+00	5.78E-01		
Repeat 2							
BY4742	NoUV	9.04E-03	1.59E-03	5.69E+00	1.00E+00		
BY4742	0mins	9.09E-03	2.32E-03	3.91E+00	6.87E-01		
BY4742	30mins	2.22E-03	1.98E-03	1.12E+00	1.97E-01		

SD = Standard deviation

Excel files of quantification available on DVD (D:/Chapter 3/Figure 3.8)

ChIP qPCR quantification at ARS231 (Chapter 3, Fig. 3.8)

Genotype	Timepoint	SQ Mean		IP/input	Normalise to 1	Averaged Dataset	
		Abf IP	Input			Mean	SD
BY4742	NoUV	2.70E-03	1.43E-03	1.89E+00	1.00E+00	1.00E+00	0.00E+00
BY4742	0mins	3.94E-03	1.31E-03	3.02E+00	1.60E+00	1.39E+00	3.86E-01
BY4742	30mins	1.46E-03	1.91E-03	7.63E-01	4.04E-01	3.85E-01	8.86E-02
Repeat 1							
BY4742	NoUV	6.39E-03	1.49E-03	4.28E+00	1.00E+00		
BY4742	0mins	8.84E-03	1.27E-03	6.97E+00	1.63E+00		
BY4742	30mins	3.09E-03	1.56E-03	1.98E+00	4.62E-01		
Repeat 2							
BY4742	NoUV	5.83E-03	1.57E-03	3.73E+00	1.00E+00		
BY4742	0mins	9.08E-03	2.58E-03	3.53E+00	9.47E-01		
BY4742	30mins	2.27E-03	2.11E-03	1.08E+00	2.88E-01		

SD = Standard deviation

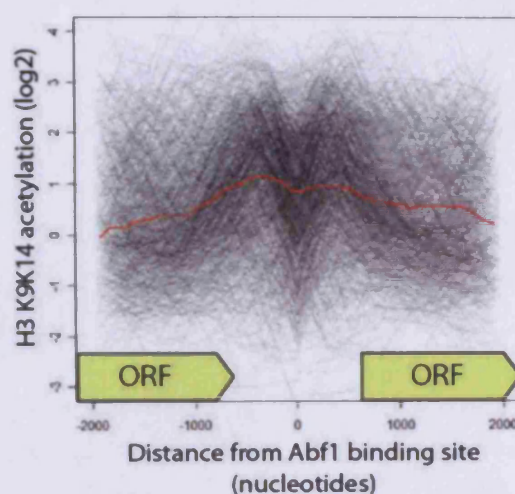
Excel files of quantification available on DVD (D:/Chapter 3/Figure 3.8)

ChIP micorarray quantification (Chapter 3, Fig. 3.7 and 3.8)

		Quantile normalised data		
		Repeat		
Locus	Timepoint	1	2	3
HML α	NoUV	1.23E+01	7.63E+00	6.02E+00
	0mins	5.99E+00	5.82E+00	4.84E+00
	30mins	5.06E+00	4.56E+00	5.38E+00
NAT4	NoUV	4.62E+01	6.00E+01	5.14E+01
	0mins	7.13E+01	6.52E+01	5.93E+01
	30mins	4.55E+01	5.20E+01	3.85E+01
ARS231	NoUV	7.23E+00	6.15E+00	6.11E+00
	0mins	4.50E+00	4.28E+00	4.29E+00
	30mins	1.69E+00	1.42E+00	1.67E+00
prRPL24A	NoUV	8.98E+00	1.19E+01	1.37E+01
	0mins	9.11E+00	6.59E+00	9.63E+00
	30mins	2.18E+00	3.10E+00	3.22E+00

		Normalised to 1				
		Repeat				
Locus	Timepoint	1	2	3	Mean	SD
HML α	NoUV	1.00E+00	1.00E+00	1.00E+00	1.00E+00	0.00E+00
	0mins	4.88E-01	7.63E-01	8.03E-01	6.85E-01	1.71E-01
	30mins	4.12E-01	5.98E-01	8.93E-01	6.34E-01	2.42E-01
NAT4	NoUV	1.00E+00	1.00E+00	1.00E+00	1.00E+00	0.00E+00
	0mins	1.54E+00	1.09E+00	1.16E+00	1.26E+00	2.46E-01
	30mins	9.84E-01	8.67E-01	7.50E-01	8.67E-01	1.17E-01
ARS231	NoUV	1.00E+00	1.00E+00	1.00E+00	1.00E+00	0.00E+00
	0mins	6.23E-01	6.97E-01	7.02E-01	6.74E-01	4.40E-02
	30mins	2.34E-01	2.30E-01	2.74E-01	2.46E-01	2.41E-02
prRPL24A	NoUV	1.00E+00	1.00E+00	1.00E+00	1.00E+00	0.00E+00
	0mins	1.01E+00	5.53E-01	7.01E-01	7.56E-01	2.35E-01
	30mins	2.43E-01	2.60E-01	2.35E-01	2.46E-01	1.29E-02

The distribution of histone H3 K9K14 acetylation at promoters in relation to the position of a TSS



In the above figure histone H3 K9K14 acetylation (U) is plotted at Abf1 binding sites found at promoters only (does not include divergent promoters). The data has been orientated such that the TSS of the promoter is always found to the right of the Abf1 binding site. Note that when the data is orientated in this manner a peak of hyperacetylation is still found either side of the Abf1 binding site.

Appendix III – Raw data and supplementary information for Chapter 4

ChIP qPCR quantification at prRAD23 (Chapter 4, Fig. 4.1)

		SQ mean		
Genotype	Timepoint	Myc IP	Input	IP/input
BY4742 RAD16::18xMyc-URA3	NoUV	1.10E-03	6.78E-04	1.63E+00
BY4742 RAD16::18xMyc-URA3	30mins	1.03E-03	4.33E-04	2.37E+00
BY4742	NoUV	2.77E-04	1.11E-03	2.50E-01
BY4742	30mins	2.95E-04	1.11E-03	2.66E-01
Repeat 1				
BY4742 RAD16::18xMyc-URA3	NoUV	3.73E-03	5.60E-04	6.67E+00
BY4742 RAD16::18xMyc-URA3	30mins	1.97E-03	5.83E-04	3.37E+00
BY4742	NoUV	1.94E-04	4.89E-04	3.97E-01
BY4742	30mins	6.84E-04	6.10E-04	1.12E+00
Repeat 2				
BY4742 RAD16::18xMyc-URA3	NoUV	1.68E-03	4.34E-04	3.88E+00
BY4742 RAD16::18xMyc-URA3	30mins	2.94E-03	4.23E-04	6.96E+00
BY4742	NoUV	1.68E-04	7.08E-04	2.38E-01
BY4742	30mins	6.01E-04	6.71E-04	8.96E-01

		SQ mean	Averaged Dataset	
Genotype	Timepoint	Normalise to 1	Mean	SD
BY4742 RAD16::18xMyc-URA3	NoUV	1.00E+00	1.00E+00	7.61E-16
BY4742 RAD16::18xMyc-URA3	30mins	1.46E+00	1.25E+00	6.68E-01
BY4742	NoUV	1.54E-01	9.16E-02	5.39E-02
BY4742	30mins	1.64E-01	1.88E-01	3.79E-02
Repeat 1				
BY4742 RAD16::18xMyc-URA3	NoUV	1.00E+00		
BY4742 RAD16::18xMyc-URA3	30mins	5.06E-01		
BY4742	NoUV	5.95E-02		
BY4742	30mins	1.68E-01		
Repeat 2				
BY4742 RAD16::18xMyc-URA3	NoUV	1.00E+00		
BY4742 RAD16::18xMyc-URA3	30mins	1.79E+00		
BY4742	NoUV	6.14E-02		
BY4742	30mins	2.31E-01		

SD = Standard deviation

Excel files of quantification available on DVD (D:/Chapter 4/Figure 4.1)

ChIP qPCR quantification at IRC5 (Chapter 4, Fig. 4.1)

		SQ mean		
Genotype	Timepoint	Myc IP	Input	IP/input
BY4742 RAD16::18xMyc-URA3	NoUV	6.27E-04	5.13E-04	1.22E+00
BY4742 RAD16::18xMyc-URA3	30mins	5.53E-04	4.06E-04	1.36E+00
BY4742	NoUV	2.82E-04	1.04E-03	2.73E-01
BY4742	30mins	2.59E-04	9.57E-04	2.71E-01
Repeat 1				
BY4742 RAD16::18xMyc-URA3	NoUV	8.77E-04	4.72E-04	1.86E+00
BY4742 RAD16::18xMyc-URA3	30mins	2.48E-03	5.15E-04	4.81E+00
BY4742	NoUV	1.31E-04	4.77E-04	2.75E-01
BY4742	30mins	4.37E-04	5.49E-04	7.96E-01
Repeat 2				
BY4742 RAD16::18xMyc-URA3	NoUV	8.82E-04	4.20E-04	2.10E+00
BY4742 RAD16::18xMyc-URA3	30mins	1.80E-03	3.72E-04	4.84E+00
BY4742	NoUV	1.62E-04	5.74E-04	2.83E-01
BY4742	30mins	5.88E-04	6.08E-04	9.68E-01

		SQ mean	Averaged Dataset	
Genotype	Timepoint	Normalise to 1	Mean	SD
BY4742 RAD16::18xMyc-URA3	NoUV	1.00E+00	1.00E+00	1.25E-15
BY4742 RAD16::18xMyc-URA3	30mins	1.12E+00	2.00E+00	7.82E-01
BY4742	NoUV	2.23E-01	1.68E-01	4.76E-02
BY4742	30mins	2.21E-01	3.70E-01	1.30E-01
Repeat 1				
BY4742 RAD16::18xMyc-URA3	NoUV	1.00E+00		
BY4742 RAD16::18xMyc-URA3	30mins	2.59E+00		
BY4742	NoUV	1.48E-01		
BY4742	30mins	4.28E-01		
Repeat 2				
BY4742 RAD16::18xMyc-URA3	NoUV	1.00E+00		
BY4742 RAD16::18xMyc-URA3	30mins	2.30E+00		
BY4742	NoUV	1.35E-01		
BY4742	30mins	4.61E-01		

SD = Standard deviation

Excel files of quantification available on DVD (D:/Chapter 4/Figure 4.1)

ChIP qPCR quantification at MFA2 (Chapter 4, Fig. 4.1)

		SQ mean		
Genotype	Timepoint	Myc IP	Input	IP/input
BY4742 RAD16::18xMyc-URA3	NoUV	7.87E-04	5.02E-04	1.57E+00
BY4742 RAD16::18xMyc-URA3	30mins	9.53E-04	3.41E-04	2.79E+00
BY4742	NoUV	3.06E-04	9.69E-04	3.16E-01
BY4742	30mins	3.35E-04	7.68E-04	4.36E-01
Repeat 1				
BY4742 RAD16::18xMyc-URA3	NoUV	2.57E-03	4.11E-04	6.24E+00
BY4742 RAD16::18xMyc-URA3	30mins	1.98E-03	5.22E-04	3.80E+00
BY4742	NoUV	2.49E-04	4.33E-04	5.75E-01
BY4742	30mins	7.74E-04	5.89E-04	1.32E+00
Repeat 2				
BY4742 RAD16::18xMyc-URA3	NoUV	1.73E-03	4.33E-04	4.00E+00
BY4742 RAD16::18xMyc-URA3	30mins	1.90E-03	3.42E-04	5.56E+00
BY4742	NoUV	2.79E-04	5.40E-04	5.16E-01
BY4742	30mins	6.40E-04	5.37E-04	1.19E+00

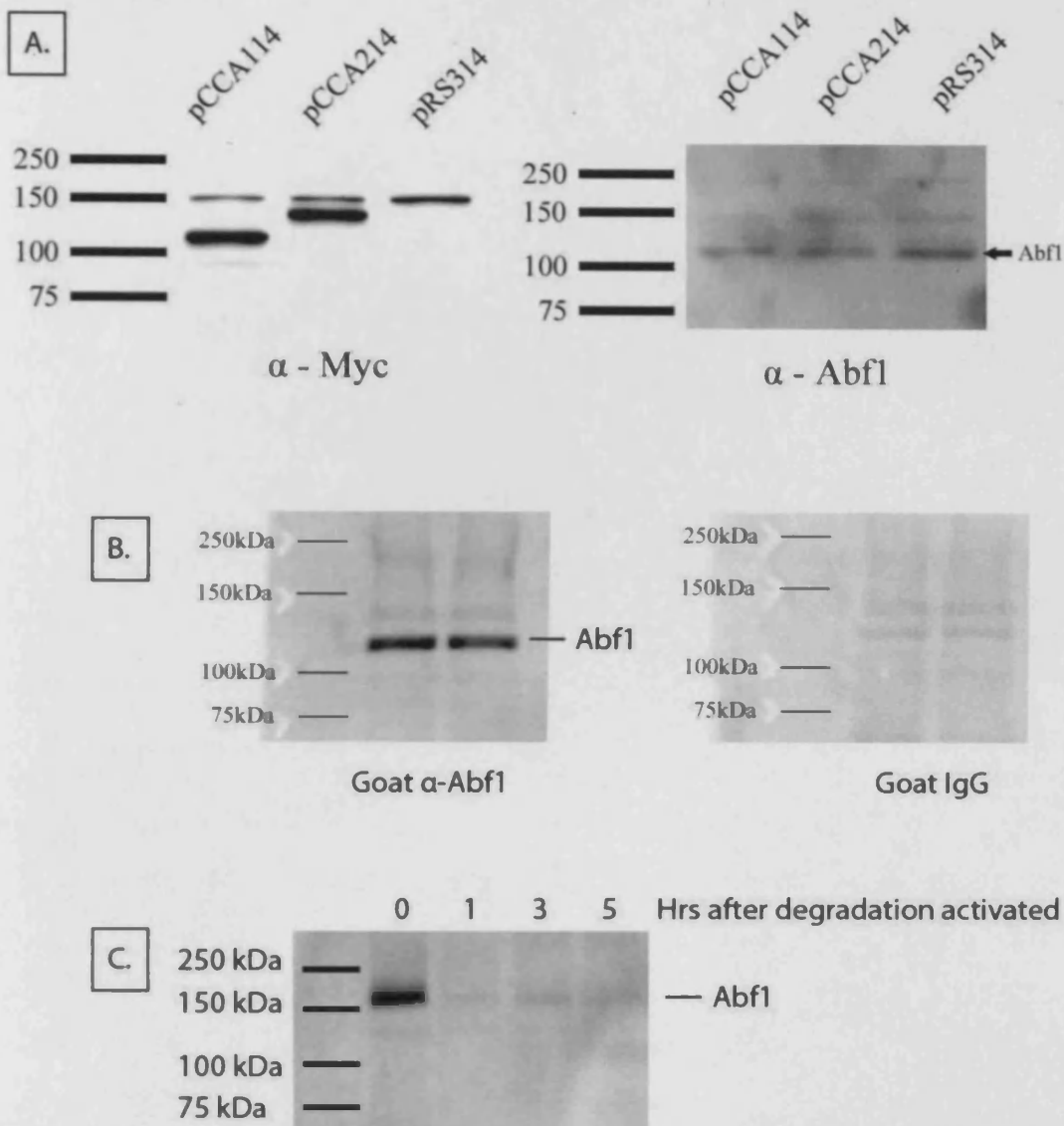
		SQ mean	Averaged Dataset	
Genotype	Timepoint	Normalise to 1	Mean	SD
BY4742 RAD16::18xMyc-URA3	NoUV	1.00E+00	1.00E+00	1.32E-15
BY4742 RAD16::18xMyc-URA3	30mins	1.78E+00	1.26E+00	5.97E-01
BY4742	NoUV	2.01E-01	1.41E-01	5.56E-02
BY4742	30mins	2.78E-01	2.62E-01	4.59E-02
Repeat 1				
BY4742 RAD16::18xMyc-URA3	NoUV	1.00E+00		
BY4742 RAD16::18xMyc-URA3	30mins	6.08E-01		
BY4742	NoUV	9.20E-02		
BY4742	30mins	2.11E-01		
Repeat 2				
BY4742 RAD16::18xMyc-URA3	NoUV	1.00E+00		
BY4742 RAD16::18xMyc-URA3	30mins	1.39E+00		
BY4742	NoUV	1.29E-01		
BY4742	30mins	2.98E-01		

SD = Standard deviation

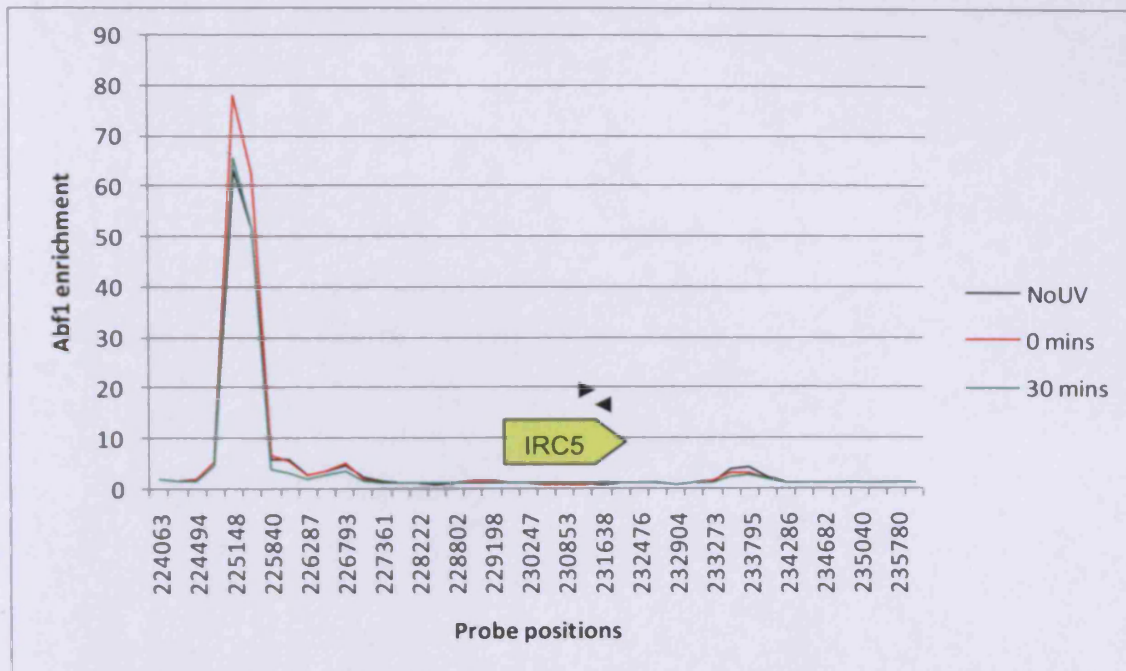
Excel files of quantification available on DVD (D:/Chapter 4/Figure 4.1)

Appendix IV – Raw data and supplementary information for Chapter 5**Primers used for cloning/sequencing**

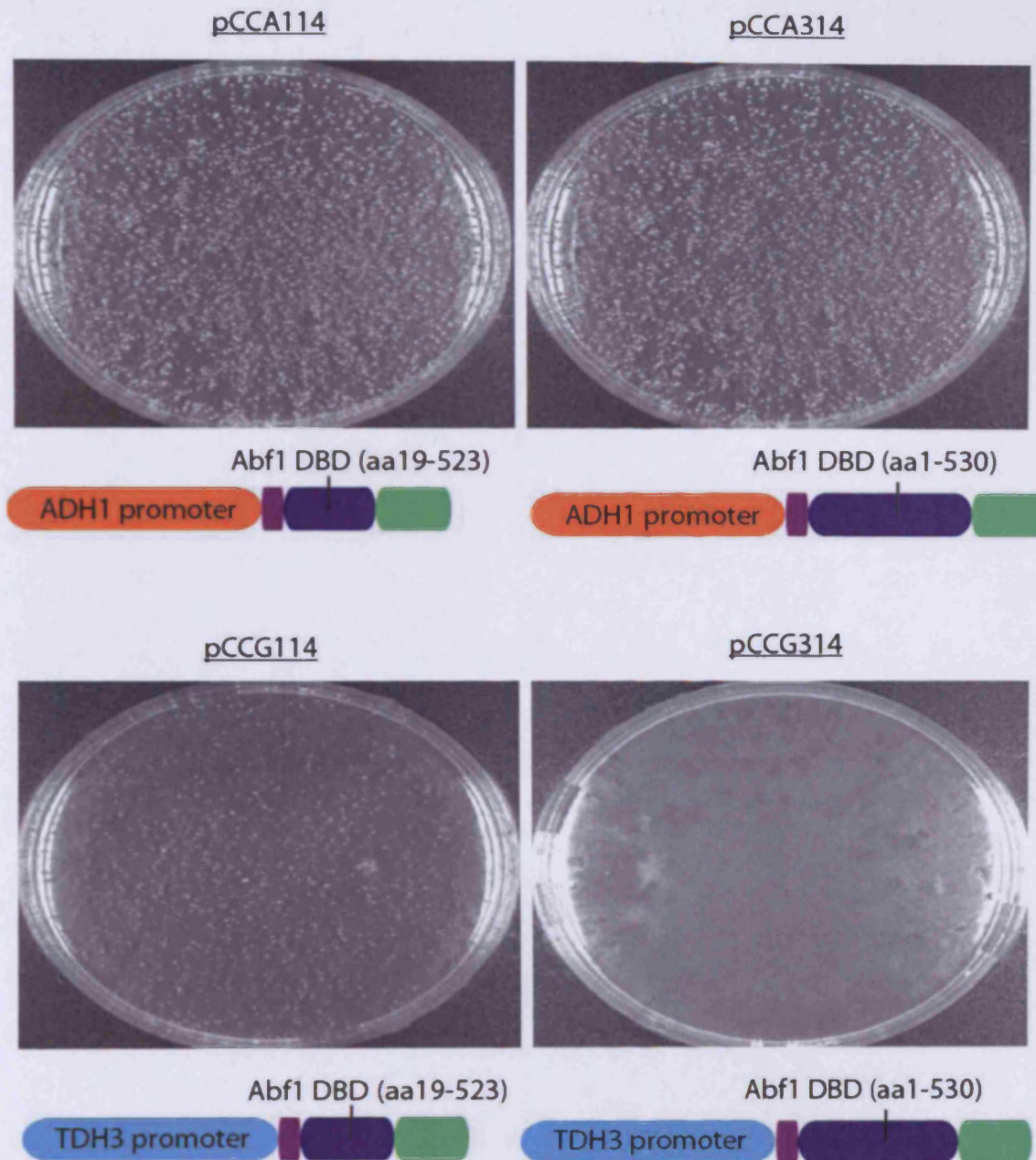
Cloning primer	Sequence (annotations below)
ABF1_1569R	5'- CCGGTGACTAGAGGTTTATC
ABF1_1590R	5'- TGGCATCTTCTTGGGTTGAT
ABF1_1590R#2	5'- TATAC <u>CTCGAG</u> CTAGACTTATACCTTTCTCTTCTTTTGG..... <u>XhoI</u> STOP <u>PKKKRKV</u> TGGCATCTTCTTGGGTTGAT – 3' 3' ABF1 DBD
ABF1_55F	5'- GACCTGGCCATTGGAGCC
ABF1_60R	5'- GTT TGTTCCTATGCGAATTC
ABF1_1F	5'- ATAT <u>CTCGGG</u> AATATGGACAAATTAGTCGTGAATTATT <u>AvaI</u> ABF1 +1-25
ABF1_1F#2	5'- ATATCTCGGGAATATGGACAAA
ABF1_1F#3	5'- ATGGACAAATTAGTCGTGAATTATT
ADH1_F	5'- ATAT <u>GGATCC</u> GGGATCGAAGAAATGATGGTA <u>BamHI</u> 5' ADH1 coding region
ADH1_F#2	5'- ATATGGATCCGGGATCGAAG
ADH1_R	5'- <u>GCACCCAAGGTGGGAAATTTTTGCCTCCATGGGCTCCAATGGCCAGGTC</u> <u>ABF1 +55-105</u> ATTCCCGAGGTCCTCTTC – 3' 3' Myc tag
ER_F	5'- <u>ACGCCTCAAATTTAATGGAAAGTGTGCTAGATAAAACCTCTAGTCACCGG</u> <u>ABF1 +1519-1569</u> TCTGCTGGAGACATGAGAG – 3' 5' ER α LBD
ER_F#2	5'- TCTGCTGGAGACATGAGAG
ER_F#3	5'- ATAT <u>CTCGGG</u> AATTCTGCTGGAGACATGAGAG <u>AvaI</u>
ER_fus_F	5'- <u>GTGTGCTAGATAAAACCTCTAGTCACCGGTATCAACCCAAGAAGATGCCA</u> <u>ABF1 +1540-1590</u> TCTGCTGGAGACATGAGAG – 3' 5' ER α LBD ORF
ER_fus_R	5'- <u>TTAATTATAGGGTGCTTGTATTTCATAATAATTCACGACTAATTTGTCCAT</u> <u>ABF1 +1-50</u> GACTGTGGCAGGGAAACC – 3' 3' of ER α LBD
ER_R	5'- TATAC <u>CTCGAG</u> CTAGACTTATACCTTTCTCTTCTTTTGGGACTGTGGCAGGGAAACC <u>XhoI</u> STOP <u>PKKKRKV</u> 3' ER α LBD
ER_R#2	5'- TATAC <u>CTCGAG</u> CTAGACTTATACCTTTCTCTTCTTTTGGCCACCGTACTCGTCAAT <u>XhoI</u> STOP <u>PKKKRKV</u> 3' VP16 AD
ER_R#3	5'- TATACTCGAGCTAGACTTATACC
Myc_F	5'- CAGAAACTTATCTCAGAAGAGG
ORF_F	5'- <u>AGTTTAAAAACCAAGAAGCTTAGTTTCGAATAAACACACATAAAACAAA CAAA</u> <u>3' of TDH3 promoter</u> ATGGAGCAGAACTTATCTCAG – 3' 5' of competitor ORF
ORF_R	5'- TATACTCGAGCTAGACTTATACCT
TEF2_-1R	5'- ATAT <u>CCCGAGG</u> CTCTTCTGAGATAAGTTTCTGCTCCATGTTTAGTTAATTATAGTTCGTTG <u>AvaI</u> Myc tag 3' of prTEF2
TEF2_-402F	5'- ATAT <u>GGATCC</u> ATTACCCATAAGGTTGTTTGTTG <u>BamHI</u>
TDH_F	5'- CACGCTTTTTCAGTTCGAGTT
TDH_F#2	5'- ATAT <u>GGATCC</u> CACGCTTTTTCAGTTCGAGTT <u>BamHI</u> 5' prTDH3
TDH_R	5'- GTTTGTTTATGTGTGTTTATTCG
Sequencing primer	
5' ADH1 seq	5'-GATGTGCTGCAAGGCGATTA
3' ADH1 seq	5'- GGAAGGGAAGCTT TACACTTCT
5' ORF seq	5'- AAGTTTGCTGTCTTGCTATCA
ABF1 DBD seq	5'- TCAAGAACGACACTGAAGATG
5' ER-LBD seq	5'- TCCCAAATAGCCAGACGTA
3' ORF seq	5'- CTTGCTCTTGGACAGGAA
3' TDH3 seq	5'- GAAATTATCCCTACTTGA
3' TEF2 seq	5'- GAGATGATCGAGCCGGTAG

Characterising the Abf1 antibody (sc6679) for western blotting

All western analysis and ChIP experiments of Abf1 were performed with goat α -Abf1 (yC-20 #sc-6679 Santa Cruz Biotechnology). A. Western blot as shown in Fig. 5.5. The arrow indicates the band that represents the Abf1 protein. This band is weaker than usually observed by western blot because the blot has been striped and reprobed following detection of the competitor with α -Myc (see Chapter 2.6.3). B. Protein WCE from SX46a was blotted (see as described in Chapter 5.2) using with either goat α -Abf1 (left blot) or goat IgG (sc-2028 Santa Cruz Biotechnology). Note that the only band clearly detected by the antibody exactly maps to the Abf1 band identified in A. Abf1 has previously been observed by western blot at an apparent molecular mass of ~135 kDa despite an estimated mass of ~80 kDa predicted from its primary sequence, as seen here (Rhode et al., 1989). C. As further evidence that the only clear band that α -Abf1 (sc-6679) detects is truly Abf1, SX46a expressing a temperature degradable version of Abf1 was analysed at various timepoints following activation of degradation as described (Reed et al., 1999). The protein has a higher molecular mass because it includes an N-terminal degron.

Abf1 binding level at IRC5.

The picture above displays the mean trace of Abf1 binding at a domain of chromosome 6 (taken from the ChIP-chip work performed in Chapter 3) for unirradiated (NoUV), 0 minutes and 30 minutes after UV. The binding level is not given in \log_2 . The yellow bar represents the approximate position of the ORF of IRC5. The black arrows above this represent the forward and reverse primers that are used to amplify IRC5 for qPCR in Chapter 5. This region is considered a negative control region for Abf1 DNA binding in vivo.

The effect upon changing domains of the competitor in SX46a

The picture above illustrates 4 plates where equal volumes of SX46a were transformed with an equal amount of plasmid DNA in the same experiment. The transformed plates were all left for ~2 days. The plasmid used for each transformation is given above the picture. Each plasmid core structure is pRS314. The only difference is the ORF insert; the structures of which are shown below each picture. As can be seen, expressing the competitor with the non-functional DBD (aa19-523) from the very powerful promoter of TDH3 suppresses efficient transformation and cell growth. Under the weak promoter ADH1, changing the competitor DBD to the functional DBD (aa1-530) has little effect upon efficient transformation and cell growth. However, changing the promoter of the competitor with the functional DBD (aa1-530) from the weak ADH1 promoter to the powerful TDH3 promoter drastically reduces efficient transformation and cell growth in a manner far greater than would be expected due to over expression alone.

ChIP qPCR quantification at HML α and ARS121 (Chapter 5, Fig. 5.6)

Genomic locus	Plasmid	Time after β -oestradiol (mins)	Mean Abf1 (IP/input) Normalised	Abf1 SD	Mean Competitor (IP/input) Normalised	Comp SD
HML- α	pCCA114	-1	1.00E+00	0.00E+00	2.10E-02	8.21E-03
	pCCA114	30	8.80E-01	2.26E-01	5.32E-02	2.25E-03
	pCCA114	60	8.15E-01	2.12E-01	3.22E-02	5.22E-03
IRC5	pCCA114	-1	9.88E-02	1.84E-02	2.06E-02	8.39E-03
	pCCA114	30	7.27E-02	1.10E-02	1.95E-02	1.22E-02
	pCCA114	60	6.84E-02	5.88E-03	1.95E-02	4.29E-03
HML- α	pCCA214	-1	1.00E+00	0.00E+00	2.67E-02	1.14E-02
	pCCA214	30	6.63E-01	6.13E-02	3.43E-02	1.99E-02
	pCCA214	60	6.60E-01	3.97E-02	1.99E-02	8.46E-03
IRC5	pCCA214	-1	8.00E-02	5.02E-02	1.94E-02	1.39E-02
	pCCA214	30	7.73E-02	1.38E-02	2.16E-02	1.63E-02
	pCCA214	60	6.57E-02	2.57E-02	1.45E-02	7.78E-03

Genomic locus	Plasmid	Time after β -oestradiol (mins)	Mean Abf1 (IP/input) Normalised	Abf1 SD	Mean Competitor (IP/input) Normalised	Comp SD
ARS121	pCCA114	-1	1.00E+00	0.00E+00	9.58E-03	7.74E-04
	pCCA114	30	9.93E-01	1.54E-01	1.53E-02	3.56E-03
	pCCA114	60	6.61E-01	3.71E-02	1.02E-02	2.88E-03
IRC5	pCCA114	-1	5.47E-02	1.89E-03	1.12E-02	2.96E-03
	pCCA114	30	4.04E-02	4.55E-06	1.04E-02	5.21E-03
	pCCA114	60	3.82E-02	2.53E-03	1.08E-02	7.49E-04
ARS121	pCCA214	-1	1.00E+00	0.00E+00	1.30E-02	2.71E-03
	pCCA214	30	9.62E-01	2.42E-01	1.28E-02	1.07E-03
	pCCA214	60	6.21E-01	2.45E-01	7.07E-03	6.24E-04
IRC5	pCCA214	-1	5.17E-02	1.43E-03	1.21E-02	1.71E-03
	pCCA214	30	5.84E-02	2.63E-02	1.33E-02	2.52E-03
	pCCA214	60	4.62E-02	1.13E-02	9.65E-03	7.74E-04

SD = Standard deviation

Excel files for the quantification of replicates and averaged values available on DVD (D:/Chapter 5/Figure 5.6)

ChIP qPCR quantification at NAT4 (Chapter 5, Fig. 5.7A)

Genotype	Timepoint (mins)	Abfl (IP/input)	Normalise to 1	Mean	SD
JCA30 pRS314	-1	3.91E+01	1.00E+00	1.00E+00	0.00E+00
	30	5.92E+01	1.51E+00	1.12E+00	5.59E-01
JCA31 pRS314	-1	3.88E+00	9.93E-02	1.01E-01	1.92E-03
	30	2.16E+00	5.53E-02	4.35E-02	1.67E-02
Repeat					
JCA30 pRS314	-1	2.86E+01	1.00E+00		
	30	2.07E+01	7.25E-01		
JCA31 pRS314	-1	2.92E+00	1.02E-01		
	30	9.05E-01	3.17E-02		

ChIP qPCR quantification at NAT4 (Chapter 5, Fig. 5.7B)

Genotype	Timepoint (mins)	Mean Abfl (IP/input) Normalised	Abfl SD	Mean competitor (IP/Input) Normalised	Competitor SD
JCA31 pRS314	-1	1.00E+00	0.00E+00		
JCA31 pCCG114	30	5.73E-01	1.04E-01	3.04E-02	2.07E-02

ChIP qPCR quantification at IRC5 (Chapter 5, Fig. 5.7B)

Genotype	Timepoint (mins)	Mean Abfl (IP/input) Normalised	Abfl SD	Mean competitor (IP/Input) Normalised	Competitor SD
JCA31 pCCG114	30			1.01E-02	4.23E-03

SD = Standard deviation

Excel files for the quantification of replicates and averaged values available on DVD
(D:/Chapter 5/Figure 5.7)

ChIP qPCR quantification at NAT4 (Chapter 5, Fig. 5.11)

Locus	Plasmid	Time after β-oestradiol (mins)	Mean Abf1 (IP/input) Normalised	Abf1 SD	Mean Competitor (IP/input) Normalised	Competitor SD
NAT4	pRS314	-1	1.00E+00	0.00E+00		
	pCCT314	-1	6.34E-01	6.20E-02	2.07E+00	1.02E+00
	pCCT314	30	6.10E-01	2.53E-01	5.00E+00	5.25E-01
NAT4	pRS314	-1	1.00E+00	0.00E+00		
	pCCT414	-1	3.99E-01	4.55E-02	1.91E+00	4.79E-01
	pCCT414	30	3.37E-01	4.66E-02	3.29E+00	9.32E-01
IRC5	pRS314	-1	1.00E+00	0.00E+00		
	pCCT314	-1	3.99E-02	5.94E-03	2.54E-02	1.61E-02
	pCCT314	30	2.77E-02	1.04E-03	4.38E-02	1.31E-02
IRC5	pRS314	-1	1.00E+00	0.00E+00		
	pCCT414	-1	2.99E-02	1.07E-02	2.90E-02	3.29E-03
	pCCT414	30	1.61E-02	8.27E-03	2.78E-02	8.59E-03

SD = Standard deviation

Excel files for the quantification of replicates and averaged values available on DVD
(D:/Chapter 5/Figure 5.11)

ChIP qPCR quantification at NAT4 (Chapter 5, Fig. 5.12)

Locus	Plasmid	Time after β-oestradiol (mins)	Mean Abfl (IP/input) Normalised	Abfl SD	Mean Competitor (IP/input) Normalised	Competitor SD
NAT4	pRS314	-1	1.00E+00	0.00E+00		
	pCCG514	-1	4.34E-01	1.62E-01	1.15E-02	6.08E-03
	pCCG514	30	3.40E-01	4.34E-02	4.59E-01	1.51E-01
NAT4	pRS314	-1	1.00E+00	0.00E+00		
	pCCG614	-1	4.33E-01	2.44E-01	2.09E-02	1.07E-02
	pCCG614	30	2.37E-01	1.62E-01	2.13E-01	3.97E-02

SD = Standard deviation

Excel files for the quantification of replicates and averaged values available on DVD
(D:/Chapter 5/Figure 5.12)

Appendix V – Raw data and supplementary information for chapter 6**Primers used for cloning**

Cloning primer	Sequence (annotations below)
ABF1_1MF	5'- ATAT <u>CTCGGA</u> AATATGGACAAATTAGTCGTGAATTATT Aval ABF1 nt+1-25
ABF1_1437F	5' - GCGGGTACCTCATCGAACA
ABF1_1593F	5' - AGCGTCAATAAATGGAGCAAGC
ABF1_2193R	5'-TATA <u>CTCGAG</u> CTAGACTTATACCTTTCTCTTCTTTTTTGG..... XhoI STOP <u>PKKKRKV</u> ATCCACGTCCACCATTACATC – 3' 3' of ABF1
ABF1_2924MR	5'- TATA <u>CTCGAG</u> TTAGACCTATTGACCTCTTAATTCTGG Aval STOP ABF1 nt+2906-2924
ABF1_fus_R	5' – GACACGTCTGAATGAGTTATTTGATCTGGCTTGCTCCATTTATTGACGC..... ABF1 +2143-2193 <u>.....TGACTGTGGCAGGGAAAC – 3'</u> <u>3' of ERα LBD</u>
ER_R#3	5'- TATACTCGAGCTAGACTTATACC
RAP1_1746F	5' - AAGAGGCCTGGCGTTCC
RAP1_2076R	5'- TATA <u>CTCGAG</u> CTAGACTTATACCTTTCTCTTCTTTTTTGG..... XhoI STOP <u>PKKKRKV</u> GCTTATGGTATCAGGATCAATA – 3' 3' of ERα LBD
RAP1_fus_R	5' – CTCTTGCGGCAGAGTTATAATTGCCAGGAGTGGAACGCCAGGCCTCT..... RAP1+2026-2076 <u>.....TGACTGTGGCAGGGAAAC – 3'</u> <u>3' of ERα LBD</u>

ChIP qPCR quantification at NAT4 (Chapter 6, Fig. 6.1)

β-oestradiol concentration (μM)	SQ Mean			IP/input		Normalise to 1	
	Abfl IP	Competitor IP	Input	Abfl	Competitor	Abfl	Competitor
1	2.89E-02	3.47E-03	1.19E-03	2.43E+01	2.91E+00	1.00E+00	1.20E-01
10≤	1.27E-02	5.85E-03	7.86E-04	1.61E+01	7.45E+00	6.64E-01	3.07E-01
20≤	7.03E-03	5.88E-03	5.78E-04	1.22E+01	1.02E+01	5.01E-01	4.19E-01
200≤	9.42E-03	1.07E-02	8.79E-04	1.07E+01	1.22E+01	4.41E-01	5.02E-01

ChIP qPCR quantification at HMLα (Chapter 6, Fig. 6.1)

β-oestradiol concentration (μM)	SQ Mean			IP/input		Normalise to 1	
	Abfl IP	Competitor IP	Input	Abfl	Competitor	Abfl	Competitor
1	2.74E-03	1.47E-04	1.10E-03	2.50E+00	1.34E-01	1.00E+00	5.37E-02
10≤	1.68E-03	4.55E-04	9.51E-04	1.76E+00	4.78E-01	7.06E-01	1.91E-01
20≤	1.03E-03	6.06E-04	7.07E-04	1.46E+00	8.57E-01	5.86E-01	3.43E-01
200≤	9.82E-04	3.85E-04	9.32E-04	1.05E+00	4.13E-01	4.22E-01	1.65E-01

Raw data is available on the accompanying DVD (D:/Chapter 6/Figure 6.1).

ChIP qPCR quantification at NAT4 for pRS316 (Chapter 6, Fig. 6.2A)

	SQ Mean			Normalise to 1
Time after β -oestradiol addition (mins)	Abfl IP	Input	IP/input	
-1	3.81E-03	1.27E-03	3.00E+00	1.00E+00
60	3.73E-03	9.70E-04	3.84E+00	1.28E+00
120	2.48E-03	8.83E-04	2.81E+00	9.37E-01

ChIP qPCR quantification at NAT4 for pCCG516 (Chapter 6, Fig. 6.2B)

Time after β -oestradiol addition (mins)	SQ Mean			IP/input		Normalise to 1	
	Abfl IP	Competitor IP	Input	Abfl	Competitor	Abfl	Competitor
-1	1.82E-02	4.85E-05	1.11E-03	1.63E+01	4.37E-02	1.00E+00	2.67E-03
60	6.39E-03	5.41E-03	1.02E-03	6.24E+00	5.28E+00	3.82E-01	3.23E-01
120	6.87E-03	8.82E-03	8.27E-04	8.31E+00	1.07E+01	5.08E-01	6.53E-01

ChIP qPCR quantification at NAT4 for pCCG616 (Chapter 6, Fig. 6.2C)

Time after β -oestradiol addition (mins)	SQ Mean			IP/input		Normalise to 1	
	Abfl IP	Competitor IP	Input	Abfl	Competitor	Abfl	Competitor
-1	5.27E-03	8.02E-05	9.97E-04	5.29E+00	8.04E-02	1.00E+00	1.52E-02
60	2.24E-03	3.00E-03	1.28E-03	1.75E+00	2.34E+00	3.30E-01	4.42E-01
120	2.78E-03	2.96E-03	1.34E-03	2.08E+00	2.21E+00	3.93E-01	4.18E-01

Raw data is available on the accompanying DVD (D:/Chapter 6/Figure 6.2).

ChIP qPCR quantification at prSRB2 (Chapter 6, Fig. 6.3A)

Time after β -oestradiol addition (mins)	SQ Mean			IP/input		Normalise to 1	
	Abfl IP	Competitor IP	Input	Abfl	Competitor	Abfl	Competitor
-1	2.21E-02	2.43E-04	1.27E-03	1.74E+01	1.92E-01	1.00E+00	1.10E-02
10	2.10E-02	7.87E-04	1.36E-03	1.55E+01	5.79E-01	8.87E-01	3.32E-02
60	1.76E-02	4.42E-03	1.34E-03	1.31E+01	3.30E+00	7.51E-01	1.89E-01
120	1.70E-02	4.06E-03	1.25E-03	1.37E+01	3.25E+00	7.83E-01	1.87E-01

ChIP qPCR quantification at ARS121 (Chapter 6, Fig. 6.3B)

Time after β -oestradiol addition (mins)	SQ Mean			IP/input		Normalise to 1	
	Abfl IP	Competitor IP	Input	Abfl	Competitor	Abfl	Competitor
-1	5.58E-03	1.60E-04	1.38E-03	4.06E+00	1.16E-01	1.00E+00	2.87E-02
10	5.25E-03	2.67E-04	1.17E-03	4.51E+00	2.29E-01	1.11E+00	5.66E-02
60	4.95E-03	7.43E-04	1.11E-03	4.47E+00	6.72E-01	1.10E+00	1.66E-01
120	4.04E-03	9.98E-04	1.14E-03	3.53E+00	8.73E-01	8.70E-01	2.15E-01

ChIP qPCR quantification at HML α (Chapter 6, Fig. 6.3C)

Time after β -oestradiol addition (mins)	SQ Mean			IP/input		Normalise to 1	
	Abfl IP	Competitor IP	Input	Abfl	Competitor	Abfl	Competitor
-1	5.29E-03	3.24E-04	1.16E-03	4.58E+00	2.81E-01	1.00E+00	6.13E-02
10	5.17E-03	6.70E-04	1.25E-03	4.15E+00	5.38E-01	9.07E-01	1.17E-01
60	3.89E-03	2.94E-03	1.27E-03	3.06E+00	2.32E+00	6.68E-01	5.06E-01
120	3.57E-03	3.23E-03	1.32E-03	2.71E+00	2.45E+00	5.92E-01	5.36E-01

Raw data is available on the accompanying DVD (D:/Chapter 6/Figure 6.3).

ChIP qPCR quantification at NAT4 in JCA30 (Chapter 6, Fig. 6.4A)

Time after β -oestradiol addition (mins)	SQ Mean			IP/input		Normalise to 1	
	Abfl IP	Competitor IP	Input	Abfl	Competitor	Abfl	Competitor
-1	2.81E-02	1.17E-04	1.03E-03	2.75E+01	1.14E-01	1.00E+00	4.14E-03
10	2.45E-02	6.91E-03	1.27E-03	1.94E+01	5.46E+00	7.06E-01	1.99E-01
20	1.41E-02	1.05E-02	1.02E-03	1.39E+01	1.03E+01	5.04E-01	3.75E-01

ChIP qPCR quantification at NAT4 in JCA31 (Chapter 6, Fig. 6.4B)

Time after β -oestradiol addition (mins)	SQ Mean			IP/input		Normalise to 1 (relative to -1Abfl IP in JCA30)	
	Abfl IP	Competitor IP	Input	Abfl	Competitor	Abfl	Competitor
-1	4.36E-03	3.04E-04	1.36E-03	3.21E+00	2.24E-01	1.17E-01	8.15E-03
10	2.54E-03	7.02E-03	1.49E-03	1.70E+00	4.70E+00	6.20E-02	1.71E-01
20	3.68E-03	1.18E-02	1.64E-03	2.24E+00	7.22E+00	8.16E-02	2.63E-01

ChIP qPCR quantification at prSRB2 in JCA30 (Chapter 6, Fig. 6.4C)

Time after β -oestradiol addition (mins)	SQ Mean			IP/input		Normalise to 1	
	Abfl IP	Competitor IP	Input	Abfl	Competitor	Abfl	Competitor
-1	1.44E-02	7.46E-05	1.19E-03	1.21E+01	6.27E-02	1.00E+00	5.20E-03
10	1.51E-02	1.01E-03	1.10E-03	1.37E+01	9.14E-01	1.13E+00	7.58E-02
20	9.12E-03	1.91E-03	8.53E-04	1.07E+01	2.24E+00	8.86E-01	1.86E-01

ChIP qPCR quantification at prSRB2 in JCA31 (Chapter 6, Fig. 6.4D)

Time after β -oestradiol addition (mins)	SQ Mean			IP/input		Normalise to 1 (relative to -1Abfl IP in JCA30)	
	Abfl IP	Competitor IP	Input	Abfl	Competitor	Abfl	Competitor
-1	9.16E-04	5.74E-05	1.23E-03	7.44E-01	4.66E-02	6.17E-02	3.87E-03
10	8.48E-04	9.66E-04	1.41E-03	6.02E-01	6.86E-01	4.99E-02	5.69E-02
20	1.08E-03	1.85E-03	1.47E-03	7.33E-01	1.26E+00	6.07E-02	1.04E-01

Raw data is available on the accompanying DVD (D:/Chapter 6/Figure 6.4).

ChIP qPCR quantification at prSRB2 with pCCG516A (Chapter 6, Fig. 6.6)

Time after β -oestradiol addition (hrs)	SQ Mean			IP/input		Normalise to 1	
	Abfl IP	Competitor IP	Input	Abfl	Competitor	Abfl	Competitor
4	1.74E-02	1.89E-03	1.07E-03	1.62E+01	1.77E+00	1.00E+00	1.09E-01

ChIP qPCR quantification at prSRB2 with pCCG516R (Chapter 6, Fig. 6.6)

Time after β -oestradiol addition (hrs)	SQ Mean			IP/input		Normalise to 1	
	Abfl IP	Competitor IP	Input	Abfl	Competitor	Abfl	Competitor
4	1.92E-02	1.87E-03	2.14E-03	8.97E+00	8.73E-01	1.00E+00	9.73E-02

ChIP qPCR quantification at prSRB2 with pCCT414 (Chapter 6, Fig. 6.6)

Time after β -oestradiol addition (hrs)	SQ Mean			IP/input		Normalise to 1	
	Abfl IP	Competitor IP	Input	Abfl	Competitor	Abfl	Competitor
4	1.37E-02	1.47E-03	8.92E-04	1.54E+01	1.65E+00	1.00E+00	1.07E-01

Raw data is available on the accompanying DVD (D:/Chapter 6/Figure 6.6).

References

- Abdulovic, A.L., and Jinks-Robertson, S. (2006). The in vivo characterization of translesion synthesis across UV-induced lesions in *Saccharomyces cerevisiae*: insights into Pol zeta- and Pol eta-dependent frameshift mutagenesis. *Genetics* 172, 1487-1498.
- Aboussekhra, A., and Al-Sharif, I. (2005). Homologous recombination is involved in transcription-coupled repair of UV damage in *Saccharomyces cerevisiae*. *EMBO J* 24, 1999-2010.
- Aboussekhra, A., Biggerstaff, M., Shivji, M.K., Vilpo, J.A., Moncollin, V., Podust, V.N., Protic, M., Hubscher, U., Egly, J.M., and Wood, R.D. (1995). Mammalian DNA nucleotide excision repair reconstituted with purified protein components. *Cell* 80, 859-868.
- Agresti, A., Scaffidi, P., Riva, A., Caiolfa, V.R., and Bianchi, M.E. (2005). GR and HMGB1 interact only within chromatin and influence each other's residence time. *Mol Cell* 18, 109-121.
- Alekseev, S., Luijsterburg, M.S., Pines, A., Geverts, B., Mari, P.O., Giglia-Mari, G., Lans, H., Houtsmuller, A.B., Mullenders, L.H., Hoeijmakers, J.H., *et al.* (2008). Cellular concentrations of DDB2 regulate dynamic binding of DDB1 at UV-induced DNA damage. *Mol Cell Biol* 28, 7402-7413.
- Allis, C.D., Jenuwein, T., and Reinberg, D. (2006). *Epigenetics* (Cold Spring Harbor, N.Y.: Cold Spring Harbor Laboratory Press).
- Almeida, K.H., and Sobol, R.W. (2007). A unified view of base excision repair: lesion-dependent protein complexes regulated by post-translational modification. *DNA Repair (Amst)* 6, 695-711.
- Anindya, R., Aygün, O., and Svejstrup, J. (2007). Damage-induced ubiquitylation of human RNA polymerase II by the ubiquitin ligase Nedd4, but not Cockayne syndrome proteins or BRCA1. *Mol Cell* 28, 386-397.
- Anindya, R., Mari, P.O., Kristensen, U., Kool, H., Giglia-Mari, G., Mullenders, L.H., Foustieri, M., Vermeulen, W., Egly, J.M., and Svejstrup, J.Q. (2010). A ubiquitin-binding domain in Cockayne syndrome B required for transcription-coupled nucleotide excision repair. *Mol Cell* 38, 637-648.
- Araki, M., Masutani, C., Takemura, M., Uchida, A., Sugasawa, K., Kondoh, J., Ohkuma, Y., and Hanaoka, F. (2001). Centrosome protein centrin 2/caltractin 1 is part of the xeroderma pigmentosum group C complex that initiates global genome nucleotide excision repair. *J Biol Chem* 276, 18665-18672.
- Araujo, S.J., Nigg, E.A., and Wood, R.D. (2001). Strong functional interactions of TFIIH with XPC and XPG in human DNA nucleotide excision repair, without a preassembled repairosome. *Mol Cell Biol* 21, 2281-2291.

- Araujo, S.J., Tirode, F., Coin, F., Pospiech, H., Syvaaja, J.E., Stucki, M., Hubscher, U., Egly, J.M., and Wood, R.D. (2000). Nucleotide excision repair of DNA with recombinant human proteins: definition of the minimal set of factors, active forms of TFIIH, and modulation by CAK. *Genes Dev* 14, 349-359.
- Archer, C., Burdine, L., Liu, B., Ferdous, A., Johnston, S., and Kodadek, T. (2008a). Physical and functional interactions of monoubiquitylated transactivators with the proteasome. *J Biol Chem* 283, 21789-21798.
- Archer, C.T., Delahodde, A., Gonzalez, F., Johnston, S.A., and Kodadek, T. (2008b). Activation domain-dependent monoubiquitylation of Gal4 protein is essential for promoter binding in vivo. *J Biol Chem* 283, 12614-12623.
- Armstrong, J.D., and Kunz, B.A. (1992). Photoreactivation implicates cyclobutane dimers as the major promutagenic UVB lesions in yeast. *Mutat Res* 268, 83-94.
- Arndt, K., and Fink, G.R. (1986). GCN4 protein, a positive transcription factor in yeast, binds general control promoters at all 5' TGACTC 3' sequences. *Proc Natl Acad Sci U S A* 83, 8516-8520.
- Auclair, Y., Rouget, R., Affar el, B., and Drobetsky, E.A. (2008). ATR kinase is required for global genomic nucleotide excision repair exclusively during S phase in human cells. *Proc Natl Acad Sci U S A* 105, 17896-17901.
- Badis, G., Chan, E.T., van Bakel, H., Pena-Castillo, L., Tillo, D., Tsui, K., Carlson, C.D., Gossett, A.J., Hasinoff, M.J., Warren, C.L., *et al.* (2008). A library of yeast transcription factor motifs reveals a widespread function for Rsc3 in targeting nucleosome exclusion at promoters. *Mol Cell* 32, 878-887.
- Bailly, V., Sommers, C.H., Sung, P., Prakash, L., and Prakash, S. (1992). Specific complex formation between proteins encoded by the yeast DNA repair and recombination genes RAD1 and RAD10. *Proc Natl Acad Sci U S A* 89, 8273-8277.
- Baldini, G., Cannone, F., and Chirico, G. (2005). Pre-unfolding resonant oscillations of single green fluorescent protein molecules. *Science* 309, 1096-1100.
- Bang, D.D., Verhage, R., Goosen, N., Brouwer, J., and van de Putte, P. (1992). Molecular cloning of RAD16, a gene involved in differential repair in *Saccharomyces cerevisiae*. *Nucleic Acids Res* 20, 3925-3931.
- Bardwell, A.J., Bardwell, L., Johnson, D.K., and Friedberg, E.C. (1993). Yeast DNA recombination and repair proteins Rad1 and Rad10 constitute a complex in vivo mediated by localized hydrophobic domains. *Mol Microbiol* 8, 1177-1188.
- Bardwell, A.J., Bardwell, L., Tomkinson, A.E., and Friedberg, E.C. (1994). Specific cleavage of model recombination and repair intermediates by the yeast Rad1-Rad10 DNA endonuclease. *Science* 265, 2082-2085.
- Bastin-Shanower, S.A., and Brill, S.J. (2001). Functional analysis of the four DNA binding domains of replication protein A. The role of RPA2 in ssDNA binding. *J Biol Chem* 276, 36446-36453.

- Batty, D., Raptic'-Otrin, V., Levine, A.S., and Wood, R.D. (2000). Stable binding of human XPC complex to irradiated DNA confers strong discrimination for damaged sites. *J Mol Biol* 300, 275-290.
- Batty, D.P., and Wood, R.D. (2000). Damage recognition in nucleotide excision repair of DNA. *Gene* 241, 193-204.
- Beerens, N., Hoeijmakers, J.H., Kanaar, R., Vermeulen, W., and Wyman, C. (2005). The CSB protein actively wraps DNA. *J Biol Chem* 280, 4722-4729.
- Bergink, S., and Jentsch, S. (2009). Principles of ubiquitin and SUMO modifications in DNA repair. *Nature* 458, 461-467.
- Bergink, S., Salomons, F.A., Hoogstraten, D., Groothuis, T.A., de Waard, H., Wu, J., Yuan, L., Citterio, E., Houtsmuller, A.B., Neefjes, J., *et al.* (2006). DNA damage triggers nucleotide excision repair-dependent monoubiquitylation of histone H2A. *Genes Dev* 20, 1343-1352.
- Bernstein, B.E., Liu, C.L., Humphrey, E.L., Perlstein, E.O., and Schreiber, S.L. (2004). Global nucleosome occupancy in yeast. *Genome Biol* 5, R62.
- Bertolaet, B.L., Clarke, D.J., Wolff, M., Watson, M.H., Henze, M., Divita, G., and Reed, S.I. (2001). UBA domains of DNA damage-inducible proteins interact with ubiquitin. *Nat Struct Biol* 8, 417-422.
- Besaratinia, A., Synold, T.W., Chen, H.H., Chang, C., Xi, B., Riggs, A.D., and Pfeifer, G.P. (2005). DNA lesions induced by UV A1 and B radiation in human cells: comparative analyses in the overall genome and in the p53 tumor suppressor gene. *Proc Natl Acad Sci U S A* 102, 10058-10063.
- Beyer, A., Workman, C., Hollunder, J., Radke, D., Möller, U., Wilhelm, T., and Ideker, T. (2006). Integrated assessment and prediction of transcription factor binding. *PLoS Comput Biol* 2, e70.
- Bhatia, P.K., Verhage, R.A., Brouwer, J., and Friedberg, E.C. (1996). Molecular cloning and characterization of *Saccharomyces cerevisiae* RAD28, the yeast homolog of the human Cockayne syndrome A (CSA) gene. *J Bacteriol* 178, 5977-5988.
- Bi, X., Yu, Q., Sandmeier, J.J., and Zou, Y. (2004). Formation of boundaries of transcriptionally silent chromatin by nucleosome-excluding structures. *Mol Cell Biol* 24, 2118-2131.
- Bochkarev, A., Pfuetzner, R.A., Edwards, A.M., and Frappier, L. (1997). Structure of the single-stranded-DNA-binding domain of replication protein A bound to DNA. *Nature* 385, 176-181.
- Bochkareva, E., Korolev, S., Lees-Miller, S.P., and Bochkarev, A. (2002). Structure of the RPA trimerization core and its role in the multistep DNA-binding mechanism of RPA. *EMBO J* 21, 1855-1863.

- Bodmer-Glavas, M., Edler, K., and Barberis, A. (2001). RNA polymerase II and III transcription factors can stimulate DNA replication by modifying origin chromatin structures. *Nucleic Acids Res* 29, 4570-4580.
- Boiteux, S., and Guillet, M. (2004). Abasic sites in DNA: repair and biological consequences in *Saccharomyces cerevisiae*. *DNA Repair (Amst)* 3, 1-12.
- Boscheron, C., Maillet, L., Marcand, S., Tsai-Pflugfelder, M., Gasser, S.M., and Gilson, E. (1996). Cooperation at a distance between silencers and proto-silencers at the yeast HML locus. *EMBO J* 15, 2184-2195.
- Bosisio, D., Marazzi, I., Agresti, A., Shimizu, N., Bianchi, M.E., and Natoli, G. (2006). A hyper-dynamic equilibrium between promoter-bound and nucleoplasmic dimers controls NF-kappaB-dependent gene activity. *EMBO J* 25, 798-810.
- Bourre, F., Renault, G., and Sarasin, A. (1987). Sequence effect on alkali-sensitive sites in UV-irradiated SV40 DNA. *Nucleic Acids Res* 15, 8861-8875.
- Brady, K.L., Ponnampalam, S.N., Bumbulis, M.J., and Setzer, D.R. (2005). Mutations in TFIIIA that increase stability of the TFIIIA-5 S rRNA gene complex: unusual effects on the kinetics of complex assembly and dissociation. *J Biol Chem* 280, 26743-26750.
- Bram, R.J., and Kornberg, R.D. (1985). Specific protein binding to far upstream activating sequences in polymerase II promoters. *Proc Natl Acad Sci U S A* 82, 43-47.
- Brand, A.H., Micklem, G., and Nasmyth, K. (1987). A yeast silencer contains sequences that can promote autonomous plasmid replication and transcriptional activation. *Cell* 51, 709-719.
- Brash, D.E., and Haseltine, W.A. (1982). UV-induced mutation hotspots occur at DNA damage hotspots. *Nature* 298, 189-192.
- Brash, D.E., Seetharam, S., Kraemer, K.H., Seidman, M.M., and Bredberg, A. (1987). Photoproduct frequency is not the major determinant of UV base substitution hot spots or cold spots in human cells. *Proc Natl Acad Sci U S A* 84, 3782-3786.
- Bregman, D.B., Halaban, R., van Gool, A.J., Henning, K.A., Friedberg, E.C., and Warren, S.L. (1996). UV-induced ubiquitination of RNA polymerase II: a novel modification deficient in Cockayne syndrome cells. *Proc Natl Acad Sci U S A* 93, 11586-11590.
- Bresson, A., and Fuchs, R.P. (2002). Lesion bypass in yeast cells: Pol eta participates in a multi-DNA polymerase process. *EMBO J* 21, 3881-3887.
- Brès, V., Kiernan, R., Linares, L., Chable-Bessia, C., Plechakova, O., Tréand, C., Emiliani, S., Peloponese, J., Jeang, K., Coux, O., *et al.* (2003). A non-proteolytic role for ubiquitin in Tat-mediated transactivation of the HIV-1 promoter. *Nat Cell Biol* 5, 754-761.

References

- Buchman, A.R., Kimmerly, W.J., Rine, J., and Kornberg, R.D. (1988). Two DNA-binding factors recognize specific sequences at silencers, upstream activating sequences, autonomously replicating sequences, and telomeres in *Saccharomyces cerevisiae*. *Mol Cell Biol* 8, 210-225.
- Buchman, A.R., and Kornberg, R.D. (1990). A yeast ARS-binding protein activates transcription synergistically in combination with other weak activating factors. *Mol Cell Biol* 10, 887-897.
- Buck, M.J., and Lieb, J.D. (2006). A chromatin-mediated mechanism for specification of conditional transcription factor targets. *Nat Genet* 38, 1446-1451.
- Buck, M.J., Nobel, A.B., and Lieb, J.D. (2005). ChIPOTle: a user-friendly tool for the analysis of ChIP-chip data. *Genome Biol* 6, R97.
- Budd, M.E., and Campbell, J.L. (1995). DNA polymerases required for repair of UV-induced damage in *Saccharomyces cerevisiae*. *Mol Cell Biol* 15, 2173-2179.
- Buterin, T., Meyer, C., Giese, B., and Naegeli, H. (2005). DNA quality control by conformational readout on the undamaged strand of the double helix. *Chem Biol* 12, 913-922.
- Caldecott, K., Aoufouchi, S., Johnson, P., and Shall, S. (1996). XRCC1 polypeptide interacts with DNA polymerase beta and possibly poly (ADP-ribose) polymerase, and DNA ligase III is a novel molecular 'nick-sensor' in vitro. *Nucleic Acids Res* 24, 4387-4394.
- Camenisch, U., Dip, R., Schumacher, S.B., Schuler, B., and Naegeli, H. (2006). Recognition of helical kinks by xeroderma pigmentosum group A protein triggers DNA excision repair. *Nat Struct Mol Biol* 13, 278-284.
- Camenisch, U., Trautlein, D., Clement, F.C., Fei, J., Leitenstorfer, A., Ferrando-May, E., and Naegeli, H. (2009). Two-stage dynamic DNA quality check by xeroderma pigmentosum group C protein. *EMBO J* 28, 2387-2399.
- Campalans, A., Marsin, S., Nakabeppu, Y., O'connor, T., Boiteux, S., and Radicella, J. (2005). XRCC1 interactions with multiple DNA glycosylases: a model for its recruitment to base excision repair. *DNA Repair (Amst)* 4, 826-835.
- Chasman, D.I., Lue, N.F., Buchman, A.R., LaPointe, J.W., Lorch, Y., and Kornberg, R.D. (1990). A yeast protein that influences the chromatin structure of UASG and functions as a powerful auxiliary gene activator. *Genes Dev* 4, 503-514.
- Chaudhuri, S., Wyrick, J.J., and Smerdon, M.J. (2009). Histone H3 Lys79 methylation is required for efficient nucleotide excision repair in a silenced locus of *Saccharomyces cerevisiae*. *Nucleic Acids Res* 37, 1690-1700.
- Chen, D., Herman, T., and Demple, B. (1991). Two distinct human DNA diesterases that hydrolyze 3'-blocking deoxyribose fragments from oxidized DNA. *Nucleic Acids Res* 19, 5907-5914.

References

- Chen, L., and Madura, K. (2002). Rad23 promotes the targeting of proteolytic substrates to the proteasome. *Mol Cell Biol* 22, 4902-4913.
- Chen, L., Shinde, U., Ortolan, T.G., and Madura, K. (2001). Ubiquitin-associated (UBA) domains in Rad23 bind ubiquitin and promote inhibition of multi-ubiquitin chain assembly. *EMBO Rep* 2, 933-938.
- Chen, X., Ding, B., LeJeune, D., Ruggiero, C., and Li, S. (2009). Rpb1 sumoylation in response to UV radiation or transcriptional impairment in yeast. *PLoS One* 4, e5267.
- Cho, G., Kim, J., Rho, H.M., and Jung, G. (1995). Structure-function analysis of the DNA binding domain of *Saccharomyces cerevisiae* ABF1. *Nucleic Acids Res* 23, 2980-2987.
- Christians, F.C., and Hanawalt, P.C. (1992). Inhibition of transcription and strand-specific DNA repair by alpha-amanitin in Chinese hamster ovary cells. *Mutat Res* 274, 93-101.
- Citterio, E., Rademakers, S., van der Horst, G.T., van Gool, A.J., Hoeijmakers, J.H., and Vermeulen, W. (1998). Biochemical and biological characterization of wild-type and ATPase-deficient Cockayne syndrome B repair protein. *J Biol Chem* 273, 11844-11851.
- Citterio, E., Van Den Boom, V., Schnitzler, G., Kanaar, R., Bonte, E., Kingston, R.E., Hoeijmakers, J.H., and Vermeulen, W. (2000). ATP-dependent chromatin remodeling by the Cockayne syndrome B DNA repair-transcription-coupling factor. *Mol Cell Biol* 20, 7643-7653.
- Clapier, C.R., and Cairns, B.R. (2009). The biology of chromatin remodeling complexes. *Annu Rev Biochem* 78, 273-304.
- Coin, F., Oksenych, V., and Egly, J.M. (2007). Distinct roles for the XPB/p52 and XPD/p44 subcomplexes of TFIIH in damaged DNA opening during nucleotide excision repair. *Mol Cell* 26, 245-256.
- Coin, F., Oksenych, V., Mocquet, V., Groh, S., Blattner, C., and Egly, J.M. (2008). Nucleotide excision repair driven by the dissociation of CAK from TFIIH. *Mol Cell* 31, 9-20.
- Coin, F., Proietti De Santis, L., Nardo, T., Zlobinskaya, O., Stefanini, M., and Egly, J. (2006). p8/TTD-A as a repair-specific TFIIH subunit. *Mol Cell* 21, 215-226.
- Collins, G.A., Lipford, J.R., Deshaies, R.J., and Tansey, W.P. (2009). Gal4 turnover and transcription activation. *Nature* 461, E7; discussion E8.
- Collins, G.A., and Tansey, W.P. (2006). The proteasome: a utility tool for transcription? *Curr Opin Genet Dev* 16, 197-202.
- Constantin, N., Dzantiev, L., Kadyrov, F.A., and Modrich, P. (2005). Human mismatch repair: reconstitution of a nick-directed bidirectional reaction. *J Biol Chem* 280, 39752-39761.

References

- Constantinou, A., Gunz, D., Evans, E., Lalle, P., Bates, P.A., Wood, R.D., and Clarkson, S.G. (1999). Conserved residues of human XPG protein important for nuclease activity and function in nucleotide excision repair. *J Biol Chem* 274, 5637-5648.
- Cortes Ledesma, F., El Khamisy, S., Zuma, M., Osborn, K., and Caldecott, K. (2009). A human 5'-tyrosyl DNA phosphodiesterase that repairs topoisomerase-mediated DNA damage. *Nature* 461, 674-678.
- Courdavault, S., Baudouin, C., Charveron, M., Canguilhem, B., Favier, A., Cadet, J., and Douki, T. (2005). Repair of the three main types of bipyrimidine DNA photoproducts in human keratinocytes exposed to UVB and UVA radiations. *DNA Repair (Amst)* 4, 836-844.
- Courdavault, S., Baudouin, C., Charveron, M., Favier, A., Cadet, J., and Douki, T. (2004). Larger yield of cyclobutane dimers than 8-oxo-7,8-dihydroguanine in the DNA of UVA-irradiated human skin cells. *Mutat Res* 556, 135-142.
- Crouse, G.F. (2010). An end for mismatch repair. *Proc Natl Acad Sci U S A* 107, 20851-20852.
- Dantuma, N.P., Heinen, C., and Hoogstraten, D. (2009). The ubiquitin receptor Rad23: At the crossroads of nucleotide excision repair and proteasomal degradation. *DNA Repair (Amst)* 8, 449-460.
- Datta, A., Bagchi, S., Nag, A., Shiyanov, P., Adami, G.R., Yoon, T., and Raychaudhuri, P. (2001). The p48 subunit of the damaged-DNA binding protein DDB associates with the CBP/p300 family of histone acetyltransferase. *Mutat Res* 486, 89-97.
- Daviet, S., Couvé-Privat, S., Gros, L., Shinozuka, K., Ide, H., Saparbaev, M., and Ishchenko, A. (2007). Major oxidative products of cytosine are substrates for the nucleotide incision repair pathway. *DNA Repair (Amst)* 6, 8-18.
- de Laat, W.L., Appeldoorn, E., Jaspers, N.G., and Hoeijmakers, J.H. (1998a). DNA structural elements required for ERCC1-XPF endonuclease activity. *J Biol Chem* 273, 7835-7842.
- de Laat, W.L., Appeldoorn, E., Sugasawa, K., Weterings, E., Jaspers, N.G., and Hoeijmakers, J.H. (1998b). DNA-binding polarity of human replication protein A positions nucleases in nucleotide excision repair. *Genes Dev* 12, 2598-2609.
- de Laat, W.L., Sijbers, A.M., Odijk, H., Jaspers, N.G., and Hoeijmakers, J.H. (1998c). Mapping of interaction domains between human repair proteins ERCC1 and XPF. *Nucleic Acids Res* 26, 4146-4152.
- de Murcia, G., and Ménissier de Murcia, J. (1994). Poly(ADP-ribose) polymerase: a molecular nick-sensor. *Trends Biochem Sci* 19, 172-176.

- de Winde, J.H., and Grivell, L.A. (1992). Global regulation of mitochondrial biogenesis in *Saccharomyces cerevisiae*: ABF1 and CPF1 play opposite roles in regulating expression of the QCR8 gene, which encodes subunit VIII of the mitochondrial ubiquinol-cytochrome c oxidoreductase. *Mol Cell Biol* 12, 2872-2883.
- Deaconescu, A.M., Savery, N., and Darst, S.A. (2007). The bacterial transcription repair coupling factor. *Curr Opin Struct Biol* 17, 96-102.
- Della Seta, F., Ciafre, S.A., Marck, C., Santoro, B., Presutti, C., Sentenac, A., and Bozzoni, I. (1990). The ABF1 factor is the transcriptional activator of the L2 ribosomal protein genes in *Saccharomyces cerevisiae*. *Mol Cell Biol* 10, 2437-2441.
- Deminoff, S.J., and Santangelo, G.M. (2001). Rap1p requires Gcr1p and Gcr2p homodimers to activate ribosomal protein and glycolytic genes, respectively. *Genetics* 158, 133-143.
- den Dulk, B., Sun, S.M., de Ruijter, M., Brandsma, J.A., and Brouwer, J. (2006). Rad33, a new factor involved in nucleotide excision repair in *Saccharomyces cerevisiae*. *DNA Repair (Amst)* 5, 683-692.
- den Dulk, B., van Eijk, P., de Ruijter, M., Brandsma, J.A., and Brouwer, J. (2008). The NER protein Rad33 shows functional homology to human Centrin2 and is involved in modification of Rad4. *DNA Repair (Amst)* 7, 858-868.
- Deshaies, R.J., and Joazeiro, C.A. (2009). RING domain E3 ubiquitin ligases. *Annu Rev Biochem* 78, 399-434.
- Diffley, J.F. (1992). Global regulators of chromosome function in yeast. *Antonie Van Leeuwenhoek* 62, 25-33.
- Diffley, J.F., and Stillman, B. (1989). Similarity between the transcriptional silencer binding proteins ABF1 and RAP1. *Science* 246, 1034-1038.
- Dion, M.F., Kaplan, T., Kim, M., Buratowski, S., Friedman, N., and Rando, O.J. (2007). Dynamics of replication-independent histone turnover in budding yeast. *Science* 315, 1405-1408.
- Dobbin, K.K., Kawasaki, E.S., Petersen, D.W., and Simon, R.M. (2005). Characterizing dye bias in microarray experiments. *Bioinformatics* 21, 2430-2437.
- Donahue, B.A., Fuchs, R.P., Reines, D., and Hanawalt, P.C. (1996). Effects of aminofluorene and acetylaminofluorene DNA adducts on transcriptional elongation by RNA polymerase II. *J Biol Chem* 271, 10588-10594.
- Dorsman, J.C., van Heeswijk, W.C., and Grivell, L.A. (1988). Identification of two factors which bind to the upstream sequences of a number of nuclear genes coding for mitochondrial proteins and to genetic elements important for cell division in yeast. *Nucleic Acids Res* 16, 7287-7301.
- Douki, T., and Cadet, J. (2001). Individual determination of the yield of the main UV-induced dimeric pyrimidine photoproducts in DNA suggests a high mutagenicity of CC photolesions. *Biochemistry* 40, 2495-2501.

- Douki, T., Court, M., Sauvaigo, S., Odin, F., and Cadet, J. (2000). Formation of the main UV-induced thymine dimeric lesions within isolated and cellular DNA as measured by high performance liquid chromatography-tandem mass spectrometry. *J Biol Chem* 275, 11678-11685.
- Douki, T., Reynaud-Angelin, A., Cadet, J., and Sage, E. (2003). Bipyrimidine photoproducts rather than oxidative lesions are the main type of DNA damage involved in the genotoxic effect of solar UVA radiation. *Biochemistry* 42, 9221-9226.
- Drapkin, R., Reardon, J., Ansari, A., Huang, J., Zawel, L., Ahn, K., Sancar, A., and Reinberg, D. (1994). Dual role of TFIIH in DNA excision repair and in transcription by RNA polymerase II. *Nature* 368, 769-772.
- Drobetsky, E.A., Grosovsky, A.J., and Glickman, B.W. (1987). The specificity of UV-induced mutations at an endogenous locus in mammalian cells. *Proc Natl Acad Sci U S A* 84, 9103-9107.
- Dumstorf, C.A., Clark, A.B., Lin, Q., Kissling, G.E., Yuan, T., Kucherlapati, R., McGregor, W.G., and Kunkel, T.A. (2006). Participation of mouse DNA polymerase iota in strand-biased mutagenic bypass of UV photoproducts and suppression of skin cancer. *Proc Natl Acad Sci U S A* 103, 18083-18088.
- Dunand-Sauthier, I., Hohl, M., Thorel, F., Jaquier-Gubler, P., Clarkson, S.G., and Scharer, O.D. (2005). The spacer region of XPG mediates recruitment to nucleotide excision repair complexes and determines substrate specificity. *J Biol Chem* 280, 7030-7037.
- Durr, H., Flaus, A., Owen-Hughes, T., and Hopfner, K.P. (2006). Snf2 family ATPases and DExx box helicases: differences and unifying concepts from high-resolution crystal structures. *Nucleic Acids Res* 34, 4160-4167.
- Dzantiev, L., Constantin, N., Genschel, J., Iyer, R.R., Burgers, P.M., and Modrich, P. (2004). A defined human system that supports bidirectional mismatch-provoked excision. *Mol Cell* 15, 31-41.
- Einerhand, A.W., Kos, W., Smart, W.C., Kal, A.J., Tabak, H.F., and Cooper, T.G. (1995). The upstream region of the FOX3 gene encoding peroxisomal 3-oxoacyl-coenzyme A thiolase in *Saccharomyces cerevisiae* contains ABF1- and replication protein A-binding sites that participate in its regulation by glucose repression. *Mol Cell Biol* 15, 3405-3414.
- El-Khamisy, S.F., Masutani, M., Suzuki, H., and Caldecott, K.W. (2003). A requirement for PARP-1 for the assembly or stability of XRCC1 nuclear foci at sites of oxidative DNA damage. *Nucleic Acids Res* 31, 5526-5533.
- El-Mahdy, M.A., Zhu, Q., Wang, Q.E., Wani, G., Praetorius-Ibba, M., and Wani, A.A. (2006). Cullin 4A-mediated proteolysis of DDB2 protein at DNA damage sites regulates in vivo lesion recognition by XPC. *J Biol Chem* 281, 13404-13411.
- Elbi, C., Walker, D.A., Romero, G., Sullivan, W.P., Toft, D.O., Hager, G.L., and DeFranco, D.B. (2004). Molecular chaperones function as steroid receptor nuclear mobility factors. *Proc Natl Acad Sci U S A* 101, 2876-2881.

- Elf, J., Li, G.W., and Xie, X.S. (2007). Probing transcription factor dynamics at the single-molecule level in a living cell. *Science* 316, 1191-1194.
- Elsasser, S., Chandler-Militello, D., Muller, B., Hanna, J., and Finley, D. (2004). Rad23 and Rpn10 serve as alternative ubiquitin receptors for the proteasome. *J Biol Chem* 279, 26817-26822.
- Elsasser, S., Gali, R.R., Schwickart, M., Larsen, C.N., Leggett, D.S., Muller, B., Feng, M.T., Tubing, F., Dittmar, G.A., and Finley, D. (2002). Proteasome subunit Rpn1 binds ubiquitin-like protein domains. *Nat Cell Biol* 4, 725-730.
- Essers, J., Theil, A.F., Baldeyron, C., van Cappellen, W.A., Houtsmuller, A.B., Kanaar, R., and Vermeulen, W. (2005). Nuclear dynamics of PCNA in DNA replication and repair. *Mol Cell Biol* 25, 9350-9359.
- Evans, E., Fellows, J., Coffey, A., and Wood, R.D. (1997a). Open complex formation around a lesion during nucleotide excision repair provides a structure for cleavage by human XPG protein. *EMBO J* 16, 625-638.
- Evans, E., Moggs, J.G., Hwang, J.R., Egly, J.M., and Wood, R.D. (1997b). Mechanism of open complex and dual incision formation by human nucleotide excision repair factors. *EMBO J* 16, 6559-6573.
- Fan, W., and Luo, J. (2010). SIRT1 regulates UV-induced DNA repair through deacetylating XPA. *Mol Cell* 39, 247-258.
- Ferdous, A., Sikder, D., Gillette, T., Nalley, K., Kodadek, T., and Johnston, S.A. (2007). The role of the proteasomal ATPases and activator monoubiquitylation in regulating Gal4 binding to promoters. *Genes Dev* 21, 112-123.
- Finley, D. (2009). Recognition and processing of ubiquitin-protein conjugates by the proteasome. *Annu Rev Biochem* 78, 477-513.
- Fitch, M.E., Nakajima, S., Yasui, A., and Ford, J.M. (2003). In vivo recruitment of XPC to UV-induced cyclobutane pyrimidine dimers by the DDB2 gene product. *J Biol Chem* 278, 46906-46910.
- Flaus, A., Martin, D.M., Barton, G.J., and Owen-Hughes, T. (2006). Identification of multiple distinct Snf2 subfamilies with conserved structural motifs. *Nucleic Acids Res* 34, 2887-2905.
- Fletcher, T.M., Ryu, B.W., Baumann, C.T., Warren, B.S., Fragoso, G., John, S., and Hager, G.L. (2000). Structure and dynamic properties of a glucocorticoid receptor-induced chromatin transition. *Mol Cell Biol* 20, 6466-6475.
- Fletcher, T.M., Xiao, N., Mautino, G., Baumann, C.T., Wolford, R., Warren, B.S., and Hager, G.L. (2002). ATP-dependent mobilization of the glucocorticoid receptor during chromatin remodeling. *Mol Cell Biol* 22, 3255-3263.
- Fourel, G., Miyake, T., Defossez, P.A., Li, R., and Gilson, E. (2002). General regulatory factors (GRFs) as genome partitioners. *J Biol Chem* 277, 41736-41743.

- Fousteri, M., Vermeulen, W., van Zeeland, A., and Mullenders, L. (2006a). Cockayne syndrome A and B proteins differentially regulate recruitment of chromatin remodeling and repair factors to stalled RNA polymerase II in vivo. *Mol Cell* 23, 471-482.
- Fousteri, M., Vermeulen, W., van Zeeland, A.A., and Mullenders, L.H. (2006b). Cockayne syndrome A and B proteins differentially regulate recruitment of chromatin remodeling and repair factors to stalled RNA polymerase II in vivo. *Mol Cell* 23, 471-482.
- Fox, D.L., and Good, D.J. (2008). Nescient helix-loop-helix 2 interacts with signal transducer and activator of transcription 3 to regulate transcription of prohormone convertase 1/3. *Mol Endocrinol* 22, 1438-1448.
- Francesconi, S.C., and Eisenberg, S. (1989). Purification and characterization of OBF1: a *Saccharomyces cerevisiae* protein that binds to autonomously replicating sequences. *Mol Cell Biol* 9, 2906-2913.
- Freeman, B.C., Felts, S.J., Toft, D.O., and Yamamoto, K.R. (2000). The p23 molecular chaperones act at a late step in intracellular receptor action to differentially affect ligand efficacies. *Genes Dev* 14, 422-434.
- Freeman, B.C., and Yamamoto, K.R. (2002). Disassembly of transcriptional regulatory complexes by molecular chaperones. *Science* 296, 2232-2235.
- Friedberg, E.C. (2006). DNA repair and mutagenesis, 2nd edn (Washington: ASM Press).
- Frit, P., Kwon, K., Coin, F., Auriol, J., Dubaele, S., Salles, B., and Egly, J.M. (2002). Transcriptional activators stimulate DNA repair. *Mol Cell* 10, 1391-1401.
- Ganapathi, M., Palumbo, M.J., Ansari, S.A., He, Q., Tsui, K., Nislow, C., and Morse, R.H. (2010). Extensive role of the general regulatory factors, Abf1 and Rap1, in determining genome-wide chromatin structure in budding yeast. *Nucleic Acids Res.*
- Gary, R., Ludwig, D.L., Cornelius, H.L., MacInnes, M.A., and Park, M.S. (1997). The DNA repair endonuclease XPG binds to proliferating cell nuclear antigen (PCNA) and shares sequence elements with the PCNA-binding regions of FEN-1 and cyclin-dependent kinase inhibitor p21. *J Biol Chem* 272, 24522-24529.
- Gentleman, R. (2005). Bioinformatics and computational biology solutions using R and Bioconductor (New York ; Cambridge: Springer).
- Giannattasio, M., Follonier, C., Tourriere, H., Puddu, F., Lazzaro, F., Pasero, P., Lopes, M., Plevani, P., and Muzi-Falconi, M. (2010). Exo1 competes with repair synthesis, converts NER intermediates to long ssDNA gaps, and promotes checkpoint activation. *Mol Cell* 40, 50-62.
- Giannattasio, M., Lazzaro, F., Longhese, M.P., Plevani, P., and Muzi-Falconi, M. (2004). Physical and functional interactions between nucleotide excision repair and DNA damage checkpoint. *EMBO J* 23, 429-438.

- Gibbs, P.E., Borden, A., and Lawrence, C.W. (1995). The T-T pyrimidine (6-4) pyrimidinone UV photoproduct is much less mutagenic in yeast than in *Escherichia coli*. *Nucleic Acids Res* 23, 1919-1922.
- Gibbs, P.E., Kilbey, B.J., Banerjee, S.K., and Lawrence, C.W. (1993). The frequency and accuracy of replication past a thymine-thymine cyclobutane dimer are very different in *Saccharomyces cerevisiae* and *Escherichia coli*. *J Bacteriol* 175, 2607-2612.
- Gibbs, P.E., McDonald, J., Woodgate, R., and Lawrence, C.W. (2005). The relative roles in vivo of *Saccharomyces cerevisiae* Pol eta, Pol zeta, Rev1 protein and Pol32 in the bypass and mutation induction of an abasic site, T-T (6-4) photoadduct and T-T cis-syn cyclobutane dimer. *Genetics* 169, 575-582.
- Giglia-Mari, G., Coin, F., Ranish, J., Hoogstraten, D., Theil, A., Wijgers, N., Jaspers, N., Raams, A., Argentini, M., van der Spek, P., *et al.* (2004). A new, tenth subunit of TFIIH is responsible for the DNA repair syndrome trichothiodystrophy group A. *Nat Genet* 36, 714-719.
- Giglia-Mari, G., Miquel, C., Theil, A.F., Mari, P.O., Hoogstraten, D., Ng, J.M., Dinant, C., Hoeijmakers, J.H., and Vermeulen, W. (2006). Dynamic interaction of TTDA with TFIIH is stabilized by nucleotide excision repair in living cells. *PLoS Biol* 4, e156.
- Gillet, L.C., and Scharer, O.D. (2006). Molecular mechanisms of mammalian global genome nucleotide excision repair. *Chem Rev* 106, 253-276.
- Gillette, T.G., Huang, W., Russell, S.J., Reed, S.H., Johnston, S.A., and Friedberg, E.C. (2001). The 19S complex of the proteasome regulates nucleotide excision repair in yeast. *Genes Dev* 15, 1528-1539.
- Gillette, T.G., Yu, S., Zhou, Z., Waters, R., Johnston, S.A., and Reed, S.H. (2006). Distinct functions of the ubiquitin-proteasome pathway influence nucleotide excision repair. *EMBO J* 25, 2529-2538.
- Glynn, E.F., Megee, P.C., Yu, H.G., Mistrot, C., Unal, E., Koshland, D.E., DeRisi, J.L., and Gerton, J.L. (2004). Genome-wide mapping of the cohesin complex in the yeast *Saccharomyces cerevisiae*. *PLoS Biol* 2, E259.
- Goncalves, P.M., Maurer, K., Mager, W.H., and Planta, R.J. (1992). *Kluyveromyces* contains a functional ABF1-homologue. *Nucleic Acids Res* 20, 2211-2215.
- Goncalves, P.M., Maurer, K., van Nieuw Amerongen, G., Bergkamp-Steffens, K., Mager, W.H., and Planta, R.J. (1996). C-terminal domains of general regulatory factors Abf1p and Rap1p in *Saccharomyces cerevisiae* display functional similarity. *Mol Microbiol* 19, 535-543.
- Gong, F., Fahy, D., and Smerdon, M.J. (2006). Rad4-Rad23 interaction with SWI/SNF links ATP-dependent chromatin remodeling with nucleotide excision repair. *Nat Struct Mol Biol* 13, 902-907.

- Gordan, R., Hartemink, A.J., and Bulyk, M.L. (2009). Distinguishing direct versus indirect transcription factor-DNA interactions. *Genome Res* 19, 2090-2100.
- Gorman, J., Chowdhury, A., Surtees, J.A., Shimada, J., Reichman, D.R., Alani, E., and Greene, E.C. (2007). Dynamic basis for one-dimensional DNA scanning by the mismatch repair complex Msh2-Msh6. *Mol Cell* 28, 359-370.
- Green, C.M., and Almouzni, G. (2002). When repair meets chromatin. First in series on chromatin dynamics. *EMBO Rep* 3, 28-33.
- Green, C.M., and Almouzni, G. (2003). Local action of the chromatin assembly factor CAF-1 at sites of nucleotide excision repair in vivo. *EMBO J* 22, 5163-5174.
- Greer, S., Zika, E., Conti, B., Zhu, X., and Ting, J. (2003). Enhancement of CIITA transcriptional function by ubiquitin. *Nat Immunol* 4, 1074-1082.
- Groisman, R., Kuraoka, I., Chevallier, O., Gaye, N., Magnaldo, T., Tanaka, K., Kisselev, A., Harel-Bellan, A., and Nakatani, Y. (2006). CSA-dependent degradation of CSB by the ubiquitin-proteasome pathway establishes a link between complementation factors of the Cockayne syndrome. *Genes Dev* 20, 1429-1434.
- Groisman, R., Polanowska, J., Kuraoka, I., Sawada, J., Saijo, M., Drapkin, R., Kisselev, A.F., Tanaka, K., and Nakatani, Y. (2003). The ubiquitin ligase activity in the DDB2 and CSA complexes is differentially regulated by the COP9 signalosome in response to DNA damage. *Cell* 113, 357-367.
- Gueranger, Q., Stary, A., Aoufouchi, S., Faili, A., Sarasin, A., Reynaud, C.A., and Weill, J.C. (2008). Role of DNA polymerases eta, iota and zeta in UV resistance and UV-induced mutagenesis in a human cell line. *DNA Repair (Amst)* 7, 1551-1562.
- Guerrero-Santoro, J., Kapetanaki, M.G., Hsieh, C.L., Gorbachinsky, I., Levine, A.S., and Raptic-Otrin, V. (2008). The cullin 4B-based UV-damaged DNA-binding protein ligase binds to UV-damaged chromatin and ubiquitinates histone H2A. *Cancer Res* 68, 5014-5022.
- Guo, R., Chen, J., Mitchell, D.L., and Johnson, D.G. (2010a). GCN5 and E2F1 stimulate nucleotide excision repair by promoting H3K9 acetylation at sites of damage. *Nucleic Acids Res* 39, 1390-1397.
- Guo, R., Chen, J., Zhu, F., Biswas, A.K., Berton, T.R., Mitchell, D.L., and Johnson, D.G. (2010b). E2F1 localizes to sites of UV-induced DNA damage to enhance nucleotide excision repair. *J Biol Chem* 285, 19308-19315.
- Guzder, S.N., Habraken, Y., Sung, P., Prakash, L., and Prakash, S. (1995). Reconstitution of yeast nucleotide excision repair with purified Rad proteins, replication protein A, and transcription factor TFIIH. *J Biol Chem* 270, 12973-12976.
- Guzder, S.N., Habraken, Y., Sung, P., Prakash, L., and Prakash, S. (1996a). RAD26, the yeast homolog of human Cockayne's syndrome group B gene, encodes a DNA-dependent ATPase. *J Biol Chem* 271, 18314-18317.

- Guzder, S.N., Sommers, C.H., Prakash, L., and Prakash, S. (2006). Complex formation with damage recognition protein Rad14 is essential for *Saccharomyces cerevisiae* Rad1-Rad10 nuclease to perform its function in nucleotide excision repair in vivo. *Mol Cell Biol* 26, 1135-1141.
- Guzder, S.N., Sung, P., Bailly, V., Prakash, L., and Prakash, S. (1994). RAD25 is a DNA helicase required for DNA repair and RNA polymerase II transcription. *Nature* 369, 578-581.
- Guzder, S.N., Sung, P., Prakash, L., and Prakash, S. (1993). Yeast DNA-repair gene RAD14 encodes a zinc metalloprotein with affinity for ultraviolet-damaged DNA. *Proc Natl Acad Sci U S A* 90, 5433-5437.
- Guzder, S.N., Sung, P., Prakash, L., and Prakash, S. (1996b). Nucleotide excision repair in yeast is mediated by sequential assembly of repair factors and not by a pre-assembled repairosome. *J Biol Chem* 271, 8903-8910.
- Guzder, S.N., Sung, P., Prakash, L., and Prakash, S. (1997). Yeast Rad7-Rad16 complex, specific for the nucleotide excision repair of the nontranscribed DNA strand, is an ATP-dependent DNA damage sensor. *J Biol Chem* 272, 21665-21668.
- Guzder, S.N., Sung, P., Prakash, L., and Prakash, S. (1998a). Affinity of yeast nucleotide excision repair factor 2, consisting of the Rad4 and Rad23 proteins, for ultraviolet damaged DNA. *J Biol Chem* 273, 31541-31546.
- Guzder, S.N., Sung, P., Prakash, L., and Prakash, S. (1998b). The DNA-dependent ATPase activity of yeast nucleotide excision repair factor 4 and its role in DNA damage recognition. *J Biol Chem* 273, 6292-6296.
- Guzder, S.N., Sung, P., Prakash, L., and Prakash, S. (1999). Synergistic interaction between yeast nucleotide excision repair factors NEF2 and NEF4 in the binding of ultraviolet-damaged DNA. *J Biol Chem* 274, 24257-24262.
- Habraken, Y., Sung, P., Prakash, L., and Prakash, S. (1995). Structure-specific nuclease activity in yeast nucleotide excision repair protein Rad2. *J Biol Chem* 270, 30194-30198.
- Habraken, Y., Sung, P., Prakash, S., and Prakash, L. (1996). Transcription factor TFIIH and DNA endonuclease Rad2 constitute yeast nucleotide excision repair factor 3: implications for nucleotide excision repair and Cockayne syndrome. *Proc Natl Acad Sci U S A* 93, 10718-10722.
- Hager, G.L., Elbi, C., Johnson, T.A., Voss, T., Nagaich, A.K., Schiltz, R.L., Qiu, Y., and John, S. (2006). Chromatin dynamics and the evolution of alternate promoter states. *Chromosome Res* 14, 107-116.
- Hager, G.L., McNally, J.G., and Misteli, T. (2009). Transcription dynamics. *Mol Cell* 35, 741-753.
- Halfter, H., Kavety, B., Vandekerckhove, J., Kiefer, F., and Gallwitz, D. (1989). Sequence, expression and mutational analysis of BAF1, a transcriptional activator and ARS1-binding protein of the yeast *Saccharomyces cerevisiae*. *EMBO J* 8, 4265-4272.

- Hanawalt, P.C., and Spivak, G. (2008). Transcription-coupled DNA repair: two decades of progress and surprises. *Nat Rev Mol Cell Biol* 9, 958-970.
- Hara, R., and Sancar, A. (2002). The SWI/SNF chromatin-remodeling factor stimulates repair by human excision nuclease in the mononucleosome core particle. *Mol Cell Biol* 22, 6779-6787.
- Hara, R., and Sancar, A. (2003). Effect of damage type on stimulation of human excision nuclease by SWI/SNF chromatin remodeling factor. *Mol Cell Biol* 23, 4121-4125.
- Haracska, L., Johnson, R.E., Unk, I., Phillips, B.B., Hurwitz, J., Prakash, L., and Prakash, S. (2001). Targeting of human DNA polymerase ι to the replication machinery via interaction with PCNA. *Proc Natl Acad Sci U S A* 98, 14256-14261.
- Harbison, C.T., Gordon, D.B., Lee, T.I., Rinaldi, N.J., Macisaac, K.D., Danford, T.W., Hannett, N.M., Tagne, J.B., Reynolds, D.B., Yoo, J., *et al.* (2004). Transcriptional regulatory code of a eukaryotic genome. *Nature* 431, 99-104.
- Hartley, P.D., and Madhani, H.D. (2009). Mechanisms that specify promoter nucleosome location and identity. *Cell* 137, 445-458.
- Hartmann-Petersen, R., Hendil, K.B., and Gordon, C. (2003). Ubiquitin binding proteins protect ubiquitin conjugates from disassembly. *FEBS Lett* 535, 77-81.
- Hayes, S., Shiyanov, P., Chen, X., and Raychaudhuri, P. (1998). DDB, a putative DNA repair protein, can function as a transcriptional partner of E2F1. *Mol Cell Biol* 18, 240-249.
- Hazra, T., Izumi, T., Boldogh, I., Imhoff, B., Kow, Y., Jaruga, P., Dizdaroglu, M., and Mitra, S. (2002). Identification and characterization of a human DNA glycosylase for repair of modified bases in oxidatively damaged DNA. *Proc Natl Acad Sci U S A* 99, 3523-3528.
- He, Z., Henricksen, L.A., Wold, M.S., and Ingles, C.J. (1995). RPA involvement in the damage-recognition and incision steps of nucleotide excision repair. *Nature* 374, 566-569.
- He, Z., Wong, J.M., Maniar, H.S., Brill, S.J., and Ingles, C.J. (1996). Assessing the requirements for nucleotide excision repair proteins of *Saccharomyces cerevisiae* in an in vitro system. *J Biol Chem* 271, 28243-28249.
- Heessen, S., Masucci, M.G., and Dantuma, N.P. (2005). The UBA2 domain functions as an intrinsic stabilization signal that protects Rad23 from proteasomal degradation. *Mol Cell* 18, 225-235.
- Hegde, M.L., Hazra, T.K., and Mitra, S. (2008). Early steps in the DNA base excision/single-strand interruption repair pathway in mammalian cells. *Cell Res* 18, 27-47.

- Henning, K.A., Li, L., Iyer, N., McDaniel, L.D., Reagan, M.S., Legerski, R., Schultz, R.A., Stefanini, M., Lehmann, A.R., Mayne, L.V., *et al.* (1995). The Cockayne syndrome group A gene encodes a WD repeat protein that interacts with CSB protein and a subunit of RNA polymerase II TFIIF. *Cell* 82, 555-564.
- Hess, M.T., Schwitter, U., Petretta, M., Giese, B., and Naegeli, H. (1997). Bipartite substrate discrimination by human nucleotide excision repair. *Proc Natl Acad Sci U S A* 94, 6664-6669.
- Hesselberth, J.R., Chen, X., Zhang, Z., Sabo, P.J., Sandstrom, R., Reynolds, A.P., Thurman, R.E., Neph, S., Kuehn, M.S., Noble, W.S., *et al.* (2009). Global mapping of protein-DNA interactions in vivo by digital genomic footprinting. *Nat Methods* 6, 283-289.
- Heyer, W.D., Ehmsen, K.T., and Liu, J. (2010). Regulation of homologous recombination in eukaryotes. *Annu Rev Genet* 44, 113-139.
- Hohl, M., Thorel, F., Clarkson, S.G., and Scharer, O.D. (2003). Structural determinants for substrate binding and catalysis by the structure-specific endonuclease XPG. *J Biol Chem* 278, 19500-19508.
- Hoogstraten, D., Bergink, S., Ng, J.M., Verbiest, V.H., Luijsterburg, M.S., Geverts, B., Raams, A., Dinant, C., Hoeijmakers, J.H., Vermeulen, W., *et al.* (2008). Versatile DNA damage detection by the global genome nucleotide excision repair protein XPC. *J Cell Sci* 121, 2850-2859.
- Hoogstraten, D., Nigg, A.L., Heath, H., Mullenders, L.H., van Driel, R., Hoeijmakers, J.H., Vermeulen, W., and Houtsmuller, A.B. (2002). Rapid switching of TFIIF between RNA polymerase I and II transcription and DNA repair in vivo. *Mol Cell* 10, 1163-1174.
- Houtsmuller, A.B., Rademakers, S., Nigg, A.L., Hoogstraten, D., Hoeijmakers, J.H., and Vermeulen, W. (1999). Action of DNA repair endonuclease ERCC1/XPF in living cells. *Science* 284, 958-961.
- Hu, Y.F., Hao, Z.L., and Li, R. (1999). Chromatin remodeling and activation of chromosomal DNA replication by an acidic transcriptional activation domain from BRCA1. *Genes Dev* 13, 637-642.
- Huang, J., Svoboda, D., Reardon, J., and Sancar, A. (1992). Human nucleotide excision nuclease removes thymine dimers from DNA by incising the 22nd phosphodiester bond 5' and the 6th phosphodiester bond 3' to the photodimer. *Proc Natl Acad Sci U S A* 89, 3664-3668.
- Hwang, B.J., Ford, J.M., Hanawalt, P.C., and Chu, G. (1999). Expression of the p48 xeroderma pigmentosum gene is p53-dependent and is involved in global genomic repair. *Proc Natl Acad Sci U S A* 96, 424-428.
- Interthal, H., Pouliot, J., and Champoux, J. (2001). The tyrosyl-DNA phosphodiesterase Tdp1 is a member of the phospholipase D superfamily. *Proc Natl Acad Sci U S A* 98, 12009-12014.

- Ischenko, A., and Saparbaev, M. (2002). Alternative nucleotide incision repair pathway for oxidative DNA damage. *Nature* *415*, 183-187.
- Ito, S., Kuraoka, I., Chymkowitch, P., Compe, E., Takedachi, A., Ishigami, C., Coin, F., Egly, J.M., and Tanaka, K. (2007). XPG stabilizes TFIIH, allowing transactivation of nuclear receptors: implications for Cockayne syndrome in XP-G/CS patients. *Mol Cell* *26*, 231-243.
- Jans, J., Schul, W., Sert, Y.G., Rijksen, Y., Rebel, H., Eker, A.P., Nakajima, S., van Steeg, H., de Gruijl, F.R., Yasui, A., *et al.* (2005). Powerful skin cancer protection by a CPD-photolyase transgene. *Curr Biol* *15*, 105-115.
- Jansen, L.E., den Dulk, H., Brouns, R.M., de Ruijter, M., Brandsma, J.A., and Brouwer, J. (2000). Spt4 modulates Rad26 requirement in transcription-coupled nucleotide excision repair. *EMBO J* *19*, 6498-6507.
- Jansen, L.E., Verhage, R.A., and Brouwer, J. (1998). Preferential binding of yeast Rad4.Rad23 complex to damaged DNA. *J Biol Chem* *273*, 33111-33114.
- Jiang, Y., Rabbi, M., Kim, M., Ke, C., Lee, W., Clark, R.L., Mieczkowski, P.A., and Marszalek, P.E. (2009). UVA generates pyrimidine dimers in DNA directly. *Biophys J* *96*, 1151-1158.
- Jiang, Y., Wang, X., Bao, S., Guo, R., Johnson, D.G., Shen, X., and Li, L. (2010). INO80 chromatin remodeling complex promotes the removal of UV lesions by the nucleotide excision repair pathway. *Proc Natl Acad Sci U S A* *107*, 17274-17279.
- Jin, Y., Rodriguez, A.M., and Wyrick, J.J. (2009). Genetic and genomewide analysis of simultaneous mutations in acetylated and methylated lysine residues in histone H3 in *Saccharomyces cerevisiae*. *Genetics* *181*, 461-472.
- Jiricny, J. (2006a). MutLalpha: at the cutting edge of mismatch repair. *Cell* *126*, 239-241.
- Jiricny, J. (2006b). The multifaceted mismatch-repair system. *Nat Rev Mol Cell Biol* *7*, 335-346.
- Johnson, R.E., Haracska, L., Prakash, S., and Prakash, L. (2001). Role of DNA polymerase zeta in the bypass of a (6-4) TT photoproduct. *Mol Cell Biol* *21*, 3558-3563.
- Johnson, R.E., Kondratick, C.M., Prakash, S., and Prakash, L. (1999a). hRAD30 mutations in the variant form of xeroderma pigmentosum. *Science* *285*, 263-265.
- Johnson, R.E., Prakash, S., and Prakash, L. (1999b). Efficient bypass of a thymine-thymine dimer by yeast DNA polymerase, Poleta. *Science* *283*, 1001-1004.
- Johnson, R.E., Prakash, S., and Prakash, L. (2000a). The human DINB1 gene encodes the DNA polymerase Poltheta. *Proc Natl Acad Sci U S A* *97*, 3838-3843.

- Johnson, R.E., Washington, M.T., Haracska, L., Prakash, S., and Prakash, L. (2000b). Eukaryotic polymerases ι and ζ act sequentially to bypass DNA lesions. *Nature* **406**, 1015-1019.
- Kadonaga, J.T. (2004). Regulation of RNA polymerase II transcription by sequence-specific DNA binding factors. *Cell* **116**, 247-257.
- Kadyrov, F.A., Dzantiev, L., Constantin, N., and Modrich, P. (2006). Endonucleolytic function of MutL α in human mismatch repair. *Cell* **126**, 297-308.
- Kadyrov, F.A., Genschel, J., Fang, Y., Penland, E., Edelmann, W., and Modrich, P. (2009). A possible mechanism for exonuclease 1-independent eukaryotic mismatch repair. *Proc Natl Acad Sci U S A* **106**, 8495-8500.
- Kapetanaki, M.G., Guerrero-Santoro, J., Bisi, D.C., Hsieh, C.L., Rapic-Otrin, V., and Levine, A.S. (2006). The DDB1-CUL4ADDB2 ubiquitin ligase is deficient in xeroderma pigmentosum group E and targets histone H2A at UV-damaged DNA sites. *Proc Natl Acad Sci U S A* **103**, 2588-2593.
- Kaplan, N., Moore, I.K., Fondufe-Mittendorf, Y., Gossett, A.J., Tillo, D., Field, Y., LeProust, E.M., Hughes, T.R., Lieb, J.D., Widom, J., *et al.* (2009). The DNA-encoded nucleosome organization of a eukaryotic genome. *Nature* **458**, 362-366.
- Karpova, T.S., Chen, T.Y., Sprague, B.L., and McNally, J.G. (2004). Dynamic interactions of a transcription factor with DNA are accelerated by a chromatin remodeller. *EMBO Rep* **5**, 1064-1070.
- Karpova, T.S., Kim, M.J., Spriet, C., Nalley, K., Stasevich, T.J., Kherrouche, Z., Heliot, L., and McNally, J.G. (2008). Concurrent fast and slow cycling of a transcriptional activator at an endogenous promoter. *Science* **319**, 466-469.
- Kassabov, S.R., Henry, N.M., Zofall, M., Tsukiyama, T., and Bartholomew, B. (2002). High-resolution mapping of changes in histone-DNA contacts of nucleosomes remodeled by ISW2. *Mol Cell Biol* **22**, 7524-7534.
- Kelley, M.R., Kow, Y.W., and Wilson, D.M., 3rd (2003). Disparity between DNA base excision repair in yeast and mammals: translational implications. *Cancer Res* **63**, 549-554.
- Kelly, T.J., Jallepalli, P.V., and Clyne, R.K. (1994). Replication and transcription. Silence of the ORCs. *Curr Biol* **4**, 238-241.
- Kemp, M.G., Mason, A.C., Carreira, A., Reardon, J.T., Haring, S.J., Borgstahl, G.E., Kowalczykowski, S.C., Sancar, A., and Wold, M.S. (2010). An alternative form of replication protein A expressed in normal human tissues supports DNA repair. *J Biol Chem* **285**, 4788-4797.
- Khlimankov, D., Rechkunova, N.I., Kolpashchikov, D.M., Petruseva, I.O., Khodyreva, S.N., Favr, A., and Lavrik, O.I. (2001). [Interaction of human replication protein A with DNA-duplexes, containing gaps of varying sizes]. *Mol Biol (Mosk)* **35**, 827-835.

- Kibe, T., Ono, Y., Sato, K., and Ueno, M. (2007). Fission yeast Taz1 and RPA are synergistically required to prevent rapid telomere loss. *Mol Biol Cell* 18, 2378-2387.
- Kim, C., Paulus, B.F., and Wold, M.S. (1994). Interactions of human replication protein A with oligonucleotides. *Biochemistry* 33, 14197-14206.
- Kim, C., Snyder, R.O., and Wold, M.S. (1992). Binding properties of replication protein A from human and yeast cells. *Mol Cell Biol* 12, 3050-3059.
- Kim, I., Mi, K., and Rao, H. (2004). Multiple interactions of rad23 suggest a mechanism for ubiquitylated substrate delivery important in proteolysis. *Mol Biol Cell* 15, 3357-3365.
- Kim, Y.C., Wu, S.Y., Lim, H.S., Chiang, C.M., and Kodadek, T. (2009). Non-proteolytic regulation of p53-mediated transcription through destabilization of the activator-promoter complex by the proteasomal ATPases. *J Biol Chem* 284, 34522-34530.
- Kimura, H. (2005). Histone dynamics in living cells revealed by photobleaching. *DNA Repair (Amst)* 4, 939-950.
- Klokk, T.I., Kurys, P., Elbi, C., Nagaich, A.K., Hendarwanto, A., Slagsvold, T., Chang, C.Y., Hager, G.L., and Saatcioglu, F. (2007). Ligand-specific dynamics of the androgen receptor at its response element in living cells. *Mol Cell Biol* 27, 1823-1843.
- Klug, A. (2010). The discovery of zinc fingers and their applications in gene regulation and genome manipulation. *Annu Rev Biochem* 79, 213-231.
- Kodadek, T., Sikder, D., and Nalley, K. (2006). Keeping transcriptional activators under control. *Cell* 127, 261-264.
- Kohzaki, H., Ito, Y., and Murakami, Y. (1999). Context-dependent modulation of replication activity of *Saccharomyces cerevisiae* autonomously replicating sequences by transcription factors. *Mol Cell Biol* 19, 7428-7435.
- Kohzaki, H., and Murakami, Y. (2005). Transcription factors and DNA replication origin selection. *Bioessays* 27, 1107-1116.
- Kolpashchikov, D.M., Khodyreva, S.N., Khlimankov, D.Y., Wold, M.S., Favre, A., and Lavrik, O.I. (2001). Polarity of human replication protein A binding to DNA. *Nucleic Acids Res* 29, 373-379.
- Kraakman, L.S., Mager, W.H., Grootjans, J.J., and Planta, R.J. (1991). Functional analysis of the promoter of the gene encoding the acidic ribosomal protein L45 in yeast. *Biochim Biophys Acta* 1090, 204-210.
- Kunkel, T.A., and Erie, D.A. (2005). DNA mismatch repair. *Annu Rev Biochem* 74, 681-710.

- Kusumoto, R., Masutani, C., Sugasawa, K., Iwai, S., Araki, M., Uchida, A., Mizukoshi, T., and Hanaoka, F. (2001). Diversity of the damage recognition step in the global genomic nucleotide excision repair in vitro. *Mutat Res* 485, 219-227.
- Laine, J.P., and Egly, J.M. (2006). Initiation of DNA repair mediated by a stalled RNA polymerase IIO. *EMBO J* 25, 387-397.
- Laine, J.P., Mocquet, V., and Egly, J.M. (2006). TFIIH enzymatic activities in transcription and nucleotide excision repair. *Methods Enzymol* 408, 246-263.
- Lainé, J., and Egly, J. (2006). Initiation of DNA repair mediated by a stalled RNA polymerase IIO. *EMBO J* 25, 387-397.
- Lake, R.J., Geyko, A., Hemashettar, G., Zhao, Y., and Fan, H.Y. (2010). UV-induced association of the CSB remodeling protein with chromatin requires ATP-dependent relief of N-terminal autorepression. *Mol Cell* 37, 235-246.
- Lambertson, D., Chen, L., and Madura, K. (1999). Pleiotropic defects caused by loss of the proteasome-interacting factors Rad23 and Rpn10 of *Saccharomyces cerevisiae*. *Genetics* 153, 69-79.
- Lascaris, R.F., Groot, E., Hoen, P.B., Mager, W.H., and Planta, R.J. (2000). Different roles for abf1p and a T-rich promoter element in nucleosome organization of the yeast RPS28A gene. *Nucleic Acids Res* 28, 1390-1396.
- Le Cam, L., Linares, L., Paul, C., Julien, E., Lacroix, M., Hatchi, E., Triboulet, R., Bossis, G., Shmueli, A., Rodriguez, M., *et al.* (2006). E4F1 is an atypical ubiquitin ligase that modulates p53 effector functions independently of degradation. *Cell* 127, 775-788.
- Le May, N., Mota-Fernandes, D., Velez-Cruz, R., Iltis, I., Biard, D., and Egly, J.M. (2010). NER factors are recruited to active promoters and facilitate chromatin modification for transcription in the absence of exogenous genotoxic attack. *Mol Cell* 38, 54-66.
- Lebrun, E., Revardel, E., Boscheron, C., Li, R., Gilson, E., and Fourel, G. (2001). Protosilencers in *Saccharomyces cerevisiae* subtelomeric regions. *Genetics* 158, 167-176.
- Lee, J.H., Yoo, S.J., Park, S.H., Hwang, I., Lee, J.S., and Ahn, J.H. (2007a). Role of SVP in the control of flowering time by ambient temperature in *Arabidopsis*. *Genes Dev* 21, 397-402.
- Lee, J.W., Ryan, F., Swaffield, J.C., Johnston, S.A., and Moore, D.D. (1995). Interaction of thyroid-hormone receptor with a conserved transcriptional mediator. *Nature* 374, 91-94.
- Lee, K.B., Wang, D., Lippard, S.J., and Sharp, P.A. (2002a). Transcription-coupled and DNA damage-dependent ubiquitination of RNA polymerase II in vitro. *Proc Natl Acad Sci U S A* 99, 4239-4244.

- Lee, T.I., Rinaldi, N.J., Robert, F., Odom, D.T., Bar-Joseph, Z., Gerber, G.K., Hannett, N.M., Harbison, C.T., Thompson, C.M., Simon, I., *et al.* (2002b). Transcriptional regulatory networks in *Saccharomyces cerevisiae*. *Science* 298, 799-804.
- Lee, W., Tillo, D., Bray, N., Morse, R.H., Davis, R.W., Hughes, T.R., and Nislow, C. (2007b). A high-resolution atlas of nucleosome occupancy in yeast. *Nat Genet* 39, 1235-1244.
- Li, L., Lu, X., Peterson, C.A., and Legerski, R.J. (1995a). An interaction between the DNA repair factor XPA and replication protein A appears essential for nucleotide excision repair. *Mol Cell Biol* 15, 5396-5402.
- Li, L., Peterson, C.A., Lu, X., and Legerski, R.J. (1995b). Mutations in XPA that prevent association with ERCC1 are defective in nucleotide excision repair. *Mol Cell Biol* 15, 1993-1998.
- Li, R., Yu, D.S., Tanaka, M., Zheng, L., Berger, S.L., and Stillman, B. (1998). Activation of chromosomal DNA replication in *Saccharomyces cerevisiae* by acidic transcriptional activation domains. *Mol Cell Biol* 18, 1296-1302.
- Li, S., Chen, X., Ruggiero, C., Ding, B., and Smerdon, M. (2006a). Modulation of Rad26- and Rpb9-mediated DNA repair by different promoter elements. *J Biol Chem* 281, 36643-36651.
- Li, S., Chen, X., Ruggiero, C., Ding, B., and Smerdon, M.J. (2006b). Modulation of Rad26- and Rpb9-mediated DNA repair by different promoter elements. *J Biol Chem* 281, 36643-36651.
- Li, S., Ding, B., Chen, R., Ruggiero, C., and Chen, X. (2006c). Evidence that the transcription elongation function of Rpb9 is involved in transcription-coupled DNA repair in *Saccharomyces cerevisiae*. *Mol Cell Biol* 26, 9430-9441.
- Li, S., Ding, B., LeJeune, D., Ruggiero, C., Chen, X., and Smerdon, M.J. (2007). The roles of Rad16 and Rad26 in repairing repressed and actively transcribed genes in yeast. *DNA Repair (Amst)* 6, 1596-1606.
- Li, S., and Smerdon, M. (2002). Rpb4 and Rpb9 mediate subpathways of transcription-coupled DNA repair in *Saccharomyces cerevisiae*. *EMBO J* 21, 5921-5929.
- Li, S., and Smerdon, M.J. (2004). Dissecting transcription-coupled and global genomic repair in the chromatin of yeast GAL1-10 genes. *J Biol Chem* 279, 14418-14426.
- Lia, G., Praly, E., Ferreira, H., Stockdale, C., Tse-Dinh, Y.C., Dunlap, D., Croquette, V., Bensimon, D., and Owen-Hughes, T. (2006). Direct observation of DNA distortion by the RSC complex. *Mol Cell* 21, 417-425.
- Lieber, M.R. (2010). The mechanism of double-strand DNA break repair by the nonhomologous DNA end-joining pathway. *Annu Rev Biochem* 79, 181-211.

- Lipford, J.R., and Bell, S.P. (2001). Nucleosomes positioned by ORC facilitate the initiation of DNA replication. *Mol Cell* 7, 21-30.
- Lippke, J.A., Gordon, L.K., Brash, D.E., and Haseltine, W.A. (1981). Distribution of UV light-induced damage in a defined sequence of human DNA: detection of alkaline-sensitive lesions at pyrimidine nucleoside-cytidine sequences. *Proc Natl Acad Sci U S A* 78, 3388-3392.
- Loch, C.M., Mosammaparast, N., Miyake, T., Pemberton, L.F., and Li, R. (2004). Functional and physical interactions between autonomously replicating sequence-binding factor 1 and the nuclear transport machinery. *Traffic* 5, 925-935.
- Lommel, L., Bucheli, M., and Sweder, K. (2000a). Transcription-coupled repair in yeast is independent from ubiquitylation of RNA pol II: implications for Cockayne's syndrome. *Proc Natl Acad Sci U S A* 97, 9088-9092.
- Lommel, L., Chen, L., Madura, K., and Sweder, K. (2000b). The 26S proteasome negatively regulates the level of overall genomic nucleotide excision repair. *Nucleic Acids Res* 28, 4839-4845.
- Lommel, L., Ortolan, T., Chen, L., Madura, K., and Sweder, K.S. (2002). Proteolysis of a nucleotide excision repair protein by the 26 S proteasome. *Curr Genet* 42, 9-20.
- Loo, S., Laurenson, P., Foss, M., Dillin, A., and Rine, J. (1995). Roles of ABF1, NPL3, and YCL54 in silencing in *Saccharomyces cerevisiae*. *Genetics* 141, 889-902.
- Loo, S., and Rine, J. (1994). Silencers and domains of generalized repression. *Science* 264, 1768-1771.
- Louvion, J.F., Havaux-Copf, B., and Picard, D. (1993). Fusion of GAL4-VP16 to a steroid-binding domain provides a tool for gratuitous induction of galactose-responsive genes in yeast. *Gene* 131, 129-134.
- Luijsterburg, M.S., Goedhart, J., Moser, J., Kool, H., Geverts, B., Houtsmuller, A.B., Mullenders, L.H., Vermeulen, W., and van Driel, R. (2007). Dynamic in vivo interaction of DDB2 E3 ubiquitin ligase with UV-damaged DNA is independent of damage-recognition protein XPC. *J Cell Sci* 120, 2706-2716.
- Luscombe, N.M., Babu, M.M., Yu, H., Snyder, M., Teichmann, S.A., and Gerstein, M. (2004). Genomic analysis of regulatory network dynamics reveals large topological changes. *Nature* 431, 308-312.
- Mahe, Y., Lemoine, Y., and Kuchler, K. (1996). The ATP binding cassette transporters Pdr5 and Snq2 of *Saccharomyces cerevisiae* can mediate transport of steroids in vivo. *J Biol Chem* 271, 25167-25172.
- Maillard, O., Solyom, S., and Naegeli, H. (2007). An aromatic sensor with aversion to damaged strands confers versatility to DNA repair. *PLoS Biol* 5, e79.

- Malik, S., Chaurasia, P., Lahudkar, S., Durairaj, G., Shukla, A., and Bhaumik, S.R. (2010). Rad26p, a transcription-coupled repair factor, is recruited to the site of DNA lesion in an elongating RNA polymerase II-dependent manner in vivo. *Nucleic Acids Res* 38, 1461-1477.
- Marahrens, Y., and Stillman, B. (1992). A yeast chromosomal origin of DNA replication defined by multiple functional elements. *Science* 255, 817-823.
- Martens, J.A., and Brandl, C.J. (1994). GCN4p activation of the yeast TRP3 gene is enhanced by ABF1p and uses a suboptimal TATA element. *J Biol Chem* 269, 15661-15667.
- Martinez, E., Palhan, V.B., Tjernberg, A., Lyman, E.S., Gamper, A.M., Kundu, T.K., Chait, B.T., and Roeder, R.G. (2001). Human STAGA complex is a chromatin-acetylating transcription coactivator that interacts with pre-mRNA splicing and DNA damage-binding factors in vivo. *Mol Cell Biol* 21, 6782-6795.
- Masson, M., Niedergang, C., Schreiber, V., Muller, S., Menissier-de Murcia, J., and de Murcia, G. (1998). XRCC1 is specifically associated with poly(ADP-ribose) polymerase and negatively regulates its activity following DNA damage. *Mol Cell Biol* 18, 3563-3571.
- Masutani, C., Araki, M., Sugasawa, K., van der Spek, P.J., Yamada, A., Uchida, A., Maekawa, T., Bootsma, D., Hoeijmakers, J.H., and Hanaoka, F. (1997). Identification and characterization of XPC-binding domain of hHR23B. *Mol Cell Biol* 17, 6915-6923.
- Masutani, C., Araki, M., Yamada, A., Kusumoto, R., Nogimori, T., Maekawa, T., Iwai, S., and Hanaoka, F. (1999a). Xeroderma pigmentosum variant (XP-V) correcting protein from HeLa cells has a thymine dimer bypass DNA polymerase activity. *EMBO J* 18, 3491-3501.
- Masutani, C., Kusumoto, R., Yamada, A., Dohmae, N., Yokoi, M., Yuasa, M., Araki, M., Iwai, S., Takio, K., and Hanaoka, F. (1999b). The XPV (xeroderma pigmentosum variant) gene encodes human DNA polymerase eta. *Nature* 399, 700-704.
- Mathieu, N., Kaczmarek, N., and Naegeli, H. (2010). Strand- and site-specific DNA lesion demarcation by the xeroderma pigmentosum group D helicase. *Proc Natl Acad Sci U S A* 107, 17545-17550.
- Matsumoto, Y., and Kim, K. (1995). Excision of deoxyribose phosphate residues by DNA polymerase beta during DNA repair. *Science* 269, 699-702.
- Matsunaga, T., Mu, D., Park, C.H., Reardon, J.T., and Sancar, A. (1995). Human DNA repair excision nuclease. Analysis of the roles of the subunits involved in dual incisions by using anti-XPG and anti-ERCC1 antibodies. *J Biol Chem* 270, 20862-20869.
- Matsunaga, T., Park, C.H., Bessho, T., Mu, D., and Sancar, A. (1996). Replication protein A confers structure-specific endonuclease activities to the XPF-ERCC1 and XPG subunits of human DNA repair excision nuclease. *J Biol Chem* 271, 11047-11050.

- McBroom, L.D., and Sadowski, P.D. (1994a). Contacts of the ABF1 protein of *Saccharomyces cerevisiae* with a DNA binding site at MATa. *J Biol Chem* 269, 16455-16460.
- McBroom, L.D., and Sadowski, P.D. (1994b). DNA bending by *Saccharomyces cerevisiae* ABF1 and its proteolytic fragments. *J Biol Chem* 269, 16461-16468.
- McNally, F.J., and Rine, J. (1991). A synthetic silencer mediates SIR-dependent functions in *Saccharomyces cerevisiae*. *Mol Cell Biol* 11, 5648-5659.
- McNally, J., Müller, W., Walker, D., Wolford, R., and Hager, G. (2000a). The glucocorticoid receptor: rapid exchange with regulatory sites in living cells. *Science* 287, 1262-1265.
- McNally, J.G., Muller, W.G., Walker, D., Wolford, R., and Hager, G.L. (2000b). The glucocorticoid receptor: rapid exchange with regulatory sites in living cells. *Science* 287, 1262-1265.
- Mellon, I., Spivak, G., and Hanawalt, P.C. (1987). Selective removal of transcription-blocking DNA damage from the transcribed strand of the mammalian DHFR gene. *Cell* 51, 241-249.
- Mer, G., Bochkarev, A., Gupta, R., Bochkareva, E., Frappier, L., Ingles, C.J., Edwards, A.M., and Chazin, W.J. (2000). Structural basis for the recognition of DNA repair proteins UNG2, XPA, and RAD52 by replication factor RPA. *Cell* 103, 449-456.
- Metivier, R., Penot, G., Hubner, M.R., Reid, G., Brand, H., Kos, M., and Gannon, F. (2003). Estrogen receptor- α directs ordered, cyclical, and combinatorial recruitment of cofactors on a natural target promoter. *Cell* 115, 751-763.
- Min, J.H., and Pavletich, N.P. (2007). Recognition of DNA damage by the Rad4 nucleotide excision repair protein. *Nature* 449, 570-575.
- Missura, M., Buterin, T., Hindges, R., Hubscher, U., Kasparkova, J., Brabec, V., and Naegeli, H. (2001). Double-check probing of DNA bending and unwinding by XPA-RPA: an architectural function in DNA repair. *EMBO J* 20, 3554-3564.
- Mitchell, D.L., Jen, J., and Cleaver, J.E. (1992). Sequence specificity of cyclobutane pyrimidine dimers in DNA treated with solar (ultraviolet B) radiation. *Nucleic Acids Res* 20, 225-229.
- Miyake, T., Loch, C.M., and Li, R. (2002). Identification of a multifunctional domain in autonomously replicating sequence-binding factor 1 required for transcriptional activation, DNA replication, and gene silencing. *Mol Cell Biol* 22, 505-516.
- Miyake, T., Reese, J., Loch, C.M., Auble, D.T., and Li, R. (2004). Genome-wide analysis of ARS (autonomously replicating sequence) binding factor 1 (Abf1p)-mediated transcriptional regulation in *Saccharomyces cerevisiae*. *J Biol Chem* 279, 34865-34872.

- Mocquet, V., Kropachev, K., Kolbanovskiy, M., Kolbanovskiy, A., Tapias, A., Cai, Y., Broyde, S., Geacintov, N.E., and Egly, J.M. (2007). The human DNA repair factor XPC-HR23B distinguishes stereoisomeric benzo[a]pyrenyl-DNA lesions. *EMBO J* 26, 2923-2932.
- Mocquet, V., Laine, J.P., Riedl, T., Yajin, Z., Lee, M.Y., and Egly, J.M. (2008). Sequential recruitment of the repair factors during NER: the role of XPG in initiating the resynthesis step. *EMBO J* 27, 155-167.
- Moggs, J.G., Yarema, K.J., Essigmann, J.M., and Wood, R.D. (1996). Analysis of incision sites produced by human cell extracts and purified proteins during nucleotide excision repair of a 1,3-intrastrand d(GpTpG)-cisplatin adduct. *J Biol Chem* 271, 7177-7186.
- Morris, M.C., Kaiser, P., Rudyak, S., Baskerville, C., Watson, M.H., and Reed, S.I. (2003). Cks1-dependent proteasome recruitment and activation of CDC20 transcription in budding yeast. *Nature* 423, 1009-1013.
- Moser, J., Kool, H., Giakzidis, I., Caldecott, K., Mullenders, L.H., and Foustieri, M.I. (2007). Sealing of chromosomal DNA nicks during nucleotide excision repair requires XRCC1 and DNA ligase III alpha in a cell-cycle-specific manner. *Mol Cell* 27, 311-323.
- Moser, J., Volker, M., Kool, H., Alekseev, S., Vrieling, H., Yasui, A., van Zeeland, A.A., and Mullenders, L.H. (2005). The UV-damaged DNA binding protein mediates efficient targeting of the nucleotide excision repair complex to UV-induced photo lesions. *DNA Repair (Amst)* 4, 571-582.
- Mouret, S., Baudouin, C., Charveron, M., Favier, A., Cadet, J., and Douki, T. (2006). Cyclobutane pyrimidine dimers are predominant DNA lesions in whole human skin exposed to UVA radiation. *Proc Natl Acad Sci U S A* 103, 13765-13770.
- Mouret, S., Philippe, C., Gracia-Chantegrel, J., Banyasz, A., Karpati, S., Markovitsi, D., and Douki, T. (2010). UVA-induced cyclobutane pyrimidine dimers in DNA: a direct photochemical mechanism? *Org Biomol Chem* 8, 1706-1711.
- Mu, D., Hsu, D., and Sancar, A. (1996a). Reaction mechanism of human DNA repair excision nuclease. *J Biol Chem* 271, 8285-8294.
- Mu, D., Hsu, D.S., and Sancar, A. (1996b). Reaction mechanism of human DNA repair excision nuclease. *J Biol Chem* 271, 8285-8294.
- Mu, D., and Sancar, A. (1997). Model for XPC-independent transcription-coupled repair of pyrimidine dimers in humans. *J Biol Chem* 272, 7570-7573.
- Mu, D., Wakasugi, M., Hsu, D., and Sancar, A. (1997). Characterization of reaction intermediates of human excision repair nuclease. *J Biol Chem* 272, 28971-28979.
- Mueller, F., Mazza, D., Stasevich, T.J., and McNally, J.G. (2010). FRAP and kinetic modeling in the analysis of nuclear protein dynamics: what do we really know? *Curr Opin Cell Biol* 22, 403-411.

- Mueller, J.P., and Smerdon, M.J. (1996). Rad23 is required for transcription-coupled repair and efficient overall repair in *Saccharomyces cerevisiae*. *Mol Cell Biol* *16*, 2361-2368.
- Muftuoglu, M., Sharma, S., Thorslund, T., Stevnsner, T., Soerensen, M.M., Brosh, R.M., Jr., and Bohr, V.A. (2006). Cockayne syndrome group B protein has novel strand annealing and exchange activities. *Nucleic Acids Res* *34*, 295-304.
- Mukherjee, S., Berger, M.F., Jona, G., Wang, X.S., Muzzey, D., Snyder, M., Young, R.A., and Bulyk, M.L. (2004). Rapid analysis of the DNA-binding specificities of transcription factors with DNA microarrays. *Nat Genet* *36*, 1331-1339.
- Mumberg, D., Muller, R., and Funk, M. (1995). Yeast vectors for the controlled expression of heterologous proteins in different genetic backgrounds. *Gene* *156*, 119-122.
- Muratani, M., Kung, C., Shokat, K., and Tansey, W. (2005). The F box protein Dsg1/Mdm30 is a transcriptional coactivator that stimulates Gal4 turnover and cotranscriptional mRNA processing. *Cell* *120*, 887-899.
- Naegeli, H., Bardwell, L., and Friedberg, E. (1992). The DNA helicase and adenosine triphosphatase activities of yeast Rad3 protein are inhibited by DNA damage. A potential mechanism for damage-specific recognition. *J Biol Chem* *267*, 392-398.
- Nagaich, A.K., Walker, D.A., Wolford, R., and Hager, G.L. (2004). Rapid periodic binding and displacement of the glucocorticoid receptor during chromatin remodeling. *Mol Cell* *14*, 163-174.
- Nalley, K., Johnston, S.A., and Kodadek, T. (2006). Proteolytic turnover of the Gal4 transcription factor is not required for function in vivo. *Nature* *442*, 1054-1057.
- Nelson, J.R., Lawrence, C.W., and Hinkle, D.C. (1996). Thymine-thymine dimer bypass by yeast DNA polymerase zeta. *Science* *272*, 1646-1649.
- Nelson, M., and Silver, P. (1989). Context affects nuclear protein localization in *Saccharomyces cerevisiae*. *Mol Cell Biol* *9*, 384-389.
- Newman, J.C., Bailey, A.D., and Weiner, A.M. (2006). Cockayne syndrome group B protein (CSB) plays a general role in chromatin maintenance and remodeling. *Proc Natl Acad Sci U S A* *103*, 9613-9618.
- Ng, J.M., Vermeulen, W., van der Horst, G.T., Bergink, S., Sugawara, K., Vrieling, H., and Hoeijmakers, J.H. (2003). A novel regulation mechanism of DNA repair by damage-induced and RAD23-dependent stabilization of xeroderma pigmentosum group C protein. *Genes Dev* *17*, 1630-1645.
- Ni, L., Bruce, C., Hart, C., Leigh-Bell, J., Gelperin, D., Umansky, L., Gerstein, M.B., and Snyder, M. (2009). Dynamic and complex transcription factor binding during an inducible response in yeast. *Genes Dev* *23*, 1351-1363.

- Nichols, M., Rientjes, J.M., Logie, C., and Stewart, A.F. (1997). FLP recombinase/estrogen receptor fusion proteins require the receptor D domain for responsiveness to antagonists, but not agonists. *Mol Endocrinol* 11, 950-961.
- Nick McElhinny, S.A., Kissling, G.E., and Kunkel, T.A. (2010). Differential correction of lagging-strand replication errors made by DNA polymerases {alpha} and {delta}. *Proc Natl Acad Sci U S A* 107, 21070-21075.
- Nicolas, A. (1998). Relationship between transcription and initiation of meiotic recombination: toward chromatin accessibility. *Proc Natl Acad Sci U S A* 95, 87-89.
- Nishi, R., Okuda, Y., Watanabe, E., Mori, T., Iwai, S., Masutani, C., Sugasawa, K., and Hanaoka, F. (2005). Centrin 2 stimulates nucleotide excision repair by interacting with xeroderma pigmentosum group C protein. *Mol Cell Biol* 25, 5664-5674.
- O'Donovan, A., Davies, A.A., Moggs, J.G., West, S.C., and Wood, R.D. (1994). XPG endonuclease makes the 3' incision in human DNA nucleotide excision repair. *Nature* 371, 432-435.
- Oberye, E.H., Maurer, K., Mager, W.H., and Planta, R.J. (1993). Structure of the ABF1-homologue from *Kluyveromyces marxianus*. *Biochim Biophys Acta* 1173, 233-236.
- Ogi, T., and Lehmann, A.R. (2006). The Y-family DNA polymerase kappa (pol kappa) functions in mammalian nucleotide-excision repair. *Nat Cell Biol* 8, 640-642.
- Ogi, T., Limsirichaikul, S., Overmeer, R.M., Volker, M., Takenaka, K., Cloney, R., Nakazawa, Y., Niimi, A., Miki, Y., Jaspers, N.G., *et al.* (2010). Three DNA polymerases, recruited by different mechanisms, carry out NER repair synthesis in human cells. *Mol Cell* 37, 714-727.
- Okano, S., Lan, L., Caldecott, K.W., Mori, T., and Yasui, A. (2003). Spatial and temporal cellular responses to single-strand breaks in human cells. *Mol Cell Biol* 23, 3974-3981.
- Oksenysh, V., de Jesus, B., Zhovmer, A., Egly, J., and Coin, F. (2009). Molecular insights into the recruitment of TFIIH to sites of DNA damage. *EMBO J* 28, 2971-2980.
- Ono, Y., Tomita, K., Matsuura, A., Nakagawa, T., Masukata, H., Uritani, M., Ushimaru, T., and Ueno, M. (2003). A novel allele of fission yeast rad11 that causes defects in DNA repair and telomere length regulation. *Nucleic Acids Res* 31, 7141-7149.
- Orelli, B., McClendon, T.B., Tsodikov, O.V., Ellenberger, T., Niedernhofer, L.J., and Scharer, O.D. (2009). The XPA-binding domain of ERCC1 is required for nucleotide excision repair but not other DNA repair pathways. *J Biol Chem* 285, 3705-3712.
- Orren, D.K., Selby, C.P., Hearst, J.E., and Sancar, A. (1992). Post-incision steps of nucleotide excision repair in *Escherichia coli*. Disassembly of the UvrBC-DNA complex by helicase II and DNA polymerase I. *J Biol Chem* 267, 780-788.

- Ortolan, T.G., Chen, L., Tongaonkar, P., and Madura, K. (2004). Rad23 stabilizes Rad4 from degradation by the Ub/proteasome pathway. *Nucleic Acids Res* 32, 6490-6500.
- Ortolan, T.G., Tongaonkar, P., Lambertson, D., Chen, L., Schaubert, C., and Madura, K. (2000). The DNA repair protein rad23 is a negative regulator of multi-ubiquitin chain assembly. *Nat Cell Biol* 2, 601-608.
- Palomera-Sanchez, Z., and Zurita, M. (2011). Open, repair and close again: chromatin dynamics and the response to UV-induced DNA damage. *DNA Repair (Amst)* 10, 119-125.
- Paumi, C.M., Chuk, M., Snider, J., Stagljar, I., and Michaelis, S. (2009). ABC transporters in *Saccharomyces cerevisiae* and their interactors: new technology advances the biology of the ABCC (MRP) subfamily. *Microbiol Mol Biol Rev* 73, 577-593.
- Perdiz, D., Grof, P., Mezzina, M., Nikaido, O., Moustacchi, E., and Sage, E. (2000). Distribution and repair of bipyrimidine photoproducts in solar UV-irradiated mammalian cells. Possible role of Dewar photoproducts in solar mutagenesis. *J Biol Chem* 275, 26732-26742.
- Perlmann, T., Eriksson, P., and Wrangé, O. (1990). Quantitative analysis of the glucocorticoid receptor-DNA interaction at the mouse mammary tumor virus glucocorticoid response element. *J Biol Chem* 265, 17222-17229.
- Pfeifer, G.P., You, Y.H., and Besaratinia, A. (2005). Mutations induced by ultraviolet light. *Mutat Res* 571, 19-31.
- Phair, R.D., Scaffidi, P., Elbi, C., Vecerova, J., Dey, A., Ozato, K., Brown, D.T., Hager, G., Bustin, M., and Misteli, T. (2004). Global nature of dynamic protein-chromatin interactions in vivo: three-dimensional genome scanning and dynamic interaction networks of chromatin proteins. *Mol Cell Biol* 24, 6393-6402.
- Phillips, J.E., and Corces, V.G. (2009). CTCF: master weaver of the genome. *Cell* 137, 1194-1211.
- Picard, D. (1999). *Nuclear receptors : a practical approach* (Oxford: Oxford University Press).
- Picard, D. (2006). Chaperoning steroid hormone action. *Trends Endocrinol Metab* 17, 229-235.
- Picard, D., Kumar, V., Chambon, P., and Yamamoto, K.R. (1990). Signal transduction by steroid hormones: nuclear localization is differentially regulated in estrogen and glucocorticoid receptors. *Cell Regul* 1, 291-299.
- Picard, D., Salser, S.J., and Yamamoto, K.R. (1988). A movable and regulable inactivation function within the steroid binding domain of the glucocorticoid receptor. *Cell* 54, 1073-1080.

- Pluciennik, A., Dzantiev, L., Iyer, R.R., Constantin, N., Kadyrov, F.A., and Modrich, P. (2010). PCNA function in the activation and strand direction of MutLalpha endonuclease in mismatch repair. *Proc Natl Acad Sci U S A* 107, 16066-16071.
- Pockwinse, S.M., Kota, K.P., Quaresma, A.J., Imbalzano, A.N., Lian, J.B., van Wijnen, A.J., Stein, J.L., Stein, G.S., and Nickerson, J.A. (2011). Live cell imaging of the cancer-related transcription factor RUNX2 during mitotic progression. *J Cell Physiol* 226, 1383-1389.
- Podust, V.N., Georgaki, A., Strack, B., and Hubscher, U. (1992). Calf thymus RF-C as an essential component for DNA polymerase delta and epsilon holoenzymes function. *Nucleic Acids Res* 20, 4159-4165.
- Pokholok, D.K., Harbison, C.T., Levine, S., Cole, M., Hannett, N.M., Lee, T.I., Bell, G.W., Walker, K., Rolfe, P.A., Herbolzheimer, E., *et al.* (2005). Genome-wide map of nucleosome acetylation and methylation in yeast. *Cell* 122, 517-527.
- Popescu, A., Miron, S., Blouquit, Y., Duchambon, P., Christova, P., and Craescu, C.T. (2003). Xeroderma pigmentosum group C protein possesses a high affinity binding site to human centrin 2 and calmodulin. *J Biol Chem* 278, 40252-40261.
- Pouliot, J., Yao, K., Robertson, C., and Nash, H. (1999). Yeast gene for a Tyr-DNA phosphodiesterase that repairs topoisomerase I complexes. *Science* 286, 552-555.
- Prakash, S., Johnson, R.E., and Prakash, L. (2005). Eukaryotic translesion synthesis DNA polymerases: specificity of structure and function. *Annu Rev Biochem* 74, 317-353.
- Prakash, S., and Prakash, L. (2000). Nucleotide excision repair in yeast. *Mutat Res* 451, 13-24.
- Pryde, F.E., and Louis, E.J. (1999). Limitations of silencing at native yeast telomeres. *EMBO J* 18, 2538-2550.
- Ptashne, M. (1988). How eukaryotic transcriptional activators work. *Nature* 335, 683-689.
- Punga, T., Bengoechea-Alonso, M., and Ericsson, J. (2006). Phosphorylation and ubiquitination of the transcription factor sterol regulatory element-binding protein-1 in response to DNA binding. *J Biol Chem* 281, 25278-25286.
- Raasi, S., Varadan, R., Fushman, D., and Pickart, C.M. (2005). Diverse polyubiquitin interaction properties of ubiquitin-associated domains. *Nat Struct Mol Biol* 12, 708-714.
- Rademakers, S., Volker, M., Hoogstraten, D., Nigg, A.L., Mone, M.J., Van Zeeland, A.A., Hoeijmakers, J.H., Houtsmuller, A.B., and Vermeulen, W. (2003). Xeroderma pigmentosum group A protein loads as a separate factor onto DNA lesions. *Mol Cell Biol* 23, 5755-5767.

- Ramsey, K.L., Smith, J.J., Dasgupta, A., Maqani, N., Grant, P., and Auble, D.T. (2004). The NEF4 complex regulates Rad4 levels and utilizes Snf2/Swi2-related ATPase activity for nucleotide excision repair. *Mol Cell Biol* 24, 6362-6378.
- Rao, H., and Sastry, A. (2002). Recognition of specific ubiquitin conjugates is important for the proteolytic functions of the ubiquitin-associated domain proteins Dsk2 and Rad23. *J Biol Chem* 277, 11691-11695.
- Rapic-Otrin, V., McLenigan, M.P., Bisi, D.C., Gonzalez, M., and Levine, A.S. (2002). Sequential binding of UV DNA damage binding factor and degradation of the p48 subunit as early events after UV irradiation. *Nucleic Acids Res* 30, 2588-2598.
- Ratner, J.N., Balasubramanian, B., Corden, J., Warren, S.L., and Bregman, D.B. (1998). Ultraviolet radiation-induced ubiquitination and proteasomal degradation of the large subunit of RNA polymerase II. Implications for transcription-coupled DNA repair. *J Biol Chem* 273, 5184-5189.
- Ravanat, J.L., Douki, T., and Cadet, J. (2001). Direct and indirect effects of UV radiation on DNA and its components. *J Photochem Photobiol B* 63, 88-102.
- Rayasam, G.V., Elbi, C., Walker, D.A., Wolford, R., Fletcher, T.M., Edwards, D.P., and Hager, G.L. (2005). Ligand-specific dynamics of the progesterone receptor in living cells and during chromatin remodeling in vitro. *Mol Cell Biol* 25, 2406-2418.
- Reagan, M.S., and Friedberg, E.C. (1997). Recovery of RNA polymerase II synthesis following DNA damage in mutants of *Saccharomyces cerevisiae* defective in nucleotide excision repair. *Nucleic Acids Res* 25, 4257-4263.
- Reardon, J., and Sancar, A. (2004). Thermodynamic cooperativity and kinetic proofreading in DNA damage recognition and repair. *Cell Cycle* 3, 141-144.
- Reed, S.H., Akiyama, M., Stillman, B., and Friedberg, E.C. (1999). Yeast autonomously replicating sequence binding factor is involved in nucleotide excision repair. *Genes Dev* 13, 3052-3058.
- Reed, S.H., and Gillette, T.G. (2007). Nucleotide excision repair and the ubiquitin proteasome pathway--do all roads lead to Rome? *DNA Repair (Amst)* 6, 149-156.
- Reed, S.H., You, Z., and Friedberg, E.C. (1998). The yeast RAD7 and RAD16 genes are required for postincision events during nucleotide excision repair. In vitro and in vivo studies with rad7 and rad16 mutants and purification of a Rad7/Rad16-containing protein complex. *J Biol Chem* 273, 29481-29488.
- Reid, G., Hubner, M.R., Metivier, R., Brand, H., Denger, S., Manu, D., Beaudouin, J., Ellenberg, J., and Gannon, F. (2003). Cyclic, proteasome-mediated turnover of unliganded and liganded ERalpha on responsive promoters is an integral feature of estrogen signaling. *Mol Cell* 11, 695-707.
- Reid, J.L., Iyer, V.R., Brown, P.O., and Struhl, K. (2000). Coordinate regulation of yeast ribosomal protein genes is associated with targeted recruitment of Esa1 histone acetylase. *Mol Cell* 6, 1297-1307.

- Remacle, J.E., and Holmberg, S. (1992). A REB1-binding site is required for GCN4-independent ILV1 basal level transcription and can be functionally replaced by an ABF1-binding site. *Mol Cell Biol* 12, 5516-5526.
- Ren, B., Robert, F., Wyrick, J.J., Aparicio, O., Jennings, E.G., Simon, I., Zeitlinger, J., Schreiber, J., Hannett, N., Kanin, E., *et al.* (2000). Genome-wide location and function of DNA binding proteins. *Science* 290, 2306-2309.
- Rhode, P.R., Elsasser, S., and Campbell, J.L. (1992). Role of multifunctional autonomously replicating sequence binding factor 1 in the initiation of DNA replication and transcriptional control in *Saccharomyces cerevisiae*. *Mol Cell Biol* 12, 1064-1077.
- Rhode, P.R., Sweder, K.S., Oegema, K.F., and Campbell, J.L. (1989). The gene encoding ARS-binding factor I is essential for the viability of yeast. *Genes Dev* 3, 1926-1939.
- Riedl, T., Hanaoka, F., and Egly, J. (2003). The comings and goings of nucleotide excision repair factors on damaged DNA. *EMBO J* 22, 5293-5303.
- Rivier, D.H., Ekena, J.L., and Rine, J. (1999). HMR-I is an origin of replication and a silencer in *Saccharomyces cerevisiae*. *Genetics* 151, 521-529.
- Robertson, A.B., Klungland, A., Rognes, T., and Leiros, I. (2009). DNA repair in mammalian cells: Base excision repair: the long and short of it. *Cell Mol Life Sci* 66, 981-993.
- Robson, C., and Hickson, I. (1991). Isolation of cDNA clones encoding a human apurinic/apyrimidinic endonuclease that corrects DNA repair and mutagenesis defects in *E. coli* xth (exonuclease III) mutants. *Nucleic Acids Res* 19, 5519-5523.
- Rochette, P.J., Therrien, J.P., Drouin, R., Perdiz, D., Bastien, N., Drobetsky, E.A., and Sage, E. (2003). UVA-induced cyclobutane pyrimidine dimers form predominantly at thymine-thymine dipyrimidines and correlate with the mutation spectrum in rodent cells. *Nucleic Acids Res* 31, 2786-2794.
- Runger, T.M., and Kappes, U.P. (2008). Mechanisms of mutation formation with long-wave ultraviolet light (UVA). *Photodermatol Photoimmunol Photomed* 24, 2-10.
- Russell, S.J., Reed, S.H., Huang, W., Friedberg, E.C., and Johnston, S.A. (1999). The 19S regulatory complex of the proteasome functions independently of proteolysis in nucleotide excision repair. *Mol Cell* 3, 687-695.
- Saeki, Y., Sone, T., Toh-e, A., and Yokosawa, H. (2002). Identification of ubiquitin-like protein-binding subunits of the 26S proteasome. *Biochem Biophys Res Commun* 296, 813-819.
- Saha, A., Wittmeyer, J., and Cairns, B.R. (2006). Chromatin remodelling: the industrial revolution of DNA around histones. *Nat Rev Mol Cell Biol* 7, 437-447.

- Salas, T.R., Petruseva, I., Lavrik, O., and Saintome, C. (2009). Evidence for direct contact between the RPA3 subunit of the human replication protein A and single-stranded DNA. *Nucleic Acids Res* 37, 38-46.
- Salghetti, S., Caudy, A., Chenoweth, J., and Tansey, W. (2001). Regulation of transcriptional activation domain function by ubiquitin. *Science* 293, 1651-1653.
- San Filippo, J., Sung, P., and Klein, H. (2008). Mechanism of eukaryotic homologous recombination. *Annu Rev Biochem* 77, 229-257.
- Sarkar, S., Kiely, R., and McHugh, P.J. (2010). The Ino80 chromatin-remodeling complex restores chromatin structure during UV DNA damage repair. *J Cell Biol* 191, 1061-1068.
- Sarker, A.H., Tsutakawa, S.E., Kostek, S., Ng, C., Shin, D.S., Peris, M., Campeau, E., Tainer, J.A., Nogales, E., and Cooper, P.K. (2005). Recognition of RNA polymerase II and transcription bubbles by XPG, CSB, and TFIIH: insights for transcription-coupled repair and Cockayne Syndrome. *Mol Cell* 20, 187-198.
- Schaeffer, L., Moncollin, V., Roy, R., Staub, A., Mezzina, M., Sarasin, A., Weeda, G., Hoeijmakers, J., and Egly, J. (1994). The ERCC2/DNA repair protein is associated with the class II BTF2/TFIIH transcription factor. *EMBO J* 13, 2388-2392.
- Schaeffer, L., Roy, R., Humbert, S., Moncollin, V., Vermeulen, W., Hoeijmakers, J., Chambon, P., and Egly, J. (1993). DNA repair helicase: a component of BTF2 (TFIIH) basic transcription factor. *Science* 260, 58-63.
- Schauber, C., Chen, L., Tongaonkar, P., Vega, I., Lambertson, D., Potts, W., and Madura, K. (1998). Rad23 links DNA repair to the ubiquitin/proteasome pathway. *Nature* 391, 715-718.
- Schlecht, U., Erb, I., Demougin, P., Robine, N., Borde, V., Nimwegen, E., Nicolas, A., and Primig, M. (2008). Genome-wide expression profiling, in vivo DNA binding analysis, and probabilistic motif prediction reveal novel Abf1 target genes during fermentation, respiration, and sporulation in yeast. *Mol Biol Cell* 19, 2193-2207.
- Schroeder, S.C., and Weil, P.A. (1998). Biochemical and genetic characterization of the dominant positive element driving transcription of the yeast TBP-encoding gene, SPT15. *Nucleic Acids Res* 26, 4186-4195.
- Scrima, A., Konickova, R., Czyzewski, B.K., Kawasaki, Y., Jeffrey, P.D., Groisman, R., Nakatani, Y., Iwai, S., Pavletich, N.P., and Thoma, N.H. (2008). Structural basis of UV DNA-damage recognition by the DDB1-DDB2 complex. *Cell* 135, 1213-1223.
- Seki, M., and Wood, R.D. (2008). DNA polymerase theta (POLQ) can extend from mismatches and from bases opposite a (6-4) photoproduct. *DNA Repair (Amst)* 7, 119-127.
- Selby, C., Drapkin, R., Reinberg, D., and Sancar, A. (1997a). RNA polymerase II stalled at a thymine dimer: footprint and effect on excision repair. *Nucleic Acids Res* 25, 787-793.

- Selby, C.P., Drapkin, R., Reinberg, D., and Sancar, A. (1997b). RNA polymerase II stalled at a thymine dimer: footprint and effect on excision repair. *Nucleic Acids Res* 25, 787-793.
- Selby, C.P., and Sancar, A. (1997). Human transcription-repair coupling factor CSB/ERCC6 is a DNA-stimulated ATPase but is not a helicase and does not disrupt the ternary transcription complex of stalled RNA polymerase II. *J Biol Chem* 272, 1885-1890.
- Shachar, S., Ziv, O., Avkin, S., Adar, S., Wittschieben, J., Reissner, T., Chaney, S., Friedberg, E.C., Wang, Z., Carell, T., *et al.* (2009). Two-polymerase mechanisms dictate error-free and error-prone translesion DNA synthesis in mammals. *EMBO J* 28, 383-393.
- Shang, Y., Hu, X., DiRenzo, J., Lazar, M.A., and Brown, M. (2000). Cofactor dynamics and sufficiency in estrogen receptor-regulated transcription. *Cell* 103, 843-852.
- Shareef, A., Angove, M.J., Wells, J.D., and Johnson, B.B. (2006). Aqueous Solubilities of Estrone, 17 β -Estradiol, 17 α -Ethinylestradiol, and Bisphenol A. *J Chem Eng Data* 51, 879-881.
- Sharp, Z.D., Mancini, M.G., Hinojos, C.A., Dai, F., Berno, V., Szafran, A.T., Smith, K.P., Lele, T.P., Ingber, D.E., and Mancini, M.A. (2006). Estrogen-receptor- α exchange and chromatin dynamics are ligand- and domain-dependent. *J Cell Sci* 119, 4101-4116.
- Shell, S.M., Li, Z., Shkriabai, N., Kvaratskhelia, M., Brosey, C., Serrano, M.A., Chazin, W.J., Musich, P.R., and Zou, Y. (2009). Checkpoint kinase ATR promotes nucleotide excision repair of UV-induced DNA damage via physical interaction with xeroderma pigmentosum group A. *J Biol Chem* 284, 24213-24222.
- Shivji, K.K., Kenny, M.K., and Wood, R.D. (1992). Proliferating cell nuclear antigen is required for DNA excision repair. *Cell* 69, 367-374.
- Shivji, M.K., Podust, V.N., Hubscher, U., and Wood, R.D. (1995). Nucleotide excision repair DNA synthesis by DNA polymerase epsilon in the presence of PCNA, RFC, and RPA. *Biochemistry* 34, 5011-5017.
- Sijbers, A.M., de Laat, W.L., Ariza, R.R., Biggerstaff, M., Wei, Y.F., Moggs, J.G., Carter, K.C., Shell, B.K., Evans, E., de Jong, M.C., *et al.* (1996a). Xeroderma pigmentosum group F caused by a defect in a structure-specific DNA repair endonuclease. *Cell* 86, 811-822.
- Sijbers, A.M., van der Spek, P.J., Odijk, H., van den Berg, J., van Duin, M., Westerveld, A., Jaspers, N.G., Bootsma, D., and Hoeijmakers, J.H. (1996b). Mutational analysis of the human nucleotide excision repair gene ERCC1. *Nucleic Acids Res* 24, 3370-3380.
- Sikder, D., Johnston, S.A., and Kodadek, T. (2006). Widespread, but non-identical, association of proteasomal 19 and 20 S proteins with yeast chromatin. *J Biol Chem* 281, 27346-27355.

- Simpson, R.T. (1990). Nucleosome positioning can affect the function of a cis-acting DNA element in vivo. *Nature* **343**, 387-389.
- Smerdon, M.J., and Lieberman, M.W. (1978). Nucleosome rearrangement in human chromatin during UV-induced DNA- repair synthesis. *Proc Natl Acad Sci U S A* **75**, 4238-4241.
- Somesh, B., Sigurdsson, S., Saeki, H., Erdjument-Bromage, H., Tempst, P., and Svejstrup, J. (2007). Communication between distant sites in RNA polymerase II through ubiquitylation factors and the polymerase CTD. *Cell* **129**, 57-68.
- Somesh, B.P., Reid, J., Liu, W.F., Sogaard, T.M., Erdjument-Bromage, H., Tempst, P., and Svejstrup, J.Q. (2005). Multiple mechanisms confining RNA polymerase II ubiquitylation to polymerases undergoing transcriptional arrest. *Cell* **121**, 913-923.
- Sopko, R., Huang, D., Preston, N., Chua, G., Papp, B., Kafadar, K., Snyder, M., Oliver, S.G., Cyert, M., Hughes, T.R., *et al.* (2006). Mapping pathways and phenotypes by systematic gene overexpression. *Mol Cell* **21**, 319-330.
- Staresincic, L., Fagbemi, A.F., Enzlin, J.H., Gourdin, A.M., Wijgers, N., Dunand-Sauthier, I., Giglia-Mari, G., Clarkson, S.G., Vermeulen, W., and Scharer, O.D. (2009). Coordination of dual incision and repair synthesis in human nucleotide excision repair. *EMBO J* **28**, 1111-1120.
- Stavreva, D.A., Muller, W.G., Hager, G.L., Smith, C.L., and McNally, J.G. (2004). Rapid glucocorticoid receptor exchange at a promoter is coupled to transcription and regulated by chaperones and proteasomes. *Mol Cell Biol* **24**, 2682-2697.
- Steinfeld, I., Shamir, R., and Kupiec, M. (2007). A genome-wide analysis in *Saccharomyces cerevisiae* demonstrates the influence of chromatin modifiers on transcription. *Nat Genet* **39**, 303-309.
- Stenoien, D.L., Patel, K., Mancini, M.G., Dutertre, M., Smith, C.L., O'Malley, B.W., and Mancini, M.A. (2001). FRAP reveals that mobility of oestrogen receptor-alpha is ligand- and proteasome-dependent. *Nat Cell Biol* **3**, 15-23.
- Stigger, E., Drissi, R., and Lee, S.H. (1998). Functional analysis of human replication protein A in nucleotide excision repair. *J Biol Chem* **273**, 9337-9343.
- Sugasawa, K. (2009). Regulation of damage recognition in mammalian global genomic nucleotide excision repair. *Mutat Res*.
- Sugasawa, K., Akagi, J., Nishi, R., Iwai, S., and Hanaoka, F. (2009). Two-step recognition of DNA damage for mammalian nucleotide excision repair: Directional binding of the XPC complex and DNA strand scanning. *Mol Cell* **36**, 642-653.
- Sugasawa, K., Masutani, C., Uchida, A., Maekawa, T., van der Spek, P.J., Bootsma, D., Hoeijmakers, J.H., and Hanaoka, F. (1996). HHR23B, a human Rad23 homolog, stimulates XPC protein in nucleotide excision repair in vitro. *Mol Cell Biol* **16**, 4852-4861.

- Sugasawa, K., Ng, J.M., Masutani, C., Iwai, S., van der Spek, P.J., Eker, A.P., Hanaoka, F., Bootsma, D., and Hoeijmakers, J.H. (1998). Xeroderma pigmentosum group C protein complex is the initiator of global genome nucleotide excision repair. *Mol Cell* 2, 223-232.
- Sugasawa, K., Okamoto, T., Shimizu, Y., Masutani, C., Iwai, S., and Hanaoka, F. (2001). A multistep damage recognition mechanism for global genomic nucleotide excision repair. *Genes Dev* 15, 507-521.
- Sugasawa, K., Okuda, Y., Saijo, M., Nishi, R., Matsuda, N., Chu, G., Mori, T., Iwai, S., Tanaka, K., and Hanaoka, F. (2005). UV-induced ubiquitylation of XPC protein mediated by UV-DDB-ubiquitin ligase complex. *Cell* 121, 387-400.
- Sugasawa, K., Shimizu, Y., Iwai, S., and Hanaoka, F. (2002). A molecular mechanism for DNA damage recognition by the xeroderma pigmentosum group C protein complex. *DNA Repair (Amst)* 1, 95-107.
- Sung, P., Bailly, V., Weber, C., Thompson, L., Prakash, L., and Prakash, S. (1993). Human xeroderma pigmentosum group D gene encodes a DNA helicase. *Nature* 365, 852-855.
- Sung, P., Prakash, L., Matson, S.W., and Prakash, S. (1987). RAD3 protein of *Saccharomyces cerevisiae* is a DNA helicase. *Proc Natl Acad Sci U S A* 84, 8951-8955.
- Svejstrup, J.Q. (2003). Rescue of arrested RNA polymerase II complexes. *J Cell Sci* 116, 447-451.
- Svejstrup, J.Q. (2007). Contending with transcriptional arrest during RNAPII transcript elongation. *Trends Biochem Sci* 32, 165-171.
- Svejstrup, J.Q., Wang, Z., Feaver, W.J., Wu, X., Bushnell, D.A., Donahue, T.F., Friedberg, E.C., and Kornberg, R.D. (1995). Different forms of TFIIH for transcription and DNA repair: holo-TFIIH and a nucleotide excision repairsome. *Cell* 80, 21-28.
- Sweder, K.S., and Hanawalt, P.C. (1992). Preferential repair of cyclobutane pyrimidine dimers in the transcribed strand of a gene in yeast chromosomes and plasmids is dependent on transcription. *Proc Natl Acad Sci U S A* 89, 10696-10700.
- Tan, K., Feizi, H., Luo, C., Fan, S.H., Ravasi, T., and Ideker, T.G. (2008). A systems approach to delineate functions of paralogous transcription factors: role of the Yap family in the DNA damage response. *Proc Natl Acad Sci U S A* 105, 2934-2939.
- Tan, K., Shlomi, T., Feizi, H., Ideker, T., and Sharan, R. (2007). Transcriptional regulation of protein complexes within and across species. *Proc Natl Acad Sci U S A* 104, 1283-1288.
- Tanaka, K., Miura, N., Satokata, I., Miyamoto, I., Yoshida, M.C., Satoh, Y., Kondo, S., Yasui, A., Okayama, H., and Okada, Y. (1990). Analysis of a human DNA excision repair gene involved in group A xeroderma pigmentosum and containing a zinc-finger domain. *Nature* 348, 73-76.

- Tang, J., and Chu, G. (2002). Xeroderma pigmentosum complementation group E and UV-damaged DNA-binding protein. *DNA Repair (Amst)* 1, 601-616.
- Tang, M.S., Bohr, V.A., Zhang, X.S., Pierce, J., and Hanawalt, P.C. (1989). Quantification of aminofluorene adduct formation and repair in defined DNA sequences in mammalian cells using the UVRABC nuclease. *J Biol Chem* 264, 14455-14462.
- Tantin, D. (1998). RNA polymerase II elongation complexes containing the Cockayne syndrome group B protein interact with a molecular complex containing the transcription factor IIH components xeroderma pigmentosum B and p62. *J Biol Chem* 273, 27794-27799.
- Tapias, A., Auriol, J., Forget, D., Enzlin, J.H., Scharer, O.D., Coin, F., Coulombe, B., and Egly, J.M. (2004). Ordered conformational changes in damaged DNA induced by nucleotide excision repair factors. *J Biol Chem* 279, 19074-19083.
- Team, R.D.C. (2010). R: A language and environment for statistical computing (Vienna, Austria).
- Teng, Y., Bennett, M., Evans, K.E., Zhuang-Jackson, H., Higgs, A., Reed, S.H., and Waters, R. (2010). A novel method for the genome-wide high resolution analysis of DNA damage. *Nucleic Acids Res.*
- Teng, Y., Li, S., Waters, R., and Reed, S.H. (1997). Excision repair at the level of the nucleotide in the *Saccharomyces cerevisiae* MFA2 gene: mapping of where enhanced repair in the transcribed strand begins or ends and identification of only a partial rad16 requisite for repairing upstream control sequences. *J Mol Biol* 267, 324-337.
- Teng, Y., Liu, H., Gill, H.W., Yu, Y., Waters, R., and Reed, S.H. (2008). *Saccharomyces cerevisiae* Rad16 mediates ultraviolet-dependent histone H3 acetylation required for efficient global genome nucleotide-excision repair. *EMBO Rep* 9, 97-102.
- Teng, Y., Yu, Y., and Waters, R. (2002). The *Saccharomyces cerevisiae* histone acetyltransferase Gcn5 has a role in the photoreactivation and nucleotide excision repair of UV-induced cyclobutane pyrimidine dimers in the MFA2 gene. *J Mol Biol* 316, 489-499.
- Terleth, C., Schenk, P., Poot, R., Brouwer, J., and van de Putte, P. (1990). Differential repair of UV damage in rad mutants of *Saccharomyces cerevisiae*: a possible function of G2 arrest upon UV irradiation. *Mol Cell Biol* 10, 4678-4684.
- Thomas, M., and Chiang, C. (2006). The general transcription machinery and general cofactors. *Crit Rev Biochem Mol Biol* 41, 105-178.
- Thorel, F., Constantinou, A., Dunand-Sauthier, I., Nospikel, T., Lalle, P., Raams, A., Jaspers, N.G., Vermeulen, W., Shivji, M.K., Wood, R.D., *et al.* (2004). Definition of a short region of XPG necessary for TFIIH interaction and stable recruitment to sites of UV damage. *Mol Cell Biol* 24, 10670-10680.

- Thrower, J.S., Hoffman, L., Rechsteiner, M., and Pickart, C.M. (2000). Recognition of the polyubiquitin proteolytic signal. *EMBO J* 19, 94-102.
- Tijsterman, M., de Pril, R., Tasseront-de Jong, J.G., and Brouwer, J. (1999). RNA polymerase II transcription suppresses nucleosomal modulation of UV-induced (6-4) photoproduct and cyclobutane pyrimidine dimer repair in yeast. *Mol Cell Biol* 19, 934-940.
- Tijsterman, M., Verhage, R.A., van de Putte, P., Tasseront-de Jong, J.G., and Brouwer, J. (1997). Transitions in the coupling of transcription and nucleotide excision repair within RNA polymerase II-transcribed genes of *Saccharomyces cerevisiae*. *Proc Natl Acad Sci U S A* 94, 8027-8032.
- Tissier, A., Frank, E.G., McDonald, J.P., Iwai, S., Hanaoka, F., and Woodgate, R. (2000). Misinsertion and bypass of thymine-thymine dimers by human DNA polymerase ϵ . *EMBO J* 19, 5259-5266.
- Tornaletti, S. (2009). DNA repair in mammalian cells: Transcription-coupled DNA repair: directing your effort where it's most needed. *Cell Mol Life Sci* 66, 1010-1020.
- Tornaletti, S., and Hanawalt, P.C. (1999). Effect of DNA lesions on transcription elongation. *Biochimie* 81, 139-146.
- Tornaletti, S., Reines, D., and Hanawalt, P.C. (1999). Structural characterization of RNA polymerase II complexes arrested by a cyclobutane pyrimidine dimer in the transcribed strand of template DNA. *J Biol Chem* 274, 24124-24130.
- Trawick, J.D., Kraut, N., Simon, F.R., and Poyton, R.O. (1992). Regulation of yeast COX6 by the general transcription factor ABF1 and separate HAP2- and heme-responsive elements. *Mol Cell Biol* 12, 2302-2314.
- Tremeau-Bravard, A., Riedl, T., Egly, J.M., and Dahmus, M.E. (2004). Fate of RNA polymerase II stalled at a cisplatin lesion. *J Biol Chem* 279, 7751-7759.
- Troelstra, C., van Gool, A., de Wit, J., Vermeulen, W., Bootsma, D., and Hoeijmakers, J.H. (1992). ERCC6, a member of a subfamily of putative helicases, is involved in Cockayne's syndrome and preferential repair of active genes. *Cell* 71, 939-953.
- Tsodikov, O.V., Ivanov, D., Orelli, B., Staresinic, L., Shoshani, I., Oberman, R., Scharer, O.D., Wagner, G., and Ellenberger, T. (2007). Structural basis for the recruitment of ERCC1-XPF to nucleotide excision repair complexes by XPA. *EMBO J* 26, 4768-4776.
- Uchida, A., Sugawara, K., Masutani, C., Dohmae, N., Araki, M., Yokoi, M., Ohkuma, Y., and Hanaoka, F. (2002). The carboxy-terminal domain of the XPC protein plays a crucial role in nucleotide excision repair through interactions with transcription factor IIH. *DNA Repair (Amst)* 1, 449-461.
- Ueno, M., Murase, T., Kibe, T., Ohashi, N., Tomita, K., Murakami, Y., Uritani, M., Ushimaru, T., and Harata, M. (2004). Fission yeast Arp6 is required for telomere silencing, but functions independently of Swi6. *Nucleic Acids Res* 32, 736-741.

- Ura, K., Araki, M., Saeki, H., Masutani, C., Ito, T., Iwai, S., Mizukoshi, T., Kaneda, Y., and Hanaoka, F. (2001). ATP-dependent chromatin remodeling facilitates nucleotide excision repair of UV-induced DNA lesions in synthetic dinucleosomes. *EMBO J* 20, 2004-2014.
- Vaisman, A., Frank, E.G., Iwai, S., Ohashi, E., Ohmori, H., Hanaoka, F., and Woodgate, R. (2003). Sequence context-dependent replication of DNA templates containing UV-induced lesions by human DNA polymerase ι . *DNA Repair (Amst)* 2, 991-1006.
- Vaisman, A., Takasawa, K., Iwai, S., and Woodgate, R. (2006). DNA polymerase ι -dependent translesion replication of uracil containing cyclobutane pyrimidine dimers. *DNA Repair (Amst)* 5, 210-218.
- van den Boom, V., Citterio, E., Hoogstraten, D., Zotter, A., Egly, J.M., van Cappellen, W.A., Hoeijmakers, J.H., Houtsmuller, A.B., and Vermeulen, W. (2004). DNA damage stabilizes interaction of CSB with the transcription elongation machinery. *J Cell Biol* 166, 27-36.
- van Gool, A.J., Citterio, E., Rademakers, S., van Os, R., Vermeulen, W., Constantinou, A., Egly, J.M., Bootsma, D., and Hoeijmakers, J.H. (1997). The Cockayne syndrome B protein, involved in transcription-coupled DNA repair, resides in an RNA polymerase II-containing complex. *EMBO J* 16, 5955-5965.
- van Steensel, B., Braunschweig, U., Filion, G.J., Chen, M., van Bemmelen, J.G., and Ideker, T. (2010). Bayesian network analysis of targeting interactions in chromatin. *Genome Res* 20, 190-200.
- van Werven, F.J., van Teeffelen, H.A., Holstege, F.C., and Timmers, H.T. (2009). Distinct promoter dynamics of the basal transcription factor TBP across the yeast genome. *Nat Struct Mol Biol* 16, 1043-1048.
- Velculescu, V.E., Zhang, L., Zhou, W., Vogelstein, J., Basrai, M.A., Bassett, D.E., Jr., Hieter, P., Vogelstein, B., and Kinzler, K.W. (1997). Characterization of the yeast transcriptome. *Cell* 88, 243-251.
- Venditti, P., Costanzo, G., Negri, R., and Camilloni, G. (1994). ABFI contributes to the chromatin organization of *Saccharomyces cerevisiae* ARS1 B-domain. *Biochim Biophys Acta* 1219, 677-689.
- Venema, J., Mullenders, L.H., Natarajan, A.T., van Zeeland, A.A., and Mayne, L.V. (1990). The genetic defect in Cockayne syndrome is associated with a defect in repair of UV-induced DNA damage in transcriptionally active DNA. *Proc Natl Acad Sci U S A* 87, 4707-4711.
- Venema, J., van Hoffen, A., Karcagi, V., Natarajan, A.T., van Zeeland, A.A., and Mullenders, L.H. (1991). Xeroderma pigmentosum complementation group C cells remove pyrimidine dimers selectively from the transcribed strand of active genes. *Mol Cell Biol* 11, 4128-4134.

- Venters, B.J., Wachi, S., Mavrich, T.N., Andersen, B.E., Jena, P., Sinnamon, A.J., Jain, P., Roller, N.S., Jiang, C., Hemeryck-Walsh, C., *et al.* (2011). A comprehensive genomic binding map of gene and chromatin regulatory proteins in *Saccharomyces*. *Mol Cell* 41, 480-492.
- Verhage, R., Zeeman, A.M., de Groot, N., Gleig, F., Bang, D.D., van de Putte, P., and Brouwer, J. (1994). The RAD7 and RAD16 genes, which are essential for pyrimidine dimer removal from the silent mating type loci, are also required for repair of the nontranscribed strand of an active gene in *Saccharomyces cerevisiae*. *Mol Cell Biol* 14, 6135-6142.
- Verma, R., Oania, R., Graumann, J., and Deshaies, R.J. (2004). Multiubiquitin chain receptors define a layer of substrate selectivity in the ubiquitin-proteasome system. *Cell* 118, 99-110.
- Volker, M., Mone, M.J., Karmakar, P., van Hoffen, A., Schul, W., Vermeulen, W., Hoeijmakers, J.H., van Driel, R., van Zeeland, A.A., and Mullenders, L.H. (2001). Sequential assembly of the nucleotide excision repair factors in vivo. *Mol Cell* 8, 213-224.
- Voss, T.C., and Hager, G.L. (2008). Visualizing chromatin dynamics in intact cells. *Biochim Biophys Acta* 1783, 2044-2051.
- Wakasugi, M., Kawashima, A., Morioka, H., Linn, S., Sancar, A., Mori, T., Nikaido, O., and Matsunaga, T. (2002). DDB accumulates at DNA damage sites immediately after UV irradiation and directly stimulates nucleotide excision repair. *J Biol Chem* 277, 1637-1640.
- Wakasugi, M., Reardon, J.T., and Sancar, A. (1997). The non-catalytic function of XPG protein during dual incision in human nucleotide excision repair. *J Biol Chem* 272, 16030-16034.
- Wakasugi, M., and Sancar, A. (1998). Assembly, subunit composition, and footprint of human DNA repair excision nuclease. *Proc Natl Acad Sci U S A* 95, 6669-6674.
- Wakasugi, M., and Sancar, A. (1999). Order of assembly of human DNA repair excision nuclease. *J Biol Chem* 274, 18759-18768.
- Walker, S.S., Francesconi, S.C., and Eisenberg, S. (1990). A DNA replication enhancer in *Saccharomyces cerevisiae*. *Proc Natl Acad Sci U S A* 87, 4665-4669.
- Walker, S.S., Francesconi, S.C., Tye, B.K., and Eisenberg, S. (1989). The OBF1 protein and its DNA-binding site are important for the function of an autonomously replicating sequence in *Saccharomyces cerevisiae*. *Mol Cell Biol* 9, 2914-2921.
- Wang, H., Zhai, L., Xu, J., Joo, H.Y., Jackson, S., Erdjument-Bromage, H., Tempst, P., Xiong, Y., and Zhang, Y. (2006). Histone H3 and H4 ubiquitylation by the CUL4-DDB-ROC1 ubiquitin ligase facilitates cellular response to DNA damage. *Mol Cell* 22, 383-394.

- Wang, Q.E., Praetorius-Ibba, M., Zhu, Q., El-Mahdy, M.A., Wani, G., Zhao, Q., Qin, S., Patnaik, S., and Wani, A.A. (2007). Ubiquitylation-independent degradation of Xeroderma pigmentosum group C protein is required for efficient nucleotide excision repair. *Nucleic Acids Res* 35, 5338-5350.
- Wang, Q.E., Zhu, Q., Wani, G., El-Mahdy, M.A., Li, J., and Wani, A.A. (2005). DNA repair factor XPC is modified by SUMO-1 and ubiquitin following UV irradiation. *Nucleic Acids Res* 33, 4023-4034.
- Wang, Y., Zhang, X.S., and Xia, Y. (2009). Predicting eukaryotic transcriptional cooperativity by Bayesian network integration of genome-wide data. *Nucleic Acids Res* 37, 5943-5958.
- Wang, Z., Wei, S., Reed, S.H., Wu, X., Svejstrup, J.Q., Feaver, W.J., Kornberg, R.D., and Friedberg, E.C. (1997). The RAD7, RAD16, and RAD23 genes of *Saccharomyces cerevisiae*: requirement for transcription-independent nucleotide excision repair in vitro and interactions between the gene products. *Mol Cell Biol* 17, 635-643.
- Washington, M.T., Johnson, R.E., Prakash, L., and Prakash, S. (2002). Human DINB1-encoded DNA polymerase kappa is a promiscuous extender of mispaired primer termini. *Proc Natl Acad Sci U S A* 99, 1910-1914.
- Washington, M.T., Johnson, R.E., Prakash, S., and Prakash, L. (2000). Accuracy of thymine-thymine dimer bypass by *Saccharomyces cerevisiae* DNA polymerase eta. *Proc Natl Acad Sci U S A* 97, 3094-3099.
- Waters, R., Teng, Y., Yu, Y., Yu, S., and Reed, S.H. (2009). Tilting at windmills? The nucleotide excision repair of chromosomal DNA. *DNA Repair (Amst)* 8, 146-152.
- Watkins, J.F., Sung, P., Prakash, L., and Prakash, S. (1993). The *Saccharomyces cerevisiae* DNA repair gene RAD23 encodes a nuclear protein containing a ubiquitin-like domain required for biological function. *Mol Cell Biol* 13, 7757-7765.
- Weake, V.M., and Workman, J.L. (2010). Inducible gene expression: diverse regulatory mechanisms. *Nat Rev Genet* 11, 426-437.
- Wiederhold, L., Leppard, J., Kedar, P., Karimi-Busheri, F., Rasouli-Nia, A., Weinfeld, M., Tomkinson, A., Izumi, T., Prasad, R., Wilson, S., *et al.* (2004). AP endonuclease-independent DNA base excision repair in human cells. *Mol Cell* 15, 209-220.
- Wilson, D.r. (2003). Properties of and substrate determinants for the exonuclease activity of human apurinic endonuclease Ape1. *J Mol Biol* 330, 1027-1037.
- Wiltshire, S., Raychaudhuri, S., and Eisenberg, S. (1997). An Abf1p C-terminal region lacking transcriptional activation potential stimulates a yeast origin of replication. *Nucleic Acids Res* 25, 4250-4256.

- Winters, T., Henner, W., Russell, P., McCullough, A., and Jorgensen, T. (1994). Removal of 3'-phosphoglycolate from DNA strand-break damage in an oligonucleotide substrate by recombinant human apurinic/apyrimidinic endonuclease 1. *Nucleic Acids Res* 22, 1866-1873.
- Winzeler, E.A., Shoemaker, D.D., Astromoff, A., Liang, H., Anderson, K., Andre, B., Bangham, R., Benito, R., Boeke, J.D., Bussey, H., *et al.* (1999). Functional characterization of the *S. cerevisiae* genome by gene deletion and parallel analysis. *Science* 285, 901-906.
- Wittschieben, B.O., Iwai, S., and Wood, R.D. (2005). DDB1-DDB2 (xeroderma pigmentosum group E) protein complex recognizes a cyclobutane pyrimidine dimer, mismatches, apurinic/apyrimidinic sites, and compound lesions in DNA. *J Biol Chem* 280, 39982-39989.
- Wolski, S., Kuper, J., and Kisker, C. (2010). The XPD helicase: XPanDing archaeal XPD structures to get a grip on human DNA repair. *Biol Chem* 391, 761-765.
- Workman, C.T., Mak, H.C., McCuine, S., Tagne, J.B., Agarwal, M., Ozier, O., Begley, T.J., Samson, L.D., and Ideker, T. (2006). A systems approach to mapping DNA damage response pathways. *Science* 312, 1054-1059.
- Woudstra, E.C., Gilbert, C., Fellows, J., Jansen, L., Brouwer, J., Erdjument-Bromage, H., Tempst, P., and Svejstrup, J.Q. (2002). A Rad26-Def1 complex coordinates repair and RNA pol II proteolysis in response to DNA damage. *Nature* 415, 929-933.
- Wu, X., Braithwaite, E., and Wang, Z. (1999). DNA ligation during excision repair in yeast cell-free extracts is specifically catalyzed by the CDC9 gene product. *Biochemistry* 38, 2628-2635.
- Wu, X., Shell, S.M., Liu, Y., and Zou, Y. (2007). ATR-dependent checkpoint modulates XPA nuclear import in response to UV irradiation. *Oncogene* 26, 757-764.
- Wu, X., Shell, S.M., Yang, Z., and Zou, Y. (2006). Phosphorylation of nucleotide excision repair factor xeroderma pigmentosum group A by ataxia telangiectasia mutated and Rad3-related-dependent checkpoint pathway promotes cell survival in response to UV irradiation. *Cancer Res* 66, 2997-3005.
- Wu, Y., Reece, R.J., and Ptashne, M. (1996). Quantitation of putative activator-target affinities predicts transcriptional activating potentials. *EMBO J* 15, 3951-3963.
- Xie, Z., Liu, S., Zhang, Y., and Wang, Z. (2004). Roles of Rad23 protein in yeast nucleotide excision repair. *Nucleic Acids Res* 32, 5981-5990.
- Yang, E., Henriksen, M.A., Schaefer, O., Zakharova, N., and Darnell, J.E., Jr. (2002a). Dissociation time from DNA determines transcriptional function in a STAT1 linker mutant. *J Biol Chem* 277, 13455-13462.
- Yang, Z.G., Liu, Y., Mao, L.Y., Zhang, J.T., and Zou, Y. (2002b). Dimerization of human XPA and formation of XPA2-RPA protein complex. *Biochemistry* 41, 13012-13020.

References

- Yao, J., Munson, K.M., Webb, W.W., and Lis, J.T. (2006). Dynamics of heat shock factor association with native gene loci in living cells. *Nature* 442, 1050-1053.
- Yarragudi, A., Miyake, T., Li, R., and Morse, R.H. (2004). Comparison of ABF1 and RAP1 in chromatin opening and transactivator potentiation in the budding yeast *Saccharomyces cerevisiae*. *Mol Cell Biol* 24, 9152-9164.
- Yarragudi, A., and Morse, R. (2006). Chromatin opening and potentiation of transcriptional activation by the General Regulatory Factors, ABF1 and RAP1, in the budding yeast *Saccharomyces cerevisiae*. *Proc Indian Natn Sci Acad* 72, 13-17.
- Yarragudi, A., Parfrey, L.W., and Morse, R.H. (2007). Genome-wide analysis of transcriptional dependence and probable target sites for Abf1 and Rap1 in *Saccharomyces cerevisiae*. *Nucleic Acids Res* 35, 193-202.
- Yasuda, G., Nishi, R., Watanabe, E., Mori, T., Iwai, S., Orioli, D., Stefanini, M., Hanaoka, F., and Sugasawa, K. (2007). In vivo destabilization and functional defects of the xeroderma pigmentosum C protein caused by a pathogenic missense mutation. *Mol Cell Biol* 27, 6606-6614.
- Yokoi, M., Masutani, C., Maekawa, T., Sugasawa, K., Ohkuma, Y., and Hanaoka, F. (2000). The xeroderma pigmentosum group C protein complex XPC-HR23B plays an important role in the recruitment of transcription factor IIH to damaged DNA. *J Biol Chem* 275, 9870-9875.
- Yoo, H.Y., Jung, S.Y., Kim, Y.H., Kim, J., Jung, G., and Rho, H.M. (1995). Transcriptional control of the *Saccharomyces cerevisiae* ADH1 gene by autonomously replicating sequence binding factor 1. *Curr Microbiol* 31, 163-168.
- Yoon, J.H., Prakash, L., and Prakash, S. (2009). Highly error-free role of DNA polymerase eta in the replicative bypass of UV-induced pyrimidine dimers in mouse and human cells. *Proc Natl Acad Sci U S A* 106, 18219-18224.
- Yoon, J.H., Prakash, L., and Prakash, S. (2010). Error-free replicative bypass of (6-4) photoproducts by DNA polymerase zeta in mouse and human cells. *Genes Dev* 24, 123-128.
- You, J.S., Wang, M., and Lee, S.H. (2003). Biochemical analysis of the damage recognition process in nucleotide excision repair. *J Biol Chem* 278, 7476-7485.
- You, Y.H., Lee, D.H., Yoon, J.H., Nakajima, S., Yasui, A., and Pfeifer, G.P. (2001). Cyclobutane pyrimidine dimers are responsible for the vast majority of mutations induced by UVB irradiation in mammalian cells. *J Biol Chem* 276, 44688-44694.
- Yu, L., and Morse, R.H. (1999). Chromatin opening and transactivator potentiation by RAP1 in *Saccharomyces cerevisiae*. *Mol Cell Biol* 19, 5279-5288.
- Yu, P., and Kodadek, T. (2007). Dynamics of the hypoxia-inducible factor-1-vascular endothelial growth factor promoter complex. *J Biol Chem* 282, 35035-35045.

- Yu, Q., Qiu, R., Foland, T.B., Griesen, D., Galloway, C.S., Chiu, Y.H., Sandmeier, J., Broach, J.R., and Bi, X. (2003). Rap1p and other transcriptional regulators can function in defining distinct domains of gene expression. *Nucleic Acids Res* 31, 1224-1233.
- Yu, S., Owen-Hughes, T., Friedberg, E.C., Waters, R., and Reed, S.H. (2004). The yeast Rad7/Rad16/Abf1 complex generates superhelical torsion in DNA that is required for nucleotide excision repair. *DNA Repair (Amst)* 3, 277-287.
- Yu, S., Smirnova, J.B., Friedberg, E.C., Stillman, B., Akiyama, M., Owen-Hughes, T., Waters, R., and Reed, S.H. (2009). ABF1-binding sites promote efficient global genome nucleotide excision repair. *J Biol Chem* 284, 966-973.
- Yu, S., Teng, Y., Lowndes, N.F., and Waters, R. (2001). RAD9, RAD24, RAD16 and RAD26 are required for the inducible nucleotide excision repair of UV-induced cyclobutane pyrimidine dimers from the transcribed and non-transcribed regions of the *Saccharomyces cerevisiae* MFA2 gene. *Mutat Res* 485, 229-236.
- Yu, S., Teng, Y., Waters, R., and Reed, H.S. (2011). How chromatin is remodelled during DNA repair of UV-induced DNA damage in *Saccharomyces cerevisiae*. *PLoS Genet* 7.
- Yu, Y., Teng, Y., Liu, H., Reed, S.H., and Waters, R. (2005). UV irradiation stimulates histone acetylation and chromatin remodeling at a repressed yeast locus. *Proc Natl Acad Sci U S A* 102, 8650-8655.
- Zabel, U., and Baeuerle, P. (1990). Purified human I kappa B can rapidly dissociate the complex of the NF-kappa B transcription factor with its cognate DNA. *Cell* 61, 255-265.
- Zanton, S.J., and Pugh, B.F. (2006). Full and partial genome-wide assembly and disassembly of the yeast transcription machinery in response to heat shock. *Genes Dev* 20, 2250-2265.
- Zhai, J., and Hingorani, M.M. (2010). *Saccharomyces cerevisiae* Msh2-Msh6 DNA binding kinetics reveal a mechanism of targeting sites for DNA mismatch repair. *Proc Natl Acad Sci U S A* 107, 680-685.
- Zhang, H., and Siede, W. (2002). UV-induced T-->C transition at a TT photoproduct site is dependent on *Saccharomyces cerevisiae* polymerase eta in vivo. *Nucleic Acids Res* 30, 1262-1267.
- Zhang, L., Jones, K., and Gong, F. (2009). The molecular basis of chromatin dynamics during nucleotide excision repair. *Biochem Cell Biol* 87, 265-272.
- Zhao, Q., Wang, Q.E., Ray, A., Wani, G., Han, C., Milum, K., and Wani, A.A. (2009). Modulation of nucleotide excision repair by mammalian SWI/SNF chromatin-remodeling complex. *J Biol Chem* 284, 30424-30432.
- Zhu, Q., Wani, G., Yao, J., Patnaik, S., Wang, Q.E., El-Mahdy, M.A., Praetorius-Ibba, M., and Wani, A.A. (2007). The ubiquitin-proteasome system regulates p53-mediated transcription at p21waf1 promoter. *Oncogene* 26, 4199-4208.

- Ziv, O., Geacintov, N., Nakajima, S., Yasui, A., and Livneh, Z. (2009). DNA polymerase zeta cooperates with polymerases kappa and iota in translesion DNA synthesis across pyrimidine photodimers in cells from XPV patients. *Proc Natl Acad Sci U S A* 106, 11552-11557.
- Zotter, A., Luijsterburg, M.S., Warmerdam, D.O., Ibrahim, S., Nigg, A., van Cappellen, W.A., Hoeijmakers, J.H., van Driel, R., Vermeulen, W., and Houtsmuller, A.B. (2006). Recruitment of the nucleotide excision repair endonuclease XPG to sites of UV-induced dna damage depends on functional TFIIH. *Mol Cell Biol* 26, 8868-8879.
- Zou, Y., Yu, Q., and Bi, X. (2006). Asymmetric positioning of nucleosomes and directional establishment of transcriptionally silent chromatin by *Saccharomyces cerevisiae* silencers. *Mol Cell Biol* 26, 7806-7819.